Integration and function of new neurons generated from fibroblasts and adult neural stem cells in the pathological brain

Wood, James

2011

[Link to publication]

Citation for published version (APA):
Wood, J. (2011). *Integration and function of new neurons generated from fibroblasts and adult neural stem cells in the pathological brain*. [Doctoral Thesis (compilation), Neurology, Lund]. Laboratory of Neurogenesis and Cell Therapy.

Total number of authors:
1

Academic Dissertation

INTEGRATION AND FUNCTION OF NEW NEURONS GENERATED FROM FIBROBLASTS AND ADULT NEURAL STEM CELLS IN THE PATHOLOGICAL BRAIN

James C. W. Wood

Lund University
Faculty of Medicine

With the approval of the Faculty of Medicine at Lund University,
this thesis will be defended on December 20, 2011 at 9:00 am in Segerfalksalen,
Wallenberg Neuroscience Center, Lund, Sweden

Faculty Opponent

Professor Sebastian Jessberger, PhD
Institute of Cell Biology
Swiss Federal Institute for Technology
Zürich, Switzerland

LUND
UNIVERSITY

Organization LUND UNIVERSITY	Document name DOCTORAL DISSERTATION
Department of Clinical Sciences **Division of Neurology** **Lund University** **Lund, Sweden**	Date of issue December 20, 2011
	Sponsoring organization
Author(s) **James Wood**	

Title and subtitle   Integration and function of new neurons generated from fibroblasts and adult neural stem cells in the pathological brain

Abstract
In Papers One through Six we have investigated the function and integration of "new" neurons – new neurons born from neural stem cells in the adult brain, and new neurons in the sense that they were generated from fibroblasts. Papers One and Two focused on the new neurons generated from neural stem cells in the SVZ and SGZ after pathological insults. We investigated how the newly generated neurons migrate and integrate in the brain. These two phenomena, migration and integration are intimately linked. Without the proper migratory cues new cells exhibit ectopic placement and aberrant integration, as observed in the hippocampus after severe epileptic insults. Papers Three to Six focused on generating (and characterizing) neurons from fibroblasts. First it was crucial to investigate the functional characteristics of the newly generated neurons to demonstrate that they indeed had the properties of mature neurons. The functional properties of the new cells will determine how and importantly if they will integrate in the brain. This is of key importance if we envision using iN or iPS cells for transplantation in the future. In Paper 6 we demonstrate for the first time that transplanted iPS cells survive, migrate beyond the transplantation core, and exhibit the functional properties of mature neurons. Taken together, this thesis demonstrates that the environment encountered by new neurons will influence their migration and integration. We also demonstrate that human fibroblasts can be reprogrammed to neurons and show that fibroblast-derived neurons can integrate in the mammalian brain. Thus, fibroblasts may be a valuable source of neurons for transplantation but the environment encountered will influence their integration and function which will determine their therapeutic effect.

Key words: neurogenesis, neural stem cells, iNs, iPS cells, stroke, epilepsy, electrophysiology

Classification system and/or index termes (if any):

Supplementary bibliographical information:	Language English

ISSN and key title: 1652-8220	ISBN 978-91-86871-62-8

Recipient's notes	Number of pages	Price
	Security classification	

Distribution by (name and address)
I, the undersigned, being the copyright owner of the abstract of the above-mentioned dissertation, hereby grant to all reference sources permission to publish and disseminate the abstract of the above-mentioned dissertation.

Signature_____   Date____2011-11-07_____

Academic Dissertation

INTEGRATION AND FUNCTION OF NEW NEURONS GENERATED FROM FIBROBLASTS AND ADULT NEURAL STEM CELLS IN THE PATHOLOGICAL BRAIN

James C. W. Wood

Laboratory of Neurogenesis and Cell Therapy
Division of Neurology
Department of Clinical Sciences
Lund University

LUND
UNIVERSITY

Cover artwork by Bengt Mattsson and James Wood
5 months after transplantation into the striatum, a biocytin labeled (red),
GFP-expressing human iPS cell (green) exhibits the morphology and
functional properties of a mature neuron.

To my family

"Ah, but a man's reach should exceed his grasp,
Or what's a heaven for?"
-Robert Browning

TABLE OF CONTENTS

ABBREVIATIONS

ABM	Ascl1, Brn2, Myt1l
AMPA	2-amino-3-(5-methyl-3-oxo-1,2-oxazol-4-yl) propanoic acid
BrdU	Bromodeoxyuridine
D-AP5	(2R)-amino-5-phosphonovaleric acid
DGCs	Dentate granule cells
iNs	Induced neurons
iPS cells	Induced pluripotent stem cells
MCAO	Middle cerebral artery occlusion
mEPSCs, mIPSCs	Miniature excitatory or inhibitory postsynaptic currents
NBM	Neurogenin2, Brn2, Myt1l
NBQX	2,3-dihydroxy-6-nitro-7-sulfamoyl-benzo[f]quinoxaline-2,3-dione
NMDA	N-Methyl-D-aspartate
NSCs	Neural stem/progenitor cells
OB	Olfactory bulbs
RMS	Rostral migratory stream
RV-GFP	Retrovirus-expressing green fluorescent protein
SE	Status epilepticus
sEPSCs, sIPSCs	Spontaneous excitatory or inhibitory postsynaptic currents
SGZ	Subgranular zone
SVZ	Subventricular zone
TLE	Temporal lobe epilepsy

ORIGINAL PAPERS AND MANUSCRIPTS

I: Thored P, **Wood J**, Arvidsson A, Cammenga J, Kokaia Z, Lindvall O (2007) Long-term neuroblast migration along blood vessels in an area with transient angiogenesis and increased vascularization after stroke. Stroke 38:3032-9.

II: **Wood JC***, Jackson JS*, Jakubs K, Chapman KZ, Ekdahl CT, Kokaia Z, Kokaia M, Lindvall O (2011) Functional integration of new hippocampal neurons in adult epileptic brain is determined by characteristics of pathological environment. Exp Neurol 229:484-93.

III: Pfisterer U*, Kirkeby A*, Torper O*, **Wood J**, Nelander J, Dufour A, Bjorklund A, Lindvall O, Jakobsson J, Parmar M (2011) Direct conversion of human fibroblasts to dopamingergic neurons. Proc Natl Acad Sci U S A 108:10343-8.

IV: Pfisterer U, **Wood J**, Nihlberg K, Hallgren O, Bjermer L, Westergren-Thorsson G, Lindvall O, Parmar M (2011) Efficient induction of functional neurons from adult human fibroblasts. Cell Cycle 10:3311-6.

V: **Wood J**, Torper O, Kirkeby A, Lindvall O, Parmar M. Replacing Mash1 with Ngn2 during neural conversion of human fibroblasts influences phenotype and electrophysiological properties of generated neurons. Manuscript

VI: Oki K*, Tatarishvili J*, **Wood J***, Koch P*, Mine Y, Monni E, Wattanati S, Brüstle O, Lindvall O, Kokaia Z. Human induced pluripotent stem cells form functionally integrated neurons and improve recovery after transplantation in stroke-damaged rodent brain. Manuscript

* Equal contribution

SUMMARY

Stroke and epilepsy are devastating neurological disorders. These pathologies cause changes in neurogenesis, the process by which new neurons are added to the brain, in the brain regions affected. After a stroke, neural stem cells in the subventricular zone (SVZ) give rise to neuroblasts which migrate to the damaged region indicating the brain may have an endogenous repair mechanism. In Paper 1 we examined how a stroke influences the neural stem cell niche and vasculature, and how the new born neurons interact with the environment encountered. We showed that hypoxia is present in the SVZ after stroke, that changes in vascularization occur in the SVZ and adjacent striatum, and that newly formed neuroblasts migrate in close association with blood vessels.

Epileptic patients exhibit widespread changes in the hippocampus, the brain region where seizures often arise. Experimental animal models have shown that seizures lead to increased neurogenesis, but whether the new cells contribute to, or counteract the pathological function is unknown. We have previously shown that after severe hippocampal insults (status epilepticus and chronic inflammation), the new neurons may actually counteract the pathological function. In Paper 2, we analyzed the morphological development and electrophysiological integration of new neurons born into a less severe pathological environment characterized by recurrent stimulation-induced seizures, gradual development of hyperexcitability, but only minor transient changes in inflammation. In this case the new cells exhibited enhanced excitatory input but also a concomitant reduction in intrinsic excitability. Our results demonstrate that the severity and characteristics of pathological insults play a crucial role in determining how new neurons develop and integrate in the adult brain.

Cell replacement therapy using stem cells leads to benefits for patients with neurological disorders. However, using stem cells for transplantation has drawbacks such as the risk of tumor formation and the requirement of immunosuppression. In Paper 3, 4, and 5 we have generated neurons from human fibroblasts by direct reprogramming using defined sets of transcription factors. Paper 3 was the first study to show that human fibroblasts can be directly converted to functional neurons and also dopaminergic neurons. Paper 4 showed that lung fibroblasts from adult and elderly patients can be converted to functional neurons, and in Paper 5 we presented a novel set of transcription factors which give rise to neurons with distinct phenotype and functional properties. Finally, in Paper

6 we have transplanted induced pluripotent stem cells into adult rats and demonstrated that these cells become functionally integrated neurons and that transplantation after stroke leads to improvement. These studies may one day lead to patient-specific transplantations.

The goal of this thesis was to investigate the integration and function of firstly, new neurons born into the pathological brain and secondly, of fibroblast-derived neurons. Papers 1 and 2 demonstrate that the environment encountered by the neurons influences their migration and integration, respectively. Papers 3 to 6 focused on characterizing neurons from fibroblasts which may in the future be used in cell replacement studies. Taken together, future studies using fibroblast-derived neurons for transplantation should consider how the environment will influence the integration and function of the cells which will determine the therapeutic outcome.

INTRODUCTION

The Discovery of Adult Neurogenesis

To many, the founder of modern day neuroscience is Santiago Ramón y Cajal. He was a histologist, pathologist, and physician. One of his contributions to neuroscience is his numerous detailed illustrations of the nervous system, many of which are still used today. In 1906, for his work uncovering the mysteries of the nervous system, he was awarded the Nobel Prize. A centrally held belief in the time of Ramón y Cajal was that new neurons were not added to the adult brain. In other words, the neurons present at birth are the only neurons we ever possess. This belief was largely due to the fact that mitotic cells were not observed in the adult brain of birds and mammals, and by the absence of regenerative proliferation after traumatic brain injuries. However, in the 1960's, two researchers at MIT began questioning the long held belief that new neurons were not born in the adult brain. In a pilot study using fine-resolution autoradiography, Joseph Altman and Gopal Das observed that following intracranial injection of thymidine-H3 into young adult rats there was an accumulation of silver grains over the nuclei of a few neurons in the cortex and more commonly over granule cells in the hippocampus (Altman and Das, 1965). This led them to believe that they had discovered postnatal hippocampal neurogenesis; in fact, they did! However their publication was largely ignored at the time. Adult neurogenesis was reported again by Michael Kaplan and JW Hinds in the mid 1970's and early 1980's, but the phenomenon of adult neurogenesis continued to be overlooked by the academic community. However, thanks to the pioneering work of Altman, Das, Kaplan, and Hinds, and advances in technology, we now know that neurons are generated in specific regions of the brain throughout life, and that adult neurogenesis is a very dynamic, regulated, and reactive process.

Adult Neurogenesis

The development of nucleotide analogues (halogenated thymidines), notably, 5-bromo-2-deoxyuridine (BrdU), allowed adult neurogenesis to become more accessible for study by researchers. BrdU can be injected into experimental subjects where it rapidly incorporates into the DNA of dividing cells (Kriss et al., 1963). Thus, it is possible to visualize dividing cells by creating antibodies specific to BrdU (see Immunohistochemistry, below). Using this method throughout

the 1980's and 1990's many neuroscience groups examined which populations of cells incorporated BrdU and how various conditions could alter the number of dividing cells. However, adult neurogenesis was not a mainstream topic which appeared in the highest-impact journals until the late 1990's.

A "tipping point" is defined as the point at which the momentum for change becomes unstoppable. In the field of neuroscience, some consider the tipping point for the widespread acceptance and interest in adult neurogenesis to be in 2002, when the group of Fred Gage at the Salk Institute in San Diego reported that new born neurons added to the preexisting neural circuitry in the hippocampus become mature functional neurons (van Praag et al., 2002). This was the first evidence that adult born neurons became mature functioning cells, receiving excitatory and inhibitory input and capable of firing action potentials. The tool which made this study possible was a retrovirus (RV) encoding green-fluorescent protein (GFP) (see RV-GFP, below). This virus, RV-GFP, specifically infects dividing cells, and results in accumulation of GFP, thereby labeling the cell. Thus, using an electrophysiology rig (see Whole-cell Patch-clamp, below) equipped with a fluorescent microscope it is possible to examine the functional properties of GFP-expressing cells; the adult born neurons.

Today, it is accepted that neurogenesis occurs throughout life in all mammalian and non-mammalian species examined so far, including rodents (discussed in detail, below), birds (Goldman and Nottebohm, 1983), lizards (Goffinet et al., 1986), primates (Gould et al., 1998, 1999), and humans (Eriksson et al., 1998). The two regions of ongoing mammalian neurogenesis are the subventricular zone (SVZ) located along the walls of the lateral ventricles, and the subgranular zone (SGZ) of the dentate gyrus in the hippocampus (Figure 1).

Subventricular Zone Neurogenesis

The most prominent region of neurogenesis in the adult mammalian brain is the SVZ. In the mouse SVZ, there are believed to be four main cell types (Doetsch et al., 1997; Alvarez-Buylla and García-Verdugo, 2002) (Figure 2). The putative stem cell of the SVZ is the astrocytic Type B cell which gives rise to Type C cells. Type B cells form tubes ensheathing Type A cells and some Type B cells extend a ciliated process into the lumen of the lateral ventricle contacting the cerebrospinal fluid (CSF). The purpose of the interface between Type B cells and the CSF is currently unknown and could be an interesting issue to address.
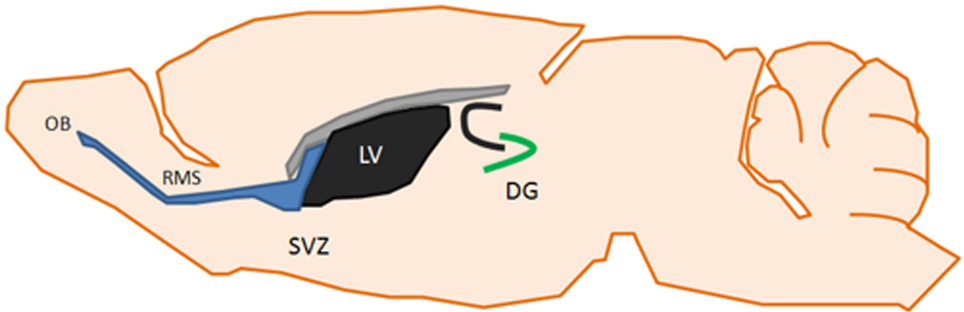
Figure 1. Regions of neurogenesis in the adult rodent brain.
The two regions of adult mammalian neurogenesis are the SVZ of the lateral ventricle (LV) and the subgranular zone of the dentate gyrus (DG). SVZ stem cells give rise to neuroblasts which migrate towards the olfactory bulb (OB) via the rostral migratory stream (RMS). Neural stem cells in the DG give rise to dentate granule cells throughout life. Adapted from Mu et al. (2010).

Type A cells form a chain-like structure and migrate tangentially towards to the olfactory bulb (OB) via the rostral migratory stream (RMS). These neuroblasts become interneurons and integrate in the granule and periglomerular layers of the OB where they have an important role in function (Gheusi et al., 2000) and maintenance (Imayoshi et al., 2008). Neuroblast migration in the RMS is a complex process which depends on many factors including, poly-sialated neural cell adhesion molecule (PSA-NCAM) expression (Rousselot et al., 1995), cyclin-dependent kinase 5 (Cdk5) (Hirota et al., 2007), serum response factor (Alberti et al., 2005), the direction of CSF flow (Sawamoto et al., 2006), β1 integrins (Belvindrah et al., 2007), and the vasculature for scaffolding (Snapyan et al., 2009).

Transit-amplifying Type C cells are highly proliferative neural precursors which form clusters next to, and give rise to Type A cells. These cells are present only in the SVZ (not the RMS). Doetsch et al. (2002) demonstrated that exposure to epidermal growth factor (EGF) can convert Type C cells into multipotent stem cells, showing they retain stem cell potential.

The ependymal layer is made up of ciliated ependymal cells (Type E cells) which form an epithelial layer separating the SVZ from the lateral ventricle. Beating of ependymal cell cilia controls the flow of the CSF in the lateral ventricles and can influence the migration of neuroblasts (Sawamoto et al., 2006).

There is evidence that the SVZ contains a vascular niche for adult neurogenesis such as the close proximity and contact of neural stem/progenitor cells (NSCs) to blood vessels, and vasculature-derived signaling (Shen et al., 2004; Shen et al.,
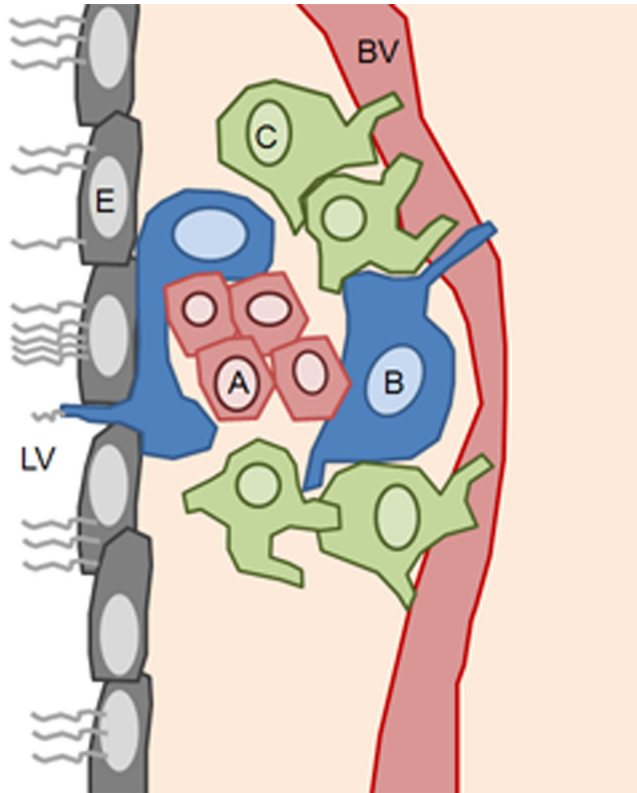
Figure 2. Schematic of neurogenesis in the mouse SVZ.
Type B cells (B), the SVZ stem cells, give rise to Type C cells (C), contact blood vessels (BV) and the lateral ventricle (LV), and form tubes ensheathing migrating Type A cells (A). Type A cells migrate in chains to the OB via the RMS. Transit-amplifying Type C cells are associated with blood vessels and give rise to Type A cells. Ependymal cells (E) separate the lateral ventricle from the SVZ, and control CSF flow with cilia. The rat SVZ is similar, but devoid of type C cells. Adapted from Tavazoie et al. (2008).

2008; Tavazoie et al., 2008) (see Neurogenesis and Angiogenesis, below). Besides the vasculature, the presence of specialized signaling pathways help maintain this neurogenic niche such as, notch signaling (Imayoshi et al., 2010), and the interaction of bone morphogenic protein (BMP) and its antagonistic ligand, noggin (Lim et al., 2000).

The rat and mouse SVZ are similar but at least one difference exists. Danilov et al. (2009) have shown that Type A, B, and E cells are present in the rat SVZ, however Transit-amplifying Type C cells are not.
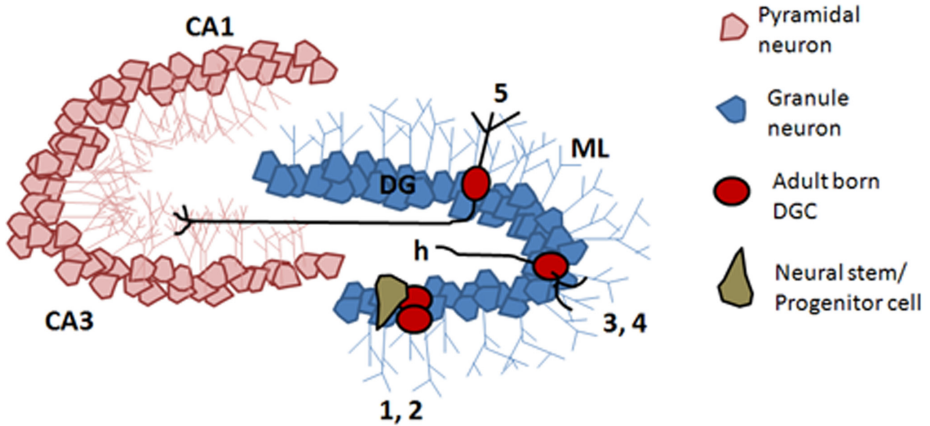
Figure 3. Schematic of neurogenesis in the rodent dentate gyrus.
The trisynaptic circuit of the hippocampus consists of input from the entorhinal cortex to the dentate gyrus (DG) whereby DGCs extend mossy fibers to CA3 pyramidal neurons (CA3) which then contact CA1 pyramidal neurons (CA1). 1, 2, NSCs in the SGZ of the dentate gyrus divide and generate lineage-committed progenitors (neuroblasts). 3,4, Adult born neurons migrate into the GCL and extend dendrites into the molecular layer (ML) and axons into the hilus (h). 5, Several weeks after birth, the new born cells become mature, functional neurons, with afferent input from the perforant path, and efferent output to CA3 pyramidal neurons. Adapted from Ming and Song (2005).

Hippocampal Neurogenesis

The hippocampus is located in the medial temporal lobe and is a major component of the mammalian brain. It belongs to the limbic system where it plays an important role in the formation of certain types of memories (Milner, 1996; Squire et al., 2004). The hippocampus is also a region of adult neurogenesis whereby new neurons are continuously added to the preexisting circuitry (Figure 3). In the rodent, there are thousands of new neurons added each day (Cameron and McKay, 2001). NSCs in the rodent granule cell layer (GCL) referred to as Type 1 cells, divide producing lineage-committed, doublecortin (DCX)-expressing neuroblasts which migrate into the GCL where they initially receive depolarizing GABAergic input (Ge et al., 2006). Over the course of several weeks, the new dentate granule cells (DGCs) extend dendrites into the molecular layer and axons into the hilus. The dendrites develop afferent glutamatergic synaptic input from the perforant path (van Praag et al., 2002) and hyperpolarizing GABAergic input from inter-

neurons (Laplagne et al., 2006). The axons, via the mossy fiber pathway, establish functional synapses with the CA3 pyramidal neurons (Toni et al., 2008; Faulkner et al., 2008).

Each step of adult hippocampal neurogenesis is a dynamic process which can be regulated by physiological and pathological changes. Hippocampal neurogenesis is increased by exposure to an enriched environment (Kempermann et al., 1997), running (van Praag et al., 1999), and hormones (Gould et al., 2000). Gobeske et al. (2009) demonstrated that exercise exerts its neurogenic effect via BMP-signaling which is depressed during and after exercise. This leads to a robust increase in hippocampal neurogenesis and also improved performance on hippocampal-dependent tasks. Another link between hippocampal-dependent tasks and neurogenesis was uncovered by Cao et al. (2004) who demonstrated that hippocampal-dependent tasks boost expression of vascular endothelial growth factor (VEGF) which in turn increases hippocampal neurogenesis. Other signaling pathways which regulate hippocampal neurogenesis include Prox1 which has important roles in neurogenesis both during development (Lavado et al., 2010) and also in the adult hippocampus (Karalay et al., 2011), and Cdk-5 signaling which has an important role in directing the migration and dendrite development of the new born DGCs (Jessberger et al., 2008).

Dendrite development and the formation of synaptic afferent inputs to the adult born DGCs is a dynamic process. Performing spatial learning tasks increases the number and size of spines which develop on the dendrites of new cells resulting in marked changes in the overall morphology (Tronel et al., 2010). Severe pathological insults such as status epilepticus and chronic inflammation cause altered synaptic integration, changes in dendrite development, and altered expression of synaptic adhesion molecules (Jakubs et al., 2006; 2008). After a less severe epileptic insult, characterized by repetitive seizures but only minor transient inflammation, adult born DGCs receive enhanced excitatory input which is counteracted by a concomitant reduction in membrane excitability (Wood et al., 2011) (these latter studies are discussed in more detail below).

Factors which lead to lower rates of DGC proliferation and neurogenesis include alcohol (He et al., 2005), repeated isofluorane exposure (Zhu et al., 2010), lead exposure (Gilbert et al., 2005), and chronic stress (Dranovsky and Hen, 2006). There is also evidence that hippocampal neurogenesis is related to the cause and cure of depression. Sahay and Hen (2007) have reviewed the evidence showing that depression coincides with reduced levels of hippocampal neurogenesis and

that successful antidepressant treatment not only enhances neurogenesis, but that this increase may in fact underlie mood improvement.

The precise role of hippocampal neurogenesis continues to be an important research question. Increasing evidence indicates neurogenesis has crucial roles in hippocampus-dependent tasks, learning, and memory formation (Drapeau et al., 2003; Clelland et al., 2009). A recent study by Deng et al. (2009) demonstrated that a transient reduction in hippocampal proliferation causes impaired long-term, but not short-term, memory retention. These are just a small handful of the many publications examining hippocampal neurogenesis, revealing the importance, complexity and sensitivity of the process.

Neurogenesis and Angiogenesis

There is evidence that neurogenesis and angiogenesis are linked in the brain. Endothelial cells secrete brain-derived neurotrophic factor (BDNF) providing sufficient trophic support for SVZ-derived neuroblast development (Leventhal et al., 1999). Furthermore, endothelial cells maintain neurogenic niches by secreting factors which stimulate self-renewal of NSCs (Shen et al., 2004). In the adult songbird brain, the higher vocal center (HVC) is a site of continuous neurogenesis and angiogenesis which is mediated by seasonal changes in testosterone levels and VEGF signaling (Louissaint et al., 2002). In the adult rat dentate gyrus, approximately 40% of adult born cells exhibit markers of endothelial cells indicating this region is a vascular and neurogenic niche (Palmer et al., 2000). Pathological insults, such as electroconvulsive shock, can induce simultaneous enhancement of angiogenesis and neurogenesis in the dentate gyrus (Hellsten et al., 2005). There is evidence that the vasculature plays an important role maintaining the SVZ neurogenic niche (Shen et al., 2008; Tavazoie et al., 2008). Experimental animals models of stroke lead to an increase in angiogenesis and neurogenesis in the SVZ and striatum (Gotts and Chesselet, 2005; Thored et al., 2007), and the newly formed cells migrate towards the damaged region in close association with blood vessels (Thored et al., 2007).

Adult Neurogenesis and Pathology

Adult neurogenesis is a very exciting field of study for researchers and clinicians, especially for those who work with neurodegenerative disease and traumatic brain injury. The discovery of lifelong neurogenesis has fostered hope that

the brain has some regenerative capacity. Even if physiological adult neurogenesis is incapable of repairing the pathological brain, perhaps a deeper understanding of how the brain incorporates new neurons into the preexisting neural circuitry will provide clues how to proceed with neural transplantations or gene therapy. For example, if after a stroke we could boost neurogenesis and guide new neurons into the damaged region of the brain, perhaps we could enhance stroke rehabilitation. Or, if we could program adult born neurons in the hippocampus to suppress seizure activity, maybe we could cure temporal lobe epilepsy. And, perhaps we could use cell transplantations to replace the neurons lost in Parkinson's disease to alleviate motor impairments. The list of potential therapeutic uses of adult neurogenesis goes on, and for this reason adult neurogenesis is studied in relation to many pathological brain states.

Epilepsy

A seizure is a neurological disorder characterized by spontaneous occurrence of repetitive synchronized firing of populations of neurons resulting in a surge of electrical activity throughout the brain. The clinical presentation of a seizure depends on the region(s) of the brain affected. Partial seizures involve a specific region of the brain and induce a brief loss of consciousness. Partial seizures can spread, or generalize, affecting the entire brain, causing loss of consciousness and tonic-clonic seizures, i.e., status epilepticus (SE). Every brain has a seizure threshold and approximately 10% of the population experiences at least one seizure in their lifetime. However, only one percent of the population develops epilepsy, a seizure disorder characterized by the occurrence of at least two unprovoked seizures. The underlying cause of a seizure disorder can be considered to be a pathological brain state which makes the brain susceptible to seizures i.e., a low seizure threshold. Epilepsy refers to any one of the array of seizure disorders and comorbidities resulting from recurrent seizures, which include poor memory, mood and anxiety disorders, and psychosis. Approximately 40% of epilepsy patients exhibit a structural abnormality in the brain such as, scars, tumors, or infections. How these abnormalities result in a lowered seizure threshold is not fully understood. The cause of epilepsy in the other 60% of patients is unknown. There is an apparent genetic component to seizure susceptibility however it is unclear how epileptic genes are passed on.

Experimental Epilepsy Models

There are numerous experimental models of epilepsy. Pilocarpine or kainic acid can be injected in experimental animals resulting in chemically-induced SE. Pilocarpine is a muscarinic receptor agonist while kainic acid exerts its epileptic effect by binding to and activating the kainate receptor. Chemically-induced models of epilepsy develop in three behavioral and electrographic changes: i) acute development of SE characterized by afterdischarges and motor seizures, ii) a silent phase, lasting approximately a month, when brain activity returns to normal, and iii) the chronic phase characterized by the occurrence of spontaneous, recurrent seizures (Cavalheiro, 1995).

Electrical SE and kindling are models of epilepsy induced by the direct electrical stimulation of the brain. There are several different versions of electrically-induced seizures, but in this thesis the relevant model involves placing a stimulating electrode in the CA3 region of the hippocampus. Stimulation in this region leads to seizure activity in both the ipsi- and contralateral hippocampus and can spread to other brain regions i.e., generalize. Various stimulation protocols can be employed, such as SE which is characterized by continuous stimulation leading to self-sustained seizures, or traditional kindling which involves daily stimulus-induced seizures leading gradually to a lowered seizures threshold and more intense seizures. Rapid kindling can be seen as a hybrid of these two techniques and has been used to induce seizures and hyperexcitability in Paper 2. The specifics of this technique are discussed in detail below.

Epilepsy and Reactive Plasticity

The most common type of epilepsy in adults is temporal lobe epilepsy (TLE), whereby seizures initiate and propagate from the hippocampus in the mesial temporal lobe (Engel et al., 1997). Neuropathological changes referred to as the reactive plasticity of the dentate gyrus, observed in patients and in animal models of epilepsy illustrates that this region has important roles in epileptogenesis. In particular, the following abnormalities observed in mature DGCs are hallmarks of the epileptic brain:

(i) Mossy fiber sprouting, whereby glutamatergic axons of DGCs sprout and extend ectopic processes into the GCL and establish functional recurrent excitatory circuits between DGCs after kindling (Elmér et al., 1996; Lynch and Sutula, 2000),

kainic acid-induced SE (Tauck and Nadler, 1985; Buckmaster and Dudek, 1997; Lynch and Sutula, 2000), pilocarpine-induced SE (Scharfman et al., 2003b), and in patients with TLE (Sutula et al., 1989; Represa et al., 1990). Epsztein et al. (2005) demonstrated that the sprouted mossy fibers can lead to the establishment of recurrent kainate receptor-operated synapses on DGCs.

(ii) Hilar basal dendrites, whereby ectopic dendrites rather than extending into the molecular layer, extend into the hilus. Ribak et al. (2000) used electron microscopy to show that after pilocarpine-induced seizures, basal dendrites have synapses and thus likely contribute to hyperexcitability.

(iii) Dispersion of the GCL and/or ectopic integration of DGCs in the hilus in animal models of epilepsy (Parent et al., 1997, Scharfman et al., 2003a) and also in TLE patients (Parent et al., 2006). Haas and Frotscher (2010) demonstrated that this dispersion is associated with a loss of the matrix protein Reelin in both epileptic patients and animal models of epilepsy and that knockdown of Reelin causes GCL dispersion in otherwise healthy mice. Another study demonstrated that elevated levels of Cystatin C correlated with GCL dispersion in human TLE patients and also in rodent models of epilepsy (Pirttilä et al., 2005).

(iv) Changes in excitatory and inhibitory synaptic input. Many studies have demonstrated that epileptic insults cause changes in the synaptic input to mature DGCs (Wuarin and Dudek, 1996; Buhl et al., 1996; Simmons et al., 1997; Wuarin and Dudek, 2001; Kobyashi and Buckmaster, 2003; Jakubs et al., 2006; Feng et al., 2008; Zhan and Nadler, 2009). These studies and others are discussed in more detail in Paper 2.

Hippocampal interneurons in TLE patients and in animal models of epilepsy are also susceptible to repeated seizures and may be lost or exhibit morphological and functional changes (Wittner et al., 2001; Dinocourt et al., 2003; Sayin et al., 2003; Zhang et al., 2009; Zhang and Buckmaster, 2009).

Together, the reactive plasticity of the dentate gyrus after SE may contribute to the generation of spontaneous, recurrent seizures. Indeed, under certain conditions, seizure activity can be induced in acute brain slice preparations taken from patients with epilepsy (Gabriel et al., 2004).

Epilepsy and Neurogenesis

Neurogenesis in the dentate gyrus is altered in TLE patients and in animal models of epilepsy. It has become increasingly evident that the newborn neurons are at least equally, if not even more susceptible to the reactive plasticity observed in the hippocampus. Indeed, all of the above listed changes are also seen in adult born neurons. Thus it is highly likely that the new neurons born into the epileptic hippocampus contribute to the overall network reorganization observed in the chronic stages of epilepsy.

In all animal models of epilepsy examined so far, after a seizure there is an initial increase in DGC NSC proliferation (Bengzon et al., 1997; Parent et al., 1997; Scott et al., 2000; Ekdahl et al., 2001), however in the later phase, i.e., chronic stage of epilepsy, there is a marked decline in hippocampal neurogenesis (Hattiangady et al., 2004). Loss or decline of neurogenesis may contribute to comorbidities of epilepsy, including, depression or memory loss (for neurogenesis-depression link, see Malberg et al., 2000; Santarelli et al., 2003; Kondziella et al., 2007; Eisch et al., 2008). DGCs which develop several weeks before, or after SE exhibit numerous abnormalities. Parent et al. (1997) demonstrated that new neurons migrate ectopically into the hilus, exhibit mossy fiber sprouting, and display abnormal axon development in response to pilocarpine-induced seizures. Walter et al. (2007), using BrdU at various time-points before and after pilocarpine-induced seizures, revealed that new neurons which are young at the time of seizures are more susceptible to the pathological insult. Specifically, new cells which were 1 week old at the time of seizures were far more likely to exhibit hilar basal dendrites and migrate ectopically than 4-week old cells. A similar study performed by Kron et al. (2010) using a retrovirus to label the new born cells drew the same conclusion, whereby young neurons at the time of SE were more prone to developing mossy fiber sprouting and hilar basal dendrites. New neurons born after SE exhibit more extensive dendrite development leading to earlier functional integration with the perforant path compared to new neurons born in healthy rodents (Overstreet-Wadiche et al., 2006). Jessberger et al. (2007) demonstrated that kainic-acid induced seizures induce alterations in neuronal polarity and spine density. Epileptic insults induce functional changes at the afferent synapses of the new born neurons. Jakubs et al. (2006) demonstrated that new neurons born after electrically-induced SE receive reduced excitatory and enhanced inhibitory input compared to new neurons generated in response to a physiological stimulus (running). A comparably mild epileptic insult characterized by recurring seizures, development of hy-

perexcitability, but only minor inflammation, results in enhanced excitatory input and reduced intrinsic excitability of the new born neurons (Wood et al., 2011) *(The complete details of this study are presented below in Paper 2)*. How these numerous changes in adult born DGCs influence the network activity of the epileptic hippocampus remains to be completely understood. Of key importance in determining whether new neurons born into the epileptic brain will contribute or counteract the pathology, will be uncovering how these new neurons interact with the hippocampal network at their efferent outputs.

Experimental Epilepsy Therapy

The wide array of changes in the epileptic brain has led to many ideas on how to prevent or suppress epileptogenesis. A few are discussed here:

Modulating Neurotrophins

Modulating neurotrophin expression after seizures has shown promise in preventing epileptogenesis. For example, BDNF expression is increased by seizures (Lindvall et al., 1994a) and has been shown to enhance excitatory transmission (Kang and Schuman, 1995) and reduce inhibitory transmission in the hippocampus (Tanaka et al., 1997) which may underlie hyperexcitability. Indeed, blocking BDNF signaling can suppress epileptogenesis (Kokaia et al., 1995). Other neurotrophins involved with epileptogenesis include neurotrophin-3 (NT-3) and glial cell line-derived neurotrophic factor (GDNF). Mice lacking components of these signaling pathways exhibit reduced epileptogenesis (Elmér et al., 1997; Nanobashvili et al., 2000).

Targeting Hippocampal Neurogenesis

Because epilepsy causes changes throughout the hippocampus and the newly formed neurons contribute to the overall network reorganization, controversy exists over their role, i.e., are adult born neurons contributing to, or counteracting epileptogenesis? Blocking hippocampal neurogenesis with cytosine-b-D-arabino-furanoside (Ara-C) in a model of pilocarpine-induced SE has been shown to reduce the occurrence of spontaneous recurrent seizures (Jung et al., 2004). Rapamycin treatment before kainic acid-induced SE has been shown to interfere with epileptogenesis and coincides with reduced mossy fiber sprouting and hippocampal neurogenesis (Zeng et al., 2009). In a mild epileptic environment, characterized by repeated seizures but minor inflammatory changes, new born neurons exhibit

enhanced excitatory input at their afferent synapses, but reduced intrinsic excitability and conserved morphology (Wood et al., 2011). However, after electrically-induced SE, a much more severe model of epilepsy, new born DGCs receive less excitatory input, and could therefore attenuate network hyperexcitability (Jakubs et al., 2006). There are still many questions surrounding the role of adult born neurons and epileptogenesis. For example, what is the functional significance of new born neurons migrating into the hilus? By incorporating into the network circuitry, are they contributing to seizure activity or counteracting hyperexcitability by stimulating inhibitory interneurons? Does mossy fiber sprouting of adult born neurons copy the sprouting of mature DGCs and lead to efferent connections with neighboring cells? More research is needed to determine the precise role of adult born neurons in the epileptic brain.

Optogenetics

An exciting, new approach to reduce epileptic activity in the hippocampus is to control the excitability of hippocampal neurons. A light-driven chloride pump, NpHR, can be inserted into the cell membrane of neurons, which can be activated by light of a specific wavelength causing chloride influx, cell hyperpolarization, and thus reduced excitability (Zhang et al., 2007a). Light activation of NpHR expressed in hippocampal neurons can suppress epileptiform activity indicating this experimental approach to treating epilepsy therapy has potential (Tønnesen et al., 2009). In theory, one can envision a clinical application of optogenetics whereby NpHR is expressed at the epileptic focus, i.e., in cells which are the source of seizure activity, and light is used to suppress abnormal activity when detected. However, additional research is needed to prove that this technique is safe and would be more effective and cause fewer adverse effects then surgical resection in pharmacoresistant patients.

Stroke

Cerebrovascular disease, or stroke, is the third most common cause of death and is a leading cause of serious long-term disability in adults. A stroke is defined as a loss of blood supply to any region of the brain. The resulting brain injury, including neuronal loss, can affect different areas of the brain resulting in varying degrees of speech, sight, and motor impairments, and changes in cognition, memory, and emotions. Early recovery after stroke is limited and variable. Recovery in some patients may be due to populations of neurons which survive and may

resume functioning, and/or reorganization of brain. In general, rehabilitation af-
ter stroke is limited, resulting in profound emotional and economic consequences,
and therefore research is necessary. Current experimental therapies to enhance
stroke recovery include enhancing the brain plasticity, regenerating or replacing
damaged neural circuitry, and modulating inflammation and angiogenesis (see
Experimental Stroke Therapy, below).

Experimental Stroke Models

There are numerous experimental models of stroke. The method used in this
thesis is middle cerebral artery occlusion (MCAO) which involves the introduc-
tion of a filament into the common carotid artery and extending it to the base of
the middle cerebral artery to block blood flow. In this way, ischemia is induced in
a particular region of the brain. Withdrawal of the filament after two hours or 30
minutes, depending on the requisite severity, allows reperfusion.

Other groups have established embolic models of stroke whereby a small em-
bolus is placed in a specific blood vessel causing ischemia in the desired region of
the brain. A more severe model of stroke is global ischemia. Typically, blood flow
is irreversibly blocked by ligation of the common carotid artery causing ischemia
to one hemisphere of the brain. This model would be lethal if not for the contra-
lateral carotid artery which provides below normal perfusion.

Stroke and Endogenous Repair

An exciting discovery in the fields of neurogenesis and stem cell biology was
that after MCAO, an animal model of stroke (see Experimental Stroke Models,
above), there is enhanced endogenous neurogenesis which may have the poten-
tial for brain repair. SVZ-derived, DCX-expressing neuroblasts migrate through
the penumbra into the ischemic core where they differentiate towards the phe-
notype of neurons destroyed by the lesion (Arvidsson et al., 2002) (Figure 4). The
penumbra is characterized by transient hypoxia and minor cell death, while the
ischemic core is characterized by extensive cell death i.e., necrosis, and glial scar
formation. After MCAO, changes in cell cycle length lead to increased numbers
of SVZ NSCs (Zhang et al., 2006; Zhang et al., 2007b). There is also evidence that
ependymal cells transform into NSCs after MCAO, thus contributing to endog-
enous neurogenesis (Zhang et al., 2007; Carlén et al., 2009). Stroke-induced neu-
rogenesis is extensive and long-lasting (Thored et al., 2006). Neuroblast migration
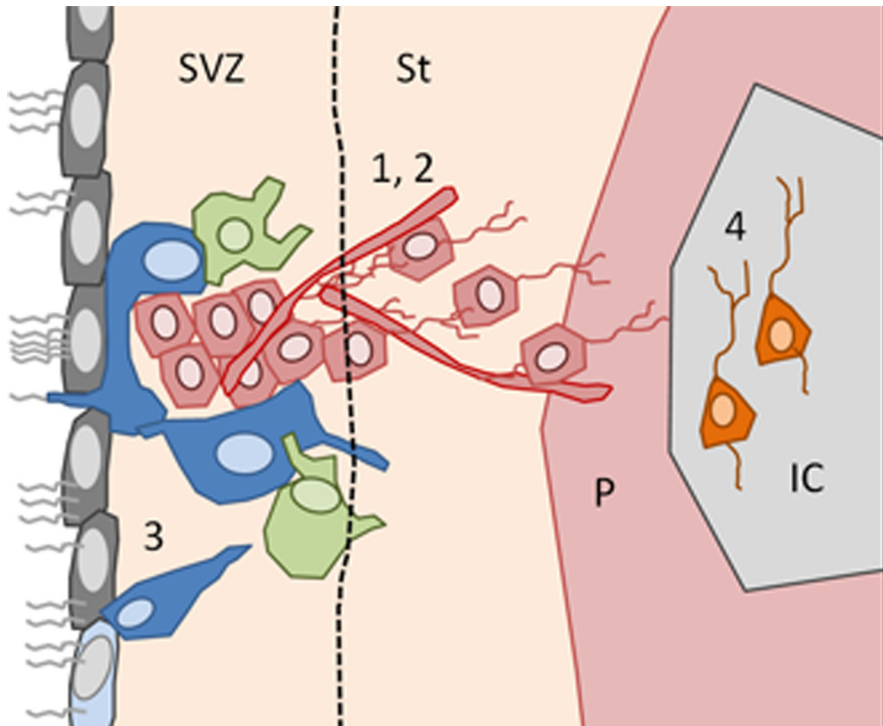
Figure 4. Schematic of endogenous SVZ neurogenesis after MCAO.
 1, 2, SVZ NSCs give rise to neuroblasts which migrate along blood vessels into the striatum (St), through the penumbra (P), and into the ischemic core (IC). 3, Ependymal cells can become NSCs after MCAO, thus contributing to the neurogenic response. 4, SVZ-derived neuroblasts differentiate in the ischemic core and possibly become functional neurons.

towards the ischemic core is attributable to chemotaxis mediated by stromal cell-derived factor-1 (SDF-1)/CXCR4 signaling (Thored et al., 2006), which has been shown to be regulated by hypoxic gradients and hypoxia-inducible factor-1 (HIF-1) (Ceradini et al., 2004). The neuroblasts migrate towards the damaged striatum in association with blood vessels, which likely provide trophic or mechanical support (Thored et al., 2007). There is evidence SVZ-derived neuroblasts develop into functional neurons (Hou et al., 2008; Lai et al., 2008). There is also evidence of an endogenous neurogenic response in human patients with cerebrovascular disease (Minger et al., 2007; Sgubin et al., 2007). Thus, enhancing endogenous neurogenesis in stroke survivors could provide a means of regenerating damaged brain tissue, perhaps improving stroke rehabilitation. However, further research is needed to find ways to overcome obstacles of brain repair.

Experimental Cell Replacement Therapy

The challenges and potential benefits of brain repair are discussed here:

Fibroblast Reprogramming

Research over the past decades has demonstrated that cell replacement therapy can have beneficial results in patients, particularly with Parkinson's disease (Lindvall et al., 1994b; Piccini et al., 1999). Finding the optimal cell source for transplantation remains a key issue. There are currently several methods of generating neuronal cell types with the potential for cell transplantation (Figure 5). Stem cells can be used to generate neurons (reviewed by Svendson et al., 2001). However, since stem cells have the ability to self-renew, the risk of uncontrolled cell cycling and tumor formation is high and thus limits their therapeutic potential. Furthermore, stem cells may be difficult or impossible to obtain from adult patients, reducing the likelihood of patient-specific transplantations and therefore necessitating ongoing immunosuppressant therapy.

More recently, induced pluripotent stem (iPS) cells have received much attention, also in this thesis, for their potential to generate patient-specific cells. These cells are derived from somatic cells and can be converted to a pluripotent cell using transcription factors (Takahashi and Yamanaka, 2006). Remarkably these cells can contribute to the germline and generate live chimeras demonstrating their close resemblance to actual embryonic stem cells (Okita et al., 2007; Wernig et al., 2007). We have shown in Paper 6, (Oki et al.) that iPS cells derived from human fibroblasts develop into functional neurons when transplanted into the rodent brain. Patient-derived cells may be the ideal candidate for transplantation as this overcomes the risk of graft rejection by the host.

Another remarkable breakthrough has occurred with the discovery that fibroblasts can be directly converted to functional neurons, termed induced neurons (iNs) (Vierbuchen et al., 2010; Pfisterer et al., 2011a; Pang et al., 2011; Caiazzo et al., 2011; Qiang et al., 2011; Pfisterer et al., 2011b and Paper 5). Conversion occurs by over-expressing specific transcription factors (via a viral vector) in fully differentiated fibroblasts which alters gene expression and 'reprograms' the cells identity. In this way, these cells bypass the pluripotent stage of iPS cells and thus may impose a lower risk of uncontrolled cell cycling and tumor growth. Furthermore, we here, and others have shown that human fibroblasts can be converted to dopaminergic iNs using viral overexpression of additional specific transcription factors (Pfisterer et al., 2011a; Caiazzo et al., 2011). More recently, fibroblasts taken
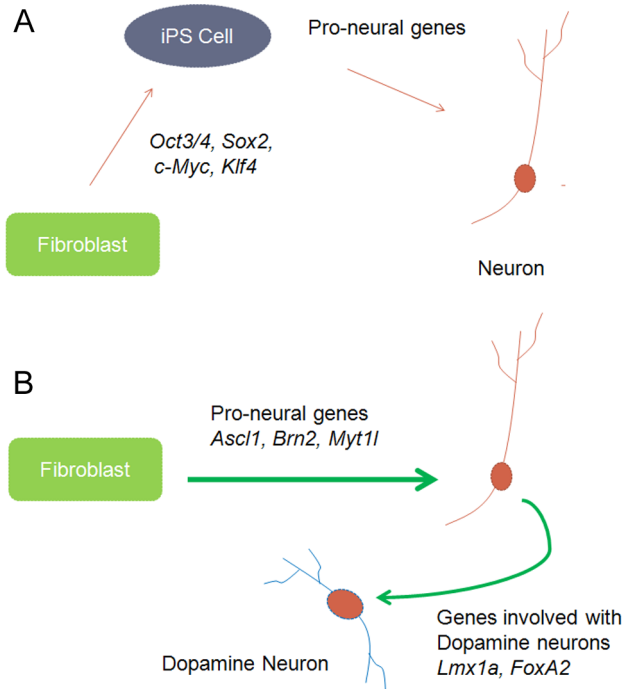
Figure 5. Neurons can be generated via a pluripotent stage or directly.
(A) Fibroblasts can be first reprogrammed to embryonic stem cell-like iPS cells using transcription factors and then directed to neurons, or (B) can be directly converted to neurons by overexpression of a different combination of factors.

from Alzheimer's patients have been directly converted to iNs using a different combination of transcription factors (Qiang et al., 2011). This study indicates that direct conversion may have a potential diagnostic value and can be used for disease-modeling. Future experiments should address whether these cells can be transplanted into an adult mammalian brain and not only maintain their neuronal properties, but also integrate with the preexisting neural circuitry. The rapid developments in the field of reprogramming differentiated cells for the generation of novel neurons will hopefully pave the way for patient-specific cures in the future.

Cell Transplantation after Stroke

Cell transplantation has been used in an attempt to replace damaged or dead cells in experimental animal models of stroke. Human fetal cortical and striatal neural stem cells have the potential to differentiate into neurons when transplanted into the rat striatum (Kallur et al., 2006). When transplanted into the stroke damaged striatum, these cells have been shown to express factors characteristic of striatal neurons (Darsalia et al., 2007). Mouse-derived embryonic stem cells transplanted into the rat stroke damaged brain have been shown to develop electrophysiological properties of neurons, suggesting transplanted cells have the potential to become functional (Bühnemann et al., 2006). Median ganglionic eminence cells derived from embryonic rats have been transplanted into the stroke damaged rodent brain. Four weeks after transplantation, these cells differentiate into cells with neuronal characteristics, develop synapses with host cells, and receive spontaneous excitatory input (Daadi et al., 2009). Transplanted human fibroblast-derived iPS cells exhibit immunohistochemical markers characteristic of neurons, establish axonal connections with distant brain regions and improve functional recovery in mice after stroke (Oki et al., Paper 6).

A multitude of diverse cell transplantation experiments have been conducted in the rodent stroke damaged brain, many of which have resulted in improved functional recovery (Bliss et al., 2007). Although this is a positive result, the mechanism behind the recovery is largely unknown. There is currently very little evidence that observed recovery is due to integration of the graft and renewal of the lost neural circuitry, which may be the ultimate goal of a cell-based stroke therapy. The implanted cells are believed to elicit functional improvement by either providing trophic support to damaged and dying cells, or by modulating the inflammatory response in the host brain (Lindvall and Kokaia, 2010).

Together, these studies show that cell transplantation has the potential to repair the stroke-damaged brain. However, more research is needed to optimize cell transplantation, and complications such as, tumor formation and graft rejection must be addressed before clinical studies can be conducted (Lindvall and Kokaia, 2006, 2010).

Enhancing Angiogenesis and Neurogenesis

Angiogenesis is an important factor in brain repair as new vessels are needed to nourish cells as they enter the damaged regions. There are several studies which report vascular changes associated with enhanced neurogenesis and re-

covery. For example, Erythropoietin and Atorvastatin treatment after stroke in rodents has been shown to enhance angiogenesis and neurogenesis with a concomitant increase of VEGF and BDNF expression at the ischemic border (Wang et al., 2004; Chen et al., 2005). These studies also report improved motor recovery in treated rodents. There is also evidence that SVZ-derived neuroblasts require blood vessels for mechanical or trophic support as they migrate towards the damaged region (Thored et al., 2007; Kojima et al., 2010).

Overcoming the Glial Scar

A challenge of repairing the central nervous system (CNS) after injury is overcoming the formation of a glial scar (Silver and Miller, 2004). After brain injury, astrocytes become hypertrophic and express higher levels of intermediate filaments, including, glial fibrillary acidic protein (GFAP), creating a web of astroglia and connective tissue elements such as proteoglycans. The glial scar creates a physical barrier blocking neurite outgrowth and axon extension, and also contains growth-inhibiting molecules such as chondroitin sulfate proteoglycans (CSPGs), degenerating myelin, and the neurite outgrowth-inhibitor, Nogo-A (Schwab, 2002; Filbin, 2003). However, the glial scar does perform an important protective role after brain injury. In a model of spinal cord injury, preventing glial scar formation by depletion of reactive astrocytes leads to disruption of the blood brain barrier (BBB), leukocyte infiltration, and more severe cell death (Faulkner et al., 2004). Thus, when considering methods of improving recovery, the key is to optimize the benefits and minimize the limitations of the glial scar (for detailed review, see Rolls et al., 2009).

Methods to neutralize the growth-inhibiting properties of the glial scar have been investigated, such as specifically blocking Nogo-A, after MCAO (Wiessner et al., 2003; Cheatwood et al., 2008). Digesting CSPGs by administration of the enzyme chondroitinase (chABC) has been shown to enhance regeneration and plasticity in various experimental models (Pizzorusso et al., 2002; Massey et al., 2006; García-Alías et al., 2009, Wang et al., 2011). When considering cell replacement therapy, for instance in spinal cord injury or stroke patients, it may also be worth considering ways to concomitantly provide a neuron-receptive environment by altering the properties of the glial scar.

Inflammation, Microglia, and Neurogenesis

Pathological brain insults, including severe seizures and stroke, induce an inflammatory response. A major player in brain inflammation is the resident microglia. These cells are believed to act as 'sensors' in the brain which can detect and react to homeostatic and pathological changes (Kreutzberg, 1996; Hanisch and Kettenmann, 2007). In response to inflammation, microglia shift activation states and can mediate inflammation by secreting a wide-array of pro- and anti-inflammatory cytokines (Minghetti and Levi, 1998). For example, in response to bacterial invasion, microglia release pro-inflammatory cytokines such as tumor necrosis factor-alpha (TNF-α) and interleukin-6 (IL-6) (Hanisch et al., 2001). In contrast, microglia secrete anti-inflammatory factors such as interleukin-10 (IL-10) when phagocytosing apoptotic cells (Magnus et al., 2001).

Severe brain inflammation, induced by the bacterial endotoxin, lipopolysaccharide (LPS) injection or radiation exposure, causes microglia to shift into a highly activated state which is detrimental to hippocampal neurogenesis (Ekdahl et al., 2003; Monje et al., 2003). In these experimental models, inhibiting the inflammatory response restores hippocampal neurogenesis. LPS-induced chronic inflammation leads to changes in the afferent inputs and expression of gephyrin, a GABA-related scaffolding protein, in adult born DGCs (Jakubs et al., 2008). Stroke-induced neurogenesis may be suppressed by microglia production of TNF- α, which has been shown to suppress NSC proliferation (Iosif et al., 2008). However, microglia are complex cells, and may not always have a negative effect on neurogenesis. For example, cytokines secreted by T-helper cells cause microglia to express insulin-like growth factor-1 (IGF-1) which is beneficial to neurogenesis (Butovsky et al., 2006). Furthermore, after stroke, microglia accumulate in the SVZ and express IGF-1, indicating they can modulate apoptosis, proliferation and differentiation of NSCs (Thored et al., 2009). This has led to the notion that whether microglia exert a positive or negative effect on neurogenesis depends on the balance between pro- and anti-inflammatory signals (Ekdahl et al., 2009). Thus, modulating the microglial response after seizures or stroke could potentially be used for altering endogenous neurogenesis, and perhaps have the potential to improve recovery.

AIMS OF THIS THESIS

1. Investigate how neural stem cell-derived neurons migrate and integrate in the pathological brain *(Papers 1 and 2)*

> To characterize the distribution of hypoxia during 2h MCAO, measure changes in vasculature, and investigate how the new neurons migrate

> To investigate how an epileptic insult resulting in development of hyperexcitability but only minor inflammatory changes influences the development and functional integration of new born cells

2. Characterize the integration and function of fibroblast-derived neurons *(Papers 3 to 6)*

> To investigate the electrophysiological characteristics of fibroblast-derived iNs and dopaminergic iNs

> To investigate how the functional properties of iNs are influenced by replacing *Ascl1* with *Neurogenin2*

> To determine whether neural-committed iPS cells transplanted into the adult mammalian brain become functionally integrated neurons

SUMMARY OF PAPERS

Paper 1: Long-term neuroblast migration along blood vessels in an area with transient angiogenesis and increased vascularization after stroke

Background and Rationale

Stroke induced by 2h MCAO in rats causes increased SVZ NSC proliferation. Newly formed DCX-expressing cells normally migrate to the olfactory bulb, but after stroke migrate towards the damaged region. Once there, the new cells express immunohistochemical markers specific for medium spiny neurons e.g., Meis2, DARP-32, which are the cell type primarily affected by MCAO (Arvidsson et al., 2002). These results suggest that new neurons generated from the SVZ may have the potential for brain repair. The mechanisms underlying this phenomenon are largely unknown. In Paper 1 we investigated whether MCAO leads to hypoxia in the SVZ, changes in vessel density, and angiogenesis in the ipsilateral SVZ and adjacent striatum and investigated the relationship between migrating neuroblasts and the vasculature.

Results

Hypoxyprobe-1 immunoreactivity demonstrated that 2hr MCAO caused transient hypoxia in the ipsilateral SVZ and striatum (hypoxia was not present 6 weeks after MCAO). Within the SVZ, hypoxia was more pronounced in the caudal than rostral sections. Hypoxia was present throughout the SVZ in the most ventral-caudal sections, while only penetrating a few cell layers in the more dorsal-rostral sections. Hypoxia in the striatum overlapped with the regions where cell death occurred as demonstrated by the loss of NeuN-expressing cells and immunoreactivity of fluoro-jade (a marker of cell death).

The volume of the SVZ was increased 2, 6 and 16 weeks after MCAO compared to sham operated animals. This increase in volume resulted in decreased vessel density at 2 and 6 weeks after MCAO but returned to baseline levels at 16 weeks. This observation coincided with gradual increase of vessel length which took place between 2 and 16 weeks after MCAO. Using triple-labeling (BrdU, RECA, and Laminin) we determined that low levels of angiogenesis was taking place within the SVZ during the first 2 weeks after MCAO. In the adjacent

striatum, in the region where neuroblast migration primarily occurs (zone 1a), blood vessel density and length gradually increased between 2 and 16 weeks after MCAO. Triple-labeling again demonstrated that angiogenesis was taking place in this region within the first 2 weeks after MCAO.

We observed that the new neurons migrated in clusters in close proximity to blood vessels. To determine whether an association between blood vessels and migrating neuroblasts existed, we measured the distance between migrating neuroblasts and the nearest blood vessel. Using this method of quantification, we demonstrated that the majority of neuroblasts (~85%) were within 15 μm of a blood vessel.

Discussion

In this study we demonstrated that 2h MCAO induces hypoxia throughout the brain regions associated with the neurogenic response: the striatum and SVZ. Vascular reorganization and angiogenesis was present in this region and the new neurons migrated in close proximity to blood vessels.

We reported that low levels of angiogenesis occurred in the SVZ after MCAO which was at the time unexpected since in the SGZ neurogenesis and angiogenesis are linked (Palmer et al., 2000). Furthermore, Gotts and Chesselet (2005) reported that a robust angiogenic response was present in the SVZ after stroke. What we did observe was a close association between the migrating neuroblasts and the vasculature. Consistent with our results, ongoing angiogenesis has not been detected in the SVZ but the vasculature provides the SVZ with important signaling cues (Shen et al., 2008; Tavazoie et al., 2008). Notably, recent studies have demonstrated that neurons use the vasculature as scaffolding while migrating in the RMS (Snapyan et al., 2009) and towards the stroke-damaged striatum (Kojima et al., 2010).

Paper 2: Functional integration of new hippocampal neurons in adult epileptic brain is determined by characteristics of pathological environment

Background and Rationale

How new neurons develop in the pathological adult brain will determine whether they counteract or contribute to pathology. We have previously shown that after severe insults (status epilepticus and chronic inflammation) the new neurons may counteract the pathology. New neurons born into the epileptic brain, characterized by recurrent seizures, cell death and inflammation, exhibit reduced excitatory input, and enhanced inhibitory input at their afferent synapses (Jakubs et al., 2006). Born into an environment characterized by chronic inflammation, new neurons exhibit increased excitatory input but also enhanced inhibitory input. Here we have studied the morphological development and electrophysiological integration of new neurons born into a less severe pathological environment characterized by recurrent stimulation-induced seizures, gradual development of hyperexcitability, but only minor transient changes in inflammation.

Results

In order to answer our primary question we needed to establish a kindling protocol which would be characterized by recurrent seizures, gradual development of hyperexcitability, but little or no inflammatory changes. Based on previous studies (Elmér et al., 1998), and a pilot study demonstrating that inflammation was influenced by the severity and frequency of seizures, rapid kindling with subsequent stimulation induced seizures was used. The inflammatory response to the seizure paradigm used was investigated 1 and 7 weeks after rapid kindling. At 1 week after rapid kindling there tended to be more activated microglia (Iba1+/ED1+) present in the hippocampus compared to sham animals, however the increase was much lower than the increase observed in SE animals. The phenotype of the microglia indicated that they were not in a highly activated state. Consistent with the notion that the seizure paradigm resulted in only minor inflammatory changes, cytokines associated with inflammation were not elevated in seizure-exposed compared to sham animals 1 week after rapid kindling. At 7 weeks after rapid kindling there was no difference in the number of activated microglia between the groups. Taken together, these results demonstrate that the seizure paradigm used caused only minor inflammatory changes compared to

those induced by SE or chronic inflammation. The development of hyperexcitability was apparent by the increase in mean seizure grade and the decrease in seizure threshold measured over the course of 6-8 weeks of twice weekly stimulation-induced seizures.

Morphological analysis of GFP+ neurons at 6-8 weeks after labeling demonstrated that the seizure paradigm used here did not cause any major changes in gross morphology. No differences were detected in the location or orientation of GFP+ cells, the structure of the dendrites, or the pattern of gephyrin expression. However, using confocal imaging techniques an increase in the proportion of stubby spines was detected.

Electrophysiological analysis performed 6-8 weeks after virus labeling demonstrated that GFP+ cells born into the pathological environment had similar passive and active membrane properties compared to both mature DGCs and GFP+ cells in sham animals. However, the seizure-exposed new cells exhibited increased rheobase (the amount of current required to depolarize the membrane to action potential threshold) and fired fewer action potentials in response to depolarizing current injection. Whole-cell, voltage clamp recordings demonstrated that seizure-exposed new cells received enhanced excitatory input evidenced by the occurrence of miniature excitatory postsynaptic currents (mEPSCs) of larger amplitude and faster rise time. Furthermore, mEPSCs occurred with shorter inter-event-intervals in seizure-exposed new cells compared to control new cells. Taken together, these results demonstrate a net increase of excitatory afferent input to seizure-exposed new cells. Whole-cell, voltage clamp recordings of miniature inhibitory postsynaptic currents (mIPSCs) demonstrated that seizure-exposed new cells received reduced inhibitory input compared to control new cells. mIPSCs occurred at longer IEIs, and exhibited slower rise times likely indicating a reduction in perisomatic inhibition. Taken together, the electrophysiological analysis suggests that seizure-exposed new cells experience a net increase in excitatory input (larger amplitude of excitatory currents and reduced inhibition). However, increased rheobase in these cells may partially or completely counteract the enhanced synaptic excitability.

The conclusions of this study are two-fold: firstly, that new cells born into a pathological environment characterized by recurring seizures and the gradual development of hyperexcitability but without a major inflammatory response receive enhanced excitatory input likely counteracted by reduced intrinsic excitability; and secondly that, taken together with our previous studies (Jakubs et

al., 2006; 2008), the functional integration of new neurons, and whether they will contribute or counteract pathology, will depend on the characteristics of the pathological environment.

Discussion

In this study we show that new neurons born into an environment characterized by repeated seizures, the gradual development of hyperexcitability, but only minor transient inflammatory changes exhibit conserved gross morphology, altered synapse development, enhanced excitatory input, and reduced intrinsic excitability.

The finding that the new neurons exhibit increased excitatory input is consistent with results from experiments investigating the excitatory input to mature DGCs in animal models of epilepsy (Simmons et al., 1997; Wuarin and Dudek, 2001). However, it is the opposite of what was observed by Jakubs et al. (2006), whereby new born DGCs received reduced excitatory input and enhanced inhibition. It must be emphasized that the seizure models used in these two studies differed greatly. In the Jakubs et al. (2006) study, rats were subjected to SE i.e., 3 hours of seizure activity resulting in neuronal death, spontaneous seizures and widespread inflammatory changes. The seizure model used in the present was comparably mild resulting in a total of ~ 30 minutes of seizures and only a minor and transient inflammatory response. The differences observed indicate that the characteristics of the pathological environment will influence functional integration. Interestingly, adaptation to the pathological environment was seen in both studies. Jakubs et al. (2006) reported reduced excitability and enhanced inhibition. In the present study, we detected enhanced excitatory input but a concomitant reduction of intrinsic excitability, whereby the amount of current required to generate action potentials was greater in the new seizure-exposed cells. This finding suggests that the new cells may have a mechanism to prevent the propagation of the increased excitability. Whether or not adult born cells contribute to or counteract pathological brain states will depend on how they interact with their targets. In the future it would be very interesting to investigate what proportion of excitatory synaptic input is propagated by the new cells in various seizure models.

Paper 3: Direct conversion of human fibroblasts to dopamingergic neurons

Background and Rationale

Lineage reprogramming is the process whereby a fully differentiated cell is converted to a different cell type without passing through a pluripotent stem cell-like stage. This technique may be a valuable tool for disease-modeling and cell replacement therapy. Vierbuchen et al. (2010) were the first to demonstrate that mouse fibroblasts can be directly converted to functional neurons (termed induced neurons; iNs) by viral overexpression of 3 transcription factors. Of particular interest is whether this technique could also be used with human fibroblasts. To this end, we here have used human fibroblasts from three sources for direct conversion to neurons (embryonic fibroblasts, fetal lung fibroblasts and postnatal fibroblasts). We show for the first time, that also human fibroblasts can be converted to functional neurons using this technique. We have also shown, for the first time, that the iNs can be further differentiated into specific neuronal subtypes by additional factors.

Results

Fibroblasts from human embryos (HEFs), fetal lung fibroblasts (HFLs), and postnatal fibroblasts were used in conversions. A lentivirus was used to deliver the transcription factors Ascl1, Brn2, Myt1l (ABM). By 12 days after transduction, many cells exhibited neuronal morphology and expressed immunohistochemical markers characteristic of neurons i.e., MAP2 and βIII-tubulin. Whole-cell patch clamp recordings demonstrated that the majority of cells with neuronal morphology had properties of mature functional neurons (termed induced-neurons, iNs). Action potentials and whole-cell currents were readily induced by depolarizing the membrane potential.

Parkinson's disease involves the selective loss of the dopamine system and therefore is a neurodegenerative disorder that may benefit from transplantation. We thus focused our efforts on transforming the fibroblast-derived neurons to dopamine neurons. 10 genes were selected for overexpression in HEFs and HFLs based on their role in midbrain development. By 24 days after conversion, a proportion of iNs expressed tyrosine hydroxylase (TH), a marker characteristic of dopaminergic neurons due to its role in the synthesis of dopamine. We found that using two genes, Lmx1a and FoxA2 together with the 3 transcription factors

(ABM) was sufficient to convert HEFs to TH-expressing cells. Furthermore, a proportion of iNs expressed another enzyme involved with dopamine synthesis; aromatic L-amino acid decarboxylase. Electrophysiological recordings demonstrated that the majority of iNs converted using these 5 genes were functionally mature neurons and that a proportion exhibited characteristics similar to dopaminergic neurons, i.e., spontaneous pacemaker action potentials, rebound action potentials, and comparable passive membrane properties.

Discussion

This was the first study to demonstrate that human fibroblasts can be reprogrammed to neurons using the same technique used for reprogramming mouse fibroblasts (Wernig et al., 2010). This was also the first study to show that iNs can be further reprogrammed to subtype specific neurons, in this case dopaminergic neurons. These breakthroughs are an important step on the path towards patient-specific neural cell replacement therapies.

Patients with Parkinson's disease can benefit from cell transplantations (Piccini et al., 1999; Lindvall and Björklund, 2011) and thus a patient-specific source of dopaminergic neurons may be very valuable. We generated dopaminergic neurons by using additional transcription factors associated with dopaminergic neuron development. Two lines of evidence show that dopaminergic neurons were generated. Firstly, patterned cells expressed tyrosine hydroxylase and aromatic-L-amino acid decarboxylase which are enzymes crucial to the synthesis of dopamine. Secondly, whole-cell patch clamp recordings demonstrated that the patterned iNs had electrophysiological characteristics similar to midbrain dopamine neurons. A proportion of cells exhibited spontaneous pace-maker like action potentials and rebound action potentials which are both characteristic of dopaminergic neurons. iNs also exhibited comparable active and passive membrane properties of dopaminergic neurons such as input resistance and action potential amplitude and duration.

The generation of neurons from fibroblasts may be a valuable tool for studying the pathogenesis of neurological disorders and also provide a source of patient-specific neurons for transplantation.

Paper 4: Efficient induction of functional neurons from adult human fibroblasts

Background and Rationale

We have previously shown that human embryonic, fetal, and postnatal fibroblasts can be reprogrammed to mature functional neurons; induced neurons (Pfisterer et al., 2011a). If one envisages iNs being used for disease-modeling or transplantation it is crucial to determine whether also fibroblasts taken from adults have the potential to become functional neurons. To this end, we obtained human lung fibroblasts taken for biopsy from adult and elderly patients to determine whether they could be reprogrammed to iNs using the same technique used in Paper 3.

Results

Immunohistochemistry and quantitative reverse transcriptase PCR confirmed the fibroblast identity of the lung fibroblasts used for conversions. Similar to our previous study (Pfisterer et al., 2011a), 3-4 days after viral delivery of the conversion factors ABM the lung fibroblasts displayed an elongated neuron-like morphology. Immunohistochemistry demonstrated that at 12 and 20 days after transduction the cells exhibited the neuronal markers MAP2 and βIII-tubulin. Fibroblasts from a total of six individuals were used for conversion and in all cases overexpression of ABM led to the generation of iNs at a comparable efficiency as we have previously described (Pfisterer et al., 2011a) indicating that the age of the individual does not influence conversion efficiency. To determine whether the iNs were functional, whole-cell patch clamp recordings were performed on iNs generated from three of the six individuals. Action potentials and whole-cell currents characteristic of fast inactivating inward sodium and outward voltage-activated potassium currents were observed. Biocytin labeling confirmed the neuronal morphology of the recorded cells.

Taken together, these results demonstrate that also lung fibroblasts taken from adult and elderly individuals have the capacity to be converted to functional iNs. Furthermore, the iNs were generated with a similar conversion efficiency and timing as when using embryonic fibroblasts, showing this technique has potential for disease-modeling and possibly patient-derived transplantations in the future.

Discussion

We report here that lung fibroblasts taken from adult and elderly individuals can be readily reprogrammed to iNs using defined sets of transcription factors as previously reported (Wernig et al., 2010; Pfisterer et al., 2011a). Remarkably, lung fibroblasts converted at similar efficiency and time course regardless of the age of donor.

Previously, we generated iNs from fetal and post-natal derived fibroblasts (Pfisterer et al., 2011A). This study shows that it is possible to take fibroblasts from adults and convert them to neurons. Therefore by using this technique one could study the iNs of patients with neurological disorders for disease progression or drug screening and maybe one day for autologous transplantation.

Paper 5: Replacing Mash1 with Ngn2 during neural conversion of human fibroblasts influences phenotype and electrophysiological properties of generated neurons

Background and Rationale

Fibroblasts can be converted to functional neurons, termed iNs by overexpression of specific sets of transcription factors (Vierbuchen et al., 2011; Pfisterer et al., 2011a, Pang et al., 2011, Caiazzo et al., 2011; , Qiang et al., 2011; Pfisterer et al., 2011b). Dopaminergic neurons (Pfisterer et al., 2011a; Caiazzo et al., 2011), glutamatergic neurons (Qiang et al., 2011) and motor neurons (Son et al., 2011) can be generated using different combinations of transcription factors. These latter studies demonstrate that the factors used for conversion influence the characteristics of the neurons generated and will thus determine their suitability for disease-modeling or cell replacement therapy. These studies all used the proneural gene Ascl1 (referred to as Mash1) for neural conversion. We have investigated here whether replacing Mash1 (which is associated with the development of GABAergic neurons) with the proneural gene Ngn2 (which is associated with the development of glutamatergic neurons) influences the phenotype and electrophysiological properties of neurons generated from human fibroblasts.

Results

When using Ngn2 in combination with Brn2 and Myt1l, we found that iN cells started to appear in the same time frame as we have previously reported using Ascl1, Brn2, Myt1l (ABM) (Pfisterer et al., 2011a; 2011b). 30 days after viral transduction, βIII-tubulin expressing cells with neuronal morphology were present in cultures of fibroblasts converted with Ngn2, Brn2, Myt1l (NBM). To determine whether using NBM instead of ABM resulted in differences in conversion efficiency, we examined NBM and ABM derived iNs 40 days after transduction. Quantification using Cellomics showed that conversion efficiency using NBM was comparable to that when using ABM. Total neurite length of iNs generated using NBM was similar to neurite length of iNs generated using ABM.

Mash1 directs GABAergic neuronal differentiation during development while Ngn2 primarily directs cells towards a glutamatergic phenotype. To determine whether the fibroblast-derived neurons were GABAergic, immunohistochemistry was performed at day 40 in vitro. In line with their respective roles

in development, while ~13% of ABM converted fibroblasts expressed GABA, no cells converted with NBM exhibited a GABAergic phenotype.

In order to directly compare the functional characteristics of NBM and ABM derived iNs, identical whole cell recordings were performed on a number of cells from each conversion setup. Action potentials were induced by a single depolarizing current injection step and whole-cell currents characteristic of sodium and potassium currents were induced by step depolarization of the membrane potential. Although both Mash1 and Ngn2, when over-expressed in combination with BM, resulted in the generation of functional neurons, differences in the passive and active membrane properties were detected.

Taken together, these results show that overexpression of NBM and ABM lead to the generation of iNs. We also report that the functional properties and phenotype of the generated iNs differ depending on the proneural gene overexpressed. This study presents another combination of genes capable of transforming fibroblasts to functional neurons.

Discussion

In the present study we demonstrate that replacing Mash1 overexpression with Ngn2 leads to the formation of mature neurons. In line with previous studies, Mash1 overexpression led to the generation of GABAergic cells, while Ngn2 did not (Berninger et al., 2007; Heinrich et al., 2011). Electrophysiological recordings demonstrated differences in the passive and active membrane properties of the iNs generated. Differences in membrane properties of iNs have also been reported when fetal (Caiazzo et al., 2011) or post-natal fibroblasts (Ambasudhan et al., 2011) were used instead of adult-derived fibroblasts. Interestingly, iPS-derived neurons generated from patients with schizophrenia exhibit similar electrophysiological properties to those generated from healthy individuals but altered gene expression (Brennand et al., 2011). Taken together, these observations indicate that the genes used for conversion in combination with the starting material will influence the functional and morphological properties of iNs.

We have shown for the first time that viral overexpression of Ngn2, Brn2 and Myt1l in fibroblasts leads to the formation of iNs and report that they exhibit different characteristics from iNs generated using ABM. It remains unclear how each transcription factor influences the properties of the iNs generated, however this is an important issue when considering using iNs for disease-modeling, drug

screening, and also transplantation. It is important that the iNs generated mirror as closely as possible the relevant cell type.

Paper 6: Human induced pluripotent stem cells form functionally integrated neurons and improve recovery after transplantation in stroke-damaged rodent brain

Background and Rationale

Ischemic stroke causes death of brain cells in the affected regions. To date, recovery after stroke is limited and thus cell replacement therapies have been considered. Human fetal cortical and striatal neural stem cells have the potential to differentiate into striatal neurons when transplanted into the rat striatum (Kallur et al., 2006; Darsalia et al., 2007). Embryonic stem cells from rodents transplanted into the rat stroke damaged brain have been shown to develop electrophysiological properties of neurons (Bühnemann et al., 2006; Daadi et al., 2009). Many cell replacement therapies have yielded functional improvement in rodents (see Bliss et al., 2007).

Ideally, cells for transplantation should come from the patient themselves to avoid graft rejections or long-term immunosuppression. Induced pluripotent (iPS) cells are somatic cells which can be derived from an individual and reprogrammed to various fates (Takahashi and Yamanaka, 2006; Wernig et al., 2007; Wernig et al., 2008; Dimos et al., 2008). In the present study we have transplanted human-derived iPS cells into the healthy and stroke-damaged rodent brain. We demonstrate that these iPS cells differentiate into neurons, improve recovery after stroke, extend processes to long-range targets in the brain and exhibit the functional properties of mature, synaptically integrated neurons.

Results

iPS cells were generated from human dermal fibroblasts by overexpression of Oct4, Sox2, Klf4, and c-Myc and were indistinguishable from human embryonic stem cells, as previously described (Koch et al., 2009). Withdrawal of growth factors during culturing led to the differentiation of βIII-tubulin-expressing cells demonstrating the neuronal potential of the iPS cells.

Mice subjected to middle cerebral artery occlusion (MCAO) were transplanted with iPS cells 1 week after stroke into the damaged brain region. Interestingly, already 1 week and up to 9 weeks after transplantation mice transplanted with iPS cells exhibited improved performance on the staircase test (which measures fine and coordinated forelimb movement) compared to vehicle-transplanted

mice. Conversely, mice transplanted with iPS cells and vehicle did not show any behavioral improvement after MCAO when challenged with the corridor test which analyzes paired lateralized sensorimotor integration (neglect).

We next examined the immunohistochemical properties of the transplanted iPS cells. Ten weeks after transplantation, ~80% of the iPS cells expressed HuNu (a human-specific antibody) and HuD (a marker for young and mature neurons) indicating that the majority of transplanted iPS cells became neurons. We next used a retrograde tracer, fluoro-gold to determine the axonal outgrowth of the transplanted iPS cells. Remarkably, when fluoro-gold was injected in the globus pallidus iPS cells grafted in the striatum became immunoreactive for fluoro-gold indicating the iPS cells establish long-range connections.

We next sought to perform long-term experiments to follow the path of iPS cell differentiation after MCAO. To this end, T-cell deficient, so called nude-rats (to avoid requiring immunosuppression), were transplanted with iPS cells 2 days after MCAO. Two and four months after transplantation over 65% of grafted iPS cells exhibited the neuronal marker NeuN indicating that the iPS cells survive in the MCAO damaged brain and undergo neuronal differentiation, similar to what we observed in the mouse brain at earlier time-points. Many of the transplanted iPS cells also exhibited markers of neuronal subtypes such as GABA and parvalbumin (markers associated with GABAergic interneurons) and DARP-32 (marker of medium-spiny projection neurons).

Finally, we performed a separate set of experiments designed to investigate the electrophysiological characteristics of the transplanted iPS cells. Whole-cell patch-clamp recordings were performed on iPS cells grafted in either the cortex or the striatum 4.5-5.5 months after transplantation. Transplanted cells in the striatum were classified as either neuronal or glial based on resting membrane potential and input resistance. A proportion of the transplanted iPS cells became mature, functional neurons exhibiting action potentials in response to depolarizing current injection. In voltage-clamp configuration, depolarizing voltage steps induced voltage-activated Na^+ and K^+ currents characteristic of neurons. Spontaneous postsynaptic currents were frequently observed indicating the iPS cells developed functional synapses. Spontaneous excitatory postsynaptic currents (sEPSCs) were recorded in the presence of the $GABA_A$ receptor antagonist, picrotoxin. Addition of glutamate receptor antagonists (NBQX and D-AP5) blocked all postsynaptic currents indicating iPS cells have functional excitatory synapses.

Whole-cell patch clamp recordings demonstrated that also iPS cells transplanted in the cortex became functional neurons and fired action potentials in response to depolarizing current injection. Depolarizing voltage steps induced whole-cell currents characteristic of Na+ and K+ currents. Voltage-clamp recordings demonstrated that spontaneous and miniature (action potential-independent) postsynaptic currents occurred frequently in the transplanted iPS cells. sEPSCs were frequently detected. Interestingly, in 2 of 10 cells, excitatory, AMPA receptor-mediated currents could be evoked by stimulating the cortex at a distance from the transplant, suggesting iPS cells can integrate with the host brain. Taken together, these results demonstrate that transplanted iPS cells become functionally mature neurons.

Discussion

In the present study we have shown that transplanted human iPS cells give rise to neurons in the mammalian brain. Transplantation led to rapid and persistent functional recovery after stroke. At later time-points grafted cells expressed markers of neurons and neuronal subtypes and developed long range processes. We also demonstrate that iPS cells grafted in the cortex and striatum possess the electrophysiological characteristics of mature, functional neurons.

Transplantation after stroke often leads to enhanced recovery at a time-point before the cells would be expected to integrate. Thus the recovery is likely due to neuroprotection, immune modulation or angiogenesis (Lindvall and Kokaia, 2010). Here we have detected improved performance in the staircase test, but not the corridor test after cell transplantation. This is an interesting observation which may be explained by the fact that the staircase test is harder to improvise than the corridor test. Specifically, the staircase test is designed such that pellets placed on the impaired side cannot easily be reached by the intact side, while in the corridor test it is relatively easy to use either paw (Montoya et al., 1991; Dowd et al., 2005).

We also demonstrate that iPS cells express neuronal markers, develop long processes, possess the electrophysiological properties of functional neurons and at least partially integrate with the host brain. These results demonstrate that human iPS cells are capable of becoming neurons when transplanted into the mammalian brain. This is an important step in the process of developing patient-specific transplantations capable of rebuilding the lost neural circuitry.

CONCLUDING REMARKS

In Papers One through Six we have investigated the function and integration of "new" neurons – new neurons born from neural stem cells in the adult brain, and new neurons in the sense that they were generated from fibroblasts.

Papers One and Two focused on the new neurons generated from neural stem cells in the SVZ and SGZ after pathological insults. We investigated how the newly generated neurons migrate and integrate in the brain. These two phenomena, migration and integration are intimately linked. Without the proper migratory cues new cells exhibit ectopic placement and aberrant integration, as observed in the hippocampus after severe epileptic insults.

Papers Three to Six focused on generating (and characterizing) neurons from fibroblasts. First it was crucial to investigate the functional characteristics of the newly generated neurons to demonstrate that they indeed had the properties of mature neurons. The functional properties of the new cells will determine how and importantly if they will integrate in the brain. This is of key importance if we envision using iN or iPS cells for transplantation in the future. In Paper 6 we demonstrate for the first time that transplanted iPS cells survive, migrate beyond the transplantation core, and exhibit the functional properties of mature neurons.

Taken together, this thesis demonstrates that the environment encountered by new neurons will influence their migration and integration. We also demonstrate that human fibroblasts can be reprogrammed to neurons and show that fibroblast-derived neurons can integrate in the mammalian brain. Thus, fibroblasts may be a valuable source of neurons for transplantation but the environment encountered will influence their integration and function which will determine their therapeutic effect.

MATERIALS AND METHODS SUMMARY

General Methods (detailed methods are found in reprints, below)

Middle cerebral artery occlusion (MCAO)

Rats or mice were anesthetized during surgery. The right common carotid (CCA) and its proximal branches were exposed. The CCA and external common carotid artery were ligated and the internal common carotid was temporarily clamped. A small incision was made in the external common carotid and a microfilament was inserted and guided to the middle cerebral artery for occlusion. At the end of occlusion (30 minutes or 2 hours) the filament was withdrawn and the external common carotid artery was permanently ligated.

Immunohistochemistry

Immunohistochemistry (IHC) is a technique commonly used to identify various cell types and extracellular components such as blood vessels. Briefly, primary antibodies recognize and bind to antigens, e.g., proteins, which are often specific to the entity of interest. Secondary antibodies bind to primary antibodies and have some intrinsic property to allow their visualization, such as fluorescence or enzymatic activity, i.e., peroxidase which oxidizes DAB to create a dark brown color. Thus, by sequential exposure of a sample, such as tissue specimens or cell cultures, to primary and secondary antibodies, it is possible to detect antigens-of-interest.

Whole-Cell Patch-Clamp

The best way to study the functional characteristics of a cell is to measure its electrophysiological parameters. Although electrophysiology may seem complicated to those unfamiliar with the field, all aspects of the technique can be explained using Ohm's Law, whereby the voltage (V), current (I), and resistance (R) are related by the equation: $V = IR$. For example, if we wish to measure the resistance of a cell we can induce a voltage change of for example 5 mV, measure the current that travels across the membrane in response, and solve for R (for additional information see Molleman, 1983).

Whole-cell patch-clamp recordings involve an electrode housed in a pipette connected to an amplifier establishing an electrical circuit with a single cell (Figure 6). This is achieved by placing the tip of a recording pipette on the cell mem-
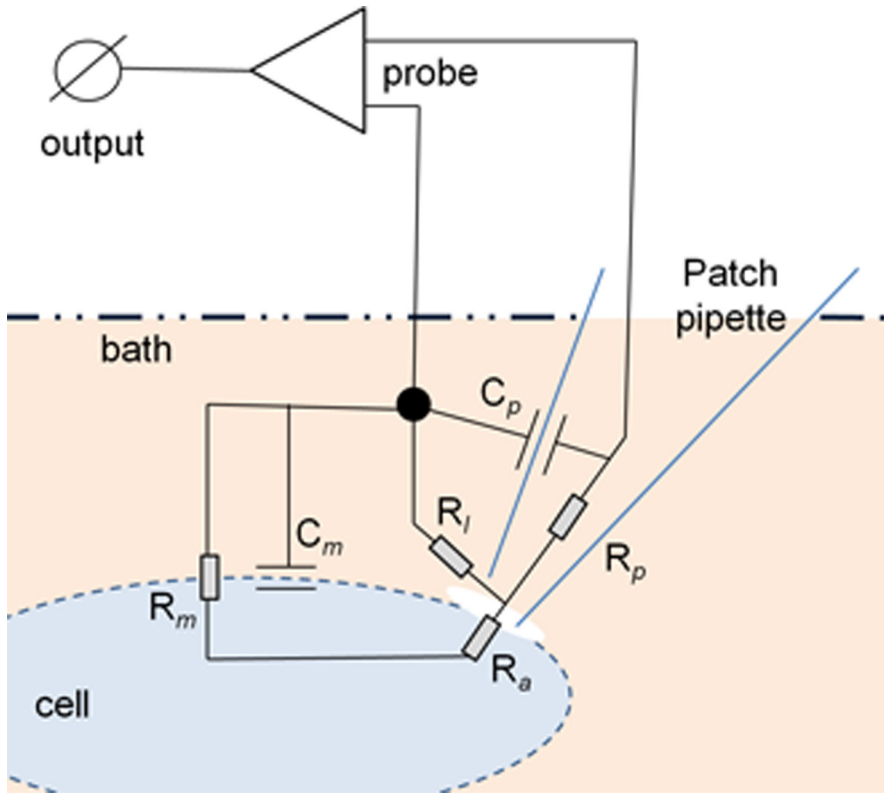
Figure 6. Circuit diagram of whole-cell patch-clamp configuration.
The patch pipette disrupts the cell membrane allowing access to the cell with relatively low access resistance (Ra) compared to the pipette resistance (Rp) and membrane resistance (Rm). The membrane resistance is the largest current-limiting resistor in the circuit so currents through the membrane can be observed. The pipette-membrane interface creates a leak resistance (Rl) which should be very high to prevent short-circuiting. The capacitance of the pipette (Cp) and membrane (Cm) affects the amount of time which elapses before fluctuations in voltage can be observed. The probe within the patch pipette is connected to an amplifier connected to a computer for recording and post hoc analysis. Adapted from Molleman (2003).

brane and applying negative pressure to rupture the membrane. In this way, the pipette has electrical access to the cell which depends on the resistance of the pipette opening, membrane resistance, and leak resistance. Thus, it is possible to manipulate, and/or measure the membrane potential or the current traveling across the cell membrane.

Intrinsic membrane properties of cells include the resting membrane potential (RMP), action potential threshold, and current-voltage relationship. These parameters allow a detailed characterization and identification of cells. In voltage-clamp mode it is possible to hold the membrane potential constant by modulating the 'holding current' across the membrane creating an 'artificial' RMP. Current crossing the membrane (e.g. postsynaptic Na2+, Ca2+, Cl- currents) cause deflections in the holding current and can thus be measured. Conversely, in current-clamp mode it is possible to observe the intrinsic properties of cells by mimicking depolarizing or hyperpolarizing postsynaptic currents by injecting specific quantities of current into the cell and measuring changes in the membrane potential. For example, injecting sufficient depolarizing current into mature neurons will activate voltage-gated sodium channels thus eliciting action potentials. In this way passive and active membrane properties can be studied. For a description of exactly how this technique was used in each paper, see reprints in next section.

Electrophysiology

For acute brain slice preparations, whole brains were placed in cold cutting solution and cut into 225 μm to 300 μm thick slices using a vibratome. Cultured cells or brain slices were constantly perfused with artificial cerebrospinal fluid. Cells for recording were visualized using infrared light with differential interference contrast or fluorescent light using an Olympus upright microscope equipped with a digital camera and a 40X water-immersion lens. Recording pipettes were filled with intracellular solution resulting in pipette resistances of 2–5 MΩ. Intrinsic properties were measured using current- and voltage-clamp experiments. Action potentials were generated by either step or ramp current injection protocols. Whole-cell currents were measured by membrane depolarizations in voltage-clamp. Spontaneous and miniature postsynaptic currents were measured in voltage-clamp mode whereby cells were typically held at a membrane potential of either -70 mV or -80 mV. GABA$_A$ receptors were blocked using Picrotoxin, NMDA receptors were blocked using D-AP5 and AMPA receptors were blocked using NBQX. Action potentials and voltage-gated Na+ currents were blocked using tetrodotoxin. Voltage-activated K+ currents were blocked using tetraethylammonium (TEA). Data were obtained using an EPC9 patch-clamp amplifier connected to a MacMini (Apple Inc.) installed with Patchmaster (HEKA, Elektronic).

Paper 1

Hypoxyprobe-1

Hypoxyprobe-1 (Chemicon) forms irreversible adducts with intracellular and extracellular proteins under hypoxic conditions ($PO_2 < 10$ mm Hg) with a half-life of 0.5 hours (Noto et al., 2006). To determine the extent hypoxia induced by 2 hour MCAO, Hypoxyprobe-1 was administered to rats via intraperitoneal injection (60 mg/kg) 30 minutes after MCAO induction, or 6 weeks later to detect long-lasting hypoxia. Hypoxyprobe-1 adducts were visualized combining the monoclonal mouse Hypoxyprobe-1 primary antibody and 3, 3'-diaminobenzidine (DAB) with cresyl violet counter-stain to label cell nuclei (see Immunohistochemistry, above).

Vessel Density and Length Quantification

Blood vessels were quantified in brain sections immunostained with rat-endothelial cell antigen (RECA) to label vessels and cresyl violet counter-stain to label cells, using a Nikon Eclipse 80i microscope with a motorized specimen stage. The density and length of blood vessels in the SVZ and striatum was estimated using computer-assisted stereology (CAST, version 2.3.5.1; Visiopharm) (Larsen et al., 1998). The software generates a sampling box with isotropic virtual planes which intersect the tissue sample. The density and length of vessels were calculated by the software based on the number of intersections between virtual planes and blood vessels, taking into account the number of sampling box corners hitting the reference space (area of interest), and the total area of isotropic planes in each sampling box.

Paper 2

Rapid Kindling and Extra Stimulations

"The term kindling refers to a procedure and to a process, which leads to a state"
– Graham V. Goddard 1938 – 1987 (from Elmér, 1997)

Kindling is the process by which repeated electrical stimulation of the brain leads to the development of spontaneous seizures. This is a model of epileptogenesis. Rats were anesthetized and implanted with a bipolar stainless steel stimulating/recording electrode in the ventral hippocampal CA1-CA3 region. A reference electrode was placed between the skull and adjacent muscle. Seven days later, animals were subjected to the rapid kindling protocol (40 stimulations; 1 ms

square-wave pulses of 400 μA intensity with 100 Hz intratrain frequency for 10 s every 5 min). 2 days after retrovirus administration (9 days after rapid kindling) animals were subjected to stimulus evoked seizures, twice weekly for 6-8 weeks. Using this protocol we induced seizures and hyperexcitability without causing major inflammatory changes.

ELISA

Enzyme-linked immunosorbent assay (ELISA), is a technique used to detect the presence and concentration of antigens. Briefly, a primary antibody is attached to the sides of a well. A sample with unknown concentration of an antigen is added to the well allowing the antigen to bind to the primary antibody. A secondary antibody conjugated to peroxidase (see Immunohistochemistry, above) recognizes and binds to the antigen-antibody complex. A substrate to peroxidase is added to the well, and the quantity of antigen can be determined based on the magnitude of sample color change (change in optical density) using a microtiter plate reader.

RV-GFP

RV-GFP was used to label adult born neurons. This virus specifically infects dividing cells. GFP expression was driven by the CMV early enhancer/chicken β actin (CAG) promoter. Using RV-GFP allowed temporal and spatial control when labeling the adult born neurons, i.e., RV-GFP has a short half-life, is replication incompetent, and remains localized to the site of injection (Zhao et al., 2006).

Paper 3, 4 and 5

Cell culturing and viral transduction

For neural conversion, fibroblasts were plated in medium in culture plates coated with gelatin. Cells were transduced with the doxycycline regulated lentiviral vectors Ascl1, Brn2, Myt1l (ABM) and a separate vector containing the transactivator TET-ON (FUW .rtTZ-SM2). When transduced with Neurog2, Brn2, Myt1l (NBM), a non-regulated lentiviral vector expressing the mouse open-reading-frame for Neurog2 was used. For detailed methods see reprints in next section.

Quantification and Efficiency Calculations

Neuronal conversions were evaluated either by counting cells using random sampling at 20x magnification or using Cellomics (Thermo Scientific). Neurite outgrowth was determined using Cellomics.

Quantitative RT-PCR

RNA (1-4 mg) was used for reverse transcription using random primers and SuperScriptIII (Invitrogen). SYBR Green qRT-PCR was performed with LightCycler 480 SYBR Green I Master (Roche) in a two-step cycling protocol. For detailed methods see reprints in next section.

Paper 6

Generation of human iPS cells and neuronal differentiation

Dermal fibroblasts obtained from a 33 year old male were transduced with the reprogramming factors Oct4, Sox2, KLF4, and c-Myc and were grown in culture medium. Neural differentiation was induced by applying the appropriate media conditions as previously described (Koch et al., 2009) and can be found in the reprint.

Cell transplantation and fluoro-gold injection

Intracerebral transplantation was performed on anesthetized rodents secured in a stereotax. Cell suspensions were injected into the desired brain region using a microcapillary connected to a Hamilton syringe. Similarly, fluoro-gold was injected and delivered iontophoretically by applying repeated 5 μA current pulses.

Behavioral tests

The staircase test measures side-specific forelimb reaching and grasping abilities. Sugar pellets were placed on 6 steps on each side of the mice giving them the opportunity to grasp and eat the pellets with the impaired or unimpaired paw. Similarly, the corridor test involves giving mice the opportunity to take food from 10 pairs of adjacent pots in a narrow corridor. Performance was calculated as the number of pellets taken by the impaired paw divided by the total number of pellets taken by both paws.

ACKNOWLEDGEMENTS

REFERENCES

Alberti S, Krause SM, Kretz O, Philippar U, Lemberger T, Casanova E, Wiebel FF, Schwarz H, Frotscher M, Schütz G, Nordheim A (2005) Neuronal migration in the murine rostral migratory stream requires serum response factor. Proc Natl Acad Sci U S A 102:6148-53.

Altman J, Das GD (1965) Autoradiographic and histological evidence of postnatal hippo-campal neurogenesis in rats. J Comp Neurol 124:319-35.

Alvarez-Buylla A, Garcia-Verdugo JM (2002) Neurogenesis in adult subventricular zone. J Neurosci 22:629-34. Review.

Arvidsson A, Collin T, Kirik D, Kokaia Z, Lindvall O (2002) Neuronal replacement from endogenous precursors in the adult brain after stroke. Nat Med 8:963-70.

Belvindrah R, Hankel S, Walker J, Patton BL, Müller U (2007) Beta1 integrins control the formation of cell chains in the adult rostral migratory stream. J Neurosci 27:2704-17.

Bengzon J, Kokaia Z, Elmér E, Nanobashvili A, Kokaia M, Lindvall O (1997) Apoptosis and proliferation of dentate gyrus neurons after single and intermittent limbic seizures. Proc Natl Acad Sci U S A 94:10432-7.

Berninger B, Guillemot F, Götz M (2007) Directing neurotransmitter identity of neurones derived from expanded adult neural stem cells. Eur J Neurosci 25:2581-90.

Bliss T, Guzman R, Daadi M, Steinberg GK (2007) Cell transplantation therapy for stroke. Stroke 38:817-26. Review.

Brennand KJ, Simone A, Jou J, Gelboin-Burkhart C, Tran N, Sangar S, Li Y, Mu Y, Chen G, Yu D, McCarthy S, Sebat J, Gage FH (2011) Modelling schizophrenia using human induced pluripotent stem cells. Nature 473:221-5.

Buckmaster PS, Dudek FE (1997) Neuron loss, granule cell axon reorganization, and func-tional changes in the dentate gyrus of epileptic kainate-treated rats. J Comp Neurol 385:385-404.

Buhl EH, Otis TS, Mody I (1996) Zinc-induced collapse of augmented inhibition by GABA in a temporal lobe epilepsy model. Science 271:369-373.

Butovsky O, Ziv Y, Schwartz A, Landa G, Talpalar AE, Pluchino S, Martino G, Schwartz M (2006) Microglia activated by IL-4 or IFN-gamma differentially induce neurogen-esis and oligodendrogenesis from adult stem/progenitor cells. Mol Cell Neurosci 31:149-60.

Bühnemann C, Scholz A, Bernreuther C, Malik CY, Braun H, Schachner M, Reymann KG, Dihné M (2006) Neuronal differentiation of transplanted embryonic stem cell-derived precursors in stroke lesions of adult rats. Brain 129:3238-48.

Caiazzo M, Dell'anno MT, Dvoretskova E, Lazarevic D, Taverna S, Leo D, Sotnikova TD, Menegon A, Roncaglia P, Colciago G, Russo G, Carninci P, Pezzoli G, Gainetdinov RR, Gustincich S, Dityatev A, Broccoli V (2011) Direct generation of functional dopaminergic neurons from mouse and human fibroblasts. Nature 476:224-7.

Cameron HA, McKay RD (2001) Adult neurogenesis produces a large pool of new granule cells in the dentate gyrus. J Comp Neurol 435:406-17.

Cao L, Jiao X, Zuzga DS, Liu Y, Fong DM, Young D, During MJ (2004) VEGF links hippocampal activity with neurogenesis, learning and memory. Nat Genet 36:827-35.

Carlén M, Meletis K, Göritz C, Darsalia V, Evergren E, Tanigaki K, Amendola M, Barnabé-Heider F, Yeung MS, Naldini L, Honjo T, Kokaia Z, Shupliakov O, Cassidy RM, Lindvall O, Frisén J (2009) Forebrain ependymal cells are Notch-dependent and generate neuroblasts and astrocytes after stroke. Nat Neurosci 12:259-67.

Cavalheiro EA (1995) The pilocarpine model of epilepsy. Ital J Neurol Sci. 16:33-7. Review.

Ceradini DJ, Kulkarni AR, Callaghan MJ, Tepper OM, Bastidas N, Kleinman ME, Capla JM, Galiano RD, Levine JP, Gurtner GC (2004) Progenitor cell trafficking is regulated by hypoxic gradients through HIF-1 induction of SDF-1. Nat Med 10:858-64.

Cheatwood JL, Emerick AJ, Schwab ME, Kartje GL (2008) Nogo-A expression after focal ischemic stroke in the adult rat. Stroke 39:2091-8.

Clelland CD, Choi M, Romberg C, Clemenson GD Jr, Fragniere A, Tyers P, Jessberger S, Saksida LM, Barker RA, Gage FH, Bussey TJ (2009) A functional role for adult hippocampal neurogenesis in spatial pattern separation. Science 325:210-3.

Chen J, Zhang C, Jiang H, Li Y, Zhang L, Robin A, Katakowski M, Lu M, Chopp M (2005) Atorvastatin induction of VEGF and BDNF promotes brain plasticity after stroke in mice. J Cereb Blood Flow Metab 25:281-90.

Daadi MM, Lee SH, Arac A, Grueter BA, Bhatnagar R, Maag AL, Schaar B, Malenka RC, Palmer TD, Steinberg GK (2009) Functional engraftment of the medial ganglionic eminence cells in experimental stroke model. Cell Transplant 18:815-26.

Danilov AI, Gomes-Leal W, Ahlenius H, Kokaia Z, Carlemalm E, Lindvall O (2009) Ultrastructural and antigenic properties of neural stem cells and their progeny in adult rat subventricular zone. Glia 57:136-52.

Darsalia V, Kallur T, Kokaia Z (2007) Survival, migration and neuronal differentiation of human fetal striatal and cortical neural stem cells grafted in stroke-damaged rat striatum. Eur J Neurosci 26:605-14.

Deng W, Saxe MD, Gallina IS, Gage FH (2009) Adult-born hippocampal dentate granule cells undergoing maturation modulate learning and memory in the brain. J Neurosci 29:13532-42.

Dimos JT, Rodolfa KT, Niakan KK, Weisenthal LM, Mitsumoto H, Chung W, Croft GF, Saphier G, Leibel R, Goland R, Wichterle H, Henderson CE, Eggan K (2008) Induced pluripotent stem cells generated from patients with ALS can be differentiated into motor neurons. Science 321:1218-21.

Dinocourt C, Petanjek Z, Freund TF, Ben-Ari Y, Esclapez M (2003) Loss of interneurons innervating pyramidal cell dendrites and axon initial segments in the CA1 region of the hippocampus following pilocarpine-induced seizures. J Comp Neurol 459:407-25.

Doetsch F, García-Verdugo JM, Alvarez-Buylla A (1997) Cellular composition and three-dimensional organization of the subventricular germinal zone in the adult mammalian brain. J Neurosci 17:5046-61.

Doetsch F, Petreanu L, Caille I, Garcia-Verdugo JM, Alvarez-Buylla A (2002) EGF converts transit-amplifying neurogenic precursors in the adult brain into multipotent stem cells. Neuron 36:1021-34.

Dowd E, Monville C, Torres EM, Dunnett SB (2005) The Corridor Task: a simple test of lateralised response selection sensitive to unilateral dopamine deafferentation and graft-derived dopamine replacement in the striatum. Brain Res Bull 68:24-30.

Dranovsky A, Hen R (2006) Hippocampal neurogenesis: regulation by stress and antidepressants. Biol Psychiatry 59:1136-43. Review.

Drapeau E, Mayo W, Aurousseau C, Le Moal M, Piazza PV, Abrous DN (2003) Spatial memory performances of aged rats in the water maze predict levels of hippocampal neurogenesis. Proc Natl Acad Sci U S A 100:14385-90.

Eisch AJ, Cameron HA, Encinas JM, Meltzer LA, Ming GL, Overstreet-Wadiche LS (2008) Adult neurogenesis, mental health, and mental illness: hope or hype? J Neurosci 28:11785-91. Review.

Ekdahl CT, Mohapel P, Elmér E, Lindvall O (2001) Caspase inhibitors increase short-term survival of progenitor-cell progeny in the adult rat dentate gyrus following status epilepticus. Eur J Neurosci 14:937-45.

Ekdahl CT, Claasen JH, Bonde S, Kokaia Z, Lindvall O (2003) Inflammation is detrimental for neurogenesis in adult brain. Proc Natl Acad Sci U S A 100:13632-7.

Ekdahl CT, Kokaia Z, Lindvall O (2009) Brain inflammation and adult neurogenesis: the dual role of microglia. Neuroscience 158:1021-9. Epub 2008 Jul 3. Review.

Elmér E, Kokaia M, Kokaia Z, Ferencz I, Lindvall O (1996) Delayed kindling development after rapidly recurring seizures: relation to mossy fiber sprouting and neurotrophin, GAP-43 and dynorphin gene expression. Brain Res 712:19-34.

Elmér E (1997) Mechanisms of hyperexcitability in the kindling model of epilepsy. Doctoral Dissertation. (pp. 4) Lund University, Sweden.

Elmér E, Kokaia M, Ernfors P, Ferencz I, Kokaia Z, Lindvall O (1997) Suppressed kindling epileptogenesis and perturbed BDNF and TrkB gene regulation in NT-3 mutant mice. Exp Neurol 145:93-103.

Elmér E, Kokaia Z, Kokaia M, Carnahan J, Nawa H, Lindvall O (1998) Dynamic changes of brain-derived neurotrophic factor protein levels in the rat forebrain after single and recurring kindling-induced seizures. Neuroscience 83:351-362.

Engel J Jr, Williamson PD, Wieser HG (1997) Mesial temporal lobe epilepsy. In: Epilepsy: a comprehensive textbook (Engel J Jr, Pedley TA, eds), pp 2417–2426. Philadelphia: Lippincott-Raven.

Epsztein J, Represa A, Jorquera I, Ben-Ari Y, Crépel V (2005) Recurrent mossy fibers establish aberrant kainate receptor-operated synapses on granule cells from epileptic rats. J Neurosci 25:8229-39.

Eriksson PS, Perfilieva E, Björk-Eriksson T, Alborn AM, Nordborg C, Peterson DA, Gage FH (1998) Neurogenesis in the adult human hippocampus. Nat Med 4:1313-7.

Faulkner JR, Herrmann JE, Woo MJ, Tansey KE, Doan NB, Sofroniew MV (2004) Reactive astrocytes protect tissue and preserve function after spinal cord injury. J Neurosci 24:2143-55.

Faulkner RL, Jang MH, Liu XB, Duan X, Sailor KA, Kim JY, Ge S, Jones EG, Ming GL, Song H, Cheng HJ (2008) Development of hippocampal mossy fiber synaptic outputs by new neurons in the adult brain. Proc Natl Acad Sci U S A 105:14157-62.

Feng HJ, Mathews GC, Kao C, Macdonald RL (2008) Alterations of GABA A-receptor unction and allosteric modulation during development of status epilepticus. J Neurophysiol 99:1285-93.

Filbin MT (2003) Myelin-associated inhibitors of axonal regeneration in the adult mammalian CNS. Nat Rev Neurosci 4:703-13. Review.

Gabriel S, Njunting M, Pomper JK, Merschhemke M, Sanabria ER, Eilers A, Kivi A, Zeller M, Meencke HJ, Cavalheiro EA, Heinemann U, Lehmann TN (2004) Stimulus and potassium-induced epileptiform activity in the human dentate gyrus from patients with and without hippocampal sclerosis. J Neurosci 24:10416-30.

García-Alías G, Barkhuysen S, Buckle M, Fawcett JW (2009) Chondroitinase ABC treatment opens a window of opportunity for task-specific rehabilitation. Nat Neurosci 12:1145-51.

Ge S, Goh EL, Sailor KA, Kitabatake Y, Ming GL, Song H (2006) GABA regulates synaptic integration of newly generated neurons in the adult brain. Nature 439:589-93.

Gheusi G, Cremer H, McLean H, Chazal G, Vincent JD, Lledo PM (2000) Importance of newly generated neurons in the adult olfactory bulb for odor discrimination. Proc Natl Acad Sci U S A 97:1823-8.

Gilbert ME, Kelly ME, Samsam TE, Goodman JH (2005) Chronic developmental lead exposure reduces neurogenesis in adult rat hippocampus but does not impair spatial learning. Toxicol Sci 86:365-74.

Gobeske KT, Das S, Bonaguidi MA, Weiss C, Radulovic J, Disterhoft JF, Kessler JA (2009) BMP signaling mediates effects of exercise on hippocampal neurogenesis and cognition in mice. PLoS One 4:e7506.

Goffinet AM, Daumerie C, Langerwerf B, Pieau C (1986) Neurogenesis in reptilian cortical structures: 3H-thymidine autoradiographic analysis. J Comp Neurol 243:106-16.

Goldman SA, Nottebohm F (1983) Neuronal production, migration, and differentiation in a vocal control nucleus of the adult female canary brain. Proc Natl Acad Sci U S A 80:2390-4.

Gotts JE, Chesselet MF (2005) Vascular changes in the subventricular zone after distal cortical lesions. Exp Neurol 194:139-50.

Gould E, Tanapat P, McEwen BS, Flügge G, Fuchs E (1998) Proliferation of granule cell precursors in the dentate gyrus of adult monkeys is diminished by stress. Proc Natl Acad Sci U S A 95:3168-71.

Gould E, Reeves AJ, Graziano MS, Gross CG (1999) Neurogenesis in the neocortex of adult primates. Science 286:548-52.

Gould E, Tanapat P, Rydel T, Hastings N (2000) Regulation of hippocampal neurogenesis in adulthood. Biol Psychiatry 48:715-20.

Haas CA, Frotscher M (2010) Reelin deficiency causes granule cell dispersion in epilepsy. Exp Brain Res 200:141-9.

Hanisch UK, Prinz M, Angstwurm K, Häusler KG, Kann O, Kettenmann H, Weber JR (2001) The protein tyrosine kinase inhibitor AG126 prevents the massive microglial cytokine induction by pneumococcal cell walls. Eur J Immunol 31:2104-15.

Hanisch UK, Kettenmann H (2007) Microglia: active sensor and versatile effector cells in the normal and pathologic brain. Nat Neurosci 10:1387-94. Review.

Hattiangady B, Rao MS, Shetty AK (2004) Chronic temporal lobe epilepsy is associated with severely declined dentate neurogenesis in the adult hippocampus. Neurobiol Dis 17:473-90.

He J, Nixon K, Shetty AK, Crews FT (2005) Chronic alcohol exposure reduces hippocampal neurogenesis and dendritic growth of newborn neurons. Eur J Neurosci 21:2711-20.

Heinrich C, Gascón S, Masserdotti G, Lepier A, Sanchez R, Simon-Ebert T, Schroeder T, Götz M, Berninger B (2011) Generation of subtype-specific neurons from postnatal astroglia of the mouse cerebral cortex. Nat Protoc 6:214-28.

Hellsten J, West MJ, Arvidsson A, Ekstrand J, Jansson L, Wennström M, Tingström A (2005) Electroconvulsive seizures induce angiogenesis in adult rat hippocampus. Biol Psychiatry 58:871-8.

Hirota Y, Ohshima T, Kaneko N, Ikeda M, Iwasato T, Kulkarni AB, Mikoshiba K, Okano H, Sawamoto K (2007) Cyclin-dependent kinase 5 is required for control of neuroblast migration in the postnatal subventricular zone. J Neurosci 27:12829-38.

Hou SW, Wang YQ, Xu M, Shen DH, Wang JJ, Huang F, Yu Z, Sun FY (2008) Functional integration of newly generated neurons into striatum after cerebral ischemia in the adult rat brain. Stroke 39:2837-44.

Imayoshi I, Sakamoto M, Ohtsuka T, Takao K, Miyakawa T, Yamaguchi M, Mori K, Ikeda T, Itohara S, Kageyama R (2008) Roles of continuous neurogenesis in the structural and functional integrity of the adult forebrain. Nat Neurosci 11:1153-61.

Imayoshi I, Sakamoto M, Yamaguchi M, Mori K, Kageyama R (2010) Essential roles of Notch signaling in maintenance of neural stem cells in developing and adult brains. J Neurosci 30:3489-98.

Iosif RE, Ahlenius H, Ekdahl CT, Darsalia V, Thored P, Jovinge S, Kokaia Z, Lindvall O (2008) Suppression of stroke-induced progenitor proliferation in adult subventricular zone by tumor necrosis factor receptor 1. J Cereb Blood Flow Metab 28:1574-87.

Jakubs K, Nanobashvili A, Bonde S, Ekdahl CT, Kokaia Z, Kokaia M, Lindvall O (2006) Environment matters: synaptic properties of neurons born in the epileptic adult brain develop to reduce excitability. Neuron 52:1047-1059.

Jakubs K, Bonde S, Iosif RE, Ekdahl CT, Kokaia Z, Kokaia M, Lindvall O (2008) Inflammation regulates functional integration of neurons born in adult brain. J Neurosci 28:12477-12488.

Jessberger S, Zhao C, Toni N, Clemenson GD, Jr., Li Y, Gage FH (2007) Seizure-associated, aberrant neurogenesis in adult rats characterized with retrovirus-mediated cell labeling. J Neurosci 27:9400-9407.

Jessberger S, Aigner S, Clemenson GD Jr, Toni N, Lie DC, Karalay O, Overall R, Kempermann G, Gage FH (2008) Cdk5 regulates accurate maturation of newborn granule cells in the adult hippocampus. PLoS Biol 6:e272.

Jung KH, Chu K, Kim M, Jeong SW, Song YM, Lee ST, Kim JY, Lee SK, Roh JK (2004) Continuous cytosine-b-D-arabinofuranoside infusion reduces ectopic granule cells in adult rat hippocampus with attenuation of spontaneous recurrent seizures following

pilocarpine-induced status epilepticus. Eur J Neurosci 19:3219-26.

Kallur T, Darsalia V, Lindvall O, Kokaia Z (2006) Human fetal cortical and striatal neural stem cells generate region-specific neurons in vitro and differentiate extensively to neurons after intrastriatal transplantation in neonatal rats. J Neurosci Res 84:1630-44.

Kang HJ, Schuman EM (1995) Neurotrophin-induced modulation of synaptic transmission in the adult hippocampus. J Physiol Paris 89:11-22.

Karalay O, Doberauer K, Vadodaria KC, Knobloch M, Berti L, Miquelajauregui A, Schwark M, Jagasia R, Taketo MM, Tarabykin V, Lie DC, Jessberger S (2010) Prospero-related homeobox 1 gene (Prox1) is regulated by canonical Wnt signaling and has a stage-specific role in adult hippocampal neurogenesis. Proc Natl AcadSci U S A 108:5807-12.

Kempermann G, Kuhn HG, Gage FH (1997) More hippocampal neurons in adult mice living in an enriched environment. Nature 386:493-5.

Kobayashi M, Buckmaster PS (2003) Reduced inhibition of dentate granule cells in a model of temporal lobe epilepsy. J Neurosci 23:2440-2452.

Koch P, Opitz T, Steinbeck JA, Ladewig J, Brüstle O (2009) A rosette-type, self-renewing human ES cell-derived neural stem cell with potential for in vitro instruction and synaptic integration. Proc Natl Acad Sci U S A 106:3225-30.

Kojima T, Hirota Y, Ema M, Takahashi S, Miyoshi I, Okano H, Sawamoto K (2010) Subventricular zone-derived neural progenitor cells migrate along a blood vessel scaffold toward the post-stroke striatum. Stem Cells 28:545-54.

Kokaia M, Ernfors P, Kokaia Z, Elmér E, Jaenisch R, Lindvall O (1995) Suppressed epileptogenesis in BDNF mutant mice. Exp Neurol 133:215-24.

Kondziella D, Alvestad S, Vaaler A, Sonnewald U (2007) Which clinical and experimental data link temporal lobe epilepsy with depression? J Neurochem 103:2136-52.

Kreutzberg GW (1996) Microglia: a sensor for pathological events in the CNS. Trends Neurosci 19:312-8. Review.

Kriss JP, Maruyama Y, Tung LA, Bond SB, Revesz L (1963) The fate of 5-bromodeoxyuridine, 5-bromodeoxycytidine, and 5-iododeoxycytidine in man. Cancer Res 23:260-8.

Kron MM, Zhang H, Parent JM (2010) The developmental stage of dentate granule cells dictates their contribution to seizure-induced plasticity. J Neurosci 30:2051-9.

Lai B, Mao XO, Xie L, Jin K, Greenberg DA (2008) Electrophysiological neurodifferentiation of subventricular zone-derived precursor cells following stroke. Neurosci Lett 442:305-8.

Laplagne DA, Esposito MS, Piatti VC, Morgenstern NA, Zhao C, van Praag H, Gage FH, Schinder AF (2006) Functional convergence of neurons generated in the developing and adult hippocampus. PLoS Biol 4:e409.

Larsen JO, Gundersen HJ, Nielsen J (1998) Global spatial sampling with isotropic virtual planes: Estimators of length density and total length in thick, arbitrarily orientated sections. J Microsc 191:238 –248.

Lavado A, Lagutin OV, Chow LM, Baker SJ, Oliver G (2010) Prox1 is required for granule cell maturation and intermediate progenitor maintenance during brain neurogenesis. PLoS Biol 8 pii: e1000460.

Leventhal C, Rafii S, Rafii D, Shahar A, Goldman SA (1999) Endothelial trophic support of neuronal production and recruitment from the adult mammalian subependyma. Mol Cell Neurosci 13:450-64.

Lim DA, Tramontin AD, Trevejo JM, Herrera DG, García-Verdugo JM, Alvarez-Buylla A (2000) Noggin antagonizes BMP signaling to create a niche for adult neurogenesis. Neuron 28:713-26.

Lindvall O, Kokaia Z, Bengzon J, Elmér E, Kokaia M (1994a) Neurotrophins and brain insults. Trends Neurosci 17:490-6. Review.

Lindvall O, Sawle G, Widner H, Rothwell JC, Björklund A, Brooks D, Brundin P, Frackowiak R, Marsden CD, Odin P, et al (1994b). Evidence for long-term survival and function of dopaminergic grafts in progressive Parkinson's disease. Ann Neurol 35:172-80.

Lindvall O, Kokaia Z (2006) Stem cells for the treatment of neurological disorders. Nature 441:1094-6. Review.

Lindvall O, Kokaia Z (2010) Stem cells in human neurodegenerative disorders—time for clinical translation? J Clin Invest 120:29-40. Review.

Lindvall O, Björklund A (2011) Cell Therapeutics in Parkinson's Disease. Neurotherapeutics, in press

Louissaint A Jr, Rao S, Leventhal C, Goldman SA (2002) Coordinated interaction of neurogenesis and angiogenesis in the adult songbird brain. Neuron 34:945-60.

Lynch M, Sutula M (2000) Recurrent excitatory connectivity in the dentate gyrus of kindled and kainic acid-treated rats. J Neurophysiol 83:693-704.

Magnus T, Chan A, Grauer O, Toyka KV, Gold R (2001) Microglial phagocytosis of apoptotic inflammatory T cells leads to down-regulation of microglial immune activation. J Immunol 167:5004-10.

Malberg JE, Eisch AJ, Nestler EJ, Duman RS (2000) Chronic antidepressant treatment increases neurogenesis in adult rat hippocampus. J Neurosci 20:9104-10.

Massey JM, Hubscher CH, Wagoner MR, Decker JA, Amps J, Silver J, Onifer SM (2006) Chondroitinase ABC digestion of the perineuronal net promotes functional collateral sprouting in the cuneate nucleus after cervical spinal cord injury. J Neurosci 26:4406-14.

Milner, B (1966) Amnesia following operation on the temporal lobe. In C. W M. Whitty &O. L. Zangwill (Eds.), Amnesia (pp. 109-133) London: Butterworth & Co.

Ming GL, Song H (2005) Adult neurogenesis in the mammalian central nervous system. Annu Rev Neurosci 28:223-50. Review.

Minger SL, Ekonomou A, Carta EM, Chinoy A, Perry RH, Ballard CG (2007) Endogenous neurogenesis in the human brain following cerebral infarction. Regen Med 1:69-74.

Minghetti L, Levi G (1998) Microglia as effector cells in brain damage and repair: focus on prostanoids and nitric oxide. Prog Neurobiol 54:99-125. Review.

Molleman A (1983) Patch clamping: An introductory guide to patch clamp electrophysiology. (pp. 39-40) John Wiley & Sons Ltd.

Monje ML, Toda H, Palmer TD (2003) Inflammatory blockade restores adult hippocampal neurogenesis. Science 302:1760-5.

Montoya CP, Campbell-Hope LJ, Pemberton KD, Dunnett SB (1991) The "staircase test": a measure of independent forelimb reaching and grasping abilities in rats. J Neurosci Methods 36:219-28.

Mu Y, Lee SW, Gage FH (2010) Signaling in adult neurogenesis. Curr Opin Neurobiol 4:416-23.

Nanobashvili A, Airaksinen MS, Kokaia M, Rossi J, Asztély F, Olofsdotter K, Mohapel P, Saarma M, Lindvall O, Kokaia Z (2000) Development and persistence of kindling epilepsy are impaired in mice lacking glial cell line-derived neurotrophic factor family receptor alpha 2. Proc Natl Acad Sci U S A 97:12312-7.

Noto T, Furuichi Y, Ishiye M, Matsuoka N, Aramori I, Mutoh S, Yanagihara T, Manabe N (2006) Temporal and topographic profiles of tissue hypoxia following transient focal cerebral ischemia in rats. J Vet Med Sci 68:803–807.

Okita K, Ichisaka T, Yamanaka S (2007) Generation of germline-competent induced pluripotent stem cells. Nature. 448:313-7.

Overstreet-Wadiche LS, Bromberg DA, Bensen AL, Westbrook GL (2006) Seizures accelerate functional integration of adult-generated granule cells. J Neurosci 26:4095-103.

Palmer TD, Willhoite AR, Gage FH (2000) Vascular niche for adult hippocampal neurogenesis. J Comp Neurol 425:479-94.

Pang ZP, Yang N, Vierbuchen T, Ostermeier A, Fuentes DR, Yang TQ, Citri A, Sebastiano V, Marro S, Südhof TC, Wernig M (2011) Induction of human neuronal cells by defined transcription factors. 476:220-3.

Parent JM, Yu TW, Leibowitz RT, Geschwind DH, Sloviter RS, Lowenstein DH (1997) Dentate granule cell neurogenesis is increased by seizures and contributes to aberrant network reorganization in the adult rat hippocampus. J Neurosci 17:3727–3738.

Parent JM, Elliott RC, Pleasure SJ, Barbaro NM, Lowenstein DH (2006) Aberrant seizure-induced neurogenesis in experimental temporal lobe epilepsy. Ann Neurol 59:81-91.

Pfisterer U, Kirkeby A, Torper O, Wood J, Nelander J, Dufour A, Björklund A, Lindvall O, Jakobsson J, Parmar M (2011a) Direct conversion of human fibroblasts to dopaminergic neurons. Proc Natl Acad Sci U S A. 108:10343-8.

Pfisterer U, Wood J, Nihlberg K, Hallgren O, Bjermer L, Westergren-Thorsson G, Lindvall O, Parmar M (2011b) Efficient induction of functional neurons from adult human fibroblasts. Cell Cycle 10:3311-6

Piccini P, Brooks DJ, Björklund A, Gunn RN, Grasby PM, Rimoldi O, Brundin P, Hagell P, Rehncrona S, Widner H, Lindvall O (1999) Dopamine release from nigral transplants visualized in vivo in a Parkinson's patient. Nat Neurosci 2:1137-40.

Pirttilä TJ, Manninen A, Jutila L, Nissinen J, Kälviäinen R, Vapalahti M, Immonen A, Paljärvi L, Karkola K, Alafuzoff I, Mervaala E, Pitkänen A (2005) Cystatin C expression is associated with granule cell dispersion in epilepsy. Ann Neurol 58:211-23.

Pizzorusso T, Medini P, Berardi N, Chierzi S, Fawcett JW, Maffei L (2002) Reactivation of ocular dominance plasticity in the adult visual cortex. Science 298:1248-51.

Qiang L, Fujita R, Yamashita T, Angulo S, Rhinn H, Rhee D, Doege C, Chau L, Aubry L, Vanti WB, Moreno H, Abeliovich A (2011) Directed conversion of Alzheimer's disease patient skin fibroblasts into functional neurons. Cell 146:359-71.

Represa A, Tremblay E, Ben-Ari Y (1990) Sprouting of mossy fibers in the hippocampus of epileptic human and rat. Adv Exp Med Biol 268:419-24.

Ribak CE, Tran PH, Spigelman I, Okazaki MM, Nadler JV (2000) Status epilepticus-induced hilar basal dendrites on rodent granule cells contribute to recurrent excitatory circuitry. J Comp Neurol 428:240-53.

Rolls A, Shechter R, Schwartz M (2009) The bright side of the glial scar in CNS repair. Nat Rev Neurosci 10:235-41. Review.

Rousselot P, Lois C, Alvarez-Buylla A (1995) Embryonic (PSA) N-CAM reveals chains of migrating neuroblasts between the lateral ventricle and the olfactory bulb of adult mice. J Comp Neurol 351:51-61.

Sahay A, Hen R. Adult hippocampal neurogenesis in depression (2007) Nat Neurosci 10:1110-5. Review.

Santarelli L, Saxe M, Gross C, Surget A, Battaglia F, Dulawa S, Weisstaub N, Lee J, Duman R, Arancio O, Belzung C, Hen R (2003) Requirement of hippocampal neurogenesis for the behavioral effects of antidepressants. Science 301:805-9.

Sawamoto K, Wichterle H, Gonzalez-Perez O, Cholfin JA, Yamada M, Spassky N, Murcia NS, Garcia-Verdugo JM, Marin O, Rubenstein JL, Tessier-Lavigne M, Okano H, Alva-

rez-Buylla A (2006) New neurons follow the flow of cerebrospinal fluid in the adult brain. Science 311:629-32.

Sayin U, Osting S, Hagen J, Rutecki P, Sutula T (2003) Spontaneous seizures and loss of axo-axonic and axo-somatic inhibition induced by repeated brief seizures in kindled rats. J Neurosci 23:2759-68.

Scharfman HE, Sollas AL, Berger RE, Goodman JH, Pierce JP (2003a) Perforant path activation of ectopic granule cells that are born after pilocarpine-induced seizures. Neuroscience 121:1017-29.

Scharfman HE, Sollas AL, Berger RE, Goodman JH (2003b) Electrophysiological evidence of monosynaptic excitatory transmission between granule cells after seizure-induced mossy fiber sprouting. J Neurophysiol 90:2536-47.

Schwab ME (2002) Increasing plasticity and functional recovery of the lesioned spinal cord. Prog Brain Res 137:351-9. Review.

Scott BW, Wojtowicz JM, Burnham WM (2000) Neurogenesis in the dentate gyrus of the rat following electroconvulsive shock seizures. Exp Neurol 165:231-6.

Sgubin D, Aztiria E, Perin A, Longatti P, Leanza G (2007) Activation of endogenous neural stem cells in the adult human brain following subarachnoid hemorrhage. J Neurosci Res 85:1647-55.

Shen Q, Goderie SK, Jin L, Karanth N, Sun Y, Abramova N, Vincent P, Pumiglia K, Temple S (2004) Endothelial cells stimulate self-renewal and expand neurogenesis of neural stem cells. Science 304:1338-40.

Shen Q, Wang Y, Kokovay E, Lin G, Chuang SM, Goderie SK, Roysam B, Temple S (2008) Adult SVZ stem cells lie in a vascular niche: a quantitative analysis of niche cell-cell interactions. Cell Stem Cell 3:289-300.

Silver J, Miller JH (2004) Regeneration beyond the glial scar. Nat Rev Neurosci 5:146-56. Review.

Simmons ML, Terman GW, Chavkin C (1997) Spontaneous excitatory currents and kappa-opioid receptor inhibition in dentate gyrus are increased in the rat pilocarpine model of temporal lobe epilepsy. J Neurophysiol 78:1860-1868.

Snapyan M, Lemasson M, Brill MS, Blais M, Massouh M, Ninkovic J, Gravel C, Berthod F, Götz M, Barker PA, Parent A, Saghatelyan A (2009) Vasculature guides migrating neuronal precursors in the adult mammalian forebrain via brain-derived neurotrophic factor signaling. J Neurosci 29:4172-88.

Son EY, Ichida JK, Wainger BJ, Toma JS, Rafuse VF, Woolf CJ, Eggan K (2011) Conversion of mouse and human fibroblasts into functional spinal motor neurons. Cell Stem Cell 9:205-18.

Squire LR, Stark CE, Clark RE (2004) The medial temporal lobe. Annu Rev Neurosci 27:279-306. Review.

Sutula T, Cascino G, Cavazos J, Parada I, Ramirez L (1989) Mossy fiber synaptic reorganization in the epileptic human temporal lobe. Ann Neurol 26:321-30.

Svendsen CN, Bhattacharyya A, Tai YT (2001) Neurons from stem cells: preventing an identity crisis. Nat Rev Neurosci. 2:831-4. Review.

Tanaka T, Saito H, Matsuki N (1997) Inhibition of GABAA synaptic responses by brain-derived neurotrophic factor (BDNF) in rat hippocampus. J Neurosci 17:2959-66.

Tauck DL, Nadler JV (1985) Evidence of functional mossy fiber sprouting in hippocampal formation of kainic acid-treated rats. J Neurosci 5:1016–1022.

Tavazoie M, Van der Veken L, Silva-Vargas V, Louissaint M, Colonna L, Zaidi B, Garcia-Verdugo JM, Doetsch F (2008) A specialized vascular niche for adult neural stem cells. Cell Stem Cell 3:279-88.

Thored P, Arvidsson A, Cacci E, Ahlenius H, Kallur T, Darsalia V, Ekdahl CT, Kokaia Z, Lindvall O (2006) Persistent production of neurons from adult brain stem cells during recovery after stroke. Stem Cells 24:739-47.

Thored P, Wood J, Arvidsson A, Cammenga J, Kokaia Z, Lindvall O (2007) Long-term neuroblast migration along blood vessels in an area with transient angiogenesis and increased vascularization after stroke. Stroke 38:3032-9.

Thored P, Heldmann U, Gomes-Leal W, Gisler R, Darsalia V, Taneera J, Nygren JM, Jacobsen SE, Ekdahl CT, Kokaia Z, Lindvall O (2009) Long-term accumulation of microglia with proneurogenic phenotype concomitant with persistent neurogenesis in adult subventricular zone after stroke. Glia 57:835-49.

Toni N, Laplagne DA, Zhao C, Lombardi G, Ribak CE, Gage FH, Schinder AF (2008) Neurons born in the adult dentate gyrus form functional synapses with target cells. Nat Neurosci 11:901-907.

Tønnesen J, Sørensen AT, Deisseroth K, Lundberg C, Kokaia M (2009) Optogenetic control of epileptiform activity. Proc Natl Acad Sci U S A 106:12162-7.

Tronel S, Fabre A, Charrier V, Oliet SH, Gage FH, Abrous DN (2010) Spatial learning sculpts the dendritic arbor of adult-born hippocampal neurons. Proc Natl Acad Sci U S A 107:7963-8.

van Praag H, Christie BR, Sejnowski TJ, Gage FH (1999) Running enhances neurogenesis, learning, and long-term potentiation in mice. Proc Natl Acad Sci U S A 96:13427-31.

van Praag H, Schinder AF, Christie BR, Toni N, Palmer TD, Gage FH (2002) Functional neurogenesis in the adult hippocampus. Nature 415:1030-4.

Vierbuchen T, Ostermeier A, Pang ZP, Kokubu Y, Südhof TC, Wernig M (2010) Direct conversion of fibroblasts to functional neurons by defined factors. Nature. 463:1035-41.

Walter C, Murphy BL, Pun RYK, Spieles-Engemann AL, Danzer SC (2007) Pilocarpine-induced seizures cause selective time-dependent changes to adult-generated hippocampal dentate granule cells. J Neurosci 27:7541-7552.

Wang L, Zhang Z, Wang Y, Zhang R, Chopp M (2004) Treatment of stroke with erythropoietin enhances neurogenesis and angiogenesis and improves neurological function in rats. Stroke 35:1732-7.

Wang D, Ichiyama RM, Zhao R, Andrews MR, Fawcett JW (2011) Chondroitinase Combined with Rehabilitation Promotes Recovery of Forelimb Function in Rats with Chronic Spinal Cord Injury. J Neurosci 31:9332-9334.

Wernig M, Meissner A, Foreman R, Brambrink T, Ku M, Hochedlinger K, Bernstein BE, Jaenisch R (2007) In vitro reprogramming of fibroblasts into a pluripotent ES-cell-like state. Nature. 448:318-24.

Wernig M, Zhao JP, Pruszak J, Hedlund E, Fu D, Soldner F, Broccoli V, Constantine-Paton M, Isacson O, Jaenisch R (2008) Neurons derived from reprogrammed fibroblasts functionally integrate into the fetal brain and improve symptoms of rats with Parkinson's disease. Proc Natl Acad Sci U S A. 105:5856-61.

Wiessner C, Bareyre FM, Allegrini PR, Mir AK, Frentzel S, Zurini M, Schnell L, Oertle T, Schwab ME (2003) Anti-Nogo-A antibody infusion 24 hours after experimental stroke improved behavioral outcome and corticospinal plasticity in normotensive and spontaneously hypertensive rats. J Cereb Blood Flow Metab 23:154-65.

Wittner L, Maglóczky Z, Borhegyi Z, Halász P, Tóth S, Eross L, Szabó Z, Freund TF (2001) Preservation of perisomatic inhibitory input of granule cells in the epileptic human dentate gyrus. Neuroscience 108:587-600.

Wood JC, Jackson JS, Jakubs K, Chapman KZ, Ekdahl CT, Kokaia Z, Kokaia M, Lindvall O (2011) Functional integration of new hippocampal neurons following insults to the adult brain is determined by characteristics of pathological environment. Exp Neurol. 229:484-93.

Wuarin JP, Dudek FE (2001) Excitatory synaptic input to granule cells increases with time after kainate treatment. J Neurophysiol 85:1067-1077.

Zeng LH, Rensing NR, Wong M (2009) The mammalian target of rapamycin signaling pathway mediates epileptogenesis in a model of temporal lobe epilepsy. J Neurosci 29:6964-72.

Zhan RZ, Nadler JV (2009) Enhanced tonic GABA current in normotopic and hilar ectopic dentate granule cells after pilocarpine-induced status epilepticus. J Neurophysiol 102:670-81.

Zhang RL, Zhang ZG, Lu M, Wang Y, Yang JJ, Chopp M (2006) Reduction of the cell cycle length by decreasing G1 phase and cell cycle reentry expand neuronal progenitor cells in the subventricular zone of adult rat after stroke. J Cereb Blood Flow Metab 26:857-63.

Zhang F, Wang LP, Brauner M, Liewald JF, Kay K, Watzke N, Wood PG, Bamberg E, Nagel G, Gottschalk A, Deisseroth K (2007a) Multimodal fast optical interrogation of neural circuitry. Nature 446:633-9.

Zhang RL, Zhang ZG, Wang Y, LeTourneau Y, Liu XS, Zhang X, Gregg SR, Wang L, Chopp M (2007b) Stroke induces ependymal cell transformation into radial glia in the subventricular zone of the adult rodent brain. J Cereb Blood Flow Metab 27:1201-12.

Zhang RL, Zhang ZG, Roberts C, LeTourneau Y, Lu M, Zhang L, Wang Y, Chopp M (2008) Lengthening the G(1) phase of neural progenitor cells is concurrent with an increase of symmetric neuron generating division after stroke. J Cereb Blood Flow Metab 28:602-11.

Zhang W, Buckmaster PS (2009) Dysfunction of the dentate basket cell circuit in a rat model of temporal lobe epilepsy. J Neurosci 29:7846-56.

Zhang W, Yamawaki R, Wen X, Uhl J, Diaz J, Prince DA, Buckmaster PS (2009) Surviving hilar somatostatin interneurons enlarge, sprout axons, and form new synapses with granule cells in a mouse model of temporal lobe epilepsy. J Neurosci 29:14247-56.

Zhao C, Teng EM, Summers RG Jr, Ming GL, Gage FH (2006) Distinct morphological stages of dentate granule neuron maturation in the adult mouse hippocampus. J Neurosci 26:3-11.

Zhu C, Gao J, Karlsson N, Li Q, Zhang Y, Huang Z, Li H, Kuhn HG, Blomgren K (2010) Isoflurane anesthesia induced persistent, progressive memory impairment, caused a loss of neural stem cells, and reduced neurogenesis in young, but not adult, rodents. J Cereb Blood Flow Metab 30:1017-30.

Paper I

Long-Term Neuroblast Migration Along Blood Vessels in an Area With Transient Angiogenesis and Increased Vascularization After Stroke

Pär Thored, PhD; James Wood, BSc; Andreas Arvidsson, MD, PhD; Jörg Cammenga, MD, PhD; Zaal Kokaia, PhD; Olle Lindvall, MD, PhD

Background and Purpose—Stroke induced by middle cerebral artery occlusion (MCAO) causes long-term formation of new striatal neurons from stem/progenitor cells in the subventricular zone (SVZ). We explored whether MCAO leads to hypoxia, changes in vessel density, and angiogenesis in the ipsilateral SVZ and adjacent striatum, and determined the relation between the migrating neuroblasts and the vasculature.

Methods—Adult rats were subjected to 2 hours of MCAO. Hypoxia was studied by injecting Hypoxyprobe-1 during MCAO or 6 weeks later. Vessel density and length was estimated using stereology. New cells were labeled with 5′-bromo-2′deoxyuridine (BrdU) during weeks 1 and 2 or 7 and 8 after MCAO, and angiogenesis was assessed immunohistochemically with antibodies against BrdU and endothelial cell markers. Distance from neuroblasts to nearest vessel was measured using confocal microscopy.

Results—The ischemic insult caused transient hypoxia and early, low-grade angiogenesis, but no damage or increase of vascular density in the SVZ. Angiogenesis was detected during the first 2 weeks in the dorsomedial striatum adjacent to the SVZ, which also showed long-lasting increase of vascularization. At 2, 6, and 16 weeks after MCAO, the majority of neuroblasts migrated through this area toward the damage, closely associated with blood vessels.

Conclusions—The vasculature plays an important role for long-term striatal neurogenesis after stroke. During several months, neuroblasts migrate close to blood vessels through an area exhibiting early vascular remodeling and persistently increased vessel density. Optimizing vascularization should be an important strategy to promote neurogenesis and repair after stroke. (***Stroke***. 2007;38:3032-3039.)

Key Words: angiogenesis ■ hypoxia ■ neurogenesis ■ stroke

I schemic stroke, induced by middle cerebral artery occlusion (MCAO), leads to increased proliferation of neural stem/progenitor cells in the ipsilateral subventricular zone (SVZ)[1,2] and migration of neuroblasts into the damaged striatum,[3–5] a region where neurogenesis does not normally occur. Many stroke-generated neuroblasts differentiate into mature neurons with the phenotype of striatal projection neurons.[3] Striatal neurogenesis continues for several months after stroke.[6]

Experimental evidence has indicated a close link between neurogenesis and angiogenesis in the adult brain. In the songbird, testosterone-induced angiogenesis leads to neurogenesis in the striatum.[7] In the subgranular zone of the rat dentate gyrus, proliferating cells giving rise to granule cells are closely associated with the vasculature and dividing endothelial cells.[8] After 1 electroconvulsive seizure, endothelial cell proliferation in the dentate gyrus occurs concomi-

tantly with proliferation of subgranular zone neural precursors.[9] These findings indicate that in the dentate gyrus, neurogenesis occurs within an angiogenic niche. Importantly, endothelial cells secrete soluble factors, which stimulate neural stem cell proliferation and neurogenesis.[10]

Stroke leads to angiogenesis in the ischemic hemisphere and peri-infarct area.[11] This area is hypoxic, which probably triggers angiogenesis through the vascular endothelial growth factor system.[12] Neuroblasts migrate in association with blood vessels in the mouse striatum during the first weeks after stroke.[13] New neuroblasts are recruited to an area in the peri-infarct cortex, exhibiting endothelial cell proliferation for the first days after cortical stroke.[14] Whether SVZ is hypoxic during transient MCAO and whether this insult triggers angiogenesis in the SVZ and the area of neuroblast migration during long-term neurogenesis is unknown. Some evidence has suggested coregulation of angiogenesis and

Stroke **is available at http://stroke.ahajournals.org**   **DOI: 10.1161/STROKEAHA.107.488445**

79

neurogenesis in the SVZ. Microarray analysis shows concomitant upregulation of genes associated with neurogenesis and angiogenesis in SVZ at 7 days after stroke in mice.[15] Moreover, a cortical lesion that induces migration of neuroblasts into the striatum[16] has been reported to trigger endothelial cell proliferation at 5 days and increased number of blood vessels 2 days later in ipsilateral SVZ.[17]

Here we studied the relation between vasculature and new neurons during long-term neurogenesis after 2 hours of MCAO in rats. The objectives were 3-fold. First, the objective was to determine the distribution of hypoxia in SVZ and adjacent striatum through which neuroblasts migrate toward the damage. This seems highly warranted because hypoxia stimulates angiogenesis[12] and proliferation and differentiation of neural progenitors in vitro[18] and in vivo.[19] The second objective was to explore whether MCAO causes changes in vascularization in SVZ and adjacent striatum, and whether these changes are attributable to angiogenesis. The third objective was to analyze the distribution of neuroblasts at various distances from blood vessels at different time points after MCAO.

Materials and Methods

Animals and Experimental Design
Male Wistar rats (280 to 320 grams; B&K Universal, Sollentuna, Sweden) were housed under 12-hour light/dark cycle with ad libitum access to food and water. Experimental procedures followed guidelines established by the Malmö-Lund Ethics Committee.

For analysis of hypoxia, animals were subjected to 2 hours of MCAO (n=10) or sham surgery (n=3) and injected with Hypoxyprobe-1 (60 mg/kg intraperitoneal; Chemicon) 30 minutes after the start of occlusion to have the probe (with half-life of 0.5 hour) present during the insult and avoid confounding effects of anesthesia or intubation. Rats were euthanized directly after the onset of reperfusion (n=6) or 4 days later (n=7). In a separate experiment, Hypoxyprobe-1 was injected 6 weeks after 2 hours of MCAO (n=3) or sham surgery (n=2), and rats were perfused 2 hours thereafter.

For analysis of angiogenesis, rats were injected with BrdU (50 mg/kg, intraperitoneal) twice daily during weeks 1 and 2 (n=5) or 7 and 8 (n=4) after 2 hours of MCAO. Sham-operated animals (n=3) were injected with BrdU during weeks 1 and 2. Rats were perfused directly after the end of injections. Another group of rats was injected with BrdU 3 times daily during days 3 and 4, 7 and 8, or 11 and 12 after 2 hours of MCAO, and perfused 48 hours after last injection (n=3 in each group).

For analysis of vessel density and length and distance between neuroblasts and blood vessels, animals were subjected to 2 hours of MCAO or sham surgery and perfused 2, 6, or 16 weeks later (n=4 in each group).

MCAO
Transient MCAO was induced by the intraluminal filament technique.[20,21] After being fasted overnight, rats were anesthetized with N_2O and O_2 (70%:30%) and 1.5% isoflurane (Abbott Scandinavia) and intubated. A silicone rubber-coated nylon monofilament was inserted into the internal carotid artery and advanced past the origin of the middle cerebral artery. For sham surgery, the filament was advanced only a few millimeters inside the internal carotid artery. After 2 hours of occlusion, the animals were re-anesthetized and the filament was withdrawn. Physiological parameters were monitored during the entire procedure. Body temperature was regulated for 4 hours after MCAO. Only animals that showed no or incomplete forelimb placing with rotational asymmetry 24 hours after MCAO were included in the subsequent analysis.

Immunohistochemistry
After transcardial perfusion with 4% ice-cold paraformaldehyde, brains were post-fixed overnight in paraformaldehyde and sectioned coronally at 30 μm on dry ice. Before stainings using diaminobenzidine, sections were quenched for 20 minutes in 3% H_2O_2 and 10% methanol. Before BrdU-stainings, sections were incubated in HCl (1 mol/L) at 65°C for 10 minutes and at room temperature for 20 minutes. After preincubation with appropriate normal sera, sections were incubated overnight at 4°C with either of the following primary antibodies: rat anti-BrdU (1:100; Harlan Sera-Laboratory, Loughborough, UK), goat anti-doublecortin (Dcx; 1:400; Santa Cruz Biotechnology, Santa Cruz, Calif), mouse anti-NeuN (1:100; Chemicon), mouse anti-rat endothelial cell antigen (RECA; 1:400; AbD Serotec, Raleigh, NC), rabbit anti-laminin (1:100; Sigma; St Louis, Mo), or mouse anti-Ki67 (1:50; Novocastra Laboratories, Newcastle-on-Tyne, UK) in appropriate normal sera. Stainings were visualized by incubation for 2 hours with Cy3-conjugated (1:200; Jackson ImmunoResearch, West Grove, Pa), Cy5-conjugated (1:200; Jackson), or biotinylated secondary antibodies (1:200; Vector Laboratories, Burlingame, Calif), followed by Alexa 488-conjugated streptavidin (1:200; Molecular Probes, Eugene, Ore) for 2 hours for double stainings, or avidin-biotin-peroxidase complex for 1 hour followed by treatment with diaminobenzidine (0.5 mg/mL) and hydrogen peroxide for single stainings. For the latter, sections were dehydrated, mounted on glass slides, and cover-slipped.

For detection of hypoxia, sections were incubated with a primary monoclonal mouse antibody against Hypoxyprobe-1 (1:200; Chemicon) overnight at 4°C, followed by diaminobenzidine visualization and cresyl violet counter stain.

For Fluoro-Jade staining, sections were pretreated with 0.06% permanganate for 15 minutes, rinsed with distilled H_2O, and immersed in Fluoro-Jade solution for 30 minutes (0.001% Fluoro-Jade in distilled H_2O with 0.1% acetic acid).

Morphometric Analysis

Estimation of Vessel Density and Length
Density of microvessels in SVZ and adjacent striatum was estimated with computer-generated isotropic virtual planes[22] using computer-assisted stereology (version 2.3.5.1; Visiopharm). Taking into consideration the number of intersections between isotropic virtual planes and vessels, number of sampling box corners hitting the reference space, and total area of isotropic planes in each box,[22] the computer-assisted stereology software calculates the vessel global spatial density.

By multiplying the global spatial density with the total volume of the reference space, measured with Cavalieri's principle,[23] an unbiased stereological assessment of global vessel length, L, is yielded. Using these methods, vessel density and length were estimated in SVZ and in a 500-μm-wide column adjacent to SVZ (zone 1). This column was further divided in the dorso-ventral direction into 3 equally spaced zones (zone 1a, zone 1b, and zone 1c).

The analysis was performed using a Nikon Eclipse 80i microscope with a motorized specimen stage controlling movements in the x–y axis. Sections were immunostained for RECA, counterstained with cresyl violet, and vessels analyzed at 40× magnification. A 3-dimensional sampling box (counting frame area 3329 μm^2; sampling box height 13 μm; guard area 2 μm at the top of the section) was focused through the section. Within this box, virtual planes were generated with a fixed plane separation of 25 μm. In each animal and region analyzed, ≈150 to 200 blood vessel intersections with the virtual planes were counted in 4 evenly distributed sections.

Estimation of Angiogenesis
Sections were stained with antibodies against BrdU, RECA, and laminin. BrdU$^+$/RECA$^+$ cells in SVZ and zone 1 were first counted in an epifluorescence microscope (Olympus BX-61), and double-labeled candidates were then analyzed for BrdU/RECA/laminin triple-labeling in a laser scanning confocal microscope (Leica).
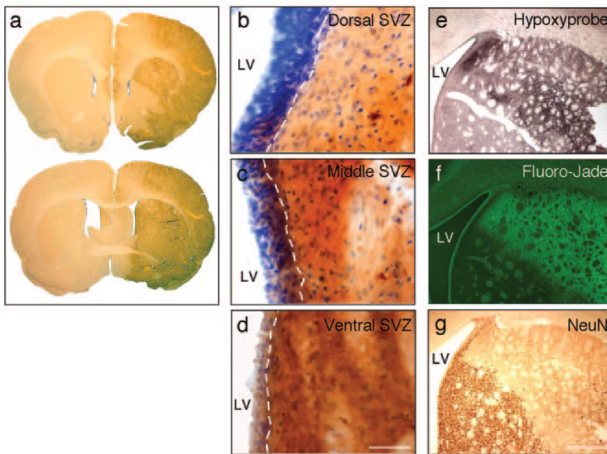
Figure 1. Stroke induces transient hypoxia in SVZ. Distribution of Hypoxyprobe-1 staining (a) at 2 coronal levels from an animal perfused directly after 2 hours of MCAO. Photographs (b through d) of different parts of ipsilateral SVZ directly after 2 hours of MCAO. Sections were stained for Hypoxyprobe-1 (brown) and counterstained with cresyl-violet (blue). Note that Hypoxyprobe-1 labeling is more extensive in ventral SVZ. Photographs of Hypoxyprobe-1 (e), Fluoro-Jade (f), and NeuN (g) staining in dorso-lateral striatum 4 days after 2 hours of MCAO in sections from the same animal. Note that the striatal area showing neuronal degeneration (labeled with Fluoro-Jade and without NeuN staining) corresponds to the hypoxic area. Scalebar is 50 μm in b through d, and 500 μm in e through g. LV indicates lateral ventricle.

Analysis of Neuroblast–Vessel Relationship

Number of Dcx$^+$ neuroblasts was quantified in zones 1a, 1b, and 1c in 3 sections double-stained with antibodies against Dcx and RECA. Approximately 100 Dcx$^+$ cells in each animal, randomly sampled in zone 1a, were then analyzed by generating 3-dimensional z-stacks in the confocal microscope. Within these z-stacks, the distance from each Dcx$^+$ cell to nearest vessel was measured.

Statistical Analysis

All values are means±SEM. One-way ANOVA with Fischer post hoc test was used to assess differences between groups, and paired t test within the same animals. Differences were considered significant at $P<0.05$.

Results

Subventricular Zone Is Transiently Hypoxic After MCAO

We first assessed the distribution of hypoxia using Hypoxyprobe-1 staining. Hypoxyprobe-1 forms irreversible adducts with intracellular and extracellular proteins under hypoxic conditions (Po$_2$ <10 mm Hg).[24] These adducts can be visualized by immunohistochemistry. After 2 hours of MCAO, with Hypoxyprobe-1 injected during the occlusion and rats euthanized immediately thereafter, all animals showed stained cells and extracellular matrix ipsilaterally in the cerebral cortex, striatum, and SVZ (Figure 1a). Caudally, Hypoxyprobe-1 staining was detected in most of the ipsilateral hemisphere (Figure 1a). Staining was absent contralaterally and in sham-operated animals.

The distribution of Hypoxyprobe-1 staining in ipsilateral SVZ directly after 2 hours of MCAO was similar in all animals. Staining was absent rostrally but, moving caudally, became visible in lateral cell layers (Figure 1c). Typically, Hypoxyprobe-1 staining was uneven and less intense in the dorsal SVZ (Figure 1b) than in the more ventral parts (Figure 1c and 1d). More caudally, labeling extended from the middle SVZ to the ventral tip, with all cell layers being stained (Figure 1d).

To determine whether the distribution of hypoxic areas correlated with those showing neuronal loss, we injected Hypoxyprobe-1 during 2 hours of MCAO or sham surgery and perfused the animals 4 days later. This time point was chosen for the stroke-induced neuronal degeneration to be virtually complete.[25] All MCAO animals showed Hypoxyprobe-1 staining in the ipsilateral SVZ, striatum, and cerebral cortex (Figure 1e), whereas we observed no staining contralaterally or in sham-operated animals. Also, the dorsal SVZ was stained, indicating that the entire SVZ had been hypoxic as a result of the insult.

We then explored whether the Hypoxyprobe-1–labeled areas exhibited ischemic damage. Fluoro-Jade staining (degenerating neurons) and loss of NeuN-positive cells (mature neurons) were found in striatal and cortical areas labeled with Hypoxyprobe-1 (Figure 1e through 1g). Fluoro-Jade labeling and loss of NeuN-stained or cresyl violet-stained cells never extended into SVZ.

Neurogenesis continues for several months after stroke,[6] and hypoxia can stimulate proliferation and differentiation of neural stem/progenitor cells.[19] We hypothesized that SVZ hypoxia may extend beyond the acute phase. Hypoxyprobe-1 was injected 6 weeks after 2 hours of MCAO or sham surgery and animals perfused 2 hours thereafter. We found no Hypoxyprobe-1 labeling in the ipsilateral SVZ.

Subventricular Zone Exhibits Long-Term Increase of Volume and Transient Decrease of Vessel Density After Stroke

We have previously shown expansion of the ipsilateral SVZ at 2 and 6 weeks after 2 hours of MCAO.[6] Here we found that the increased SVZ volume is maintained at the same level 16 weeks after the insult (Figure 2a). We hypothesized that this expansion may have been caused by increased vascularization. However, in comparison to sham-operated animals, vessel density in the SVZ of rats subjected to 2 hours of MCAO was decreased at 2 and 6 weeks but not different at 16
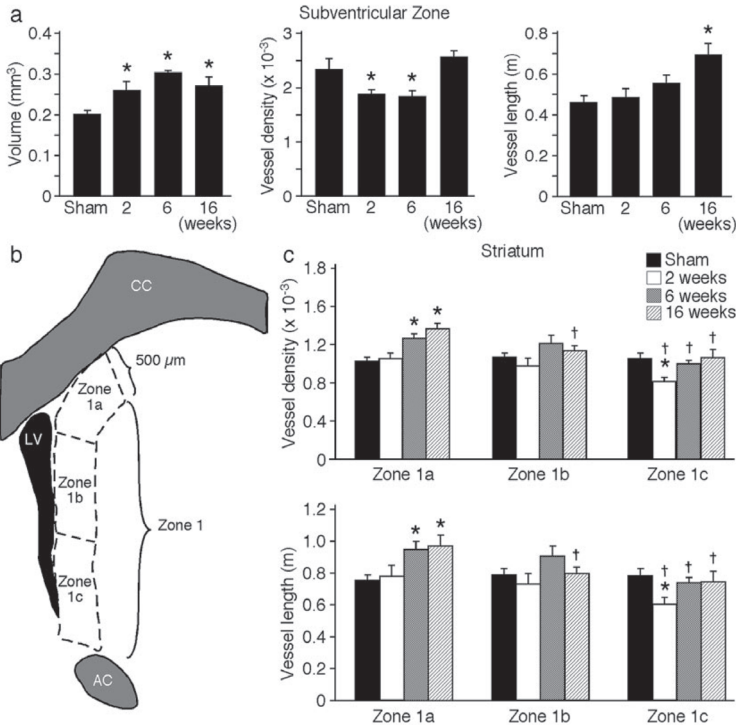
Figure 2. Stroke induces transient decrease of vessel density in SVZ and long-term increase of SVZ volume and vessel density in adjacent striatum. SVZ (a) volume, vessel density, and length in sham animals and at 2, 6, and 16 weeks after 2 hours of MCAO. Schematic drawing (b) of zone 1 and its subzones. Vessel density and length (c) in zones 1a, 1b, and 1c in sham animals and at 2, 6, and 16 weeks after 2 hours of MCAO. Means±SEM, n=4 in each group. *$P<0.05$ compared with sham, one-way ANOVA with Fisher post-hoc test. †$P<0.05$ compared with corresponding zone 1a, paired t test. AC indicates anterior commissure; CC, corpus callosum.

weeks after the insult (Figure 2a). The total vessel length was higher than sham at 16 weeks (Figure 2a).

Vessel Density Is Increased Long-Term in Striatum Adjacent to Subventricular Zone After Stroke

We wanted to determine whether 2 hours of MCAO gave rise to changes in vascularization in striatum close to SVZ. The area of striatum encompassing the first 500 μm outside the SVZ was delineated zone 1 (Figure 2b). This area, which consists mostly of intact striatal tissue located between the SVZ and the ischemic core, comprises the majority of the neuroblasts generated after stroke.[6] During 2 hours of MCAO, the ventro-caudal part of zone 1 was hypoxic, as indicated by Hypoxyprobe-1 staining (Figure 1d), and 4 days later exhibited neuronal degeneration. The dorso-rostral part of zone 1 was neither hypoxic nor damaged.

When the entire zone 1 was analyzed, no differences compared with sham-operated animals in vessel density or length were detected after MCAO. We then subdivided zone

1 in the dorso-ventral direction into 3 equally sized subzones (termed zone 1a, 1b, and 1c, respectively; Figure 2b), and found increased vessel density and length in zone 1a at both 6 and 16 weeks after 2 hours of MCAO (Figure 2c). Vessel density and length were higher in zone 1a than in the most ventral part, zone 1c, at all time points. Zone 1b did not exhibit any changes, nor did we observe any differences in vascularization between zone 1a, 1b, or 1c in sham-operated animals. Because of the variability in the extent of the ischemic lesion, analysis of vessel density in the striatal area between 750 and 1250 μm outside the SVZ was inconclusive.

Angiogenesis Occurs in Striatum and Subventricular Zone Short-Term After Stroke

To determine whether the ischemic insult and the associated hypoxia triggered angiogenesis, we counted proliferating endothelial cells in the ipsilateral SVZ and in zones 1a, 1b, and 1c of the adjacent striatum. Proliferating cells were labeled by BrdU injections during weeks 1 and 2 or weeks 7 and 8 after 2 hours of MCAO, and animals were euthanized
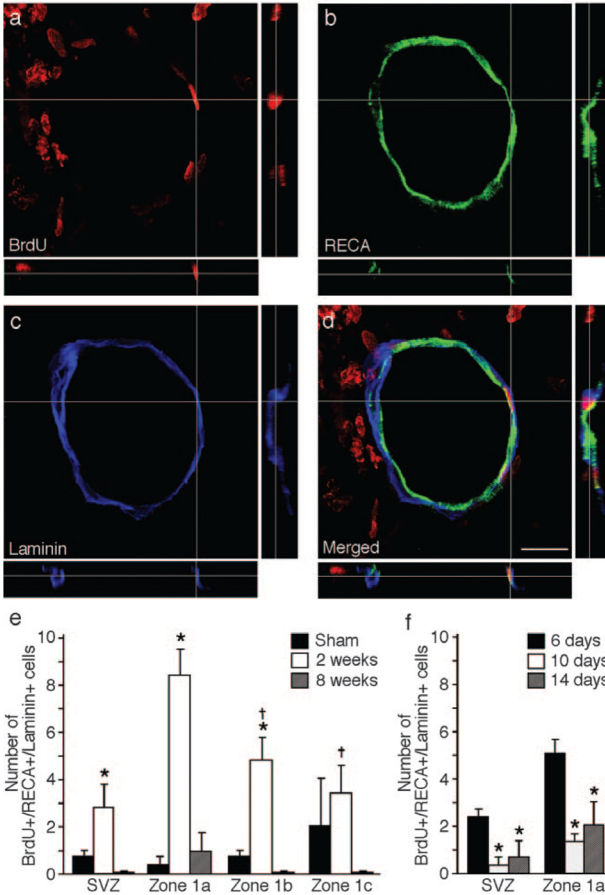
Figure 3. Stroke induces low-grade angiogenesis in SVZ and adjacent striatum. Confocal images (a through d) of a BrdU$^+$/RECA$^+$/laminin$^+$ cell in zone 1a at 2 weeks after 2 hours of MCAO. Orthogonal reconstructions of a triple-labeled cell as viewed in the x–z (bottom) and y–z (right) planes. Number of BrdU$^+$/RECA$^+$/laminin$^+$ cells (e) in zones 1a, 1b, and 1c and SVZ in animals given BrdU during weeks 1 and 2 or weeks 7 and 8 after 2 hours of MCAO and analyzed directly thereafter. Number of BrdU$^+$/RECA$^+$/laminin$^+$ cells (f) in zone 1a and SVZ in animals given BrdU days 3 and 4, 7 and 8, or 11 and 12 and perfused 48 hours later. Means±SEM, n=4 in (e) and n=3 in (f). *$P<0.05$ compared with sham or 6 days, one-way ANOVA with Fisher post-hoc test. †$P<0.05$ compared with corresponding zone 1a, paired t test. Scalebar is 15 μm.

directly thereafter. Endothelial cells were identified using antibodies against RECA, and BrdU$^+$/RECA$^+$ cells were counted in an epifluorescence microscope. To confirm that they were endothelial cells, BrdU$^+$/RECA$^+$ candidates were analyzed for triple-labeling also against laminin using confocal microscopy (Figure 3a through 3d). In the SVZ, there was a minor increase in the number of BrdU$^+$ endothelial cells at 2 weeks but not at 8 weeks after the ischemic insult (Figure 3e). These findings argue against late endothelial cell proliferation as the mechanism underlying the increased vessel length at 16 weeks. Hypothetically, vessel length had increased through so-called intussusceptive angiogenesis, ie, the splitting of 1 vessel into 2 without endothelial cell proliferation.[26] Endothelial cell proliferation in zone 1a was increased at 2 weeks after stroke (Figure 3e). Angiogenesis was also stimulated in zone 1b, but proliferating endothelial

cells were fewer than in zone 1a, and angiogenesis was unchanged in zone 1c. In all zones, BrdU$^+$ endothelial cells were found only in large, transversely cut arterioles or venules. At 8 weeks after 2 hours of MCAO, endothelial cell proliferation in zones 1a, 1b, and 1c was not different from that in sham-operated controls (Figure 3e).

We found that most of the stroke-induced angiogenesis occurred early after the insult. In animals injected with BrdU during days 3 and 4, 7 and 8, or 11 and 12 after 2 hours of MCAO and perfused 48 hours later, more BrdU$^+$ endothelial cells were detected at 6 days after stroke, compared with at 10 and 14 days in both SVZ and zone 1a (Figure 3f). However, the angiogenic response was minor and transient, as indicated also by our findings using the cell cycle marker Ki67. We observed no Ki67$^+$/RECA$^+$ cells in the either zone 1a or SVZ of rats perfused at 6, 10, or 14 days after 2 hours of MCAO.
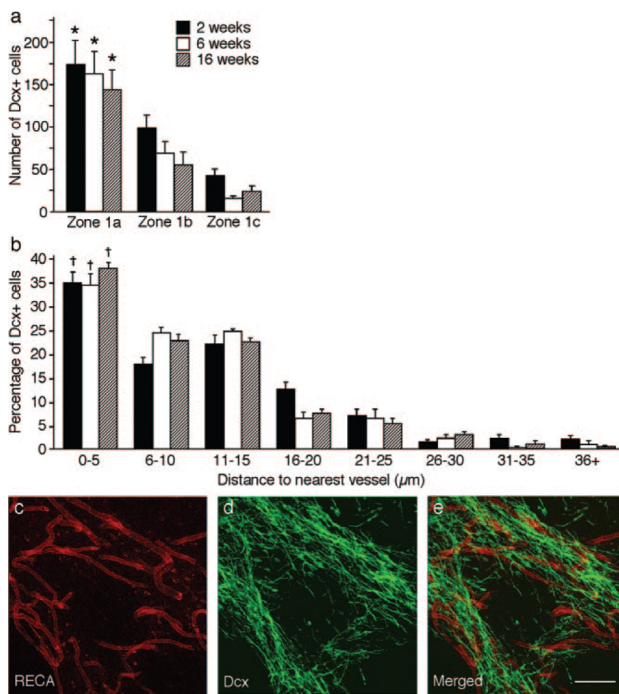
Figure 4. Neuroblasts migrate long-term after stroke close to blood vessels in striatal subzone with increased vascularization. Number of Dcx$^+$ cells (a) in zones 1a, 1b, and 1c and percentage of neuroblasts (b) located at various distances to nearest vessel at different time points after 2 hours of MCAO. Confocal images (c through e) showing close association between RECA$^+$ vessels (c) and Dcx$^+$ neuroblasts (d) in zone 1a at 2 weeks after MCAO. Generated from a z-stack of 25 planes, each 0.5 μm thick. Means±SEM, n=4 in each group. *$P<0.05$ compared with zones 1b and 1c, paired t-test. †$P<0.05$ compared with all other distances, paired t test. Scalebar is 50 μm.

Neuroblasts Formed After Stroke are Associated With Blood Vessels

We wanted to determine the relation between neuroblasts migrating toward the damage and the vasculature in the striatal area adjacent to the SVZ. Consistent with our previous findings,[6] we observed high numbers of Dcx$^+$ neuroblasts in zone 1 at 2, 6, and 16 weeks after 2 hours of MCAO (Figure 4a). There was a clear gradient in the dorso-ventral direction within zone 1, with the majority of neuroblasts being distributed within zone 1a at all time points. Thus, the neuroblasts preferentially migrated in the striatal area exhibiting low-grade angiogenesis and increased vascular density (Figure 2c).

We measured the distance from each of 100±5 randomly sampled Dcx$^+$ cells within zone 1a to the nearest RECA-stained blood vessel. At all time points after MCAO (2, 6, and 16 weeks), ≈35% of the Dcx$^+$ cells in zone 1a were located within 5 μm from a vessel and 80% within 15 μm (Figure 4b). The Dcx$^+$ cells were predominantly found in large clusters in close association with vessels (Figure 4c through 4e).

Discussion

The present data show that stroke induced by 2 hours of MCAO in rats, which gives rise to increased progenitor proliferation in the SVZ and striatal neurogenesis lasting for many months,[6] causes hypoxia and early, low-grade angiogenesis, but no increase of vascularization in ipsilateral SVZ.

The ischemic insult also induces early angiogenesis and long-lasting increase of vessel density in dorso-medial striatum adjacent to SVZ. The majority of the stroke-generated neuroblasts migrate through this striatal area toward the ischemic damage and are closely associated with blood vessels.

Similar to what was recently described after 1 hour of MCAO in rats,[24] we detected intense Hypoxyprobe-1 immunostaining in the parietal cortex and striatum after 2 hours of MCAO. In addition, we found that the SVZ expressed Hypoxyprobe-1 immunoreactivity both when animals were analyzed directly and 4 days after the insult. Our data indicate that hypoxia in SVZ induced by 2 hours of MCAO was transient since no Hypoxyprobe-1 immunoreactivity was found when the probe was injected 6 weeks after the insult. Interestingly, overall SVZ cell proliferation is increased 4 days to 2 weeks after MCAO[1–3,6,27] but has returned to baseline at 6 weeks.[6] Our finding here raises the possibility that the SVZ hypoxia caused by MCAO stimulated cell proliferation in the early postischemic phase. Consistent with this interpretation, intermittent hypoxia in adult rats[19] and hypoxia/ischemia in perinatal rats[28] and neonatal mice[29] enhance proliferation of neural stem/progenitor cells in the SVZ.

Hypoxia is an important trigger also of angiogenesis.[12] In the subgranular zone, there is a close association between

angiogenesis and neurogenesis.[8] Approximately 37% of BrdU^{+} cells in this area in the intact brain were endothelial cells, indicating that the formation of new neurons occurs within an angiogenic niche. Our findings indicate that the situation in the SVZ is markedly different. We detected increased number of BrdU/RECA/laminin triple-labeled cells, validated with confocal microscopy, in the SVZ early after 2 hours of MCAO. However, the proliferating endothelial cells were few and represented <1% of all proliferating cells within the SVZ. Our data are at variance with those of Gotts and Chesselet,[17] who reported that BrdU/RECA double-labeled cells were common in the ipsilateral SVZ after a cortical lesion. The reason for this discrepancy, apart from different injury models, is unclear. In agreement with Gotts and Chesselet,[17] we found that BrdU/RECA/laminin triple-labeled cells were rare in sham-operated animals. Taken together, our data show only minor angiogenesis in the SVZ during the early phase after stroke, and provide little experimental support for the idea of a coregulation of neurogenesis and angiogenesis in the SVZ.

We found a close association between the neuroblasts and the striatal vasculature during long-term neurogenesis after stroke. First, at all time points, the majority of neuroblasts migrated toward the damage through the striatal area, which, compared with other areas adjacent to SVZ, exhibited long-lasting increase of vessel density and, during the first 2 weeks after the insult, endothelial cell proliferation. Second, the proximity of the neuroblasts to vessels was very similar at 2, 6, and 16 weeks, indicating that they migrate in the same way throughout long-term neurogenesis. In agreement with our findings, at 18 days after 30 minutes of MCAO in mice,[13] chains of neuroblasts were wound around endothelial cells. In another model, at 7 days after cortical stroke in mice,[14] neuroblasts were located in large numbers in physical proximity to endothelial cells in the peri-infarct cortex, where active vascular remodeling occurred. Our findings suggest that blood vessels may be important for the survival, migration, and differentiation of the closely located neuroblasts during long-term neurogenesis by endothelial release of factors such as brain-derived neurotrophic factor[30] and stromal cell-derived factor 1α.[14,31] Consistent with this idea, the migration of neuroblasts that express the stromal cell-derived factor 1 receptor CXCR4,[31] was inhibited by blocking stromal cell-derived factor 1/CXCR4 signaling at 4 to 6 weeks after 2 hours of MCAO.[6] However, the widely different number of neuroblasts in areas with rather similar vascular density (comparing, eg, zones 1a, 1b, and 1c) indicates that migration is dependent also on nonvascular factors.

Our data support the notion that the vasculature plays an important role for striatal neurogenesis after stroke. Several studies have identified factors, which, when administered in the early postischemic phase, stimulate both angiogenesis and neurogenesis and lead to improved functional recovery after stroke including, eg, vascular endothelial growth factor[32] and erythropoietin.[33] Optimizing vascularization may be an important strategy to promote neurogenesis and repair in the stroke-damaged brain.

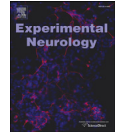## References

1. Zhang RL, Zhang ZG, Zhang L, Chopp M. Proliferation and differentiation of progenitor cells in the cortex and the subventricular zone in the adult rat after focal cerebral ischemia. *Neuroscience*. 2001;105:33–41.
2. Jin K, Minami M, Lan JQ, Mao XO, Batteur S, Simon RP, Greenberg DA. Neurogenesis in dentate subgranular zone and rostral subventricular zone after focal cerebral ischemia in the rat. *Proc Natl Acad Sci U S A*. 2001;98:4710–4715.
3. Arvidsson A, Collin T, Kirik D, Kokaia Z, Lindvall O. Neuronal replacement from endogenous precursors in the adult brain after stroke. *Nat Med*. 2002;8:963–970.
4. Parent JM, Vexler ZS, Gong C, Derugin N, Ferriero DM. Rat forebrain neurogenesis and striatal neuron replacement after focal stroke. *Ann Neurol*. 2002;52:802–813.
5. Jin K, Sun Y, Xie L, Peel A, Mao XO, Batteur S, Greenberg DA. Directed migration of neuronal precursors into the ischemic cerebral cortex and striatum. *Mol Cell Neurosci*. 2003;24:171–189.
6. Thored P, Arvidsson A, Cacci E, Ahlenius H, Kallur T, Darsalia V, Ekdahl CT, Kokaia Z, Lindvall O. Persistent production of neurons from adult brain stem cells during recovery after stroke. *Stem Cells*. 2006;24:739–747.
7. Louissaint A Jr, Rao S, Leventhal C, Goldman SA. Coordinated interaction of neurogenesis and angiogenesis in the adult songbird brain. *Neuron*. 2002;34:945–960.
8. Palmer TD, Willhoite AR, Gage FH. Vascular niche for adult hippocampal neurogenesis. *J Comp Neurol*. 2000;425:479–494.
9. Hellsten J, Wennstrom M, Bengzon J, Mohapel P, Tingstrom A. Electroconvulsive seizures induce endothelial cell proliferation in adult rat hippocampus. *Biol Psychiatry*. 2004;55:420–427.
10. Shen Q, Goderie SK, Jin L, Karanth N, Sun Y, Abramova N, Vincent P, Pumiglia K, Temple S. Endothelial cells stimulate self-renewal and expand neurogenesis of neural stem cells. *Science*. 2004;304:1338–1340.
11. Hayashi T, Deguchi K, Nagotani S, Zhang H, Sehara Y, Tsuchiya A, Abe K. Cerebral ischemia and angiogenesis. *Curr Neurovasc Res*. 2006;3:119–129.
12. Marti HJ, Bernaudin M, Bellail A, Schoch H, Euler M, Petit E, Risau W. Hypoxia-induced vascular endothelial growth factor expression precedes neovascularization after cerebral ischemia. *Am J Pathol*. 2000;156:965–976.
13. Yamashita T, Ninomiya M, Hernandez Acosta P, Garcia-Verdugo JM, Sunabori T, Sakaguchi M, Adachi K, Kojima T, Hirota Y, Kawase T, Araki N, Abe K, Okano H, Sawamoto K. Subventricular zone-derived neuroblasts migrate and differentiate into mature neurons in the post-stroke adult striatum. *J Neurosci*. 2006;26:6627–6636.
14. Ohab JJ, Fleming S, Blesch A, Carmichael ST. A neurovascular niche for neurogenesis after stroke. *J Neurosci*. 2006;26:13007–13016.
15. Liu XS, Zhang ZG, Zhang RL, Gregg S, Morris DC, Wang Y, Chopp M. Stroke induces gene profile changes associated with neurogenesis and angiogenesis in adult subventricular zone progenitor cells. *J Cereb Blood Flow Metab*. 2007;27:564–574.
16. Gotts JE, Chesselet MF. Migration and fate of newly born cells after focal cortical ischemia in adult rats. *J Neurosci Res*. 2005;80:160–171.
17. Gotts JE, Chesselet MF. Vascular changes in the subventricular zone after distal cortical lesions. *Exp Neurol*. 2005;194:139–150.
18. Zhou L, Miller CA. Mitogen-activated protein kinase signaling, oxygen sensors and hypoxic induction of neurogenesis. *Neurodegener Dis*. 2006;3:50–55.
19. Zhu LL, Zhao T, Li HS, Zhao H, Wu LY, Ding AS, Fan WH, Fan M. Neurogenesis in the adult rat brain after intermittent hypoxia. *Brain Res*. 2005;1055:1–6.
20. Koizumi J, Yoshida Y, Nakazawa T, Ooneda G. Experimental studies of ischemic brain edema. 1. A new experimental model of cerebral

embolism in rats in which recirculation can be introduced in the ischemic area. *Jpn J Stroke.* 1986;8:1–8.

21. Zhao Q, Memezawa H, Smith ML, Siesjö BK. Hyperthermia complicates middle cerebral artery occlusion induced by an intraluminal filament. *Brain Res.* 1994;649:253–259.

22. Larsen JO, Gundersen HJ, Nielsen J. Global spatial sampling with iso-tropic virtual planes: Estimators of length density and total length in thick, arbitrarily orientated sections. *J Microsc.* 1998;191:238–248.

23. Gundersen HJ, Jensen EB. The efficiency of systematic sampling in stereology and its prediction. *J Microsc.* 1987;147:229–263.

24. Noto T, Furuichi Y, Ishiye M, Matsuoka N, Aramori I, Mutoh S, Yanagihara T, Manabe N. Temporal and topographic profiles of tissue hypoxia following transient focal cerebral ischemia in rats. *J Vet Med Sci.* 2006;68:803–807.

25. Kokaia Z, Andsberg G, Martinez-Serrano A, Lindvall O. Focal cerebral ischemia in rats induces expression of p75 neurotrophin receptor in resistant striatal cholinergic neurons. *Neuroscience.* 1998;84:1113–1125.

26. Djonov V, Baum O, Burri PH. Vascular remodeling by intussusceptive angiogenesis. *Cell Tissue Res.* 2003;314:107–117.

27. Zhang R, Zhang Z, Zhang C, Zhang L, Robin A, Wang Y, Lu M, Chopp M. Stroke transiently increases subventricular zone cell division from

28. Yang Z, Levison SW. Hypoxia/ischemia expands the regenerative capacity of progenitors in the perinatal subventricular zone. *Neuroscience.* 2006;139: 555–564.

29. Plane JM, Liu R, Wang TW, Silverstein FS, Parent JM. Neonatal hypoxic-ischemic injury increases forebrain subventricular zone neuro-genesis in the mouse. *Neurobiol Dis.* 2004;16:585–595.

30. Wang H, Ward N, Boswell M, Katz DM. Secretion of brain-derived neurotrophic factor from brain microvascular endothelial cells. *Eur J Neurosci.* 2006;23:1665–1670.

31. Robin AM, Zhang ZG, Wang L, Zhang RL, Katakowski M, Zhang L, Wang Y, Zhang C, Chopp M. Stromal cell-derived factor 1alpha mediates neural progenitor cell motility after focal cerebral ischemia. *J Cereb Blood Flow Metab.* 2006;26:125–134.

32. Sun Y, Jin K, Xie L, Childs J, Mao XO, Logvinova A, Greenberg DA. VEGF-induced neuroprotection, neurogenesis, and angiogenesis after focal cerebral ischemia. *J Clin Invest.* 2003;111:1843–1851.

33. Wang L, Zhang Z, Wang Y, Zhang R, Chopp M. Treatment of stroke with erythropoietin enhances neurogenesis and angiogenesis and improves neu-rological function in rats. *Stroke.* 2004;35:1732–1737.

asymmetric to symmetric and increases neuronal differentiation in the adult rat. *J Neurosci.* 2004;24:5810–5815.

Paper II

Functional integration of new hippocampal neurons following insults to the adult brain is determined by characteristics of pathological environment

James C. Wood [a,d,1], Johanna S. Jackson [a,d,1], Katherine Jakubs [a,d,2], Katie Z. Chapman [a,d], Christine T. Ekdahl [a,d,e], Zaal Kokaia [c,d], Merab Kokaia [b], Olle Lindvall [a,d,*]

[a] Laboratory of Neurogenesis and Cell Therapy, Lund University Hospital, SE-221 84 Lund, Sweden
[b] Experimental Epilepsy Group, Wallenberg Neuroscience Center, Lund University Hospital, SE-221 84 Lund, Sweden
[c] Laboratory of Neural Stem Cell Biology and Therapy, Lund University Hospital, SE-221 84 Lund, Sweden
[d] Lund Stem Cell Center, Lund University Hospital, SE-221 84 Lund, Sweden
[e] Division of Clinical Neurophysiology, Lund University Hospital, SE-221 84 Lund, Sweden

ARTICLE INFO

ABSTRACT

We have previously shown that following severe brain insults, chronic inflammation induced by lipopolysaccharide (LPS) injection, and status epilepticus, new dentate granule cells exhibit changes of excitatory and inhibitory synaptic drive indicating that they may mitigate the abnormal brain function. Major inflammatory changes in the environment encountering the new neurons were a common feature of these insults. Here, we have asked how the morphology and electrophysiology of new neurons are affected by a comparably mild pathology: repetitive seizures causing hyperexcitability but not inflammation. Rats were subjected to rapid kindling, i.e., 40 rapidly recurring, electrically-induced seizures, and subsequently exposed to stimulus-evoked seizures twice weekly. New granule cells were labeled 1 week after the initial insult with a retroviral vector encoding green fluorescent protein. After 6–8 weeks, new neurons were analyzed using confocal microscopy and whole-cell patch-clamp recordings. The new neurons exposed to the pathological environment exhibited only subtle changes in their location, orientation, dendritic arborizations, and spine morphology. In contrast to the more severe insults, the new neurons exposed to rapid kindling and stimulus-evoked seizures exhibited enhanced afferent excitatory synaptic drive which could suggest that the cells that had developed in this environment contributed to hyperexcitability. However, the new neurons showed concomitant reduction of intrinsic excitability which may counteract the propagation of this excitability to the target cells. This study provides further evidence that following insults to the adult brain, the pattern of synaptic alterations at afferent inputs to newly generated neurons is dependent on the characteristics of the pathological environment.

© 2011 Elsevier Inc. All rights reserved.

Introduction

Neural stem/progenitor cells in the adult dentate subgranular zone (SGZ) continuously generate new granule cells (Zhao et al., 2008) which develop functional inputs from the entorhinal cortex (van Praag et al., 2002) and outputs to the hilus and CA3 region (Toni et al., 2008). Synaptic integration of adult-born hippocampal neurons in the intact brain closely resembles that during development (Laplagne et al., 2006) and is conserved throughout life and in old age (Morgenstern et al., 2008). Pathological changes in the stem cell niche and environment encountered by the new neurons influence adult neurogenesis. For example, seizures and cerebral ischemia enhance hippocampal progenitor proliferation and neurogenesis (Bengzon et al., 1997; Parent et al., 1997; Liu et al., 1998) and epileptic insults can lead to aberrant migration of new granule cells (Parent et al., 1997; Parent, 2005). Inflammation is detrimental for the survival of new neurons early after they have been born (Ekdahl et al., 2003; Monje et al., 2003) and pathologies such as Alzheimer's can impair neurogenesis and maturation of new neurons in mice (Biscaro et al., 2009).

How new neurons integrate into existing neural circuitries will determine their action in the diseased brain. Recent experimental evidence indicates that pathological environments influence the morphological and functional integration of adult-born hippocampal neurons. Following kainate-induced status epilepticus (SE) in rats, new granule cells extend abnormal basal dendrites into the hilus and have more mushroom spines on their apical dendrites (Jessberger

* Corresponding author at: Laboratory of Neurogenesis and Cell Therapy, Wallenberg Neuroscience Center, Lund University Hospital, SE-221 84 Lund, Sweden. Fax: +46 46 222 0560.
E-mail address: olle.lindvall@med.lu.se (O. Lindvall).
[1] These authors contributed equally to this work.
[2] Present address: National Institute of Neurological Disorders and Stroke, National Institutes of Health, Bethesda, MD 20892, USA.

et al., 2007). We have demonstrated that dentate granule cells born after electrically-induced SE (eSE) in rats, i.e., into an environment characterized by neuronal death, spontaneous, recurrent seizures and inflammation, exhibit more inhibitory and less excitatory synaptic drive (alterations in frequency and/or amplitude of miniature postsynaptic currents) compared to new neurons from control animals (Jakubs et al., 2006). When exposed to lipopolysaccharide (LPS)-induced inflammation without seizure activity, new neurons respond with enhanced excitatory and inhibitory drive (Jakubs et al., 2008). Chronic inflammation also gives rise to larger clusters of the postsynaptic GABA receptor scaffolding protein gephyrin on dendrites of new cells (Jakubs et al., 2008). Thus, in pathological environments, adult-born neurons exhibit a high degree of plasticity at their afferent synapses, which may act to mitigate abnormal brain function.

Integration of adult-born neurons has so far been analyzed in pathological environments with pronounced inflammation. How integration is influenced by less severe insults is unknown. The objective of the present study was to determine the morphological and electrophysiological properties of new neurons which developed in a pathological environment with repeated seizures and minimal inflammation. Rats were subjected to an epileptic insult and subsequently exposed to stimulus-evoked seizures twice weekly. New granule cells were labeled 1 week after the initial insult using a retroviral (RV) vector encoding green fluorescent protein (GFP). After 6–8 weeks, new neurons were studied using confocal microscopy and whole-cell patch-clamp recordings. We show that these cells exhibit only minor differences in morphology. Electrophysiological recordings indicate the presence of enhanced afferent excitatory input on the new cells which may be counteracted by reduced membrane excitability. Taken together with our previous studies, these findings indicate that new neurons have mechanisms to counteract or adapt to pathologies at their afferent synaptic inputs, and that the pattern of changes is dependent on the characteristics of the environment.

Materials and methods

Animal groups and rapid kindling

All experimental procedures were approved by the Malmö–Lund Ethical Committee. One hundred and thirty-two male Sprague–Dawley rats were used, weighing 200–250 g at the beginning of the experiments. Animals were anesthetized with isofluorane (1.5–2%) and implanted unilaterally with a bipolar stainless steel stimulating/recording electrode (Plastics One, Roanoke, VA) in the ventral hippocampal CA1-CA3 region (coordinates: 4.8 mm caudal and 5.2 mm lateral to bregma, 6.3 mm ventral from dura, toothbar at −3.3 mm) (Paxinos and Watson, 1997). Another electrode was positioned between the skull and the adjacent muscle to serve as reference. Seven days later, animals were subjected to the rapid kindling protocol (40 stimulations, 1 ms square-wave pulses of 400 μA intensity with 100 Hz intratrain frequency for 10 s every 5 min). For comparisons of the inflammatory response, six rats were subjected to eSE as described previously (Jakubs et al., 2006). The electroencephalogram (EEG) was recorded continuously after stimulation until cessation of focal epileptiform activity (afterdischarge, AD) using Chart 3.6.3 (PowerLab7MacLab, AD Systems). Animals were monitored during this time and behavioral seizures were characterized according to the Racine scale (Racine, 1972). Only animals exhibiting grade 2 seizures and above, and with corresponding ADs were included. Controls were electrode-implanted but not exposed to electrical stimulation.

ELISA

Seven days after rapid kindling or corresponding time point in controls, rats were transcardially perfused with saline and whole hippocampus contralateral to the electrode was rapidly removed and frozen on dry ice. Samples were homogenized on ice in buffer (pH 7.6) containing in (mM): 50.0 Tris–HCl, 150 NaCl, 5.0 CaCl$_2$, 0.02% NaN$_3$, 1% Triton X-100, and then centrifuged at 17,000 times gravity for 30 min at +4 °C. Protein concentration was determined in supernatants by BCA protein assay (Pierce, USA) and all samples equilibrated to a concentration of 2 mg/ml total protein. IL-1β, IL-6, TNF-α, IL-10, and IL-4 concentrations were determined by ELISA (Duoset; R & D Systems, USA) according to manufacturer's instructions. Results are presented as means ± SEM, and statistical comparisons were performed using Student's unpaired *t*-test. Level of significance was $p < 0.05$.

Labeling of new neurons

Seven days after the rapid kindling procedure, rats were anesthetized with isofluorane and injected with a retrovirus containing the GFP gene (RV-GFP) under the CAG promoter (1.0–1.1 transducing units/ml) (Zhao et al., 2006). Two 1.5 μl retroviral injections were made in the dorsal hippocampus contralateral to the electrode (coordinates: 3.6 mm caudal and 2.0 mm lateral to bregma, and 2.8 mm dorsal to dura; 4.4 mm caudal and 3.0 mm lateral to bregma, and 3.0 mm dorsal to dura; toothbar at −3.3 mm).

Extra stimulations and assessment of excitability

Starting 2 days after retrovirus injections, animals subjected to rapid kindling were exposed to stimulus-evoked seizures twice weekly for 6–8 weeks. Before and after stimulations, EEG was recorded to determine baseline activity and to observe ADs. Recordings continued until cessation of ADs. Stimulations were delivered for 1 s at AD threshold, as determined by a 1 s 50 Hz electrical current, starting at 10 μA and with 10 μA increments until an AD was registered. At 5 weeks after retrovirus injections, EEG recordings were made on 4 seizure-exposed and 4 non-stimulated control animals for 1 h to assess the occurrence of interictal activity. Mean AD duration (using Chart 3.6.3) and seizure grade were determined for both rapid kindling and extra stimulations. Mean AD threshold was assessed for the extra stimulations. Total AD duration, and mean number and AD duration of partial (grades 1–2) and generalized (grades 4–5) seizures were also calculated per animal. Development of seizure threshold and seizure grade in response to the consecutive extra stimulations was analyzed using linear regression. Level of significance was $p < 0.05$.

Morphological analysis

At 6–8 weeks after virus injection, animals received an overdose of pentobarbital (250 mg/kg, i.p.) and were transcardially perfused with 100 ml saline and 250 ml 4% paraformaldehyde (PFA) in 0.1 M phosphate-buffered saline (PBS), pH 7.4. Brains were cryoprotected in 20% sucrose in 0.1 M PBS overnight, cut in 30 μm coronal sections and stored in cryoprotective solution. For characterization of the environment, animals were also perfused and their brains sectioned using the same protocol 1 week after rapid kindling or corresponding time point in controls. For analysis of gephyrin distribution, rats were anesthetized and decapitated, brains were dissected and placed in ice-cold artificial cerebrospinal fluid (aCSF, described below), cut in 300 μm transverse sections and placed in gassed aCSF for 20 min and then in PFA for 10 min (Jakubs et al., 2008). Sections were cryoprotected in 20% sucrose in 0.1 M PBS overnight, cut in 12 μm sections and stored at −20 °C for at least 1 h.

For immunohistochemistry, the following primary antibodies were used: rabbit anti-Iba1 (1:1000, Wako Chemicals), mouse anti-ED1 (1:200, Serotec), rabbit anti-GFP (1:10000, Abcam), goat anti-IL-1β (1:1000, R&D Systems), and mouse anti-gephyrin (1:10000, Synaptic Systems). Free-floating sections were incubated with the

appropriate primary antibody overnight at $+4\ °C$ and secondary antibody for 1 to 2 h at room temperature. Secondary antibodies were Cy3-conjugated donkey anti-rabbit (1:200, Jackson ImmunoResearch), biotinylated horse anti-mouse (1:200, Vector Laboratories), biotinylated horse anti-goat (1:200, Vector Laboratories), and FITC-conjugated donkey anti-rabbit (1:200, Jackson ImmunoResearch). Biotinylated antibodies were visualized using Streptavidin-conjugated Alexa Fluor-488 (1:200, Invitrogen). Sections were mounted on gelatin-coated microscope slides and coverslipped. For Fluoro-Jade staining, mounted sections were pre-treated with 0.06% potassium permanganate before being agitated for 30 min in 0.001% Fluoro-Jade (Histochem) in 0.01% acetic acid, immersed in xylene, and coverslipped with Pertex mounting medium (Histolab).

Cell counting and morphological analysis were performed ipsilaterally to the virus injections in 4 to 6 hippocampal sections by an observer blind to the treatment conditions as previously described (Jakubs et al., 2008). The number of Iba1+, Iba+/ED1+, and Fluoro-Jade+ cells were counted with an Olympus BX61 epifluorescence microscope in the granule cell layer (GCL) and two cell diameters below in the SGZ. Iba1/ED1 double labeling was confirmed by confocal microscopy. The morphological phenotype of Iba1+ cells in the SGZ and GCL was classified into four different subtypes, as previously described (Lehrmann et al., 1997), in 3–4 hippocampal sections. The relative occurrence of each subtype was expressed as the mean percentage of the total number of Iba1+ microglia per section. Stained sections were also examined for double labeling of Iba1+ cells with IL-1β. GFP+ cells were counted in the GCL, SGZ, dentate hilus, and molecular layer (ML). For all GFP+ cells, axon exit point, dendrite exit points, and total number of dendrites leaving the cell soma were analyzed. Dendritic polarity was determined by classifying the angles of the dendrites leaving the cell soma as 0–22°, 22.5–67°, or 67.5–90°, where 90° was perpendicular to the GCL. Location of dendritic branching was determined by assessing the cumulative number of branching points of each dendrite from the cell soma in 15 μm increments. To measure the number of branching points and total dendrite length, a confocal stack was taken of the whole dendritic tree of GFP+ cells in 225 μm thick hippocampal sections. Dendrite length was measured using the NeuronJ plug-in of ImageJ (Meijering et al., 2004).

Spine density (number of spines per micrometer) and morphology (classified as thin, stubby, filopodia, or mushroom spines) (Zhao et al., 2006), and gephyrin cluster density (clusters per micrometer) and size (area in square micrometers) were analyzed by confocal laser scanning microscopy (Bio-Rad MRC1021UV) using Kr-Ar 488 and 568 nm excitation filters with a 63× objective and 16× digital zoom. Analysis was carried out on 12 regions-of-interest (ROI, each 221.4 μm²) per animal on proximal and distal dendrites in the inner and outer ML, respectively. Cluster area was measured using ImageJ software (Sheffield, 2007).

Results are presented as means ± SEM, and analysis was performed using Student's unpaired t-test or one-way ANOVA with Bonferroni post-hoc test for multiple comparisons. Level of significance was $p < 0.05$.

Electrophysiological recordings

Six to 8 weeks after virus injections, rats were anesthetized with isofluorane and decapitated. Brains were placed in ice-cold, gassed (95% O_2, 5% CO_2) modified-aCSF (pH 7.2–7.4, 295–300 mOsm), containing (in mM): 225 sucrose, 2.5 KCl, 0.5 $CaCl_2$, 7.0 $MgCl_2$, 28.0 $NaHCO_3$, 1.25 NaH_2PO_4, 7.0 glucose, 1.0 ascorbate, and 3.0 pyruvate. Transverse dorsal hippocampal slices (225 μm), cut on a vibratome (3000 Deluxe, Ted Pella Inc, CA), were placed in an incubation chamber with gassed (95% O_2, 5% CO_2) aCSF (pH 7.2–7.4, 295–300 mOsm) containing (in mM): 119 NaCl, 2.5 KCl, 1.3 $MgSO_4$, 2.5

$CaCl_2$, 26.2 $NaHCO_3$, 1.0 NaH_2PO_4, and 11.0 glucose, and were allowed to rest for at least 1 h at room temperature before recordings.

Individual slices were placed in a submerged recording chamber and perfused with gassed aCSF at $+32$–$34\ °C$ during recordings of miniature excitatory postsynaptic currents (mEPSCs) to optimize event frequency for analysis (Jakubs et al., 2006, 2008), or at room temperature during recordings of miniature inhibitory postsynaptic currents (mIPSCs) and measurements of intrinsic membrane properties. Cells for recording were visualized using an Olympus upright microscope equipped with a digital camera. GFP-expressing cells were identified under a 40× water immersion lens using fluorescence microscopy. Infrared light with differential interference contrast was used for visual approach and acquiring whole-cell recordings. Recording pipettes with a final tip resistance of 2.5–5.5 MΩ were filled with pipette solution (pH 7.2–7.4, 295–300 mOsm) containing the following (in mM): 122.5 K-gluconate, 12.5 KCl, 10.0 KOH-HEPES, 0.2 KOH-EGTA, 2.0 MgATP, 0.3 Na_3-GTP, and 8.0 NaCl for current-clamp recordings of intrinsic properties; 135.0 CsCl, 10.0 CsOH, 0.2 CsOH-EGTA, 2.0 Mg-ATP, 0.3 Na_3-GTP, 8.0 NaCl and 5.0 lidocaine N-ethyl bromide (QX-314) for voltage-clamp recordings of mIPSCs; or 117.5 Cs-gluconate, 17.5 CsCl, 8.0 NaCl, 10.0 CsOH-HEPES, 0.2 CsOH-EGTA, 2.0 Mg-ATP, 0.3 Na_3-GTP, and 5.0 QX-314 for voltage-clamp recordings of mEPSCs. Biocytin (0.5%, Sigma-Aldrich) was freshly dissolved in the pipette solution before recordings for *post-hoc* identification of recorded cells. Seal resistance was >1 GΩ. For analysis of intrinsic membrane properties, resting membrane potential was estimated in current-clamp mode immediately after breaking the membrane and establishing whole-cell configuration. For measuring current–voltage relationship, 500 ms hyperpolarizing and depolarizing current pulses were delivered in 30 pA increments through the whole-cell pipette. Rheobase was determined by injecting a 300 pA ramp over 1 s. Intrinsic properties were measured in aCSF containing 50 μM D-AP5 and 5 μM NBQX (both Tocris) to block NMDA and non-NMDA receptors, respectively, and 100 μM picrotoxin (PTX) (Tocris) to block GABA$_A$ receptor activation. mIPSCs were recorded in aCSF containing 50 μM D-AP5, 5 μM NBQX, and 1 μM TTX (Tocris) to block action potentials. mEPSCs were recorded with 100 μM PTX and 1 μM TTX in aCSF. To confirm that recorded cells expressed GFP, fluorescence microscopy was used to detect GFP in the recording pipette, or *post-hoc* immunohistochemical analysis of GFP colocalization with biocytin was conducted.

Data were filtered at 2.9 kHz and sampled at 10 kHz with an EPC9 patch-clamp amplifier (HEKA Elektronik, Lambrecht, Germany). Miniature postsynaptic currents were detected and analyzed using MiniAnalysis software (Synaptosoft). Minimum amplitude for detection was set at 5 times root-mean-square noise level as determined by the software. All detected events were visually controlled. The 10–90% rise time of mEPSCs and mIPSCs were analyzed using MiniAnalysis. Analysis of intrinsic membrane properties was performed using one-way ANOVA with Bonferroni *post-hoc* test for multiple comparisons. Recording duration was 3 minutes and equal numbers of mEPSCs and mIPSCs from each cell were analyzed to prevent any bias. Group interevent intervals (IEIs), amplitudes, and 10–90% rise time were compared using Kolmogorov–Smirnov's statistical test. Mean event frequency was determined from an equal number of events from each cell, and analyzed using Student's unpaired t-test. Level of significance was $p < 0.05$.

Sections from electrophysiology experiments were fixed for 12–24 h in 4% PFA immediately after recordings and stored in antifreeze medium at $-20\ °C$. For double staining of biocytin and GFP, free floating sections were preincubated for 1 h in 5% serum in 0.25% Triton X-100 in potassium PBS, and then exposed to rabbit anti-GFP primary antibody (1:10000, Abcam) overnight at room temperature. Immunoreactivity was visualized using FITC-conjugated donkey anti-rabbit secondary antibody and Cy3-streptavidin (both 1:200, Jackson ImmunoResearch).

Sections were mounted on glass slides, coverslipped and analyzed using an Olympus BX61 epifluorescence microscope.

Results

Characteristics of the pathological environment

Animals were subjected to rapid kindling (40 supra-threshold stimulations over a period of 3 h and 15 min) followed by twice weekly extra stimulations at AD threshold for 6–8 weeks in order to expose new neurons (labeled with RV-GFP one week after the initial epileptic insult) to repeated seizures but only to mild, or no inflammation during their maturation (Fig. 1A). This protocol was based on our previous data showing that rapid kindling causes AD duration of similar length in the stimulated and non-stimulated hippocampus (Elmér et al., 1998), and on a pilot experiment which indicated that the number of activated microglia (a measure of inflammation) in the dentate gyrus correlated with the number of extra stimulations and generalized seizures and the total AD duration. Using this experimental paradigm, we could address the role of seizures, without introducing major inflammatory changes, on the integration of new neurons. Only animals which showed both behavioral (grade 2 and above) and electroencephalographic seizure activity (Fig. 1B) during rapid kindling and the extra stimulations were included in the study ($n = 36$). The rapid kindling paradigm produced 23.4 ± 0.4 partial (grade 1–2) and 2.4 ± 0.2 generalized (grades 4–5) seizures per animal, the mean AD duration of partial and generalized seizures was 28.1 ± 3.2 s and 55.7 ± 9.5 s, respectively. The total AD duration per animal during the rapid kindling protocol was 18.5 ± 2 min. The extra stimulations gave rise to 17.5 ± 1.5 partial and 11.8 ± 2.0 generalized seizures and a total AD duration of 9.9 ± 0.9 min per animal. The mean seizure grade progressively increased, and the threshold required to produce an AD gradually decreased (Fig. 1C) with increasing number of extra stimulations, providing evidence for the development of hyperexcitability. However, we observed no pathological interictal activity in the EEG of the seizure-exposed group at 5 weeks after retrovirus injection or during the extra stimulations, or in the electrode-implanted, non-stimulated group ($n = 4$ rats/group). These results indicate that the seizure paradigm used here caused development of hyperexcitability in response to stimulations. The occurrences of generalized seizures, in combination with data from previously published studies (Elmér et al., 1998), indicate that the seizure activity spread to both brain hemispheres.

We next assessed in detail the magnitude of inflammation in the seizure-exposed group, first by characterizing the microglial response. At 1 week after rapid kindling, at the time point when the new cells were born (labeled with RV-GFP), there was a modest, non-significant change in the number of activated microglia (Iba1+/ED1+ cells) in the SGZ/GCL ($n = 4$ rats/group×4–6 sections/rat, $p = 0.06$, Fig. 1D–F). Control animals exhibited 13.8 ± 3.5 Iba1+/ED1+ cells/section compared with 34.2 ± 8.3 cells/section 1 week after rapid kindling (148% increase), and 68.1 ± 6.5 cells/section 1 week after eSE (395% increase, $n = 6$ rats×4–6 sections/rat), prepared as in our previous study (Jakubs et al., 2006). We then explored whether rapid kindling gave rise to a change in the morphological phenotype of the microglia. The Iba1+ cells in SGZ/GCL were classified into ramified, intermediate, amoeboid, or round phenotypes using the morphological criteria described by Lehrmann et al. (1997). The severity of a pathological insult determines the degree of microglial activation, round phenotype signifying the most activated state. We observed no change of microglia phenotype at 1 week following rapid kindling ($n = 4$ rats/group×3–4 sections/rat, Fig. 1G), arguing against microglia activation. In contrast, when we assessed the morphology of microglia in sections from animals at 1 week after eSE, there was a significant change to a more activated phenotype as compared to control animals, i.e., a decrease of ramified and an increase of intermediate microglia in eSE animals ($n = 6$ rats×3–4 sections/rat,

see Supplementary Figure 1). Taken together, these results provide evidence that rapid kindling causes a mild pathology without the pronounced microglial activation observed after eSE.

We also assessed the magnitude of hippocampal inflammation at 1 week after rapid kindling by measuring the levels of inflammatory cytokines using ELISA (Fig. 1A). Consistent with our findings that rapid kindling did not cause microglial activation, no significant changes in the levels of IL-1β (control 1188 ± 53 pg/mg; seizures 1254 ± 67 pg/mg), TNF-α (control 146.2 ± 6.5 pg/mg; seizures 156.2 ± 8.7 pg/mg), IL-4 (control 173.7 ± 8.3 pg/mg; seizures 190.2 ± 9.0 pg/mg), IL-6 (control 1928 ± 52 pg/mg; seizures 2002 ± 87 pg/mg), and IL-10 (control 689.6 ± 28.5 pg/mg; seizures 719.6 ± 59.3 pg/mg) were detected in seizure-exposed compared to control animals ($n = 8$ rats/group). We also did not detect any seizure-induced, increased expression of the pro-inflammatory cytokine IL-1β in Iba1+ microglia in SGZ/GCL using immunohistochemistry (data not shown).

Fluoro-Jade staining revealed no significant neuronal degeneration in the dentate gyrus of the seizure-exposed animals 1 week after rapid kindling stimulations ($n = 4$ rats/group×4–6 sections/rat, Fig. 1H, I). Also, we obtained no evidence for chronic inflammation induced by rapid kindling and extra stimulations. Seven weeks after rapid kindling, the number of Iba1+/ED1+ cells did not differ between seizure-exposed and control animals ($n = 4$ rats/group×4–6 sections/rat, Fig. 1F). Taken together, our findings show that the new neurons generated 1 week after rapid kindling developed in an environment characterized by repeated seizures and gradual development of hyperexcitability but without significant neuronal death or inflammation.

Morphological integration of the new neurons in the pathological environment

Six to 8 weeks after virus injection, stable GFP expression was observed in a substantial number of new dentate granule cells in non-stimulated, electrode-implanted controls and seizure-exposed animals (Fig. 2A, B). In accordance with previous studies reporting that seizures enhance neural/stem progenitor cell proliferation (Bengzon et al., 1997; Parent et al., 1997; Scott et al., 1998), there were noticeably more new GFP+ cells in seizure-exposed animals compared to control animals. The distribution of the new cells within the GCL did not differ between seizure-exposed and non-stimulated animals, the majority being located within the inner GCL ($n = 8$ control rats, 5 seizure-exposed rats×4–6 sections/rat, Fig. 2C). Very few aberrant neurons were observed in the hilus in both groups. The total number of dendrites per new cell (control 1.3 ± 0.07; seizures 1.1 ± 0.08), and the polarity of dendrites leaving the cell soma did not differ between the groups, most of the dendrites leaving at a 67.5–90° angle in relation to the GCL (control $72.0 \pm 7.1\%$; seizures $56.7 \pm 3.7\%$) ($n = 7$ control rats, 6 seizure-exposed rats×4–6 sections/rat). Dendrite development was similar in seizure-exposed and control new cells, as no differences were detected in, (i) dendrite length (control 1.87 ± 0.15 mm; seizures 1.95 ± 0.16 mm; $p > 0.05$), (ii) dendrite exit point from cell soma or number of recurrent basal dendrites (Fig. 2D), or (iii) number of branching points (control 8.3 ± 1.15 points/cell; seizures 6.3 ± 0.49 points/cell; $p > 0.05$) or location of dendrite branches (Fig. 2E). Axons primarily originated from the basal (control 80.0%; seizures 79.2%) and medial soma (control 16.0%; seizures 18.8%) and rarely from the apical side (control 4.0%; seizures 2.0%). These results indicate that the pathological environment caused by rapid kindling and repeated extra stimulations did not interfere with the gross morphological appearance of the new neurons.

We next investigated whether the pathological environment affected the morphological development of the synaptic inputs on the new granule cells. Using confocal microscopy and ImageJ we did not detect any difference in the total spine density in the inner or outer ML between the seizure-exposed and non-stimulated group ($n = 8$ rats/group×12 ROI/rat, Fig. 2F). We next examined the individual spine
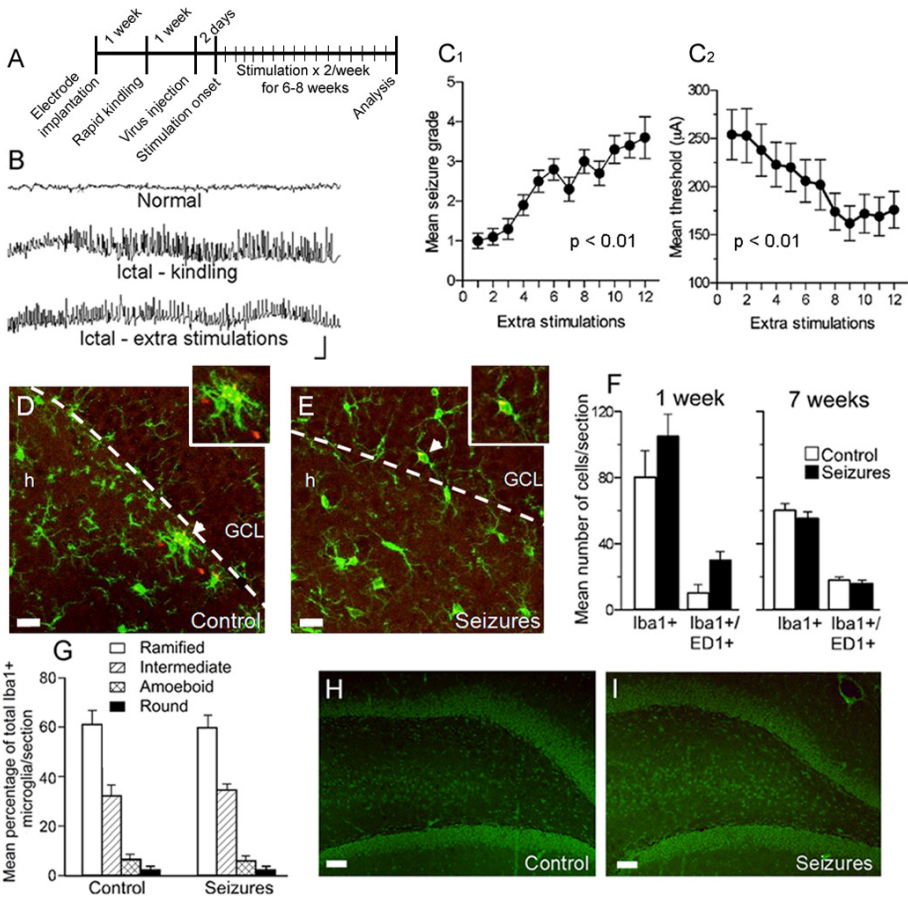
Fig. 1. Pathological environment is characterized by repeated seizures and no significant inflammation. A, Schematic representation of experimental timeline. B, EEG recordings from electrode-implanted animals showing baseline activity (top) before stimulations, high-frequency ictal activity following stimulation during the rapid kindling protocol (middle), and high-frequency ictal activity following an extra stimulation (bottom). Scale bar is 2 s, 1 mV. C_1, Increased seizure grade and (C_2) decreased seizure threshold in response to the extra stimulations (Means ± SEM, linear regression). Iba1+ (green), ED1+ (red), and Iba1+/ED1+ (yellow, arrowheads, inset) cells 1 week after rapid kindling in control (D) and seizure-exposed (E) animals (h, hilus; GCL, granule cell layer). F, Minimal increase of activated microglia (Iba1+/ED1+ cells) 1 week after rapid kindling and no difference compared to control at 7 weeks. G, No differences between seizure-exposed and control animals in morphological phenotype of Iba1+ microglia. Lack of Fluoro-Jade-stained degenerating neurons in control animals 2 weeks after electrode implantation (H) and in seizure-exposed animals 1 week after rapid kindling (I). Scale bars = 10 μm. Means ± SEM.

subtypes based on their morphology. Filopodia and stubby spines are considered immature spine phenotypes whereas thin and mushroom spines are regarded as more mature (Nimchinsky et al., 2002). There was no difference in the density of thin and mushroom spines or in filopodia between the two groups. However, the seizure-exposed group had significantly more stubby spines than the non-stimulated group (Fig. 2F), indicating that this pathological environment induced subtle alterations of excitatory synapses. We have previously reported that chronic inflammation causes increased size of gephyrin clusters on the

dendrites of new dentate granule cells (Jakubs et al., 2008). Gephyrin is a scaffolding protein associated with clustering of glycine and $GABA_A$ receptors at inhibitory synapses (Fritschy et al., 2008). Here we found that the density of gephyrin clusters on the dendrites of the new cells was similar in control and seizure-exposed animals (0.16 ± 0.03 cluster/μm and 0.20 ± 0.02 cluster/μm, respectively, $p > 0.05$, $n = 5$ rats/group × 12 ROI/rat) (Fig. 2G, H). Furthermore, the gephyrin cluster size did not differ between the groups (control 0.19 ± 0.01 μm²; seizures 0.19 ± 0.01 μm², $p > 0.05$).
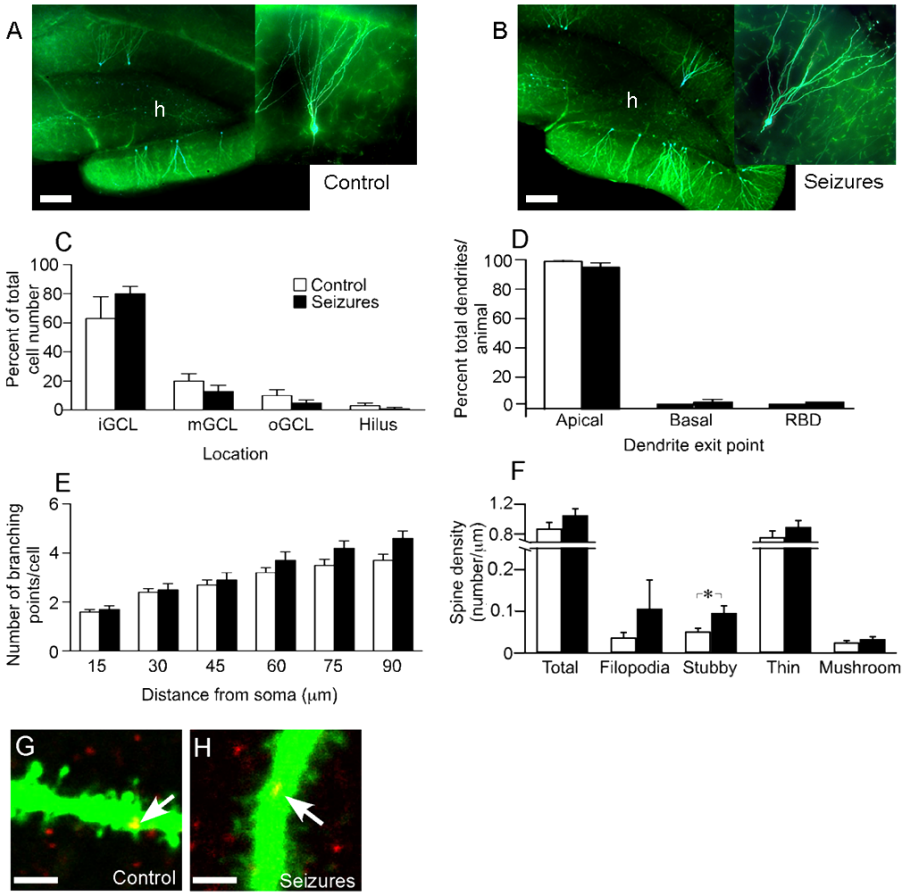
Fig. 2. New neurons exposed to repeated seizures without inflammation exhibit minor morphological changes. GFP+ cell bodies in the GCL with dendrites extending into the ML and axons into the hilus (h) 6 weeks after virus injection in control (A) and seizure-exposed (B) animals. Insets show representative images of GFP+ new cells. C, Relative location of GFP+ cells in inner, middle, or outer GCL (iGCL, mGCL, and oGCL, respectively), or hilus. D, Relative occurrence of apical, basal, or recurrent basal dendrites (RBD) on GFP+ cells. E, Cumulative number of dendritic branching points at increasing distances from the GFP+ cell body. F, Spine density on GFP+ dendrites from seizure-exposed and control animals (*, increased density on seizure-exposed compared to control new cells, Student's unpaired t-test, $p < 0.05$). Representative images of gephyrin clusters (arrows) in control (G) and seizure-exposed (H) animals. Scale bars = 50 μm (in A, B) and 1 μm (in G, H). Means ± SEM.

Functional integration of the new neurons in the pathological environment

Whole-cell patch-clamp recordings were performed from GFP+ cells (new cells, born at the time of RV–GFP injection) and neighboring GFP− cells (mature cells, most likely born before the onset of recurrent seizures) (Jakubs et al., 2006) in the GCL at 6–8 weeks after the RV-GFP injection. Mature, GFP− cells were selected based on their position within the GCL and their morphology. Immunohistochemistry performed after recordings revealed development of mature dendrites on both GFP− and GFP+ neurons. We found that the intrinsic membrane properties (resting membrane potential, input resistance, series resistance, action potential threshold, and action potential half-width) of the new and mature cells in seizure-exposed animals were not significantly different compared to new and mature cells in non-stimulated, electrode-implanted controls (Table 1, Fig. 3A, B). These properties were also similar to those characteristic of dentate granule cells (Staley et al., 1992). A recent study reported that rheobase (amount of current required to depolarize membrane potential to threshold level for action potential generation) was increased in granule cells in a model of temporal lobe epilepsy (Young et al., 2009). Interestingly, we detected an increase in rheobase in the seizure-exposed new cells compared to all other groups. Furthermore, ramp current injection elicited fewer action potentials in seizure-exposed compared to control

Table 1
Intrinsic membrane properties of GFP+ and GFP− cells in the dentate granule cell layer.

	Control GFP+	Control GFP−	Seizures GFP+	Seizures GFP−
Resting membrane potential (mV)	−79.0 ± 2.1	−80.3 ± 1.4	−80.3 ± 1.1	−81.3 ± 1.4
Input Resistance (MΩ)	321 ± 24.5	355 ± 58.9	281 ± 28.9	415 ± 34.1
Series Resistance (MΩ)	13.3 ± 2.3	10.1 ± 1.1	12.3 ± 1.1	14.4 ± 1.5
Action potential Threshold (mV)	−47.8 ± 2.1	−48.9 ± 2.5	−43.9 ± 1.3	−48.1 ± 1.6
Action potential half-width (ms)	1.26 ± 0.09	1.23 ± 0.05	1.42 ± 0.06	1.22 ± 0.05
Rheobase (pA)	131 ± 9	136 ± 19	194 ± 11*	94 ± 8

Recordings were made from new (GFP+) and mature (GFP−) cells in animals subjected to rapid kindling and repeated seizures or non-stimulated control animals at 6–8 weeks after RV-GFP injection. Means ± SEM. Comparisons using one-way ANOVA with Bonferroni *post-hoc* test revealed no significant differences ($p>0.05$) except for rheobase. *Significantly higher compared to all other groups ($p<0.05$). Number of recorded cells: new cells-seizures: 8 cells from 4 rats, new cells-control: 7 cells from 5 rats, mature cells-seizures: 8 cells from 7 rats, mature cells-control: 9 cells from 6 rats.

new cells (control 5.6 ± 0.7, $n=7$ cells from 5 rats; seizures 3.4 ± 0.5, $n=8$ cells from 4 rats; $p<0.05$, Fig 3C).

We then explored whether the environment created by the initial epileptic insult and the repeated seizures influenced the network-independent excitatory and inhibitory synaptic input to the new neurons in the GCL (for recordings of mEPSCs and mIPSCs in mature cells, see Supplementary Figure 2–3). Whole-cell voltage-clamp recordings of mEPSCs were carried out in the presence of the GABA_A receptor antagonist PTX and voltage-gated sodium channel blocker TTX. Cumulative fraction analysis showed that the new cells which were exposed to seizures throughout development exhibited mEPSCs of larger amplitude compared to new cells from control animals (Fig. 4A, E). Moreover, new cells exposed to seizures exhibited mEPSCs with faster rise times compared to control new cells (Fig. 4B). Both these changes in mEPSCs are considered to be indicative of

postsynaptic alterations. The mean frequency of mEPSCs tended to be higher in new cells exposed to seizures but this difference did not reach statistical significance, possibly due to the low number of cells accessible for recording (Fig. 4C). Since histograms of IEIs were skewed, indicating non-normal distribution (data not shown), non-parametric, cumulative fraction analysis was applied. This analysis revealed shorter IEIs of mEPSCs in new seizure-exposed cells compared to new cells from control animals (Fig. 4D), providing evidence for an increase in mEPSC frequency. Thus, our results indicate that adult-born granule cells, exposed to repeated seizures
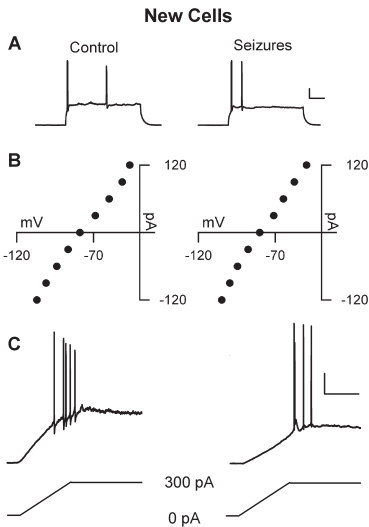

New Cells

Fig. 3. New neurons exposed to repeated seizures without inflammation have similar intrinsic membrane properties but reduced intrinsic excitability compared to new neurons in control environment. *A*, Representative traces of action potentials elicited in a control new cell and a seizure-exposed new cell. Scale bar = 100 ms, 20 mV. *B*, Voltage responses in control and seizure-exposed new cells. *C*, Representative traces of membrane potential responding to ramp current injection showing increased rheobase and fewer action potentials in seizure-exposed new cells. Scale bar = 500 ms, 20 mV. Representative traces.
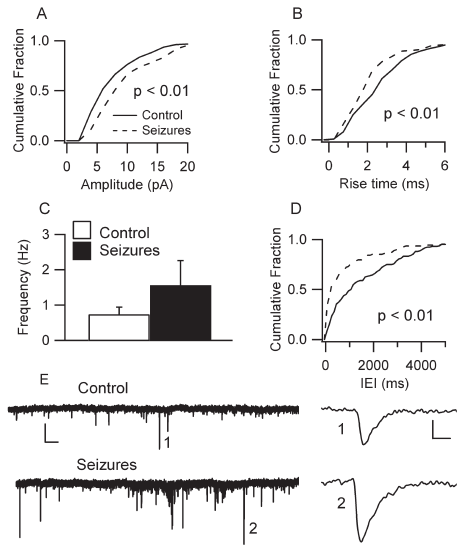

New Cells mEPSCs

Fig. 4. New neurons exposed to repeated seizures without inflammation exhibit enhanced excitatory input in the absence of network activity. Cumulative fraction curve showing increased amplitude and faster 10–90% rise time of mEPSCs in new cells from seizure-exposed compared to new cells from control animals after action potential blockade with TTX (*A*, *B*). No change in mean event frequency (Student's unpaired *t*-test, $p>0.05$), but shorter IEI of mEPSCs in new cells exposed to seizures compared to control new cells (*C*, *D*) (Kolmogorov–Smirnov test). *E*, Representative traces of mEPSCs in seizure-exposed and control cells. 1, 2 depict representative events (*left*) on an expanded time scale (*right*). Scale bar = 10 pA, 1 s and 10 pA, 5 ms, respectively. Number of recorded cells: new cells-seizures: 6 cells from 4 rats, new cells-control: 8 cells from 5 rats.

throughout development, receive enhanced excitatory drive, which is independent of network-generated action potentials.

We also determined if the new neurons exhibited altered inhibitory synaptic input when born after rapidly recurring seizures and subsequently exposed to episodes of seizure activity throughout their development. Whole-cell voltage-clamp recordings of mIPSCs were performed while blocking glutamate receptors with NBQX and D-AP5, and action potentials with TTX. Cumulative fraction analysis showed that the amplitude of mIPSCs was not different between new cells born into the seizure environment and new cells from control animals (Fig. 5A, E). However, mIPSCs from seizure-exposed new cells exhibited slower 10–90% rise times compared to control new cells (Fig. 5B), suggesting a relative decrease in the strength of perisomatic vs. dendritic inhibitory drive (Kobayashi and Buckmaster 2003; Jakubs et al., 2006; however, see Soltesz et al., 1995). We next looked at the frequency and IEIs of mIPSCs. mIPSCs occurred with lower mean frequency in seizure-exposed as compared to control new cells, but the difference was not statistically significant (Fig. 5C). However, when we used cumulative fraction analysis due to the skewed, non-normal distribution of IEIs, we detected lengthening of mIPSC IEIs in seizure-exposed compared to control new cells (Fig. 5D), suggesting a decrease in mIPSC frequency. Taken together, our results indicate that, in the absence of network-generated action potentials, adult-born granule cells exposed to repeated seizures throughout their develop-ment receive reduced perisomatic inhibition compared to new cells born in control animals.

Discussion

How neurons, which are born and develop in a pathological environment, integrate into existing neural circuitries in the adult brain will determine whether they counteract or contribute to functional impairments. Here we show that new dentate granule cells generated following an epileptic insult, comprising 40 rapidly recurring seizures, and exposed to repeated seizures during their differentiation exhibited increased overall synaptic excitability compared to new cells which had developed in a normal environment. The increased synaptic excitability of these cells may be counterbalanced, or even overridden by reduced intrinsic excitability as evidenced by higher rheobase. In contrast, detailed morphological analysis of the location, orientation, dendritic arborizations, and spines of these cells showed only minor differences between the groups.

Our finding that new granule cells received enhanced excitatory drive after seizures is consistent with studies which have reported enhanced excitability of dentate granule cells after pilocarpine-induced seizures (Simmons et al., 1997) and kainate-induced seizures (Wuarin and Dudek, 2001). How seizures influence the inhibition of granule cells is less clear as there are reports that kainate-induced seizures enhance mIPSCs (Buckmaster and Dudek, 1997) whereas pilocarpine-induced seizures reduce inhib-itory input to granule cells (Kobayashi and Buckmaster, 2003). Furthermore, after eSE, mature granule cells exhibit longer IEIs of sIPSCs with larger amplitude (Jakubs et al., 2006). Inhibition may be influenced by changes in zinc distribution. After kindling, granule cells receive increased inhibitory drive, which may collapse due to zinc released from aberrantly sprouted mossy fibers interacting with zinc-sensitive $GABA_A$ receptors (Buhl et al., 1996). We found that new granule cells born after rapid kindling and exposed to repeated seizures exhibited mIPSCs of similar amplitude but with longer IEIs compared to new cells in control animals. Taken together, it seems that changes in the inhibitory inputs to granule cells are dependent on the seizure paradigm and epilepsy model used, and may be modulated at both pre- and postsynaptic sites.

Two main lines of evidence indicate that the new neurons born after rapid kindling and exposed to repeated seizures integrate into hippocampal circuitry in a manner that may contribute to enhanced synaptic excitability. First, mEPSCs in seizure-exposed new cells had larger amplitudes and faster rise times compared to mEPSCs recorded in control new cells. These changes, including excitatory postsynaptic receptor kinetics, are consistent with alterations of AMPA receptor subunits (Koike et al., 2000; Liu and Cull-Candy, 2000). Second, mIPSCs in seizure-exposed new cells display longer rise times of mIPSCs, which suggest a relative weakening of perisomatic inhibition in seizure-exposed new cells (Kobayashi and Buckmaster 2003; Jakubs et al., 2006; however, see Soltesz et al., 1995). If this is the case, it could lead to less control over action potentials thought to be generated around the axon hillock, i.e., in the perisomatic area. These changes in postsynaptic receptor kinetics may also indicate changes in $GABA_A$ receptor subunits (Coulter, 2001). However, in the same seizure-exposed new cells, we also observed increased rheobase and fewer action potentials, which may partially, or completely, counter-act the enhanced synaptic excitability.

The exact source of the presynaptic input to the new neurons and their postsynaptic targets remain important issues. It is well established that the entorhinal cortex via the perforant path is the primary source of excitatory input to mature dentate granule cells and also adult-born neurons (Overstreet-Wadiche et al., 2006). However, there is evidence that after seizures, granule cells can provide excitatory input to each other due to mossy fiber sprouting (Tauck and Nadler, 1985; Elmér et al., 1996; Sutula et al., 1989; Represa et al., 1990). Inhibitory interneurons located throughout the hippocampus provide GABAergic input to granule cells. The number of interneurons,
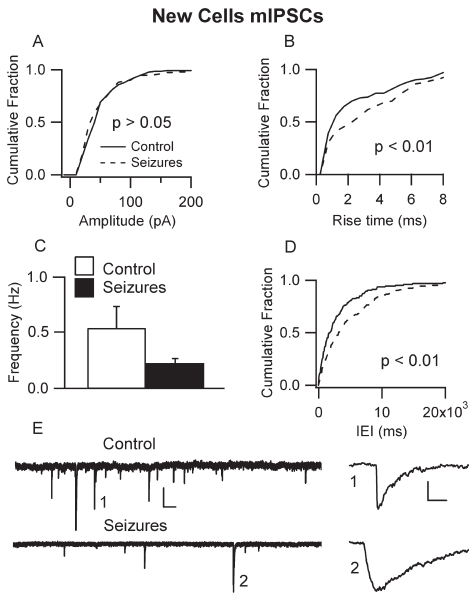
New Cells mIPSCs

Fig. 5. New neurons exposed to repeated seizures without inflammation exhibit altered inhibitory input in the absence of network activity. Cumulative fraction curves showing no change in amplitude and slower 10–90% rise time of mIPSCs in new cells from seizure-exposed compared to control animals after action potential blockade with TTX (A, B). No change in mean event frequency (Student's unpaired t-test, p>0.05), but longer IEI of mIPSCs in new cells exposed to seizures compared to control new cells (C, D). (Kolmogorov–Smirnov test). E, Representative traces of mIPSCs recorded from seizure-exposed and control cells. 1, 2 depict representative events (left) on an expanded time scale (right). Scale bar=50 pA, 1 s and 50 pA, 20 ms, respectively. Number of recorded cells: new cells-seizures: 8 cells from 4 rats, new cells-control: 7 cells from 6 rats.

their morphology, and development of synapses with granule cells is influenced by seizures (Wittner et al., 2001; Dinocourt et al., 2003; Sayin et al., 2003; Zhang and Buckmaster, 2009). To what extent mossy fiber sprouting or alterations of inhibitory interneurons influence the integration of the new neurons is not known.

The pre- and postsynaptic changes observed here indicate a net increase in the excitatory drive onto the seizure-exposed new neurons, but how this influences their functional output is unclear. Axons of dentate granule cells (mossy fibers) contact hilar mossy cells, CA3 pyramidal cells and hilar interneurons. Enhanced rheobase may prevent the cells from propagating this excitability to the targets of their efferent synapses. The changes in rheobase likely indicate alterations in the membrane properties of the seizure-exposed cells, particularly changes in the input resistance of the cell (Young et al., 2009). We found that the input resistance of the seizure-exposed new cells tended to be lower compared to that of the other recorded cells (although not statistically significant), which may partially explain the increase in rheobase. Changes in input resistance suggest alterations in the number, distribution, or composition of membrane channels in the new cells. It should be emphasized, finally, that the functional significance at the network level of the altered afferent synaptic inputs to the new cells, whether they will counteract or contribute to the development of hyperexcitability, will depend on the synaptic influence of these cells on their target neurons (Frotscher et al., 2006), an issue that is highly warranted to address in future studies.

The pattern of alterations in afferent excitatory and inhibitory synaptic drive on the new cells in the present seizure paradigm differs from that we have previously reported following eSE (Jakubs et al., 2006). In response to the eSE insult, the new neurons exhibited reduced excitatory and increased inhibitory synaptic drive (Jakubs et al., 2006). The eSE insult comprised approximately 3 h of seizure activity and the environment surrounding the new cells was characterized by neuronal death, chronic inflammation and spontaneous seizures. In contrast, we observed here no significant inflammatory changes or neuronal death in the pathological environment. The total duration of seizures induced by the rapid kindling protocol was much shorter (about 19 min). The eSE environment was associated with abnormal excitability, as evidenced by spontaneous behavioral seizures, whereas following rapid kindling, there was a progressive development of hyperexcitability but no interictal spikes or spontaneous seizures were detected. The stimulus-evoked seizures lasted for in total about 10 min. Taken together, the discrepancy in afferent synaptic connectivity, comparing the present findings with our previous data (Jakubs et al., 2006), indicates that the integration of the new cells depends on the type of pathological environment they encounter.

The characteristics of the pathological environment will also determine its influences on the morphological development of the new neurons. Walter et al. (2007) studied new granule cells exposed to 3 h of pilocarpine-induced SE in mice either at 1 week after they had been generated or when they were born into the pathological environment 3 weeks after the insult. This insult, which caused spontaneous seizures and extensive neuronal death in the dentate hilus and variable cell loss in CA1 and CA3 regions, gave rise to the formation of basal dendrites projecting into the hilus in 40–50% of new granule cells. Such dendrites are virtually absent in intact animals. Also, Jessberger et al. (2007) found basal hilar dendrites in about 20% of new granule cells born at 1 week following 2–3 h of kainate-induced SE. It is conceivable that both these severe epileptic insults were associated with inflammation. In contrast, the present epileptic insult, in which the total duration of seizure activity was much shorter, resulted in no significant inflammation or neuronal death, and the occurrence of very few basal hilar dendrites on the new granule cells. Our findings, that new neurons which develop in the presence of seizures without inflammation exhibit no major morphological changes indicate that the occurrence of morphological abnormalities is likely dependent on the severity of pathology in the environment.

We found an increased number of stubby spines on the seizure-exposed new cells. Stubby spines have been found to be more frequent on mature hippocampal dendrites in acute slices with blocked synaptic transmission, which is believed to recapitulate development (Petrak et al., 2005). Interestingly, application of brain-derived neurotrophic factor (BDNF) to hippocampal slice cultures under serum-free conditions specifically promoted the formation of stubby spines on mature CA1 pyramidal neurons (Tyler and Pozzo-Miller, 2003, however, see Chapleau et al., 2008). These stubby spines may have a role in Ca^{2+}-dependent synaptic plasticity (Tyler and Pozzo-Miller, 2003). BDNF has also been proposed to be an important regulator of morphological and functional hippocampal plasticity in response to seizures (Ernfors et al., 1991; Kokaia et al., 1995; Binder et al., 2001). Hypothetically, BDNF signaling may have contributed to the increase of stubby spines observed here on the new cells.

Inflammation regulates several steps of adult neurogenesis including survival, proliferation, migration, differentiation, and functional integration of the new neurons (reviewed by Ekdahl et al., 2009). LPS-induced chronic inflammation gave rise to a similar increase of excitatory synaptic drive in new and mature dentate granule cells, probably due to increased network activity (Jakubs et al., 2008). Also, inhibitory synaptic drive was increased by inflammation in both new and mature cells but more enhanced in the new cells. In line with this observation, larger clusters of the postsynaptic GABA$_A$ receptor scaffolding protein gephyrin were found on dendrites of new cells born in the inflammatory environment. It is conceivable that the larger gephyrin clusters indicate a more efficacious inhibitory input and contributes to the synapse-specific enhancement of the afferent inhibitory drive. In contrast, we found here that the new cells which had been born after rapid kindling and exposed to repeated seizures did not exhibit any change in mIPSC amplitude, indicating no postsynaptic alterations. In accordance, we did not observe any alteration in the density or size of gephyrin clusters at postsynaptic sites in neurons which had developed in this environment. The present findings provide further evidence for an important regulatory role of inflammation for inhibitory synaptic drive on the new cells. Our data indicate that different pathological environments, associated with varying magnitude of inflammation, differ with respect to their ability to induce postsynaptic changes in new cells which will influence the efficacy of their afferent inputs.

The present findings show that adult-born, new neurons exhibit a high degree of plasticity at their afferent synapses when developing in a pathological environment. Our previous data following eSE (Jakubs et al., 2006) and chronic inflammation (Jakubs et al., 2008) suggested that the functional integration of the new neurons may act to mitigate the pathological condition. Here, the new neurons responded to repeated seizures in an environment without inflammation by overall more synaptic excitability, which may be counteracted by the reduced intrinsic excitability compared to control new cells. If this is the case, the new neurons may have a limited contribution to the hyperexcitability which develops during the course of their maturation or even counteract the abnormal function. In conclusion, our findings indicate that the characteristics of the pathological environment, e.g., the magnitude of inflammation and the seizure paradigm, will play an important role in determining whether the new neurons will counteract or contribute to abnormal brain function.

Supplementary materials related to this article can be found online at doi:10.1016/j.expneurol.2011.03.019.

References

Bengzon, J., Kokaia, Z., Elmer, E., Nanobashvili, A., Kokaia, M., Lindvall, O., 1997. Apoptosis and proliferation of dentate gyrus neurons after single and intermittent limbic seizures. Proc. Natl. Acad. Sci. USA 94, 10432–10437.

Binder, D.K., Croll, S.D., Gall, C.M., Scharfman, H.E., 2001. BDNF and epilepsy: too much of a good thing? Trends Neurosci. 24, 47–53.

Biscaro, B., Lindvall, O., Hock, C., Ekdahl, C.T., Nitsch, R.M., 2009. Abeta immunotherapy protects morphology and survival of adult-born neurons in doubly transgenic APP/PS1 mice. J. Neurosci. 29, 14108–14119.

Buckmaster, P.S., Dudek, F.E., 1997. Neuron loss, granule cell axon reorganization, and functional changes in the dentate gyrus of epileptic kainate-treated rats. J. Comp. Neurol. 385, 385–404.

Buhl, E.H., Otis, T.S., Mody, I., 1996. Zinc-induced collapse of augmented inhibition by GABA in a temporal lobe epilepsy model. Science 271, 369–373.

Chapleau, C.A., Carlo, M.E., Larimore, J.L., Pozzo-Miller, L., 2008. The actions of BDNF on dendritic spine density and morphology in organotypic slice cultures depend on the presence of serum in culture media. J. Neurosci. Methods 169, 182–190.

Coulter, D.A., 2001. Epilepsy-associated plasticity in gamma-aminobutyric acid receptor expression, function, and inhibitory synaptic properties. Int. Rev. Neurobiol. 45, 237–252 Review..

Dinocourt, C., Petanjek, Z., Freund, T.F., Ben-Ari, Y., Esclapez, M., 2003. Loss of interneurons innervating pyramidal cell dendrites and axon initial segments in the CA1 region of the hippocampus following pilocarpine-induced seizures. J. Comp. Neurol. 459, 407–425.

Ekdahl, C.T., Kokaia, Z., Lindvall, O., 2009. Brain inflammation and adult neurogenesis: the dual role of microglia. Neuroscience 158, 1021–1029.

Ekdahl, C.T., Claasen, J.H., Bonde, S., Ekdahl, C.T., Lindvall, O., 2003. Inflammation is detrimental for neurogenesis in adult brain. Proc. Natl. Acad. Sci. USA 100, 13632–13637.

Elmér, E., Kokaia, M., Kokaia, Z., Ferencz, I., Lindvall, O., 1996. Delayed kindling development after rapidly recurring seizures: relation to mossy fiber sprouting and neurotrophin, GAP-43 and dynorphin gene expression. Brain Res. 712, 19–34.

Elmér, E., Kokaia, Z., Kokaia, M., Carnahan, J., Nawa, H., Lindvall, O., 1998. Dynamic changes of brain-derived neurotrophic factor protein levels in the rat forebrain after single and recurring kindling-induced seizures. Neuroscience 83, 351–362.

Ernfors, P., Bengzon, J., Kokaia, Z., Persson, H., Lindvall, O., 1991. Increased levels of messenger RNAs for neurotrophic factors in the brain during kindling epileptogenesis. Neuron 7, 165–176.

Fritschy, J.M., Harvey, R.J., Schwarz, G., 2008. Gephyrin: where do we stand, where do we go? Trends Neurosci. 31, 257–264.

Frotscher, M., Jonas, P., Sloviter, R.S., 2006. Synapses formed by normal and abnormal hippocampal mossy fibers. Cell Tissue Res. 326, 361–367.

Jakubs, K., Nanobashvili, A., Bonde, S., Ekdahl, C.T., Kokaia, Z., Kokaia, M., Lindvall, O., 2006. Environment matters: synaptic properties of neurons born in the epileptic adult brain develop to reduce excitability. Neuron 52, 1047–1059.

Jakubs, K., Bonde, S., Iosif, R.E., Ekdahl, C.T., Kokaia, Z., Kokaia, M., Lindvall, O., 2008. Inflammation regulates functional integration of neurons born in adult brain. J. Neurosci. 28, 12477–12488.

Jessberger, S., Zhao, C., Toni, N., Clemenson Jr., G.D., Li, Y., Gage, F.H., 2007. Seizure-associated, aberrant neurogenesis in adult rats characterized with retrovirus-mediated cell labeling. J. Neurosci. 27, 9400–9407.

Kobayashi, M., Buckmaster, P.S., 2003. Reduced inhibition of dentate granule cells in a model of temporal lobe epilepsy. J. Neurosci. 23, 2440–2452.

Koike, M., Tsukada, S., Tsuzuki, K., Kijima, H., Ozawa, S., 2000. Regulation of kinetic properties of GluR2 AMPA receptor channels by alternative splicing. J. Neurosci. 20, 2166–2174.

Kokaia, M., Ernfors, P., Kokaia, Z., Elmer, E., Jaenisch, R., Lindvall, O., 1995. Suppressed epileptogenesis in BDNF mutant mice. Exp. Neurol. 133, 215–224.

Laplagne, D.A., Esposito, M.S., Piatti, V.C., Morgenstern, N.A., Zhao, C., van Praag, H., Gage, F.H., Schinder, A.F., 2006. Functional convergence of neurons generated in the developing and adult hippocampus. PLoS Biol. 4, e409.

Lehrmann, E., Christensen, T., Zimmer, J., Diemer, N.H., Finsen, B., 1997. Microglial and macrophage reactions mark progressive changes and define the penumbra in the rat neocortex and striatum after transient middle cerebral artery occlusion. J. Comp. Neurol. 386, 461–476.

Liu, J., Solway, K., Messing, R.O., Sharp, F.R., 1998. Increased neurogenesis in the dentate gyrus after transient global ischemia in gerbils. J. Neurosci. 18, 7768–7778.

Liu, S.Q., Cull-Candy, S.G., 2000. Synaptic activity at calcium-permeable AMPA receptors induces a switch in receptor subtype. Nature 405, 454–458.

Meijering, E., Jacob, M., Sarria, J.C.F., Steiner, P., Hirling, H., Unser, M., 2004. Design and validation of a tool for neurite tracing and analysis in fluorescence microscopy images. Cytometry 2, 167–176.

Monje, M.L., Toda, H., Palmer, T.D., 2003. Inflammatory blockade restores adult hippocampal neurogenesis. Science 302, 1760–1765.

Morgenstern, N.A., Lombardi, G., Schinder, A.F., 2008. Newborn granule cells in the ageing dentate gyrus. J. Physiol. 586, 3751–3757.

Nimchinsky, E.A., Sabatini, B.L., Svoboda, K., 2002. Structure and function of dendritic spines. Annu. Rev. Physiol. 64, 313–353.

Overstreet-Wadiche, L.S., Bromberg, D.A., Bensen, A.L., Westbrook, G.L., 2006. Seizures accelerate functional integration of adult-generated granule cells. J. Neurosci. 26, 4095–4103.

Parent, J.M., 2005. When newborn neurons stray. Epilepsy Curr. 5, 231–233.

Parent, J.M., Yu, T.W., Leibowitz, R.T., Geschwind, D.H., Sloviter, R.S., Lowenstein, D.H., 1997. Dentate granule cell neurogenesis is increased by seizures and contributes to aberrant network reorganization in the adult rat hippocampus. J. Neurosci. 17, 3727–3738.

Paxinos, G., Watson, C., 1997. The Rat Brain in Stereotaxic Coordinates. Academic, San Diego.

Petrak, L.J., Harris, K.M., Kirov, S.A., 2005. Synaptogenesis on mature hippocampal dendrites occurs via filopodia and immature spines during blocked synaptic transmission. J. Comp. Neurol. 484, 183–190.

Racine, R.J., 1972. Modification of seizure activity by electrical stimulation. II. Motor seizure. Electroencephalogr. Clin. Neurophysiol. 32, 281–294.

Represa, A., Tremblay, E., Ben-Ari, Y., 1990. Sprouting of mossy fibers in the hippocampus of epileptic human and rat. Adv. Exp. Med. Biol. 268, 419–424.

Sayin, U., Osting, S., Hagen, J., Rutecki, P., Sutula, T., 2003. Spontaneous seizures and loss of axo-axonic and axo-somatic inhibition induced by repeated brief seizures in kindled rats. J. Neurosci. 23, 2759–2768.

Scott, B.W., Wang, S., Burnham, W.M., De Boni, U., Wojtowicz, J.M., 1998. Kindling-induced neurogenesis in the dentate gyrus of the rat. Neurosci. Lett. 248, 73–76.

Sheffield, J.B., 2007. ImageJ, a useful tool for biological image processing and analysis. Microsc. Microanal. 13, 200–201.

Simmons, M.L., Terman, G.W., Chavkin, C., 1997. Spontaneous excitatory currents and kappa-opioid receptor inhibition in dentate gyrus are increased in the rat pilocarpine model of temporal lobe epilepsy. J. Neurophysiol. 78, 1860–1868.

Soltesz, I., Smetters, D.K., Mody, I., 1995. Tonic inhibition originates from synapses close to the soma. Neuron 14, 1273–1283.

Staley, K.J., Otis, T.S., Mody, I., 1992. Membrane-properties of dentate gyrus granule cells—comparison of sharp microelectrode and whole-cell recordings. J. Neurophysiol. 67, 1346–1358.

Sutula, T., Cascino, G., Cavazos, J., Parada, I., Ramirez, L., 1989. Mossy fiber synaptic reorganization in the human temporal lobe. Ann. Neurol. 26, 321–330.

Tauck, D.L., Nadler, J.V., 1985. Evidence of functional mossy fiber sprouting in hippocampal formation of kainic acid-treated rats. J. Neurosci. 5, 1016–1022.

Toni, N., Laplagne, D.A., Zhao, C., Lombardi, G., Ribak, C.E., Gage, F.H., Schinder, A.F., 2008. Neurons born in the adult dentate gyrus form functional synapses with target cells. Nat. Neurosci. 11, 901–907.

Tyler, W.J., Pozzo-Miller, L., 2003. Miniature synaptic transmission and BDNF modulate dendritic spine growth and form in rat CA1 neurones. J. Physiol. London 553, 497–509.

van Praag, H., Schinder, A.F., Christie, B.R., Toni, N., Palmer, T.D., Gage, F.H., 2002. Functional neurogenesis in the adult hippocampus. Nature 415, 1030–1034.

Walter, C., Murphy, B.L., Pun, R.Y.K., Spieles-Engemann, A.L., Danzer, S.C., 2007. Pilocarpine-induced seizures cause selective time-dependent changes to adult-generated hippocampal dentate granule cells. J. Neurosci. 27, 7541–7552.

Wittner, L., Maglóczky, Z., Borhegyi, Z., Halász, P., Tóth, S., Eross, L., Szabó, Z., Freund, T.F., 2001. Preservation of perisomatic inhibitory input of granule cells in the epileptic human dentate gyrus. Neuroscience 108, 587–600.

Wuarin, J.P., Dudek, F.E., 2001. Excitatory synaptic input to granule cells increases with time after kainate treatment. J. Neurophysiol. 85, 1067–1077.

Young, C.C., Stegen, M., Bernard, R., Müller, M., Bischofberger, J., Veh, R.W., Haas, C.A., Wolfart, J., 2009. Upregulation of inward rectifier K + (Kir2) channels in dentate gyrus granule cells in temporal lobe epilepsy. J. Physiol. 587, 4213–4233.

Zhang, W., Buckmaster, P.S., 2009. Dysfunction of the dentate basket cell circuit in a rat model of temporal lobe epilepsy. J. Neurosci. 29, 7846–7856.

Zhao, C.M., Teng, E.M., Summers, R.G., Ming, G.L., Gage, F.H., 2006. Distinct morphological stages of dentate granule neuron maturation in the adult mouse hippocampus. J. Neurosci. 26, 3–11.

Zhao, C.M., Deng, W., Gage, F.H., 2008. Mechanisms and functional implications of adult neurogenesis. Cell 132, 645–660.

Paper III

Direct conversion of human fibroblasts to dopaminergic neurons

Ulrich Pfisterer[1], Agnete Kirkeby[1], Olof Torper[1], James Wood, Jenny Nelander, Audrey Dufour, Anders Björklund, Olle Lindvall, Johan Jakobsson, and Malin Parmar[2]

Departments of Experimental Medical Science and Clinical Sciences, Wallenberg Neuroscience Center, and Lund Stem Cell Center, Lund University, SE-221 84 Lund, Sweden

Recent reports demonstrate that somatic mouse cells can be directly converted to other mature cell types by using combined expression of defined factors. Here we show that the same strategy can be applied to human embryonic and postnatal fibroblasts. By overexpression of the transcription factors Ascl1, Brn2, and Myt1l, human fibroblasts were efficiently converted to functional neurons. We also demonstrate that the converted neurons can be directed toward distinct functional neurotransmitter phenotypes when the appropriate transcriptional cues are provided together with the three conversion factors. By combining expression of the three conversion factors with expression of two genes involved in dopamine neuron generation, Lmx1a and FoxA2, we could direct the phenotype of the converted cells toward dopaminergic neurons. Such subtype-specific induced neurons derived from human somatic cells could be valuable for disease modeling and cell replacement therapy.

Cellular reprogramming, the process by which somatic cells can be converted into induced pluripotent stem (iPS) cells and subsequently differentiated to mature cells, including specific types of neurons, has opened up new possibilities for disease modeling and cellular repair (1–5). Recently, it was shown that somatic cells can also be directly converted to other mature cell types by expression of a specific combinations of genes (6–9). Expression of Ascl1, Brn2, and Myt1l efficiently converted mouse embryonic fibroblasts (MEFs) and postnatal fibroblasts to functional neurons (induced neurons, or iN cells) (10). Cells generated via direct conversion do not pass through a pluripotent state, are probably not tumorigenic, and may serve as an interesting alternative to iPS cells for generating patient- and/or disease-specific neurons.

Here, we show the direct conversion of human fibroblasts to functional neurons using the same combination of neural conversion factors used for iN conversion of mouse fibroblasts (10). We also demonstrate that the expression of additional transcription factors leads to the generation of cells with properties of dopaminergic neurons, which is the cell type lost in Parkinson's disease. Our findings provide proof of principle that specific subtypes of iN cells can be produced from human somatic cells by transcription factor-mediated fate instruction combined with the three neural conversion factors.

Results

To investigate whether direct conversion into neurons from human somatic cells is possible, we established fibroblast cultures from human embryos aged 5.5–7 wk postconception (for details see Table S1). The head, the dorsal part of the embryo containing the spinal cord, and all red organs were removed, and the remaining tissue was dissociated and plated under standard fibroblast conditions (Fig. 1A). After one passage followed by a freeze–thaw cycle, the fibroblast identity and the absence of the neural crest marker SOX10 in the resulting cell lines were confirmed (Fig. 1B, Figs. S1 and S2, and Tables S2 and S3). The cells were then used for conversion by delivering lentiviral vectors coding for Ascl1, Brn2, and Myt1l, the three factors previously identified as efficiently converting MEFs to neurons (10). Expression of the conversion factors in human embryonic fibroblasts (hEFs) was verified with quantitative RT-PCR (qRT-PCR) (Fig. S2 A–C). In cultures transduced with conversion factors and subsequently grown in N3 neural induction medium (11), cells with elongated neuron-like morphology became visible

after 3–4 d (Fig. S2D). By 12 d after transduction, many cells exhibiting characteristic neuronal morphology and expressing βIII-tubulin could be detected (Fig. 2A). In parallel control cultures containing hEFs not infected with conversion factors but otherwise treated identically, neurons were never observed (Fig. 2A). The morphology of the human-derived iN (hiN) cells matured over time, and the vast majority of them had an elaborate neuronal morphology by day 24 (Fig. 2A). The efficiency of hiN generation was determined by using fibroblasts (passage 2) from three different embryos. We found that the number of hiN cells increased with time in culture. By day 24, on average, 1,600 neurons per cm^2 were present, corresponding to a conversion efficiency of $16\% \pm 4.3\%$ (Fig. 2B). The capacity to form hiN cells decreased with one additional passage (from 9.0% to 4.53%, day 12) but then remained constant until passage 8 when the cells ceased to proliferate (Fig. 2C and Fig. S2 E and F).

More than 95% of the converted neurons expressed the neuron-specific cytoskeletal protein MAP2, which is enriched in dendrites (Fig. 2D). The great majority ($\geq$90%) of the hiN cells also expressed synaptophysin, indicating the presence of synapses on the hiN cells (Fig. 2E). At 23 d after conversion, patch–clamp recordings showed that the resting membrane potential was approximately −34 mV and that depolarizing current injection did not induce action potentials, suggesting immaturity of the cells. However, at 30–32 d after transduction, the average resting membrane potential was approximately −59 mV (range: −30 mV to −78 mV), and the cells now exhibited electrophysiological properties of functional neurons (Table S4). Depolarizing current injection induced action potentials in ∼90% of recorded cells (Fig. 2F). In voltage–clamp mode, step depolarization induced fast-inactivating inward and outward currents characteristic of sodium and delayed-rectifier potassium currents, respectively (Fig. 2G). Action potentials and inward sodium currents were blocked by TTX (Fig. 2 F and G, Right). Biocytin labeling confirmed the neuronal morphology of recorded cells (Fig. S2H).

The expression of the three transgenes used for iN conversion was regulated by doxycycline, which must be supplied in the media throughout the culture period to maintain transgene expression (Fig. S2 A–C). To test whether continuous expression of the conversion factors is necessary for efficient hiN generation, we removed doxycycline at day 0 (i.e., never activated the transgenes), day 3, or day 7 after transduction. Doxycycline removal at day 0 resulted in only sporadic hiN formation, most likely because of nonspecific leakage of transgene expression, whereas withdrawal at day 3 or day 7 did not significantly change the number of neurons formed, the process length, or the number of projections (Fig. 3 A and B). These data suggest that conversion of fibroblasts into neurons using Ascl1, Brn2, and
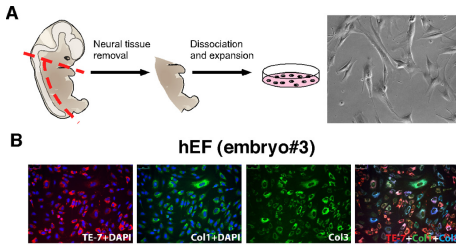
Fig. 1. Establishment of hEF cultures. (*A*) Fibroblasts isolated from human embryos were dissociated and plated under standard fibroblast conditions. The fibroblasts were passaged once, frozen, and subsequently used for experiments. (*B*) Immunostaining confirmed that the resulting cultures were composed of cells expressing collagen I and III, confirming their fibroblast identity, and TE-7 confirmed their mesodermal origin.
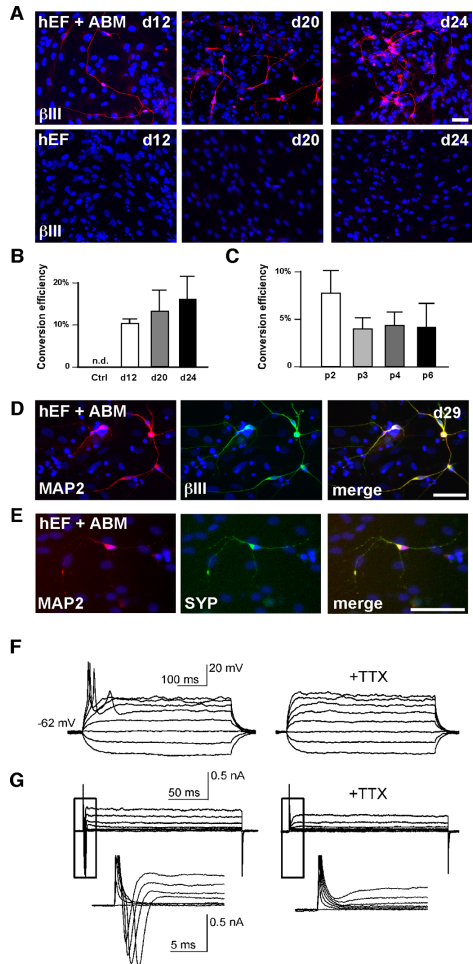

Fig. 2. Conversion of neurons from hEFs. (*A*) Neurons expressing βIII-tubulin (red) obtained by direct conversion of hEFs at 12, 20, and 24 d after Ascl1, Brn2, and Myt1l expression (ABM). Blue indicates DAPI counterstain. (*B* and *C*) Conversion efficiency estimation of hiN cell formation. (*n* = 5 for *B* and *n* = 2–4 for *C*.) (*D* and *E*) Immunocytochemical staining for MAP2 and synaptophysin (SYP) on the hEF-derived hiN cells. (*F*) Representative traces of membrane potential changes induced by current injection steps from −20 pA to +50 pA in 10-pA increments before (*Left*) and after (*Right*) TTX. (*G*) Representative traces of whole-cell currents induced by 10-mV depolarizing voltage steps from −60 mV to +10 mV before (*Left*; with inward Na⁺ current) and after (*Right*; blocked Na⁺ current) TTX. *Insets* show respective traces on an expanded scale. Bars represent average conversion efficiency from three to six separate experiments ± SD. (Scale bars: *A*, 50 µm; *D* and *E*, 100 µm.)

Myt1l only requires a pulse of transgene expression during the initiation of the conversion phase, after which the hiN cells mature into neurons without exogenous gene expression.

To determine the contribution of each conversion factor to the generation of hiN cells, we performed conversions using each of the three factors individually or pairwise. Although Ascl1 alone was sufficient to induce a neuron-like phenotype, including expression of MAP2 and βIII-tubulin without significant reduction in conversion efficiency, neither Brn2a nor Myt1l alone resulted in the formation of a substantial number of hiN cells (Fig. 3 *C* and *D*). However, the Ascl1-alone cells had a markedly different morphology with shorter processes than those observed for the cells converted with the three factors Ascl1, Brn2, and Myt1l (Fig. 3*C*). When combining the factors into pairs, we found that Ascl1 + Brn2 and Myt1l + Brn2 produced mature-looking neurons, whereas Ascl1 + Myt1l resulted in cells with less pronounced neuronal morphology (Fig. 3*C*). Thus, based on number of cells and morphological criteria, Ascl1 + Brn2 may be as efficient as Ascl1, Brn2, and Myt1l in generating hiN cells. However, electrophysiological recordings showed that cells converted with Ascl1 + Brn2, in contrast to the cells converted with Ascl1, Brn2, and Myt1l, did not exhibit the electrophysiological properties of mature neurons (resting membrane potentials between −20 mV and −75 mV; input resistances between 50 MΩ and 2 GΩ; *n* = 12) and thus are not converted neurons. These findings demonstrate that all three factors contribute to the conversion of human fibroblasts into functional neurons.

To exclude the possibility that contaminating neural progenitors, glia, or neural crest cells served as the cellular origin of the iN cells, we performed extensive immunocytochemical characterization and PCR analysis of the starting fibroblast cultures as well as fibroblasts cultured in N3 medium and doxycycline for 6 and 12 d. With the exception of very few neural crest cells detected in low-passage hEF cultures (<0.1% at passage 2), none of the other markers could be detected (Figs. S2*G* and S3 *A–H* and Tables S2 and S3). To completely rule out the possibility that hiN cells are neural crest derivatives, we next used a commercially available, long-term expanded human fetal lung fibroblast cell line (HFL1) (12), which is a homogenous fibroblast cell line, as a starting material for conversion. Using immunohistochemistry and qRT-PCR, we confirmed that this cell line was composed purely of mesodermal fibroblasts and was completely absent of neural progenitors, glia, or neural crest cells (Figs. S2*G* and S3 *A–H* and Tables S2 and S3). Similar to what we observed with hEFs, we could detect cells with a neuronal-like morphology a few days after transduction with the three conversion factors. The hiN cells derived from fetal lung fibroblasts stained positive for βIII-tubulin and MAP2 (Fig. 4*A*) and were converted with efficiencies comparable to hEFs: 8.0% ± 4.45% at day 12 (*n* = 5) and 12.3% ± 5.9% at day 20 (*n* = 4). Whole-cell patch–clamp recordings confirmed that HFL1-derived hiN cells exhibited properties of functional neurons (Fig. 4 *B* and *C* and Table S4). Resting mem-

brane potential was approximately −62 mV, and TTX-sensitive action potentials were induced by depolarizing current in ∼80% of recorded cells (Fig. 4*B*). Depolarizing voltage steps induced in-
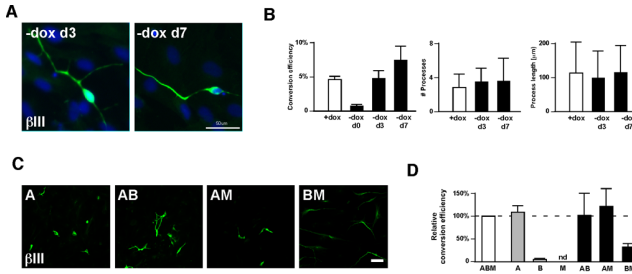
Fig. 3. Requirements for hiN conversion. (*A* and *B*) Removal of doxycycline at day 7 resulted in neurons expressing βIII (green) being formed with same efficiency and without affecting the morphological complexity of the resulting hiN cells ($n = 37$ for d3, $n = 68$ for d7, $n = 91$ for d0). (*C*) hiN cells expressing βIII-tubulin (green) obtained by conversion of hEFs in the presence of different combinations of Ascl1, Brn2, and Myt1l (ABM, A, B, M, AB, AM, and BM). (*D*) Conversion efficiency estimation of hiN cell formation using different combinations of conversion factors. Bars represent average conversion efficiency from three to six separate experiments ± SD.

ward currents (blocked by TTX) and outward currents. Several cells exhibited trains of action potentials in response to depolarizing current injection (Fig. 4*C*). Together, our data demonstrate that the hiN cells are derived from fibroblasts and provide evidence against the possibility that they originated from neural crest or other contaminating cell populations.

We next explored whether postnatal human fibroblasts could be directly converted to neurons. We used human foreskin fibroblasts (hFFs), a readily available postnatal source of cells that can be sufficiently expanded and is already used in clinical applications (13). The homogenous fibroblastic properties and absence of neural progenitors, neural crest cells, and glia was confirmed for hFFs (Figs. S1, S2*G*, and S3 and Tables S2 and S3). Similar to embryonic fibroblasts, the postnatal fibroblasts transduced with Ascl1, Brn2, and Myt1l gave rise to cells with a neuron-like morphology. When analyzed after 12 and 20 d, converted cells expressed MAP2 and βIII-tubulin with clear neuronal morphology (Fig. 5*A*). The conversion efficiency was slightly lower when using postnatal fibroblasts compared with embryonic cells as starting material: $4.3\% \pm 1.1\%$ at day 12 ($n = 3$). Whole-cell patch–clamp recordings demonstrated that, 30 d after conversion, hFF-derived iN cells had a resting membrane potential of approximately −41 mV and exhibited electrophysiological properties characteristic of neurons (Table S4). Cells fired mature action potentials in response to depolarizing current injection, and depolarizing voltage steps induced large inward currents and outward currents (Fig. 5*B*). At 36 d after transduction, several cells exhibited TTX-sensitive trains of action potentials, indicating that the neurons matured over time (Fig. 5*C*).

When investigating the neurotransmitter phenotype of the converted neurons, we found that, similar to what has been reported for mouse iN cells (10), neurons of both excitatory glutamatergic and inhibitory GABAergic phenotypes were present in the cultures (Fig. 6 *A* and *B*). Also in agreement with the mouse iN cell phenotype, we could not detect any significant number of cholinergic, serotonergic, or dopaminergic neurons

when screened for using immunocytochemistry for choline acetyltransferase, 5-hydroxytryptamine, and tyrosine hydroxylase (TH), respectively.

We next explored the possibility of directing the hiN cells into a specific neuronal subtype. We chose dopaminergic neurons, which would be of great interest from a clinical perspective because of their role in motor function and involvement in the pathogenesis of Parkinson's disease. To test whether expression of key transcription factors expressed during dopamine neuron development is sufficient to direct the hiN cells into a dopaminergic phenotype, we selected 10 genes involved in midbrain patterning and specification of dopamine neurons (*En1, Foxa2, Gli1, Lmx1a, Lmx1b, Msx1, Nurr1, Otx2, Pax2,* and *Pax5*) (14–21) and cloned them into lentiviral vectors. A pool of lentiviruses, LentiDA, containing all 10 genes was subsequently produced and validated (Fig. S4). We then performed the three-factor conversion of hEFs in combination with LentiDA and screened for the appearance of dopaminergic neurons after 12, 20, and 24 d. We found that a small, but reproducible, proportion of the hiN cells converted in the presence of LentiDA started to express TH 24 d after conversion (<1% of hiN cells) (Fig. 6 *C* and *F*). This finding provided proof of principle that formation of iN cells with specific neuronal subtypes can be achieved by transcription factor-mediated fate instruction combined with the three conversion factors.

We next set out to determine the minimal requirement for dopaminergic neuron fate specification. We found that when only Lmx1a and FoxA2 were expressed together with the three conversion factors, TH-expressing cells with typical morphology of cultured dopaminergic neurons could be detected from converted hEFs in much higher numbers (Fig. 6 *D* and *F*). Using HFL1 cells as starting material, conversion combined with expression of Lmx1a and FoxA2 gave rise to an even higher number of TH-expressing neurons (Fig. 6 *E* and *F*). The addition of Lmx1a and FoxA2 did not affect the conversion rate (Fig. S4*C*) nor did FoxA2 and Lmx1a induce neuron-like cells in the absence of the
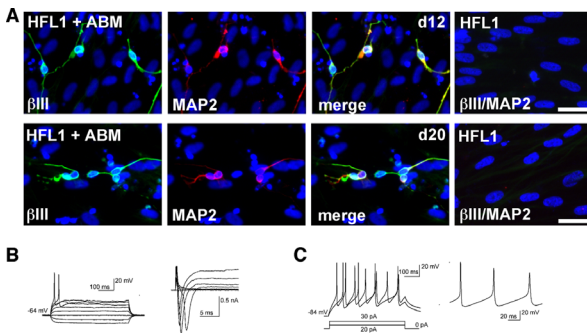

Fig. 4. Conversion of neurons from fetal lung fibroblasts. (*A*) Neurons expressing βIII-tubulin (green) and MAP2 (red) obtained by direct conversion of human fetal lung fibroblasts (HFL1) at 12 and 20 d after transduction with Ascl1, Brn2, and Myt1l (ABM). (*B*) Representative traces of membrane potential changes induced by current injection steps from −20 pA to +50 pA in 10-pA increments (*Left*) and representative traces of whole-cell currents induced by 10-mV depolarizing voltage steps from −60 mV to +10 mV (*Right*). (*C*) Representative traces of trains of action potentials induced by step injection of depolarizing current (*Right* shows traces on an expanded scale).
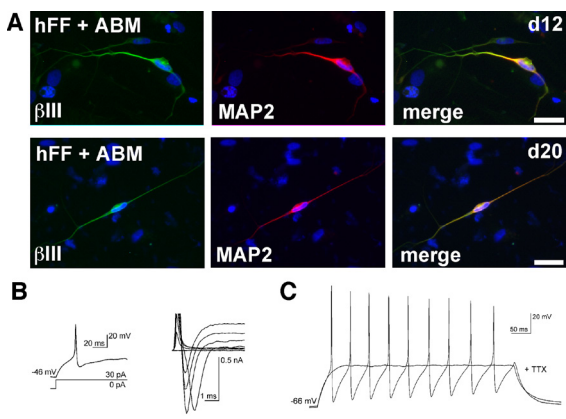
Fig. 5. Conversion of neurons from postnatal fibroblasts. (*A*) Neurons expressing βIII-tubulin (green) and MAP2 (red) obtained by direct conversion of hFFs at 12 and 20 d after transduction with Ascl1, Brn2, and Myt1l. (*B*) Representative trace of an action potential induced by depolarizing current injection (*Left*) and representative traces of whole-cell currents elicited in voltage–clamp mode by step depolarization (*Right*). (*C*) Representative trace of trains of action potentials induced by step injection of depolarizing current (20 pA) of hFF-derived iN cells, before and after TTX. (Scale bars: 50 μm.)

three conversion factors (Fig. S4C). The TH-expressing cells obtained from hEFs and HFL1 coexpressed βIII-tubulin (Fig. 6 D and E) but not the peripheral neuron marker peripherin (Fig. 6G). Aromatic L-amino acid decarboxylase (AADC), the second enzyme in dopamine synthesis and coexpression of Nurr1, an orphan nuclear receptor expressed by midbrain dopaminergic neurons, could also be detected in the TH-expressing cells (Fig. 6 H and I).

We found no TH neurons when hiN cells were generated with FoxA2 alone, whereas conversion in the presence of Lmx1a resulted in hiN cells expressing TH (Fig. 6J). However, none of the TH-expressing cells formed in the presence of Lmx1a alone coexpressed AADC (Fig. 6K). Whole-cell patch–clamp recordings demonstrated that hEF- and HFL1-derived iN cells converted in the presence of Lmx1a and FoxA2 were functional neurons (Table S5). At 28 d after conversion, action potentials could be induced by depolarizing current or occurred spontaneously (Fig. 6K). In current–clamp mode, a proportion of hEF-derived iN cells exhibited spontaneous action potentials, including pacemaker-like action potentials that were gradually blocked by adding TTX to the bath solution and rebound depolarizations resulting in action potentials after brief membrane hyperpolarizations (Fig. 6 L and M). Both spontaneous action potentials and rebound action potentials are characteristics compatible with midbrain dopamine neurons in vitro (22). Together, these data show that hiN cells generated from human fibroblasts via direct conversion can be further patterned into specific neuronal subtypes, exemplified here by the emergence of dopaminergic neurons after the addition of Lmx1a and FoxA2 during the conversion process.

Discussion

Our finding that human somatic cells, i.e., embryonic and postnatal fibroblasts, can be directly converted by using defined factors to functional neurons of a specific subtype is an important step toward developing iN cells for models of neurological disorders and brain repair.

A major concern when using primary fibroblasts for conversion is that contaminating neural progenitors, glia, or neural crest cells could be present in the starting material and selectively expanded when the embryonic fibroblasts are cultured in neural induction media and thus serve as the cellular origin of iN cells (23). To exclude this possibility, we first confirmed that our hEF cultures were indeed composed of only collagen-producing cells. We also carefully screened the cultures with a panel of antibodies against neural progenitors, glia, and neural crest cells. After the first passage, a very small fraction of cells expressing p75 and/or *Sox10* could be detected, suggesting a small contaminating neural crest population. Given the ex-

tremely low proportion of neural crest cells in low-passage hEFs and the observation that multipassaged hEFs, which do not contain any neural crest contaminants, also efficiently converted into functional neurons, it is unlikely that the hiN cells are derived from neural crest cells. Subsequent conversions using HFL1 and hFFs, two commercially available human fibroblast cell lines that do not contain any contaminating cells, confirmed that the hiN cells were in fact derived from fibroblasts.

By expressing dopamine fate determinants during the conversion, we could demonstrate that additional fate specification of iN cells is possible. The proportion of hiN cells that developed into dopaminergic neurons when converted in the presence of Lmx1a and FoxA2 was ~10%. Given that each cell needs to receive six viruses (A, B, M, Fuw, Lmx1a, and FoxA2) to differentiate into a dopamine neuron, this proportion is realistic and suggests that better delivery systems need to be developed in the future for more efficient conversion into dopamine neurons. Moreover, it will be interesting to explore the range of neuronal subtypes that can be formed via direct conversion by using combinations of other fate-determining genes or possibly by delivery of extrinsic factors.

An ultimate goal will be to use the hiN technology for disease modeling and cell therapy. As with iPS cells, iN cells circumvent the ethical concerns related to embryonic stem cell derivation and potential issues of allogenic rejection. In theory, the avoidance of reprogramming via a pluripotent state should reduce the risk of tumor formation after intracerebral grafting that is associated with the use of embryonic stem cells and iPS cells (24); thus, hiN cells may provide safer cells for transplantation in future applications. However, because the direct conversion does not go via a proliferative cell type, the number of neurons that can be obtained is limited by the accessible number of fibroblasts used as starting material for conversion. When using embryonic fibroblasts, this does not pose a serious limitation but could be limiting if generating patient-specific cells for disease modeling or autologous cell therapy.

Future studies should aim to increase the efficiency of hiN formation and the rate of dopaminergic neuron generation as well as to evaluate the converted dopaminergic neurons' ability to survive long term, reinnervate the denervated striatum, and ameliorate behavioral deficits after transplantation in rodent models of Parkinson's disease. Before clinical application of hiN cells can be considered, it will be critical to determine the optimal starting cell that can be obtained in sufficient numbers, to develop viral- and integration-free conversion systems, and to confirm the functionality and safety of hiN cells in vivo.
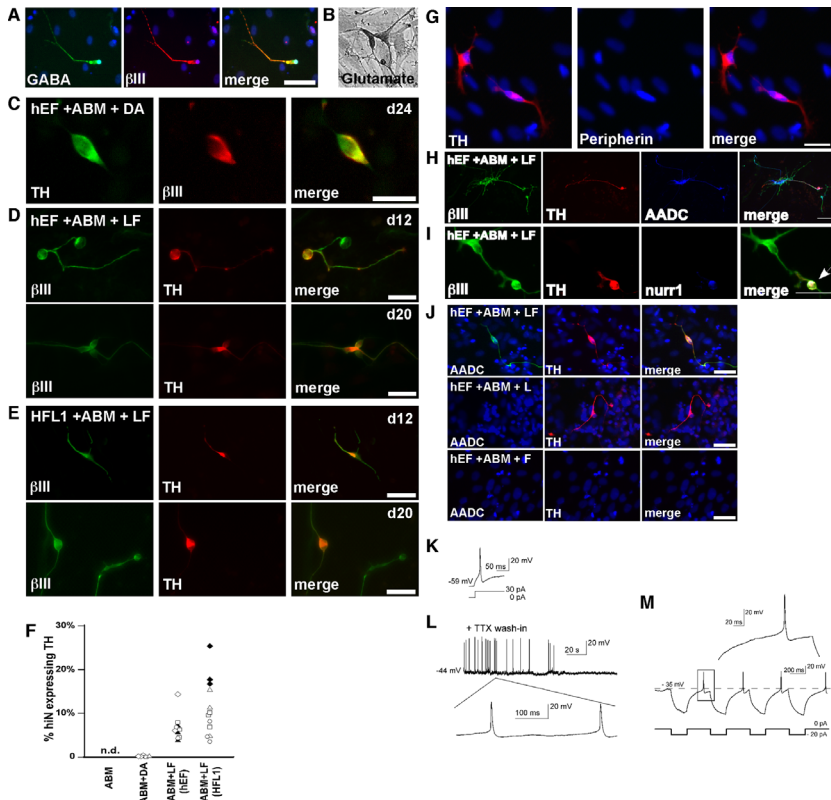
104

Fig. 6. Generation of dopamine neurons via direct conversion. (*A* and *B*) GABAergic and glutamatergic expressing hiN cells obtained by conversion with Ascl1, Brn2, and Myt1l. (*C* and *D*) hiN cells expressing TH (green) and βIII-tubulin (red) obtained by conversion of hEFs using Ascl1, Brn2, and Myt1l in combination with LentiDA, containing 10 genes involved in midbrain patterning and dopamine neuron differentiation (*C*) or in combination with Lmx1a and FoxA2 (LF) (*D*). (*E*) hiN cells expressing TH (green) and βIII-tubulin (red) obtained by conversion of HFL1 cells using Ascl1, Brn2, and Myt1l in combination with Lmx1a and Foxa2 (ABM + LF). (*F*) Quantification of dopaminergic neurons. Each symbol represents values obtained from separate biological replicates. Solid black symbols indicate data obtained when Lmx1a and FoxA2 were delivered 3 d after ABM; all other data points are from simultaneous delivery of all factors. (*G*) TH-expressing neurons (red) did not express peripherin (green). (*H* and *I*) hiN cells positive for TH (red) and βIII-tubulin (green) coexpress AADC (blue) and Nurr1 (blue; arrowhead). (*J*) TH (red) and AADC (green) expression in hiN cells obtained by conversion in the presence of Lmx1a and FoxA2 (LF; *Top*), Lmx1a alone (L; *Middle*), or FoxA2 alone (F; *Bottom*). (*K*) Example of an ABM + LF hEF iN cell exhibiting spontaneous, pacemaker-like action potentials that were gradually blocked by the addition of TTX to the bath solution. (*L*) Representative trace of an action potential induced by depolarizing current injection. (*M*) Example of an ABM + LF hEF iN cell exhibiting rebound depolarizations at the offset of brief membrane hyperpolarizations. *Insets* show respective traces on an expanded scale. (Scale bars: 50 μm.)

Methods

Tissue Sources and Cell Preparations. Fibroblasts were isolated from legally aborted fetuses aged 5.5–7 wk postconception, with approval of the Swedish National Board of Health and Welfare and the Lund/Malmö Ethics Committee (see Table S1 for details). Great care was taken to remove the head, vertebral column, dorsal root ganglia, and all inner organs to discard cells with a neurogenic potential. The remaining tissue was manually dissociated in 0.25% trypsin (Sigma), incubated at 37 °C to make a single-cell suspension, and then plated in T75 bottles. Cells were grown at 37 °C in 5% CO_2 in MEF medium, DMEM (Gibco) with 100 mg/mL penicillin/streptomycin (Sigma), 2 nM L-glutamine (Sigma), and 10% FBS (Biosera) until confluent. The cells were then dissociated with 0.25% trypsin, spun, and frozen in 50/50 DMEM/FBS with 10% DMSO (Sigma).

HFL1 (ATCC-CCL-153) and hFF (ATCC-CRL-2429) cells were obtained from the American Type Culture Collection, expanded in hEF medium until confluent, and then frozen.

For neuronal conversion, fibroblasts were plated in MEF medium at a density of 10,000 cells per cm² in tissue culture plates (Nunc) coated with 0.1% gelatin. Neuronal conversion was performed as previously described (10) with N3 medium, which is composed of DMEM/F12, 25 g/mL insulin, 50 g/mL transferrin, 30 nM sodium selenite, 20 nM progesterone (Sigma), 100 nM putrescine (Sigma), and penicillin/streptomycin.

Viral Vectors. Doxycycline-regulated lentiviral vectors expressing mouse cDNAs for Ascl1, Brn2, and Myt1l have been described elsewhere (10). The doxycycline-regulated system includes a separate lentiviral vector expressing

a Tet-On transactivator (FUW.rtTA-SM2; Addgene) that was always co-transduced in the conversion experiments.

Lentiviral vectors expressing mouse ORFs for En1, Foxa2, Gli1, Lmx1a, Lmx1b, Msx1, Nurr1, Otx2, Pax2, and Pax5 were generated by replacing GFP in a third-generation lentiviral vector containing a nonregulated, ubiquitous phospho-glycerate kinase promoter with the various ORFs (25). Plasmids containing the different cDNAs were purchased from Genecopoeia and subsequently verified by sequencing. Third-generation lentiviral vectors were produced as previously described (26) and titrated by quantitative PCR analysis (27). The titers of the vectors used in this study were in the range of 5×10^8 to 2×10^9 transducing units per mL. A multiplicity of infection of 2–3 was used for hEF and HFL1 cells.

Immunocytochemistry. Cells were fixed in 4% paraformaldehyde and preincubated for 30–60 min in blocking solution (5% normal serum and 0.25% Triton-X in 0.1 M potassium-buffered PBS). The primary antibodies (Table S6) were diluted in the blocking solution and applied overnight at 4 °C. Fluorophore-conjugated secondary antibodies (Molecular Probes or Jackson Laboratories) were diluted in blocking solution and applied for 2 h followed by three rinses in potassium PBS.

Quantifications and Efficiency Calculation. *Efficiency determination.* The total number of βIII-positive/MAP2-positive cells with a neuronal morphology and absence of fibroblast-like morphology were counted in 36 randomly selected 20× visual fields. This sampling was repeated three times, and the average number was used to calculate the mean number of positive cells per visual field. From this value, the total number of neurons per dish was estimated and, by following the method used by Vierbuchen et al. (10), the conversion efficiency was determined by dividing the number of neurons formed by the number of fibroblasts plated before infection.
TH quantifications. The total number of neurons per well was determined as described above. The total number of TH-expressing neurons per well was determined in the same manner or, when the number of TH neurons was low (<100), also by counting all of the TH-positive cells in the well.
Quantification of process length and number. Digital images were obtained with a Leica microscope and analyzed with Canvas IX. Total process length was determined by tracing each individual neuron, and the number of end processes was counted manually for the same cells.

Quantitative RT-PCR (qRT-PCR). Total RNA was isolated by using the RNeasy Micro Kit (Qiagen) according to the supplier's recommendations. For each sample, 1–4 mg of RNA was used for reverse transcription performed with random primers and SuperScriptIII (Invitrogen). SYBR green quantitative real-time PCR was performed with LightCycler 480 SYBR Green I Master (Roche) in a two-step cycling protocol. Data were quantified by the $\Delta\Delta C_T$ method and averaged upon normalization to GAPDH and β-actin expression. The specificity was confirmed by analyzing the dissociation curve and by validation in human embryonic tissue. Primer sequences are shown in Table S7.

Electrophysiology. Cells with neuronal morphology (round cell body and processes resembling neurites) were selected for whole-cell patch–clamp recordings at the indicated time points. Cells plated on coverslips were placed in a submerged recording chamber and constantly perfused with gassed bath solution (95% O_2/5% CO_2, pH 7.2–7.4, 295–300 mOsm, 32–34 °C) containing 119 mM NaCl, 2.5 mM KCl, 1.3 mM $MgSO_4$, 2.5 mM $CaCl_2$, 26 mM $NaHCO_3$, 1.25 mM NaH_2PO_4, and 25 mM glucose. Cells for recording were visualized under infrared light with differential interference contrast using an Olympus upright microscope equipped with a digital camera and a 40× water-immersion lens. Recording pipettes were filled with solution (pH 7.2–7.4, 295–300 mOsm) containing 122.5 mM potassium gluconate, 12.5 mM KCl, 10.0 mM KOH-Hepes, 0.2 mM KOH-EGTA, 2.0 mM MgATP, 0.3 mM Na_3-GTP, and 8.0 mM NaCl, resulting in pipette resistances of 3–4 Ω. Biocytin (0.5%; Sigma-Aldrich) was freshly dissolved in the pipette solution before recordings for post hoc identification of recorded cells. Resting membrane potential was estimated in current–clamp mode immediately after breaking the membrane and establishing whole-cell configuration. For measurements of action potentials and voltage responses, cells were current–clamped between −55 mV and −85 mV (depending on resting membrane potential), and 500-ms hyperpolarizing and depolarizing current steps were delivered in 10-pA increments through the whole-cell pipette. Spontaneous action potentials were measured in current–clamp mode (0 pA), and rebound action potentials were induced by brief injections of hyperpolarizing current (−20 pA). For measurements of whole-cell currents, cells were voltage–clamped between −60 mV and −70 mV, and 200-ms voltage steps were delivered in 10-mV increments. Voltage-gated sodium channels were blocked with 1 μM TTX (Tocris). Data were filtered at 2.9 kHz and sampled at 10 kHz with an EPC9 patch–clamp amplifier (HEKA Elektronik). Capacitance was compensated. Input resistance was measured at a holding potential of −60 mV by delivering −5-mV test pulses. Action potential amplitude was measured from the threshold to the peak voltage deflection, whereas half-width was measured as the duration of the action potential at half maximum amplitude. After-hyperpolarization amplitude was measured as the difference between the resting membrane potential and the maximum hyperpolarization after the action potential, whereas duration was measured as the time between the start and end of the hyperpolarization.

1. Takahashi K, et al. (2007) Induction of pluripotent stem cells from adult human fibroblasts by defined factors. *Cell* 131:861–872.
2. Takahashi K, Yamanaka S (2006) Induction of pluripotent stem cells from mouse embryonic and adult fibroblast cultures by defined factors. *Cell* 126:663–676.
3. Yu J, et al. (2007) Induced pluripotent stem cell lines derived from human somatic cells. *Science* 318:1917–1920.
4. Ebert AD, et al. (2009) Induced pluripotent stem cells from a spinal muscular atrophy patient. *Nature* 457:277–280.
5. Park IH, et al. (2008) Reprogramming of human somatic cells to pluripotency with defined factors. *Nature* 451:141–146.
6. Forsberg M, et al. (2010) Efficient reprogramming of adult neural stem cells to monocytes by ectopic expression of a single gene. *Proc Natl Acad Sci USA* 107:14657–14661.
7. Ieda M, et al. (2010) Direct reprogramming of fibroblasts into functional cardiomyocytes by defined factors. *Cell* 142:375–386.
8. Takeuchi JK, Bruneau BG (2009) Directed transdifferentiation of mouse mesoderm to heart tissue by defined factors. *Nature* 459:708–711.
9. Zhou Q, Brown J, Kanarek A, Rajagopal J, Melton DA (2008) In vivo reprogramming of adult pancreatic exocrine cells to β-cells. *Nature* 455:627–632.
10. Vierbuchen T, et al. (2010) Direct conversion of fibroblasts to functional neurons by defined factors. *Nature* 463:1035–1041.
11. Wernig M, et al. (2002) Tau EGFP embryonic stem cells: An efficient tool for neuronal lineage selection and transplantation. *J Neurosci Res* 69:918–924.
12. Breul SD, et al. (1980) Control of collagen production by human diploid lung fibroblasts. *J Biol Chem* 255:5250–5260.
13. Hovatta O, et al. (2003) A culture system using human foreskin fibroblasts as feeder cells allows production of human embryonic stem cells. *Hum Reprod* 18:1404–1409.
14. Acampora D, et al. (1995) Forebrain and midbrain regions are deleted in *Otx2*−/− mutants due to a defective anterior neuroectoderm specification during gastrulation. *Development* 121:3279–3290.
15. Andersson E, et al. (2006) Identification of intrinsic determinants of midbrain dopamine neurons. *Cell* 124:393–405.
16. Ferri AL, et al. (2007) Foxa1 and Foxa2 regulate multiple phases of midbrain dopaminergic neuron development in a dosage-dependent manner. *Development* 134:2761–2769.
17. Simon HH, Saueressig H, Wurst W, Goulding MD, O'Leary DD (2001) Fate of midbrain dopaminergic neurons controlled by the engrailed genes. *J Neurosci* 21:3126–3134.
18. Smidt MP, et al. (2000) A second independent pathway for development of mesencephalic dopaminergic neurons requires Lmx1b. *Nat Neurosci* 3:337–341.
19. Urbánek P, Fetka I, Meisler MH, Busslinger M (1997) Cooperation of *Pax2* and *Pax5* in midbrain and cerebellum development. *Proc Natl Acad Sci USA* 94:5703–5708.
20. Zervas M, Millet S, Ahn S, Joyner AL (2004) Cell behaviors and genetic lineages of the mesencephalon and rhombomere 1. *Neuron* 43:345–357.
21. Zetterström RH, et al. (1997) Dopamine neuron agenesis in Nurr1-deficient mice. *Science* 276:248–250.
22. Grace AA, Onn SP (1989) Morphology and electrophysiological properties of immunocytochemically identified rat dopamine neurons recorded in vitro. *J Neurosci* 9:3463–3481.
23. Sareen D, Svendsen CN (2010) Stem cell biologists sure play a mean pinball. *Nat Biotechnol* 28:333–335.
24. Miura K, et al. (2009) Variation in the safety of induced pluripotent stem cell lines. *Nat Biotechnol* 27:743–745.
25. Brown BD, et al. (2007) Endogenous microRNA can be broadly exploited to regulate transgene expression according to tissue, lineage and differentiation state. *Nat Biotechnol* 25:1457–1467.
26. Zufferey R, Nagy D, Mandel RJ, Naldini L, Trono D (1997) Multiply attenuated lentiviral vector achieves efficient gene delivery in vivo. *Nat Biotechnol* 15:871–875.
27. Georgievska B, et al. (2004) Regulated delivery of glial cell line-derived neurotrophic factor into rat striatum, using a tetracycline-dependent lentiviral vector. *Hum Gene Ther* 15:934–944.

106

Paper IV

Efficient induction of functional neurons from adult human fibroblasts

Ulrich Pfisterer,[1,3] James Wood,[2,3] Kristian Nihlberg,[1] Oskar Hallgren,[1,4] Leif Bjermer,[4] Gunilla Westergren-Thorsson,[1] Olle Lindvall[2,3] and Malin Parmar[1,3,*]

[1]Department of Experimental Medical Science; [2]Clinical Sciences; [3]Lund Stem Cell Center; Lund University; [4]Department of Respiratory Medicine and Allergology; Lund University Hospital; Lund, Sweden

Cellular reprogramming is a rapidly developing technology by which somatic cells are turned into pluripotent stem cells or other somatic cell types through expression of specific combinations of genes. This allows for the generation of patient-specific cell lines that can serve as tools for understanding disease pathogenesis, for drug screens and, potentially, for cell replacement therapies. Several cellular models of neurological disorders based on induced pluripotent cells (iPS cells) have been developed, and iPS-derived neurons are being explored as candidates for transplantation. Recent findings show that neurons can also be induced directly from embryonic and postnatal somatic cells by expression of defined combinations of genes. This conversion does not occur through a pluripotent stem cell stage, which eliminates the risk for tumor formation. Here, we demonstrate that functional neurons can be generated via direct conversion of fibroblasts also from adult individuals. Thus, this technology is an attractive alternative to iPS cells for generating patient- and disease-specific neurons suitable for disease modeling and autologous transplantation.

Induced pluripotent stem cells (iPS cells) obtained by reprogramming of adult human fibroblasts[1,2] are currently being used to develop models of a wide range of neurological diseases including spinal muscular atrophy, ALS, Parkinson disease and schizophrenia. Such cellular models will serve as valuable tools for understanding disease pathogenesis and progression.[3-5] The extent of genetic and epigenetic reprogramming and the mechanism for induction of pluripotency remains to be elucidated.[6-11] Nevertheless, the iPS technology has progressively been refined and human iPS cells can now be generated from different cell sources using methods that no longer rely on viral vectors or transgene integration.[12-16] These technical advancements have made iPS-derived neurons more suitable for replacement therapy, although they are still associated with substantial risk for tumor formation.[16-18]

Another approach for production of neurons from somatic cells is lineage reprogramming, in which one type of mature, differentiated somatic cell is directly transformed into another without passing through a pluripotent stage. Recent reports show that functional neurons, termed induced neurons, iNs, can be generated from mouse and human fetal and postnatal fibroblasts via direct conversion using defined sets of transcription factors such as Ascl1, Brn2 and Myt1l,[19-21] and subtype specific neurons can be obtained by varying the combination of transcription factors used.[20,22] Because of the ease of the technology, remarkably fast neural conversion and lack of a pluripotent stem cell intermediate, iN cells could become an attractive alternative to iPS cells.

However, whether the iN technology can be used to produce functional neurons from fibroblasts obtained from adult humans using the same combination of factors is unknown.

Here we used fibroblasts from six healthy adults ranging from 23 to 65 y of age. The fibroblasts were converted into neurons using the same three factors, Ascl1, Brn2 and Myt1l that previously have been shown to induce functional neurons from embryonic and postnatal fibroblasts.[19-21] We demonstrate direct conversion of the adult human fibroblasts to functional iNs with comparable efficiency as when human embryonic and postnatal were used as starting material. Interestingly, we observed no decrease in conversion efficiency with age, as fibroblasts from the older individuals converting with efficiency comparable to fibroblasts from the younger individuals. Thus, iN cells have the potential to be useful both for disease modeling and in future applications of cell replacement therapy.

Results/Discussion

We first used cultures of distal derived lung fibroblasts originating from a healthy individual in the age range of 45–65 y (For details, see Materials and Methods and **Table 1**). This line, as well as the other adult human fibroblast lines subsequently used in this study, have previously been characterized and shown to express α-SMA, a protein involved in contractile apparatus and prolyl 4-hydroxylase, an enzyme involved in collagen synthesis, but not SM22, an actin-binding protein that is expressed at high

Table 1. Clinical characterization

Name	Technique	Age (years of age)	Sex (M/F)	Distal fibroblasts
Ind1	Transplantation biopsy	45–65	F	yes
Ind2	Transplantation biospy	45–65	F	yes
Ind3	Transbronchial biopsy	29	M	yes
Ind4	Transbronchial biopsy	23	F	yes
Ind5	Transbronchial biopsy	23	M	yes
Ind6	Transbronchial biopsy	34	F	yes

levels in smooth muscle cells.[23] Before being used in the present set of experiments, the homogeneous fibroblast properties of the cells when cultured in fibroblast (MEF) medium, as well as when cultured in neural induction (N2B27) medium, were confirmed by staining for Collagen 1 and Collagen 3 (**Fig. 1A**). The absence of contaminating neural progenitors and neural crest cells in the fibroblast cultures was confirmed by qPCR as previously described in reference 20 (**Fig. 1B**). The cells were then used for conversion by delivering lentiviral vectors coding for Ascl1, Brn2 and Myt1l. In cultures transduced with conversion factors and subsequently grown in neural media, cells with elongated, neuron-like morphology became visible already 3–4 d after transgene activation, similar to what we observed for embryonic fibroblasts.[20] The cultures were fixed and analyzed by immunocytochemistry 12 and 20 d after transduction. Cells with characteristic neuronal morphology and expressing the neuronal markers βIII-tubulin and MAP2 were detected at both timepoints (**Fig. 1C**). In parallel control cultures, containing fibroblasts from the same individual and passage but not infected with conversion factors (otherwise treated identically), MAP2- and βIII-tubulin-expressing neurons were never observed (**Fig. 1C**).

We next performed similar conversion experiments on distal lung fibroblasts from a total of six healthy individuals of ages ranging from 23 to 65 y old (**Table 1**).[23] Based on cell number at each passage, theoretically a minimum of 70 x 10⁶ to 142 x 10⁶ fibroblasts from each individual were available at passage 5–6, which we used for conversion. We found that the fibroblasts from all six individuals converted into neurons expressing MAP2 and βIII-tubulin (**Fig. 2A**), with efficiencies similar to what has been reported for embryonic and postnatal fibroblasts (**Fig. 2D**).[7,8] We observed no difference in conversion efficiency between transbronchial and transplantation biopsies or gender. Interestingly, there was no correlation between age and conversion efficiency, as fibroblasts from the older individuals converting with efficiency comparable to fibroblasts from the younger individuals (**Fig. 2D**). Thus, iNs can be generated also from somatic cells of adult and elderly individuals.

To determine whether the neurons produced from the human adult-derived fibroblasts were functional, we performed whole-cell patch-clamp recordings on iN cells from three of the six individuals (Ind 1, 3 and 6) between 23 and 34 d after transduction. The induced neurons derived from all three individuals exhibited electrophysiological properties of functional neurons. Depolarizing current injection induced action potentials in ~47% of recorded cells (n = 60 cells in total, **Fig. 2B**) and in voltage-clamp mode, step depolarization gave rise to fast inactivating inward and outward currents characteristic of sodium and delayed rectifier potassium currents, respectively (**Fig. 2B**). Biocytin labeling confirmed the neuronal morphology of the recorded cells (**Fig. 2C**).

Taken together, our results demonstrate that functional neurons can be generated by direct conversion of fibroblasts from adult humans using combined expression of Ascl1, Brn2 and Myt1l. The derivation of iNs from patients with various neurological disorders should provide a novel platform for disease modeling. Moreover, patient-specific iNs could potentially be suitable for autologous cell replacement therapies. Because the iNs do not pass via a proliferative pluripotent stem cell stage, which has the advantage of circumventing the tumorigenicity concerns associated with grafting of pluripotent cells such as iPS cells,[18] the number of neurons that can be obtained is finite. However, we successfully used fibroblasts 5–6 passages after being isolated from each individual, which should provide a sufficient number of fibroblasts for potential therapeutic applications. If iN cells in the future can be obtained without the use of lentiviral vectors or transgene integration, they could provide a safe source of clinically applicable, patient-specific neurons in regenerative therapies for neurological disorders.

Materials and Methods

Subjects and sampling of tissue. Distal derived lung fibroblasts from 6 healthy individuals with no clinical history of lung disease were used. All sampling was done under approval of local Ethics committee (Dnr 413/2008 and 412/03). In four of these subjects (Ind 3–6), transbronchial specimens were taken with biopsy forceps (Olympus FB211D) guided by a fluoroscope. Biopsies were chopped into small pieces and immediately transferred to cell culture medium [DMEM supplemented with 10% FBS, Gentamicin and Amphotericin B (Gibco BRL, Paisley, UK)]. The tissue pieces were allowed to adhere to the plastic of cell culture flasks for 4 h, and then kept in cell culture medium at 37°C until outgrowth of fibroblasts was observed. For the remaining two individuals (Ind 1–2), fibroblasts were isolated from explants. Alveolar parenchymal specimens were collected 2–3 cm from the pleura in the lower lobes, i.e., from the same location where transbronchial biopsies were taken. Vessels and small airways were removed from the peripheral lung tissues and remaining tissues were chopped into small pieces. After rinsing, parenchymal pieces were allowed to adhere to the plastic of cell culture flasks for 4 h and were then kept in cell culture medium in 37°C cell incubators until outgrowth of fibroblasts was observed. For the first 2 passages, the cells were always split 1:3 (T25). Cells were then transferred to T75 and passaged 1:2 for subsequent passages. Passage 5–6 fibroblasts were used for experiments.
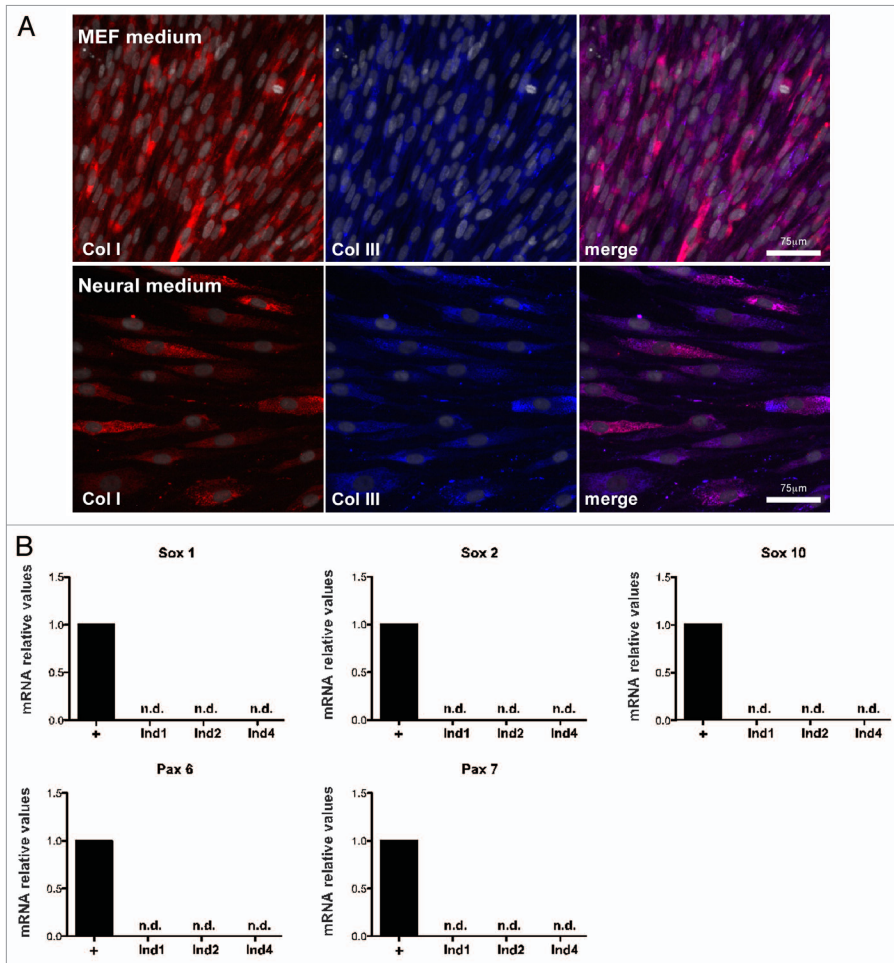
110

Figure 1A–B (For part C, see page 4). Direct conversion of adult human fibroblasts into human induced neural (iN) cells. (A) Fibroblast identity was validated by expression of collagen type I and collagen type III (ColI, ColIII). Fibroblasts were analyzed both when cultured in mouse embryonic fibroblast (MEF) medium and when cultured in neural induction (N2B27) medium. White indicates DAPI nuclear stain. (B) qRT-PCR analysis showed absence of the neural progenitor and neural crest markers *SOX1, SOX2, SOX10, PAX6* and *PAX7* from non-converted fibroblasts (cultured in N2B27 for 20 d; normalized to positive control (+), non passaged primary hEF cultures for *SOX* genes and whole head of human embryo for P*AX* genes).

Viral vectors and neural conversion. Doxycycline-regulated lentiviral vectors expressing mouse cDNAs for AsclI, Brn2 and Myt1l have been described in reference 20. The doxycycline regulated system includes a separate lentiviral vector expressing a TET-ON transactivator (FUW.rtTA-SM2, Addgene) that was always co-transduced in the conversion experiments. The titers of the vectors used in this study were in the range of 1.3 x 10^8– 2.9 x 10^9 TU/ml. A MOI of 5 for ABM and 10 for Fuw was used for conversion.

For neuronal conversion, fibroblasts were plated in MEF medium at a density of 10,000 cells/cm^2 in tissue culture plates (NUNC) coated with 0.1% gelatine. Neuronal conversion was
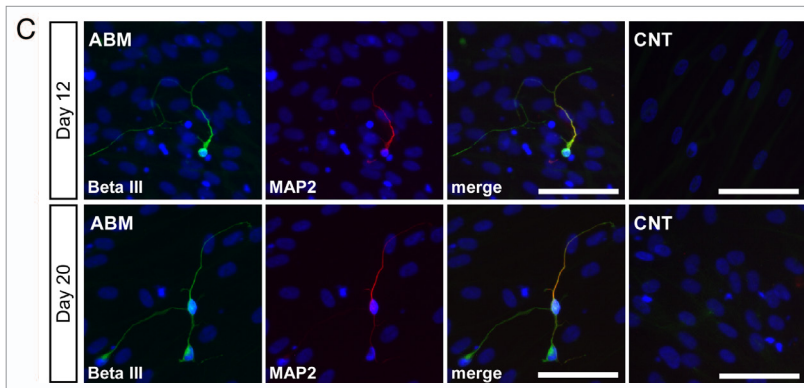
111

Figure 1C (For parts A–B, see previous page). Direct conversion of adult human fibroblasts into human induced neural (iN) cells. (C) Neurons expressing ßIII-tubulin (green) and MAP2 (red) obtained by direct conversion of adult fibroblasts at day 12 and day 20 after Ascl1, Brn2 and Myt1l expression was activated. In parallel cultures treated the same but without delivering transgenes no neurons were ever observed (right part C). Blue indicates DAPI nuclear stain. Scale bars = 75 μm.

performed as previously described in reference 20, using N2/B27 (Stem Cell Sciences) as neural induction media.

Immunocytochemistry. Cells were fixed in 4% paraformaldehyde (PFA) and pre-incubated for 30 min-1 h in blocking solution (5% normal serum and 0.25% triton-X in 0.1 M KPBS). The primary antibodies (MAP2 1:500, βIII-tubulin 1:5,000) were diluted in the blocking solution and applied over night in 4°C. Fluorophore-conjugated secondary antibodies (Molecular Probes or Jackson Laboratories) were diluted in blocking solution and applied for 2 h followed by 3 rinses in KPBS. All images were obtained using a Leica inverted microscope.

Electrophysiology. Recordings were performed as previously described in reference 20. Briefly, converted cells grown on coverslips were constantly perfused with heated (32–34°C), gassed (95% O_2, 5% CO_2) bath solution (pH 7.2–7.4, 295–300 mOsm) containing (in mM): 119 NaCl, 2.5 KCl, 1.3 $MgSO_4$, 2.5 $CaCl_2$, 26 $NaHCO_3$, 1.25 NaH_2PO_4 and 25 glucose. Recording pipettes were filled with solution (pH 7.2–7.4, 295–300 mOsm) containing (in mM): 122.5 potassium gluconate, 12.5 KCl, 10.0 KOH-Hepes, 0.2 KOH-EGTA, 2 MgATP, 0.3 Na_3-GTP and 8 NaCl, resulting in pipette resistances of 3–5 MΩ. Voltage-gated sodium channels were blocked using 1 μm tetrodotoxin (TTX, Tocris).

Quantitative RT-PCR. Total RNA was isolated using the RNeasy Micro kit (Qiagen) according to the supplier's recommendations. For each sample, 300 ng of RNA was used for reverse transcription performed with random primers and SuperScriptIII (Invitrogen). SYBR green quantitative real-time PCR was performed with LightCycler 480 SYBR Green I Master (Roche) in a 2-step cycling protocol. Data were quantified using the ΔΔCt-method and averaged upon normalization to GAPDH and β-actin expression. The specificity was confirmed by analyzing the dissociation curve and by validation in human embryonic tissue. Primer sequences were the same as previously reported in reference 20.

References

1. Takahashi K, Tanabe K, Ohnuki M, Narita M, Ichisaka T, Tomoda K, et al. Induction of pluripotent stem cells from adult human fibroblasts by defined factors. Cell 2007; 131:861-72; DOI:10.1016/j.cell.2007.11.019; PMID:18035408.

2. Yu J, Vodyanik MA, Smuga-Otto K, Antosiewicz-Bourget J, Frane JL, Tian S, et al. Induced pluripotent stem cell lines derived from human somatic cells. Science 2007; 318:1917-20; DOI:10.1126/science.1151526; PMID:18029452.

3. Brennand KJ, Simone A, Jou J, Gelboin-Burkhart C, Tran N, Sangar S, et al. Modelling schizophrenia using human induced pluripotent stem cells. Nature 2011; 473:221-5; DOI:10.1038/nature09915; PMID:21490598.

4. Ebert AD, Yu J, Rose FF Jr, Mattis VB, Lorson CL, Thomson JA, et al. Induced pluripotent stem cells from a spinal muscular atrophy patient. Nature 2009; 457:277-80; DOI:10.1038/nature07677; PMID:19098894.

5. Park IH, Arora N, Huo H, Maherali N, Ahfeldt T, Shimamura A, et al. Disease-specific induced pluripotent stem cells. Cell 2008; 134:877-86; DOI:10.1016/j.cell.2008.07.041; PMID:18691744.
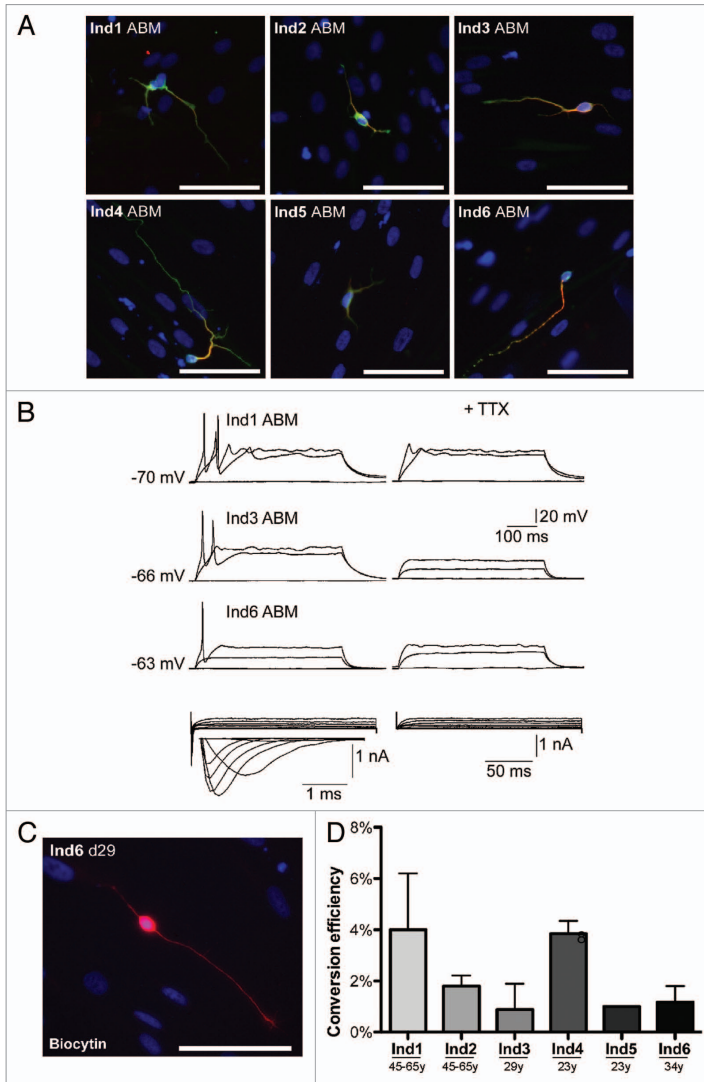
Figure 2. Efficiency and functionality of direct conversion from six individual adults. (A) iNs expressing ßIII-tubulin (green) and MAP2 (red) were formed by direct conversion of fibroblasts (Passage 5–6) from all six individuals, Ind1–6 (n = 4–6 for each individual). Blue indicates DAPI nuclear stain. (B) Representative traces of action potentials induced by step injection of depolarizing current (10 pA increments) and of whole cell currents induced by depolarizing voltage steps from -60 mV to +20 mV in 10 mV increments. Action potentials and Na$^+$ currents were blocked by bath application of TTX (right part). (C) Biocytin filled hiN cell confirmed neuronal morphology of recorded cells. (D) Conversion efficiency estimation of hiN formation at days 12, Passage 5–6 (n = 4 for Ind1; n = 2 for Ind2; n = 2 for Ind3; n = 2 for Ind4; n = 1 for Ind5; n = 3 Ind6). Scale bars: (A) 75 μm; (B) 50 μm.

113

6. Menendez S, Camus S, Izpisua Belmonte JC. p53: guardian of reprogramming. Cell Cycle 2010; 9:3887-91; DOI:10.4161/cc.9.19.13301; PMID:20948296.

7. Saunders LR, Sharma AD, Tawney J, Nakagawa M, Okita K, Yamanaka S, et al. miRNAs regulate SIRT1 expression during mouse embryonic stem cell differentiation and in adult mouse tissues. Aging 2010; 2:415-31; PMID:20634564.

8. Plath K, Lowry WE. Progress in understanding reprogramming to the induced pluripotent state. Nat Rev Genet 2011; 12:253-65; DOI:10.1038/nrg2955; PMID:21415849.

9. Kim K, Doi A, Wen B, Ng K, Zhao R, Cahan P, et al. Epigenetic memory in induced pluripotent stem cells. Nature 2010; 467:285-90; DOI:10.1038/nature09342; PMID:20644535.

10. Stadtfeld M, Hochedlinger K. Induced pluripotency: history, mechanisms and applications. Genes Dev 2010; 24:2239-63; DOI:10.1101/gad.1963910; PMID:20952534.

11. Lagarkova MA, Shutova MV, Bogomazova AN, Vassina EM, Glazov EA, Zhang P, et al. Induction of pluripotency in human endothelial cells resets epigenetic profile on genome scale. Cell Cycle 2010; 9:937-46; DOI:10.4161/cc.9.5.10869; PMID:20160486.

12. Ichida JK, Blanchard J, Lam K, Son EY, Chung JE, Egli D, et al. A small-molecule inhibitor of tgfBeta signaling replaces sox2 in reprogramming by inducing nanog. Cell Stem Cell 2009; 5:491-503; DOI:10.1016/j.stem.2009.09.012; PMID:19818703.

13. Woltjen K, Michael IP, Mohseni P, Desai R, Mileikovsky M, Hamalainen R, et al. piggyBac transposition reprograms fibroblasts to induced pluripotent stem cells. Nature 2009; 458:766-70; DOI:10.1038/nature07863; PMID:19252478.

14. Kaji K, Norrby K, Paca A, Mileikovsky M, Mohseni P, Woltjen K. Virus-free induction of pluripotency and subsequent excision of reprogramming factors. Nature 2009; 458:771-5; DOI:10.1038/nature07864; PMID:19252477.

15. Soldner F, Hockemeyer D, Beard C, Gao Q, Bell GW, Cook EG, et al. Parkinson's disease patient-derived induced pluripotent stem cells free of viral reprogramming factors. Cell 2009; 136:964-77; DOI:10.1016/j.cell.2009.02.013; PMID:19269371.

16. Sun N, Longaker MT, Wu JC. Human iPS cell-based therapy: considerations before clinical applications. Cell Cycle 2010; 9:880-5; DOI:10.4161/cc.9.5.10827; PMID:20160515.

17. Patel M, Yang S. Advances in reprogramming somatic cells to induced pluripotent stem cells. Stem Cell Rev 2010; 6:367-80; DOI:10.1007/s12015-010-9123-8; PMID:20336395.

18. Miura K, Okada Y, Aoi T, Okada A, Takahashi K, Okita K, et al. Variation in the safety of induced pluripotent stem cell lines. Nat Biotechnol 2009; 27:743-5; DOI:10.1038/nbt.1554; PMID:19590502.

19. Pang ZP, Yang N, Vierbuchen T, Ostermeier A, Fuentes DR, Yang TQ, et al. Induction of human neuronal cells by defined transcription factors. Nature 2011; 476:224-7; PMID:21725324.

20. Pfisterer U, Kirkeby A, Torper O, Wood J, Nelander J, Dufour A, et al. Direct conversion of human fibroblasts to dopaminergic neurons. Proc Natl Acad Sci USA 2011; 108:10343-8; DOI:10.1073/pnas.1105135108; PMID:21646515.

21. Vierbuchen T, Ostermeier A, Pang ZP, Kokubu Y, Sudhof TC, Wernig M. Direct conversion of fibroblasts to functional neurons by defined factors. Nature 2010; 463:1035-41; DOI:10.1038/nature08797; PMID:20107439.

22. Caiazzo M, Dell'anno MT, Dvoretskova E, Lazarevic D, Taverna S, Leo D, et al. Direct generation of functional dopaminergic neurons from mouse and human fibroblasts. Nature 2011; 476:224-7; PMID:21725324.

23. Nihlberg K, Andersson-Sjöland A, Tufvesson E, Erjefält JS, Bjermer L, Westergren-Thorsson G. Altered matrix production in the distal airways of individuals with asthma.Thorax. 2010; 65:670-6. PMID: 20685740

Paper V

Replacing Mash1 with Ngn2 During Neural Conversion of Human Fibroblasts Influences Phenotype and Electrophysiological Properties of Generated Neurons

James Wood, Olof Torper, Agnete Kirkeby, Olle Lindvall, Malin Parmar

Departments of Experimental Medical Science and Clinical Sciences, Wallenberg Neuroscience Center, and Lund Stem Cell Center, Lund University, SE-221 84, Lund, Sweden

Fibroblasts can be directly reprogrammed to induced neurons (iNs) via overexpression of defined sets of transcription factors. Neuronal subtypes such as dopaminergic or motor neurons can be generated using different combinations of transcription factors. Here we have explored whether replacing Ascl1 (referrred to as Mash1) with the proneural gene Ngn2 influences the phenotype and electrophysiological properties of neurons generated from human fibroblasts. Overexpression of Ngn2, Brn2, and Myt1l in fibroblasts led the generation of functional iNs with similar frequency and time course as when using Mash1. Immunohistochemical analysis revealed that, in line with their respective roles in development, Mash1 overexpression induced the formation of GABAergic neurons while conversion using Ngn2 did not. Furthermore, electrophysiological analysis revealed differences in the passive and active membrane properties of the iNs generated. Our findings indicate that Ngn2 can substitute for Mash1 during fibroblast reprogramming to functional neurons, but that the different transcription factor combination results in iNs with different phenotype and electrophysiological properties.

INTRODUCTION

Fibroblasts can be directly converted to mature functional neurons; so-called induced-neurons (iNs), by viral overexpression of the transcription factors Ascl1, Brn2, and Myt1l (ABM) (Vierbuchen et al., 2010; Pfisterer et al., 2011a; Pang et al., 2011; Pfisterer et al 2011b). The resulting neurons can be further reprogrammed towards subtype specific neurons including dopaminergic neurons (Pfisterer et al., 2011a; Caiazzo et al., 2011), glutamatergic neurons (Qiang et al., 2011) and motor neurons

Corresponding Author: James Wood
Laboratory of Neurogenesis and Cell Therapy
Wallenberg Neuroscience Center
Lund University
SE-221 84
Sweden
Email: James.Wood@med.lu.se

(Son et al., 2011). Fibroblast reprogramming may be useful in studying disease progression (Park et al., 2008; Dimos et al., 2008; Brennand et al., 2011; Caiazzo et al., 2011; Qiang et al., 2011) and could potentially be used as a novel diagnostic tool as well as provide neurons for cell replacement. An important issue to consider is that the factors used for conversion influence the characteristics of the neurons generated and will thus determine their suitability for disease-modeling or future transplantation studies.

With few exceptions based on microRNA for reprogramming (Yoo et al., 2011; Ambasudhan et al., 2011), all neural conversion cocktails are based on the proneural gene Ascl1 (Vierbuchen et al., 2011; Pfisterer et al., 2011a, Pang et al., 2011, Caiazzo et al., 2011; , Qiang et al., 2011; Pfisterer et al., 2011b). Ascl1, also referred to as Mash1, encodes a basic-helix-loop-helix transcription factor. Vierbuchen et al.

(2010) found that excluding Mash1 reduced the conversion efficiency with which iNs are generated. During brain development, Mash1 has an important role in neuronal differentiation and subtype specification within the nervous system. Expression of Mash1 promotes the differentiation of GABAergic neurons (Letinic et al., 2002) and can transform the identity of neuronal populations (Parras et al., 2002). Forced expression of Mash1 in neural stem cells leads to the formation of GABAergic neurons (Berninger et al., 2007) and astrocytes can be transformed to GABAergic neurons by retroviral overexpression of Mash1 (Heinrich et al., 2011).

Neurogenin-2 (Ngn2, encoded by Neurog2) is another proneural gene that is primarily expressed in neural progenitor populations complementary to Mash1 in the central and peripheral nervous system. Ngn2 has important roles in the development of cortical neurons (Fode et al., 2000; Nieto et al., 2001), sensory neurons (Zirlinger et al., 2002) and dopaminergic neurons (Andersson et al., 2006; Kele et al., 2006; Andersson et al., 2007). Neural stem cells can be directed to a glutamatergic phenotype by overexpression of Ngn2 (Berninger et al., 2007) and Heinrich et al. (2011) have shown that retroviral expression of Ngn2 in astrocytes can convert them to glutamatergic neurons. To date, Ngn2 has not been used for iN conversion.

The objective of the present study was, firstly, to address whether Ngn2 could substitute for Mash1 during neural conversion, and secondly, whether this would lead to changes in the phenotype and electrophysiological properties of the generated neurons. We overexpressed either Ascl1, Brn2, and Myt1l as previously described (Pfisterer et al., 2011a; 2011b) or Ngn2, Brn2, and Myt1l in human fetal fibroblasts. We show that overexpression of Ngn2 instead of Mash1 also leads to the conversion of fibroblasts to functional neurons. The resulting iN cells were formed at a similar frequency and temporal manner but exhibited different neurotransmitter phenotype and electrophysiological properties.

MATERIALS AND METHODS

Cell culturing and viral transduction

HFL1 (ATCC-CCL-153) cells were obtained from the American Type Culture Collection, expanded in hEF medium until confluent, and then frozen. Three days before transduction, HFL1 cells were thawed in MEF medium containing DMEM (Gibco), 10% fetal bovine serum (Biosera), 2nM L-Glutamine (Gibco) and 100 mg/ml pen/strep (Gibco) and plated in a T75 flask coated with 1% gelatin (roughly 500,000 cells). One day before transduction, cells were washed twice in phosphate buffered saline (PBS) and disassociated using 2 ml of 0.025% trypsin (Sigma). Cells were then transferred to coated culture plates (0.1% gelatin) at a density of 36,000 cells/cm2 in MEF medium. Cells were transduced with the doxycycline regulated lentiviral vectors Ascl1, Brn2, Myt1l (ABM) and a separate vector containing the transactivator TET-ON (FUW .rtTZ-SM2). When transduced with Neurog2, Brn2, Myt1l (NBM), a non-regulated lentiviral vector expressing the mouse open-reading-frame for Neurog2 was used. For the transgenes, a multiplicity-of-infection (MOI) of 5 was used and for the transactivator a MOI of 10. Virus-titers were greater than 10^8. One day after transduction, MEF medium was changed to MEF medium containing 2 μg/ml doxycycline. Three days after transduction, the medium was swapped to N2B27 containing 2 μg/ml doxycycline. Medium was changed every 2-3 days thereafter.

Immunohistochemistry

Cells were fixed in 4% paraformaldehyde and preincubated for 30-60 minutes in blocking solution containing 5% normal serum and 0.25% Triton-X in 0.1 M potassium-buffered PBS. The following primary antibodies were diluted in the blocking serum and applied overnight at 4oC: mouse anti-MAP2 (1:500, Sigma), rabbit anti-GABA (1:1000, Sigma). Fluorophore-conjugated secondary antibodies (Molecular probes or Jackson laboratories) were diluted in blocking
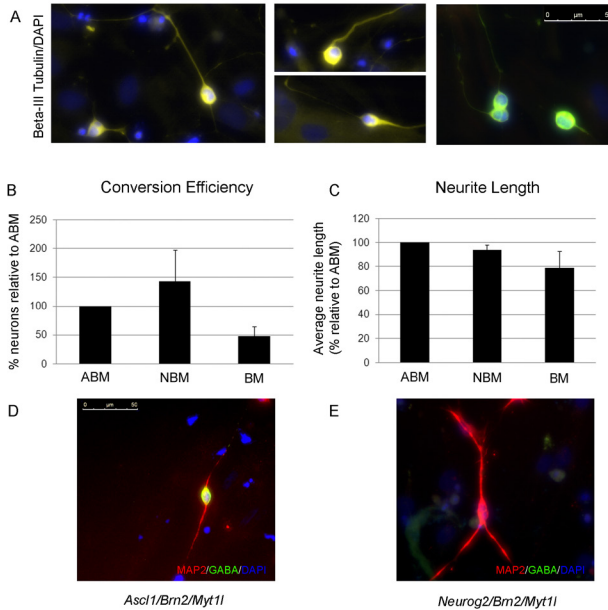
Figure 1. Overexpression of Neurogenin2 instead of Mash1 still leads to the development iNs with neuronal morphology and expression of neuronal markers. (A) Fibroblasts were converted to Beta-III Tubulin expressing iNs 30 days after transduction (B) Conversion efficiency was similar when NBM was used instead of ABM, while using BM tended to reduce efficiency. (C) iNs converted with ABM and NBM have similar neurite length. (D, E) Fibroblasts converted with ABM and NBM led to MAP2 expression and neuronal morphology, however no GABA-positive cells were observed when NBM was used.

solution and applied for 2 hours followed by three rinses in potassium PBS.

Quantification and Efficiency Calculations

Neuronal conversion and neurite outgrowth were evaluated with a Cellomics instrument (Thermo Scientific) using the neurite outgrowth algorithm. Neurite outgrowth is presented as the average neurite length sum per neuron. All data was normalized to the ABM control (ABM = 100%). The total number of MAP2- and GABA-expressing neurons was determined by counting all MAP2 and GABA positive cells in wells with fibroblasts converted using ABM or NBM. Cell counting was performed at 20x magnification using a Leica inverted microscope equipped with a DFC 360 FX camera and Leica application suite advanced fluorescent software (LAS AF).

Electrophysiology

Recordings were performed as previously described (Pfisterer et al., 2011a). Briefly, converted cells grown on coverslips were constantly perfused with heated (32-34oC), gassed (95% O2, 5% CO2) bath solution (pH 7.2-7.4, 295-300 mOsm) containing (in mM): 119 NaCl, 2.5 KCl, 1.3 MgSO4, 2.5 CaCl2, 26 NaHCO3, 1.25 NaH2PO4, and 25 glucose. Recording pipettes were filled with solution (pH 7.2–7.4, 295–300 mOsm) containing (in mM): 122.5 potassium gluconate, 12.5 KCl, 10.0 KOH-Hepes, 0.2 KOH-EGTA, 2 MgATP, 0.3 Na3-GTP, and 8 NaCl, resulting in pipette resistances of 3–5 MΩ. Voltage-gated sodium channels were blocked using 1 μm tetrodotoxin (TTX, Tocris).

RESULTS

We have previously shown that human fibroblasts can be converted to neurons by over-expression of the transcription factors Ascl1, Brn2, Myt1l (ABM) (Pfisterer et al., 2011a; 2011b). In the present study we investigated whether the proneural gene, Ngn2, could be used to generate iNs instead of Mash1. When using Ngn2 in combination with Brn2 and Myt1l, we found that iN cells started to appear in the same time frame as we have previously reported for ABM conversion (Pfisterer et al., 2011a; 2011b). When analyzing the cells 30 days after viral transduction, Beta-III Tubulin expressing cells with neuronal morphology were present in cultures of fibroblasts converted with Ngn2, Brn2, Myt1l (NBM) (Figure 1A). To determine whether using NBM instead of ABM resulted in differences in conversion efficiency, we examined NBM and ABM derived iNs 40 days after transduction. Unbiased and automated quantification using Cellomics demonstrated that 40 days after transduction the conversion efficiency using NBM was comparable to that when using ABM (Figure 1B). We next assessed the total neurite length of iNs generated using NBM and found that the total length per cell was similar to neurites of iNs generated using ABM (Figure 1C). When fibroblasts were converted with only BM, conversion efficiency was markedly reduced and neurites tended to be shorter, indicating that proneural genes have a crucial role in the reprogramming progress.

Mash1 directs GABAergic neuronal differentiation during development while Ngn2 primarily directs cells towards a glutamatergic phenotype. To determine whether the fibroblast-derived neurons were GABAergic, immunohistochemistry was performed at day 40 in vitro. In line with their respective roles in development, while ~13% of ABM converted fibroblasts expressed GABA, no cells converted with NBM exhibited a GABAergic phenotype (Figure 1D, E).
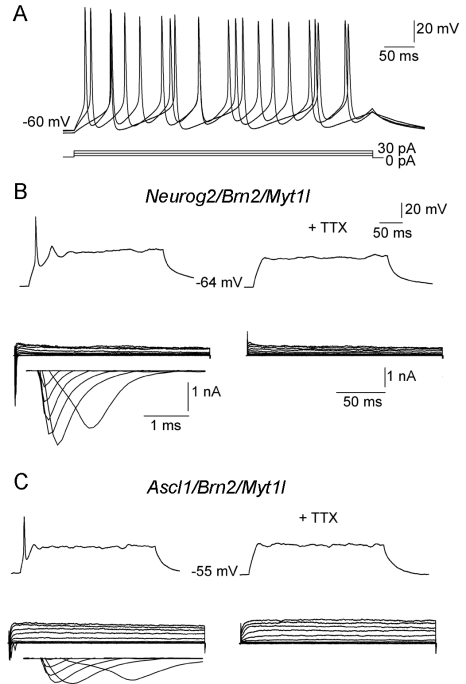

Figure 2. Fibroblasts converted with NBM are electrophysiologically functional neurons 40 days after transduction. (A) Representative traces of trains of action potentials elicited by depolarizing current injection in an iN cell generated using NBM. (B, C) Representative traces showing action potentials generated in response to depolarizing current injection (30 pA-step) and inward Na+ and outward K+ whole-cell currents in response to depolarizing voltage steps from -70 to +40 mV in iNs generated using NBM and ABM (TTX blocked action potentials and inward Na+ currents). Insets show adjacent traces on an expanded scale.

Whole-cell patch-clamp recordings performed at day 40 in vitro demonstrated that iN cells generated using NBM had properties of mature neurons, comparable to iNs generated using ABM, as we have previously reported (Pfisterer et al., 2011a). NBM generated iNs had

Table 1. Passive and active membrane properties of iN cells. *, denotes p < 0.05, Student's unpaired t-test.

	Ascl1/Brn2/Myt1l	Neurog2/Brn2/Myt1l
Resting membrane potential (mV)	-24.9 ± 1.8*	-36.8 ± 3.6
Membrane capacitance (pF)	4.3 ± 0.5*	7.6 ± 1.3
Input resistance (GΩ)	2.8 ± 0.5	2.8 ± 0.4
Peak inward Na+ current (nA)	0.57 ± 0.1*	2.9 ± 1.0
Action potentials (AP)	7 of 8 cells	9 of 9 cells
AP Threshold (mV)	-30.5 ± 1.6	-34.4 ± 1.4
AP Amplitude (mV)	38.5 ± 4.0*	58.8 ± 6.2
AP Duration (ms)	2.4 ± 0.2	2.5 ± 0.4
Afterhyperpolarization amplitude (mV)	-12.9 ± 1.5	-13.1 ± 1.2
Duration (ms)	34.1 ± 4.2*	108.8 ± 27.2

a resting membrane potential (RMP) of approximately -37 mV and frequently fired trains of action potentials in response to depolarizing current injection (Figure 2A). In order to directly compare NBM and ABM derived iNs, identical whole cell recordings were performed on a number of cells from each conversion setup. Action potentials were induced by a single depolarizing current injection step and whole-cell currents characteristic of sodium and potassium currents were induced by step depolarization of the membrane potential (Figure 2B, C). Although both Mash1 and Ngn2, when over-expressed in combination with BM, resulted in the generation of functional neurons, differences in the passive and active membrane properties were detected (Table 1). These findings, particularly the difference in peak inward Na+ current, suggest there are differences in the composition of membrane channels in iNs generated using NBM and ABM (Isom et al., 1992; Seutin and Engel 2010).

DISCUSSION

In the present study we have shown that replacing Mash1 overexpression with Ngn2 leads to the formation of functionally mature neurons with similar conversion efficiency and timing. We report that Mash1 leads to the generation of GABAergic cells, while Ngn2 does not, which is consistent with previous studies (Berninger et al., 2007; Heinrich et al., 2011). Electrophysiological recordings demonstrated that there are likely differences in the number, distribution or composition of membrane channels when Ngn2 is used rather than Mash1. This is the first study to directly compare the membrane properties of iNs generated using different combinations of transcription factors. However, differences in membrane properties of iNs have also been reported when fetal (Caiazzo et al., 2011) or postnatal fibroblasts (Ambasudhan et al., 2011) were used instead of adult-derived fibroblasts. On the other hand, Brennand et al. (2011) showed that iPS-derived neurons generated from patients with schizophrenia had similar electrophysiological properties to those generated from healthy individuals, but exhibited altered gene expression and dendrite and synapse development. These observations indicate that the genes used for conversion in combination with the starting material will influence the functional and morphological properties of iNs.

This study and others have shown that using different combinations of transcription factors can alter the characteristics of the neurons generated. Dopamine neurons can be generated from fibroblasts by overexpression of Ascl1,

Brn2, Myt1l, FoxA2, and Lmx1A (Pfisterer et al., 2011a) or Ascl1, Nurr1 and Lmx1A (Caiazzo et al., 2011) and spinal motor neurons can be generated by overexpression of Ascl1, Brn2, Myt1l, Lhx3, Hb9, Isl1, and Ngn2 (Son et al., 2011). Meanwhile, Ambasudhan et al. (2011) demonstrated that fibroblasts can be directly converted to neurons using overexpression of microRNA (miRNA-124) in combination with Myt1l and Brn2. These studies indicate that a small number of factors can alter global gene expression and thus transform a cells identity.

Direct reprogramming provides important opportunities in the study of neurodegenerative disorders such as Parkinson's (PD), Amyotrophic lateral sclerosis and Alzheimer's disease where specific regions of the brain are affected. To date, both disease progression and cell replacement therapies have been investigated using embryonic stem cells and induced pluripotent stem (iPS) cells (fibroblasts reprogrammed to an embryonic stem cell-like state). Using stem cells for cell replacement therapy has shown promise (reviewed by Lindvall and Kokaia, 2010) and stem cell-derived dopamine neurons functionally integrate with host neural circuitry in a model of PD (Tønnesen et al., 2011). Once reprogrammed, iPS cells can be directed to differentiate into neurons that have the potential to improve functional recovery when transplanted in a rodent model of PD (Wernig et al., 2008). iPS cells are an attractive source for cell replacement therapy due to the fact that they can be patient-derived and thus eliminate the need of immunosuppression. iPS cells and the neurons derived from them can also be used to model neurological disorders (Park et al., 2008; Dimos et al., 2008; Brennand et al., 2011).

Direct conversion of fibroblasts to neurons may prove to be a valuable tool for studying and treating neurodegenerative disorders. By directly converting fibroblasts to neurons without passing via a pluripotent stem cell state reduces the risk of tumor formation after grafting. In addition, this technique does not require the controversial use of embryonic or fetal cells, and may one day lead to the development of transplantable cells that are patient-specific. By converting the fibroblasts of patients with neurodegenerative disorders we can provide more accurate diagnoses and also develop a deeper understanding of disease progression. Qiang et al. (2011) have recently shown that fibroblasts taken from Alzheimer's patients, when converted to neurons, express markers associated with the disease, demonstrating that this technique has a diagnostic value and is useful in disease-modeling.

Ascl1 has been the main proneural gene used for iN conversions to date (Vierbuchen et al., 2011; Pfisterer et al., 2011a, Pang et al., 2011, Pfisterer et al., 2011b, Qiang et al., 2011, Caiazzo et al., 2011). We have demonstrated that the proneural gene Ngn2 when overexpressed with Brn2 and Myt1l leads to the generation of iNs with similar frequency and timing compared to Ascl1 with Brn2 and Myt1l. Our results indicate that these proneural genes seem to have a crucial role in high frequency conversion of fibroblasts to functional neurons. We also report that the functional properties and phenotype of the generated iNs differ depending on the proneural gene overexpressed. This study presents another combination of genes capable of transforming fibroblasts to functional neurons.

REFERENCES

Ambasudhan R, Talantova M, Coleman R, Yuan X, Zhu S, Lipton SA, Ding S (2011) Direct Reprogramming of Adult Human Fibroblasts to Functional Neurons under Defined Conditions. Cell Stem Cell 9:113-8.

Andersson E, Jensen JB, Parmar M, Guillemot F, Björklund A (2006) Development of the mesencephalic dopaminergic neuron system is compromised in the absence of neurogenin 2. Development 133:507-16.

Andersson EK, Irvin DK, Ahlsiö J, Parmar M (2007) Ngn2 and Nurr1 act in synergy to induce midbrain dopaminergic neurons from expanded neural stem and progenitor cells. Exp Cell Res 313:1172-80.

Berninger B, Guillemot F, Götz M (2007) Directing neurotransmitter identity of neurones derived from expanded adult neural stem cells. Eur J Neurosci 25:2581-90.

Brennand KJ, Simone A, Jou J, Gelboin-Burkhart C, Tran N, Sangar S, Li Y, Mu Y, Chen G, Yu D, McCarthy S, Sebat J, Gage FH (2011) Modelling schizophrenia using human induced pluripotent stem cells. Nature 473:221-5.

Caiazzo M, Dell'anno MT, Dvoretskova E, Lazarevic D, Taverna S, Leo D, Sotnikova TD, Menegon A, Roncaglia P, Colciago G, Russo G, Carninci P, Pezzoli G, Gainetdinov RR, Gustincich S, Dityatev A, Broccoli V (2011) Direct generation of functional dopaminergic neurons from mouse and human fibroblasts. Nature 476:224-7.

Dimos JT, Rodolfa KT, Niakan KK, Weisenthal LM, Mitsumoto H, Chung W, Croft GF, Saphier G, Leibel R, Goland R, Wichterle H, Henderson CE, Eggan K (2008) Induced pluripotent stem cells generated from patients with ALS can be differentiated into motor neurons. Science 321:1218-21.

Fode C, Ma Q, Casarosa S, Ang SL, Anderson DJ, Guillemot F (2000) A role for neural determination genes in specifying the dorsoventral identity of telencephalic neurons. Genes Dev 14:67-80.

Heinrich C, Gascón S, Masserdotti G, Lepier A, Sanchez R, Simon-Ebert T, Schroeder T, Götz M, Berninger B (2011) Generation of subtype-specific neurons from postnatal astroglia of the mouse cerebral cortex. Nat Protoc 6:214-28.

Isom LL, De Jongh KS, Patton DE, Reber BF, Offord J, Charbonneau H, Walsh K, Goldin AL, Catterall WA (1992) Primary structure and functional expression of the beta 1 subunit of the rat brain sodium channel. Science 256:839-42.

Kele J, Simplicio N, Ferri AL, Mira H, Guillemot F, Arenas E, Ang SL (2006) Neurogenin 2 is required for the development of ventral midbrain dopaminergic neurons. Development 133:495-505.

Letinic K, Zoncu R, Rakic P (2002) Origin of GABAergic neurons in the human neocortex. Nature 417:645-9.

Lindvall O, Kokaia Z (2010) Stem cells in human neurodegenerative disorders—time for clinical translation? J Clin Invest 120:29-40.

Nieto M, Schuurmans C, Britz O, Guillemot F (2001) Neural bHLH genes control the neuronal versus glial fate decision in cortical progenitors. Neuron 29:401-13.

Pang ZP, Yang N, Vierbuchen T, Ostermeier A, Fuentes DR, Yang TQ, Citri A, Sebastiano V, Marro S, Südhof TC, Wernig M (2011) Induction of human neuronal cells by defined transcription factors. Nature 476:220-3.

Park IH, Arora N, Huo H, Maherali N, Ahfeldt T, Shimamura A, Lensch MW, Cowan C, Hochedlinger K, Daley GQ (2008) Disease-specific induced pluripotent stem cells. Cell 134:877-86.

Parras CM, Schuurmans C, Scardigli R, Kim J, Anderson DJ, Guillemot F (2002) Divergent functions of the proneural genes Mash1 and Ngn2 in the specification of neuronal subtype identity. Genes Dev 16:324-38.

Pfisterer U, Kirkeby A, Torper O, Wood J, Nelander J, Dufour A, Björklund A, Lindvall O, Jakobsson J, Parmar M (2011a) Direct conversion of human fibroblasts to dopaminergic neurons. Proc Natl Acad Sci U S A 108:10343-8.

Ulrich Pfisterer, James Wood, Kristian Nihlberg, Oskar Hallgren, Leif Bjermer, Gunilla Westergren-Thorsson, Olle Lindvall, Malin Parmar (2011b) Efficient induction of functional neurons from adult human fibroblasts. Cell Cycle (accepted)

Qiang L, Fujita R, Yamashita T, Angulo S, Rhinn H, Rhee D, Doege C, Chau L, Aubry L, Vanti WB, Moreno H, Abeliovich A (2011) Directed conversion of Alzheimer's disease patient skin fibroblasts into functional neurons. Cell 146:359-71.

Seutin V, Engel D (2010) Differences in Na+ conductance density and Na+ channel functional properties between dopamine and GABA neurons of the rat substantia nigra. J Neurophysiol 103:3099-114.

Son EY, Ichida JK, Wainger BJ, Toma JS, Rafuse VF, Woolf CJ, Eggan K (2011) Conversion of mouse and human fibroblasts into functional spinal motor neurons. Cell Stem Cell 9:205-18.

Tønnesen J, Parish CL, Sørensen AT, Andersson A, Lundberg C, Deisseroth K, Arenas E, Lindvall O, Kokaia M (2011) Functional integration of grafted neural stem cell-derived dopaminergic neurons monitored by optogenetics in an in vitro Parkinson model. PLoS One 6:e17560.

Vierbuchen T, Ostermeier A, Pang ZP, Kokubu Y, Südhof TC, Wernig M (2010) Direct conversion of fibroblasts to functional neurons by defined factors. Nature 463:1035-41.

Wernig M, Zhao JP, Pruszak J, Hedlund E, Fu D, Soldner F, Broccoli V, Constantine-Paton M, Isacson O, Jaenisch R (2008) Neurons derived from reprogrammed fibroblasts functionally integrate

into the fetal brain and improve symptoms of rats with Parkinson's disease. Proc Natl Acad Sci U S A 105:5856-61.

Yoo AS, Sun AX, Li L, Shcheglovitov A, Portmann T, Li Y, Lee-Messer C, Dolmetsch RE, Tsien RW, Crabtree GR (2011) MicroRNA-mediated conversion of human fibroblasts to neurons. Nature 476:228-31.

Zirlinger M, Lo L, McMahon J, McMahon AP, Anderson DJ (2002) Transient expression of the bHLH factor neurogenin-2 marks a subpopulation of neural crest cells biased for a sensory but not a neuronal fate. Proc Natl Acad Sci U S A 99:8084-9.

Paper VI

Human induced pluripotent stem cells form functionally integrated neurons and improve recovery after transplantation in stroke-damaged rodent brain

Koichi Oki[1,3] , Jemal Tatarishvili[1,3], James Wood[2,3], Philipp Koch[4], Yutaka Mine[2,3], Emanuela Monni[1,3], Somsak Wattanati[1,3], Oliver Brüstle[4], Olle Lindvall[2,3] and Zaal Kokaia[1,3]

[1]Laboratory of Neural Stem Cell Biology and Therapy, University Hospital, SE-221 84 Lund, Sweden
[2]Laboratory of Neurogenesis and Cell Therapy, Wallenberg Neuroscience Center, University Hospital, SE-221 84 Lund, Sweden
[3]Lund Stem Cell Center, Lund, Sweden
[4]Institute of Reconstructive Neurobiology, Life & Brain Center, University of Bonn and Hertie Foundation, Bonn, Germany

Authorship note: Koichi Oki, Jemal Tatarishvili, James Wood and Philipp Koch contributed equally to this work.

Stroke is a leading cause of disability in humans but treatments to promote recovery are lacking. Stem cells ameliorate neurological deficits after transplantation in stroke-damaged animals. Reprogramming of adult human somatic cells to induced pluripotent stem cells (iPSCs) is a novel approach to produce patient-specific cells for autologous transplantation. Whether such cells survive long-term, differentiate to functional neurons, and induce recovery in stroke-injured brain is unclear. We have transplanted long-term self-renewing neuroepithelial-like stem (lt-NES) cells, generated from adult human fibroblast-derived iPSCs, into stroke-damaged mouse and rat striatum or cortex. Grafts improved recovery of forepaw movements already during the first 2 months after transplantation, which was not due to neuronal replacement. Transplanted cells stopped proliferating and could survive without forming tumors for at least 4 months. Morphologically mature neurons of different subtypes, expressing GABA, parvalbumin, calretinin, calbindin, and DARPP-32 were formed. Intrastriatally grafted neurons sent axonal projections to host globus pallidus. Grafted cells exhibited electrophysiological properties of mature neurons and received synaptic input from host neurons. Our study provides the first evidence that transplantation of human iPSC-derived cells is a safe and efficient approach to promote recovery after stroke and to supply the injured brain with new neurons for replacement.

INTRODUCTION

Ischemic stroke is a leading cause of mortality and disability. Occlusion of a cerebral artery leads to focal tissue loss and death of multiple neuron types as well as oligodendrocytes, astrocytes and endothelial cells. Apart from thrombolysis during the first hours after stroke, no effective treatment to improve functional recovery exists in the post-ischemic phase. Ongoing studies in animal models of stroke suggest that stem cell-based approaches could provide therapeutic benefit in a clinical setting. The observed improvements may, at least partly, be due to neuronal replacement, i.e., some level of synaptic integration of the stem cell-derived neurons into host neural circuitries (1). After transplantation

Address correspondence to: Zaal Kokaia, Lund Stem Cell Center, University Hospital BMC B10, SE-221 84 Lund, Sweden. Phone: +46 46 222 0276; Fax: +46 46 222 0560; E-mail: zaal.kokaia@med.lu.se

into stroke-damaged rodent brain, embryonic stem (ES) cell-derived neural stem cells (NSCs) differentiated into neurons and improved some impaired motor and sensorimotor functions (2-4). Electrophysiological recordings showed mature neuronal properties of the grafted cells and signs of synaptic integration into host brain (5, 6). Also human fetal NSCs gave rise to mature neurons after transplantation into stroke-damaged rat brain (7-9).

Transplanted NSCs may promote recovery also without differentiating to neurons and even without long-term survival through several other mechanisms, e.g., modulation of inflammation (10-12), neuroprotection (12), and stimulation of angiogenesis (11, 13, 14) and brain plasticity (15-17). Delayed and persistent functional improvement induced by intracerebral NSC transplantation after stroke, without cell survival and tissue replacement at 6 months after the insult, was recently documented by electrophysiology, fMRI and behavioral testing (4).

Somatic cells such as fibroblasts can be reprogrammed to pluripotent stem cells by introduction of transcription factors (18). These so-called induced pluripotent stem cells (iPSCs) can be differentiated to specific neuron types, e.g., dopaminergic neurons (19, 20) and motorneurons (21, 22). With this technology, patient-specific cells can be produced without the need for immunosuppressive treatment after transplantation, and the ethical issues associated with the use of human ES cells are avoided. Autologous transplantation of neurons generated from iPSCs seems to be more attractive in stroke than in chronic neurodegenerative disorders, in which patient-specific cells may exhibit increased susceptibility to the pathological process. Recently, mouse fibroblast-derived iPSCs, implanted into striatum and cortex in stroke-damaged mice, were reported to generate large numbers of neuroblasts and a few mature neurons but to form tumors and delay functional recovery at one month after transplantation (23). When such cells mixed with fibrin glue were delivered subdurally into the injured brain tissue in rats after

stroke, there was reduction of infarct volume and some behavioral improvement at 1, 2 and 4 weeks after the insult but no tumor formation (24). Finally, human fibroblast-derived iPSCs implanted into striatum of stroke-damaged rats were found to improve sensorimotor recovery at 4 to 16 days post-grafting but whether any neurons were formed is unclear (25). The long-term consequences after transplantation of human iPSC-derived cells in the stroke-damaged brain, if they can differentiate in vivo to morphologically and functionally mature neurons, establish connections to target areas, and improve behavioral deficits resembling those in stroke patients, are currently unknown.

Here we have transplanted long-term expandable neuroepithelial-like stem (lt-NES) cells, generated from adult human fibroblast-derived iPSCs, into the stroke-damaged mouse and rat brain. The grafted lt-NES cells cease to proliferate and survive up to at least 4 months after implantation without forming tumors. We also show, for the first time that grafted human iPSC-derived lt-NES cells generate neurons with mature morphological and electrophysiological properties in vivo, send axonal projections in the host brain, receive synaptic input from surrounding host neurons, and improve motor recovery in behavioral tests relevant for human stroke.

RESULTS

Generation and in vitro properties of lt-NES cells from human iPSCs

Induced pluripotent stem cells were generated by retroviral transduction of human dermal fibroblasts (33-year-old healthy male donor) with the reprogramming factors Oct4, Sox2, Klf4 and c-Myc. Emerging iPSC colonies were investigated for silencing of the retroviral transgenes by quantitative PCR (data not shown), and selected clones were further propagated to establish iPSC lines. The iPSC line employed in this study showed morphologies indistinguishable from those of human ES cells (Figure
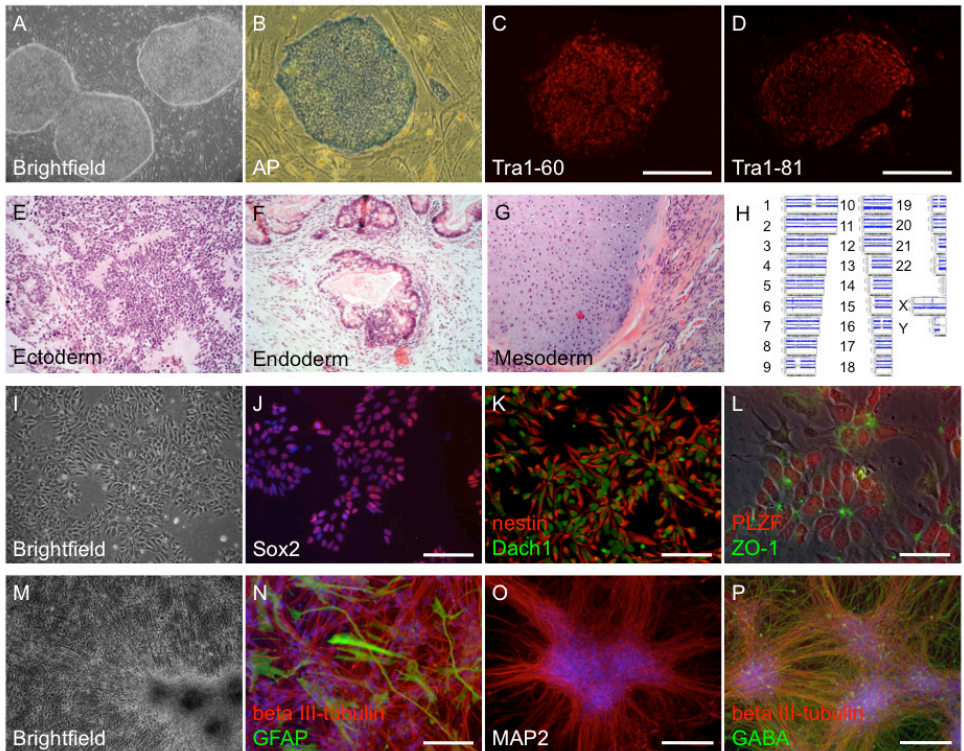
Figure 1

Generation of the human iPSC-derived lt-NES cells. (A-H) Skin fibroblast-derived iPSC colonies (A) stain positive for the pluripotency-associated markers alkaline phosphatase (B), Tra1-60 (C), and Tra1-81 (D). Following transplantation into immunodeficient mice, the iPSCs form teratomas consisting of cell types of all three germ layers such as neuroectodermal rosettes (E), glandular structures (F) and cartilage (G). Single nucleotide polymophism (SNP) analysis revealed no significant karyotypic abnormalities (F). For each chromosome, the B allele frequency (upper row) and log A ratio (lower row) is shown. Long-term self-renewing neuroepithelial stem cells generated from the iPSCs (I) express the NSC markers Sox2 (J) and nestin (K) and the rosette-associated transcription factors Dach1 (K) and PLZF (L). The tight junction protein ZO-1 is expressed apically in the rosette-like structures (L). Upon growth factor withdrawal, iPSC-derived lt-NES cells differentiate to a major proportion of neurons (M), expressing beta III-tubulin (N) and MAP2 (O). A minor fraction of GFAP-positive astrocytes is also present in the cultures (N). Many of the neurons are immunoreactive for GABA (P). Scale bars = 50 μm (L); 100 μm (J-K, N); 200 μm (C-D, O-P).

1A), and expressed the pluripotency-associated markers alkaline phosphatase (AP), Tra1-60, and Tra1-81 (Figure 1, B-D). Following transplantation into immunodeficient mice, the cells formed teratomas in vivo consisting of all three germ layers (Figure 1, E-G), and had normal karyotype as assessed by high resolution SNP analysis (Figure 1H).

A homogeneous population of iPSC-derived lt-NES cells was established using our previously established protocol (26). In the presence of the growth factors fibroblast growth factor (FGF) 2 and epidermal growth factor (EGF), these cells can be propagated along multiple passages without losing their stem cell charac-
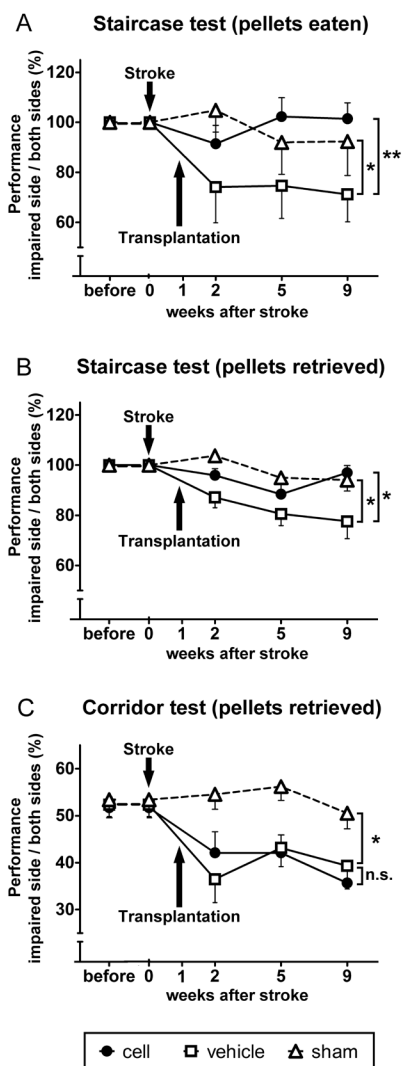
A **Staircase test (pellets eaten)**

B **Staircase test (pellets retrieved)**

C **Corridor test (pellets retrieved)**

● cell □ vehicle △ sham

Figure 2
Transplantation of human iPSC-derived lt-NES cells into striatum of stroke-damaged mice induces behavioral improvement. (A-C) Comparisons between cell-implanted ("cell"; n= 12) and vehicle-injected ("vehicle"; n= 11) mice subjected to stroke, and sham-operated, non-transplanted mice ("sham"; n= 9) in performance in the staircase (A and B) and corridor tests (C). Performance for the staircase test was calculated as the number of pellets on the impaired side divided by the total number of pellets on both sides, and expressed as percentage of performance at baseline. Performance for the corridor test was calculated by dividing the number of contralateral retrievals with the total number of retrievals from both sides. Both numbers of eaten (A) and retrieved pellets (B) are higher in the cell group as compared to the vehicle group, the performance in the stroke-damaged animals receiving cell grafts being similar to that in the sham-operated group. In contrast, cell grafts did not improve performance compared to vehicle injections in the corridor test (C). Repeated measures ANOVA between cell and vehicle group: (A) P = 0.0080, (B) P = 0.0437, (C) P = 0.9853 with *, P < 0.05; **, P < 0.01. Repeated measures ANOVA between vehicle and sham group: (A) P = 0.0472, (B) P = 0.0193, (C) P = 0.0134 with *, P < 0.05.

growth factor withdrawal and independent of passage number, human iPSC-derived lt-NES cells differentiated into a major fraction of beta III-tubulin-positive neurons (>70%) and a minor fraction of GFAP-positive astrocytes (Figure 1, M, N and P). In addition to beta III-tubulin, neurons differentiated from human iPSC-derived lt-NES cells expressed the maturation-associated neuron-specific marker microtubule associated protein (MAP2) (Figure 1O), and many cells were immunopositive the inhibitory neurotransmitter gamma-aminobutyric acid (GABA) (Figure 1P). Thus, the human iPSC-derived lt-NES cells used in this study represent a homogeneous population of NSCs with a strong neurogenic differentiation potential in vitro.

Transplantation of human iPSC-derived lt-NES cells into stroke-damaged mouse striatum improves recovery of fine forelimb movements independent of long-term graft survival

teristics or their differentiation potential. Human iPSC-derived lt-NES cells (Figure 1I) uniformly expressed the NSC-associated markers Sox2 and nestin (Figure 1, J and K). They assembled to rosette-like patterns with expression of the rosette-associated transcription factors PLZF and Dach1 and an apical accentuation of the tight junction maker ZO-1 (Figure 1, K and L). Upon
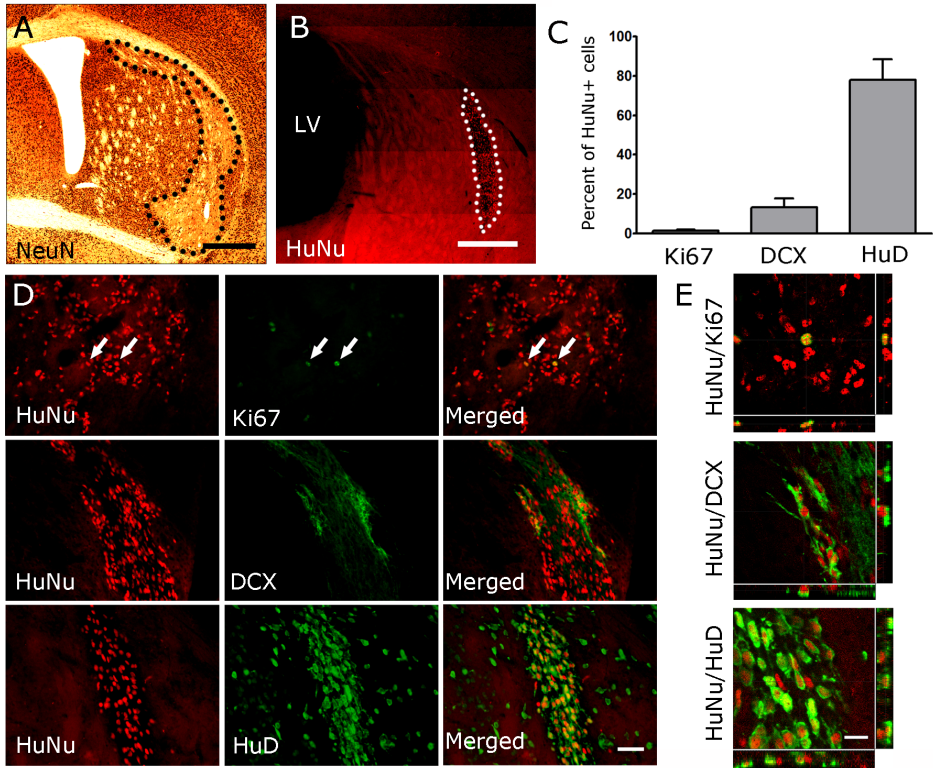
130

Figure 3

Human iPSC-derived lt-NES cells survive transplantation to striatum in stroke-damaged mice, stop to proliferate, and differentiate to neurons. NeuN-stained section showing the extent of the damage (A), mainly located in the lateral and dorsolateral parts of the striatum and HuNu-stained section showing the location of the graft in the same animal (B) at 10 weeks after transplantation. Dotted line depicts the border of the lesion (A) and of the graft (B). (C-E) Proliferation and neuronal differentiation of human iPSC-derived lt-NES cells at 10 weeks after transplantation. Fluorescence microscopic images (D) and confocal images (E) of HuNu+ cells co-expressing Ki67, DCX and HuD. Numbers of cells co-expressing each marker is presented as percentage of total number of HuNu+ cells in C. Scale bar = 500 μm (A and B), 50 μm (D) and 20 μm (E).

We first explored whether implantation of human iPSC-derived lt-NES cells could influence the functional restoration after stroke. Twenty-three mice subjected to middle cerebral artery occlusion (MCAO) were divided into 2 groups and transplanted into striatum with human iPSC-derived lt-NES cells (n=12) or vehicle (n=11) at 1 week after the ischemic insult. A third group of sham-operated animals (n=9) was given intrastriatal vehicle injection.

We evaluated fine forelimb movement using the staircase test at 2, 5 and 9 weeks after MCAO or sham surgery, i.e., 1, 4 and 8 weeks after transplantation. In this test, the number of retrieved pellets reflects the ability to move the forelimb, whereas the number of eaten pellets depends on the ability of both grasping and eating pellets, requiring fine and well-coordinated forelimb movements. Vehicle-injected, stroke-affected mice showed impairment in both parameters,

which was sustained until 9 weeks, and significantly different from sham-operated animals (Figure 2, A and B; repeated measures ANOVA: P = 0.047 for eaten pellets and P = 0.019 for retrieved pellets). In contrast, stroke-subjected animals with human iPSC grafts did not show any deficits in retrieved or eaten pellets at any time point, and performed significantly better than vehicle-treated animals (repeated measures ANOVA: P = 0.008 for eaten pellets and P = 0.044 for retrieved pellets). Taken together, our data indicate that the human iPSC-derived lt-NES cells gave rise to sustained improvement of functional recovery, probably starting already early after transplantation.

The behavioral consequences of human iPSC-derived lt-NES cell transplantation were also assessed also in the corridor test, which analyzes paired lateralized sensorimotor integration (neglect) caused by striatal damage. Animals subjected to MCAO and treated with either cells or vehicle exhibited significant impairment compared to sham-operated animals at all time-points (Figure 2C; P = 0.0134, repeated measures ANOVA). Human iPSC-derived lt-NES cell transplantation did not reverse the deficit in the corridor test.

We next determined the location, survival and proliferative activity of the grafted cells. The MCAO caused a reproducible lesion of the dorsolateral part of the striatum in all mice (Figure 3A), with shrinkage of the lateral region in some animals (27). Surviving grafts were found at 10 weeks after transplantation in 7 out of 12 animals (Figure 3B). The vast majority of the human cells, visualized by human nuclei (HuNu) staining, were located in the striatum, with diffuse distribution around the core of the ischemic lesion (n=3), or densely packed at the transplantation site (n=4). A few HuNu+ cells were also detected in cerebral cortex and corpus callosum. The number of HuNu+ cells in each graft, calculated according to the optical fractionator formula, was 9 378 ±2 517, and which was estimated at about 10% of the initial number of transplanted cells in animals with surviving grafts. Proliferation of grafted iPSCs was

evaluated by counting the number of HuNu cells coexpressing the mitotic marker Ki67 (Figure 3, C- E). Only few HuNu+ cells (1.6 ± 0.9%) were also positive for Ki67. These cells were mainly observed in animals with diffuse distribution of grafted cells. Our data indicate that at 10 weeks after transplantation, the proliferative activity of grafted iPSC-derived lt-NES cells is very low.

In 5 out of 12 animals implanted with human iPSC-derived lt-NES cells, no surviving grafts were detected 10 weeks after transplantation. We re-analyzed our behavior data and compared the impairment and magnitude of recovery between the groups with and without surviving grafts. The two groups showed no significant difference in number of retrieved or eaten pellets or in the corridor test (data not shown). These findings suggest that long-term survival of grafted cells is not necessary for the functional recovery induced by iPSC-derived lt-NES cells during the first two months after transplantation.

Extent of stroke-induced damage in mice is not affected by transplantation of human iPSC-derived lt-NES cells

One possible explanation to the improved behavioral recovery in animals subjected to human iPSC-derived lt-NES cell transplantation as compared to vehicle-implanted mice could be a graft-induced reduction in the size of the ischemic injury. However, we observed no differences in the pattern or location of the stroke-induced damage between the two groups. At 11 weeks after the insult, the volume of the injured striatum did not differ between cell-transplanted and vehicle-injected groups, (4.19 ± 0.6 mm3 and 4.69 ± 0.5 mm3, respectively). Moreover, the neurological scores at 1 h, 1 day and 1 week after MCAO were similar in the groups (data not shown).

Human iPSC-derived lt-NES cells differentiate to neurons and establish axonal connections to globus pallidus after transplantation in stroke-damaged mouse brain
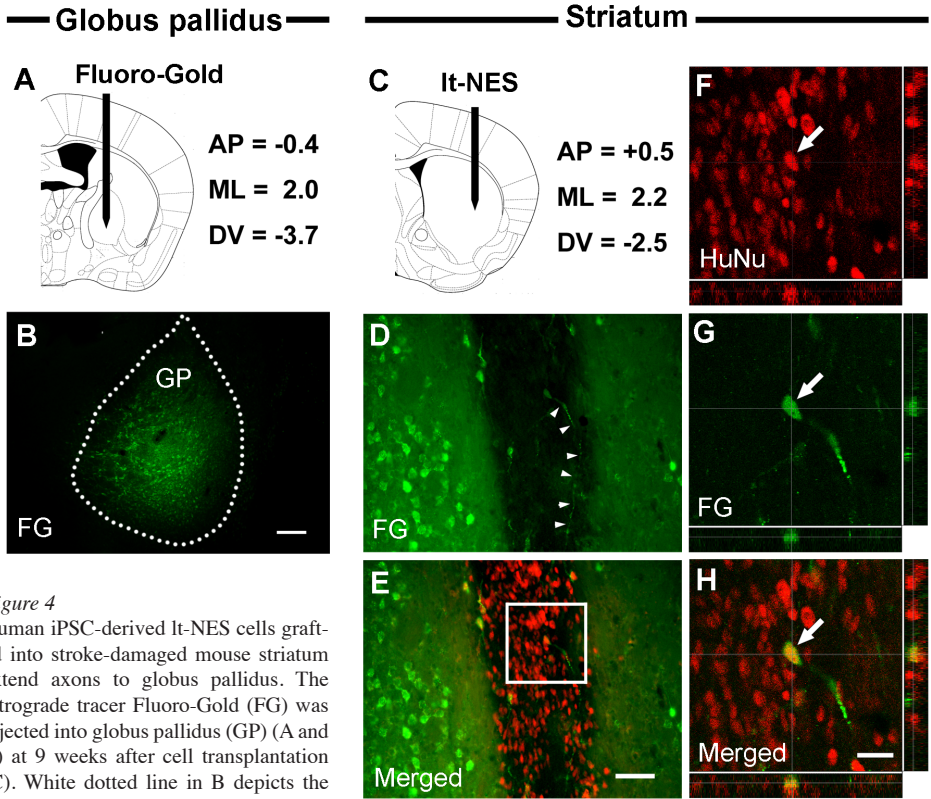
━━Globus pallidus━━ **━━━━ Striatum ━━━━**

A Fluoro-Gold

AP = -0.4
ML = 2.0
DV = -3.7

B

GP

FG

C lt-NES

AP = +0.5
ML = 2.2
DV = -2.5

D

FG

E

Merged

F

HuNu

G

FG

H

Merged

Figure 4

Human iPSC-derived lt-NES cells graft-
ed into stroke-damaged mouse striatum
extend axons to globus pallidus. The
retrograde tracer Fluoro-Gold (FG) was
injected into globus pallidus (GP) (A and
B) at 9 weeks after cell transplantation
(C). White dotted line in B depicts the
border of the GP. Staining for FG is con-
fined to GP. Fluorescence microscopic images (D and E) and high-magnification confocal images (F-H) of the
boxed area in E show a small fraction of HuNu+ cells in the intrastriatal grafts co-stained for FG at 1 week after
its injection. Arrows on F-H show the FG+ grafted iPSC-derived lt-NES cell and arrow heads on D depict an
FG+ axon extending from an HuNu+/FG+ cell. FG+ (green) cells on the left side from the grafted (red) cells in
D and E are host neurons in the intact part of the injured striatum projecting their axons to GP. Scale bar = 50
μm (A) and 20 μm (B).

We assessed the proportion of grafted cells
expressing neuronal markers such as doublecor-
tin (DCX, a marker for neuroblasts) and HuD
(a marker for young and mature neurons) at 10
weeks after transplantation (Figure 3, C-E). The
majority of grafted cells were HuNu+/HuD+
(78.5±11.2%) and mainly located in the center
of the graft. A smaller portion of the cells were
HuNu+/DCX+ (13.4 ± 4.7%), with preferential
location at the periphery of the graft. Thus, most

of grafted human iPSC-derived lt-NES cells had
differentiated to neurons.

We then examined whether neurons gener-
ated from human iPSC-derived lt-NES cells im-
planted into the stroke-damaged mouse striatum
can establish appropriate axonal projections in
the host brain. We injected the retrograde tracer
Fluoro-Gold (FG) into the globus pallidus (GP)
(Figure 4A) ipsilateral to the graft (Figure 4C)
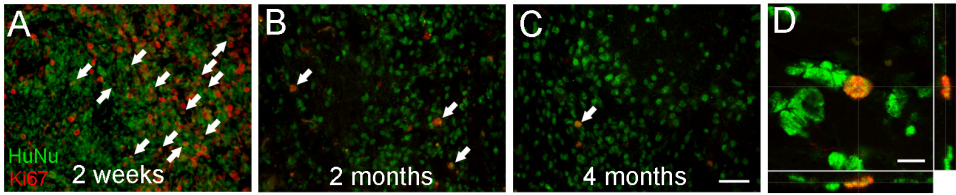at 9 weeks after transplantation (1 week prior

Figure 5

Proliferative activity of human iPSC-derived lt-NES cells decreases dramatically after transplantation into stroke-damaged rat striatum. Fluorescence photomicrographs (A-C) and confocal image (D) of HuNu+ cells co-expressing the mitotic marker Ki67 (arrows) at 2 weeks (A), 2 months (B), and 4 months (C) post-grafting. Scale bar = 50 μm (A-C) and 10 μm (D).

to sacrifice). This tracer is taken up by axon terminals or damaged axons and transported retrogradely to the soma (28). In 5 animals, FG staining was confined to GP (Figure 4B). In these animals a small fraction of HuNu+ cells in the grafts was stained with FG (1.16 ± 0.16 %; Figure 4, D-H). Axons were occasionally observed to extend from HuNu+/FG+ cells (Figure 4D). In addition, many FG+ cells were found in the remaining intact striatum ipsilateral to the lesion, demonstrating the projection of axons from host striatal neurons to GP (Figure 4, D and E). Our findings provide evidence that the neuronal progeny of the human iPSC-derived lt-NES cells, implanted into the stroke-damaged mouse striatum, can extend their axons to the GP, which is the main projection area for striatal medium-sized spiny neurons.

Human iPSC-derived lt-NES cells survive for 4 months and differentiate into neurons after transplantation into striatum of T cell-deficient rats

The sustained functional improvement which probably started already early after transplantation into the mice was independent of the
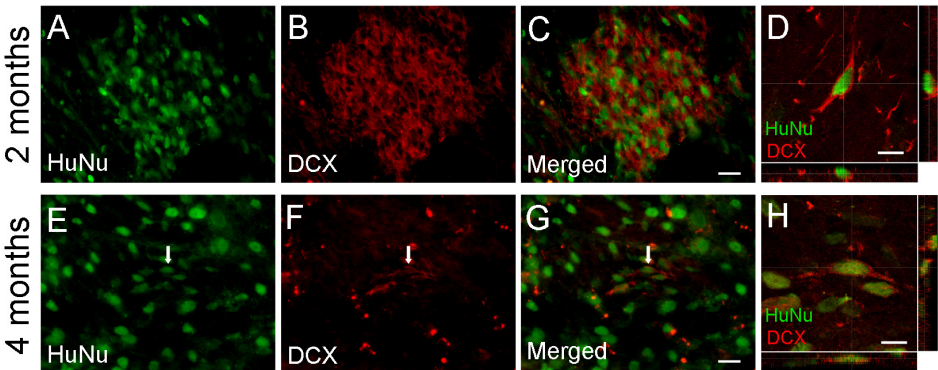

Figure 6

Number of neuroblasts generated from human iPSC-derived lt-NES cells decreases between 2 and 4 months after transplantation into stroke-damaged rat striatum. Fluorescence photomicrographs (A-C and E-G) and confocal images (D and H) show that the majority of grafted HuNu+ cells express the neuroblast marker DCX at 2 months (A-D), but only few grafted cells express DCX at 4 months post-grafting (E-H). Scale bar = 20 μm (A-C and E-G) and 10 μm (D and H).
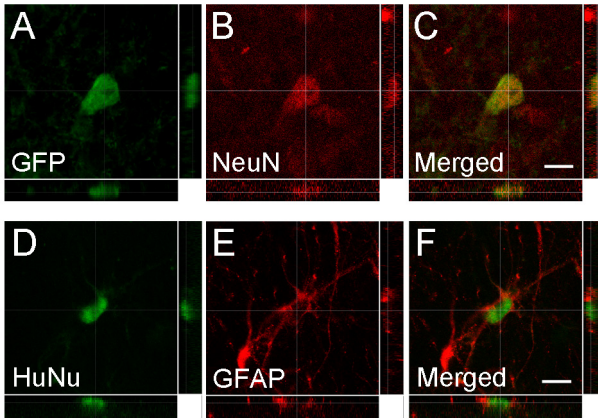
survival of the grafted cells. Therefore, it is inconceivable that the underlying mechanism was neuronal replacement and reconstruction of neural circuitry by the transplanted cells. Moreover, the development of human-derived neurons is slow (7), and it is unlikely that all neurons were fully mature at 10 weeks, when the mice were sacrificed. However, functional integration of mature neurons originating from these cells may still be an important mechanism underlying recovery at later time points. We wanted to determine whether the human iPSC-derived lt-NES cells and their progeny could survive longer than 10 weeks (the latest time-point studied in mice), differentiate to specific neuronal subtypes, and exhibit the electrophysiological properties of functional neurons. We therefore implanted the cells in Nude, T cell-deficient adult rats, which do not need immunosuppression for long-term survival of xenotransplanted human cells and also are useful for assessing long-term tumorigenicity.

Rats were subjected to MCAO and intrastriatal transplantation of green fluorescent protein (GFP)-labeled human iPSC-derived lt-NES cells at 48h after MCAO, and were perfused 2 weeks (n=3), and 2 (n=8) and 4 (n=5) months thereafter. We detected human iPSC-derived lt-NES cell grafts in all animals except 2 rats from the 2 months group, and the total number of these cells compared to the number of implanted cells being estimated at 64.8±12.4 % and 51.2±13.3% at 2 and 4 months after transplantation, respectively. The proliferative activity in the grafts (Figure 5), quantified as the percentage of HuNu+ cells co-expressing Ki67, was 40.2±4.9% at 2 weeks after transplantation but only 8.2±0.5 and 1.0±0.2% at 2 and 4 months, respectively. Our findings indicate that the human iPSC-derived cells stop dividing in vivo after transplantation. In line with this observation, we did not detect any overgrowth of grafted cells up to 4 months.

Due to the high number and density of cell bodies and fibres in the graft core of the sections immunostained for the neuroblast marker DCX, it was impossible to reliably quantify the number of HuNu+ or GFP+ cells also expressing DCX. However, microscopic examination of the sections revealed that at 2 months after transplantation, the entire core of the graft and most likely the majority of grafted cells were DCX+ (Figure 6, A-D). In contrast, at 4 months only few grafted cells exhibited DCX immunoreactivity (Figure 6, E-H). Due to cross-reactivity between the HuNu and the mature neuronal marker NeuN antibodies, the neuronal phenotype of grafted cells was determined using GFP and NeuN double-immunostaining (Figure 7, A-C). At 2 months after implantation, 65.7 ± 3.9
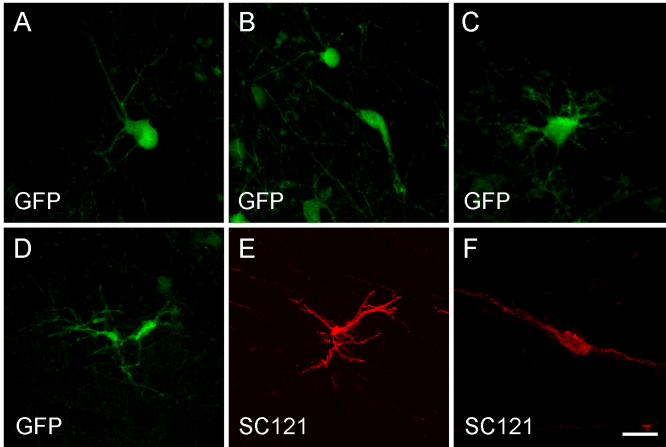
135

% of GFP+ cells in striatum co-expressed the mature neuronal marker NeuN. At 4 months, the proportion of GFP+/NeuN+ cells had increased to 72.9±4.7%. Only a fraction of grafted human iPSC-derived lt-NES cells were astrocyte marker glial fibrillary acid protein (GFAP)+ (3.8±0.5% and 6.1±1.5% at 2 and 4 months after transplantation, respectively; Figure 7, D-F). These cells were distributed mainly at the periphery of the graft core.

Human iPSC-derived lt-NES cells grafted into striatum differentiate to neurons with different phenotypes

To characterize the morphological properties of the grafted cells and their progeny, we used immunocytochemical staining for GFP and for the human cytoplasmic marker SC121. The SC121 antibody labels > 90% of human neural cells and does not cross-react with rat cells (7, 9). In the core of the graft, the high density of fibres immunoreactive to either GFP or SC121 made it difficult to distinguish the morphology of individual cells. Grafted GFP+ cells exhibiting morphological characteristics resembling those of migrating neuroblasts (Figure 8, B and F), mature neurons (Figure 8, A, D and E) or astrocytes (Figure 8, C) were more easily detectable in the areas outside the graft core. However,

GFP+ cells with typical neuronal morphology were often not immunopositive for NeuN. Also a high level of NeuN-staining in grafted cells often coincided with low GFP immunoreactivity, possibly reflecting downregulation of lentiviral promoter expression in the mature neurons.

Many of the grafted cells showed GABA immunoreactivity (Figure 9, A-D). At 2 months after transplantation, 21.9±1.8% of HuNu+ cells were also GABA+, being located mainly in the periphery, surrounding the graft core. In the 4 month group, HuNu+/GABA+ cells were evenly distributed throughout the graft but their number was lower (10.9±0.6%) as compared to the 2 month group. We also stained sections from the 4 month group for markers of the GABAergic interneurons, parvalbumin and calretinin (Figure 9, E-K). Few (3.6±0.7%) of the grafted cells were calretinin+ (Figure 9, I-K), whereas a substantial proportion were HuNu+/parvalbumin+ (15.4±2.6%) (Figure 9, E-H). Interestingly, at 4 months a small population (4.3±1.3%) of the HuNu+ cells in the intrastriatal grafts expressed dopamine- and 3':5'-monophosphate-regulated phosphoprotein 32 (DARPP-32) (Figure 9, L-O), a specific marker of medium-sized spiny striatal projection neurons. In contrast, we detected only single HuNu+/DARPP-32+ cells at 2 months.
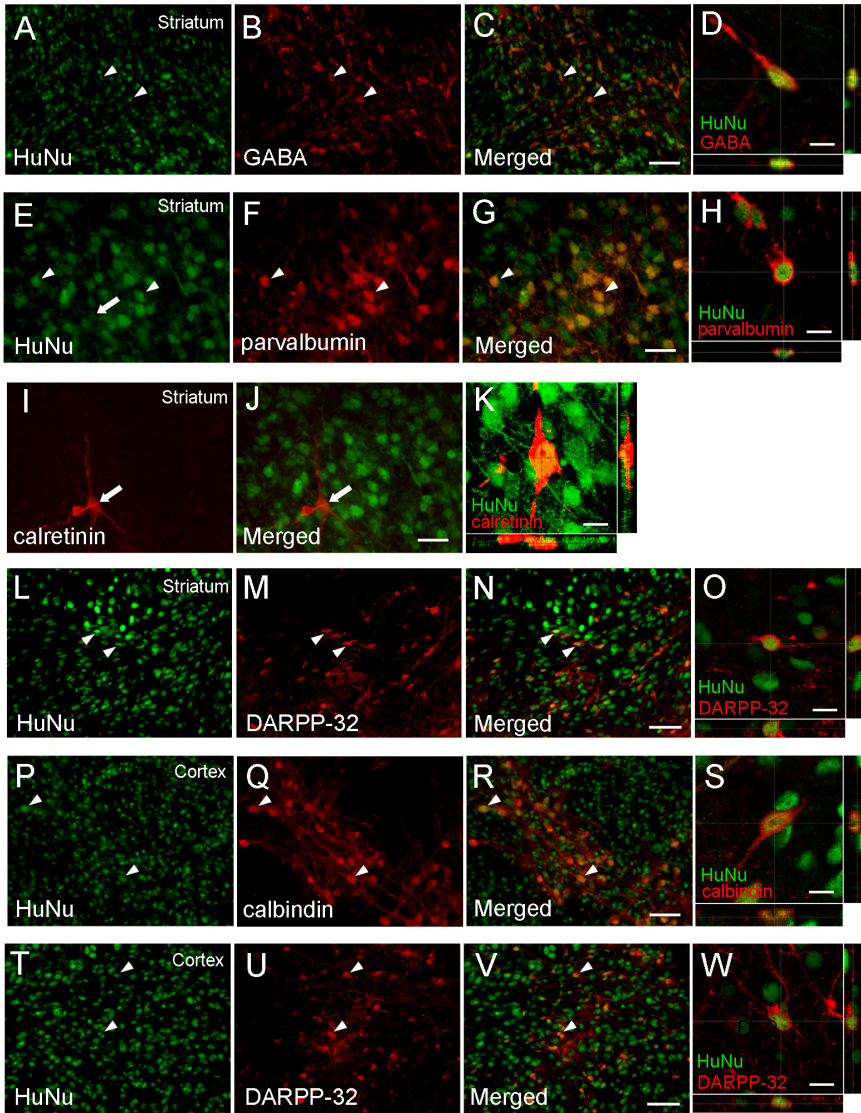
Figure 9
Human iPSC-derived lt-NES cells differentiate to neurons with different phenotype after transplantation into stroke-damaged rat brain. Fluorescence micrographs (A-C, E-G, I, J, L-N, P-R, and T-V) and confocal images (D, H, K, O, S and W) show HuNu+ cells co-expressing GABA (A-D), parvalbumin (E-H), calretinin (E, I-K) and DARPP-32 (E-H) in the striatum, and calbindin (P-S) and DARPP-32 (T-W) in cortex at 2 (A-D) and 4 (E-W) months post-grafting. Arrowheads indicate representative HuNu+ cells co-expressing GABA, DARPP-32, calbindin or parvalbumin. Arrow in E depicts a representative HuNu+ cell co-expressing calretinin (I and J). Scale bar = 50 μm (A-C, L-N, P-R, T-V), 20 μm (E-G, I and J), and 10 μm (D, H, K, O, S and W).

137

Figure 10

Human iPSC-derived lt-NES cells have developed electrophysiological properties of functional neurons at 4.5-5.5 months after transplantation into intact rat striatum. (A) Whole-cell configuration of GFP-expressing lt-NES cells. (B) Photomicrograph of a grafted, recorded cell (in the boxed area) labeled with biocytin and GFP. (C) Enlargement of boxed area in B depicting (arrows) grafted GFP+ cell filled with biocytin after recording. (D) Representative traces of membrane potential responses to step injection of hyperpolarizing and depolarizing current (10 pA steps) showing action potentials that are blocked by TTX (right). (E) Representative traces of whole-cell Na+ and K+ currents, blocked using TTX and TEA, respectively, elicited by voltage-steps from -70 mV to + 40 mV in 10 mV increments. Representative traces of spontaneous (F) and excitatory (G) postsynaptic currents recorded in the presence of PTX, in voltage-clamp configuration at -70 mV. (H) Absence of postsynaptic currents after addition of PTX and glutamate receptor antagonists, NBQX and D-AP5. Insets show respective traces on an expanded scale. DIC = differential interference contrast. LV = lateral ventricle.

Human iPSC-derived lt-NES cells survive for 4 months and differentiate to neurons after transplantation into cerebral cortex of T cell-deficient rats

In a separate group of animals, we analyzed the survival and neuronal differentiation of human iPSC-derived lt-NES cells when implanted into a brain region outside striatum. Ten rats were subjected to occlusion of the distal branch of MCA (dMCAO), which causes cortical damage, and were transplanted with iPSC-derived lt-NES cells in the cortex adjacent to the ischemic injury 48 h thereafter. Seven rats which survived these procedures were killed after 2 (n=2) or 4 (n=5) months. The number of cells in the grafts at 2 months after transplantation was esitimated at 80.8±6.2% compared to the number of implanted cells. The percentage of cells with proliferative activity resembled that of the intrastriatal grafts (7.2±1.5%). The NeuN was expressed by 71.8±8.6% of the GFP+ cells and 15.5±2.7% of HuNu+ cells were also GABA+ at 2 months. The number of cells in the grafts tapered off slightly at 4 months (60.1±10.6% of implanted number) whereas proliferative activity in cortical lt-NES cell grafts was markedly
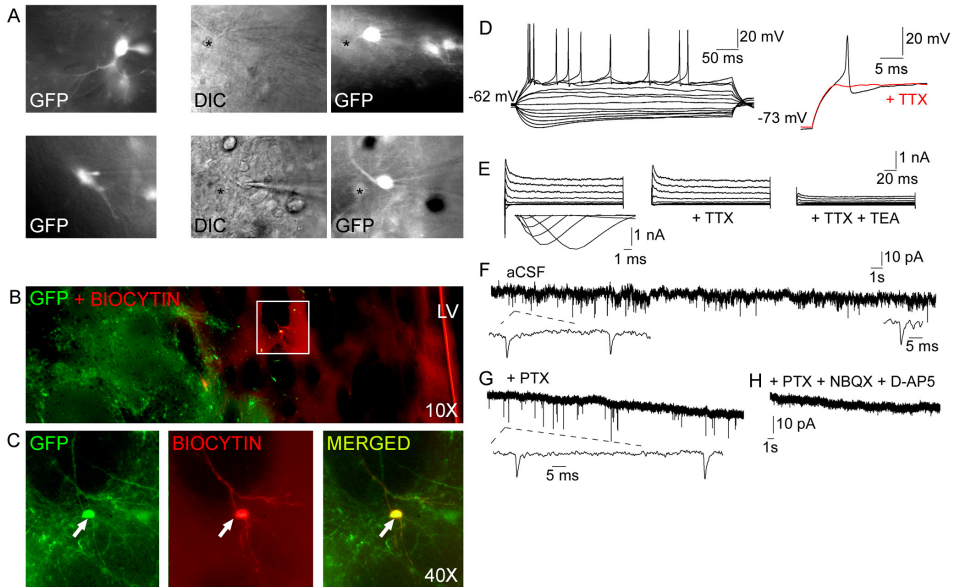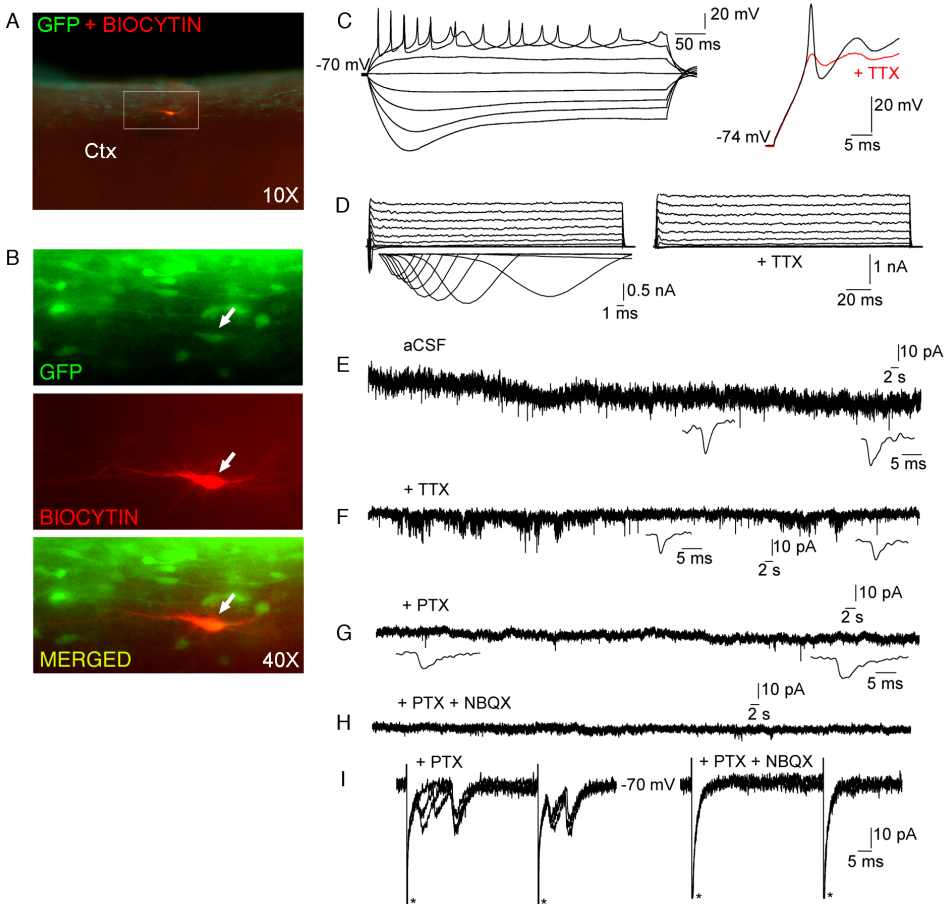
Figure 11

Human iPSC-derived lt-NES cells have developed electrophysiological properties of functional neurons at 4.5-5.5 months after transplantation into intact rat cerebral cortex. (A) Photomicrograph of a grafted, recorded cell (in the boxed area) labeled with biocytin and GFP. (B) Enlargement of boxed area in A depicting (arrows) grafted GFP+ cell filled with biocytin after recording. (C) Representative traces of membrane potential responses to step injection of hyperpolarizing and depolarizing current (10 pA steps) showing action potentials that are blocked by TTX (right). (D) Representative traces of whole-cell Na+ (blocked using TTX) and K+ currents elicited by voltage-steps from -70 mV to + 40 mV in 10 mV increments. Representative traces of spontaneous (E) and miniature (F) postsynaptic currents recorded in the presence of TTX, in voltage-clamp configuration at -70 mV. (G) Spontaneous excitatory postsynaptic currents recorded in the presence of PTX are blocked by the addition of NBQX (H). (I) Postsynaptic AMPA-receptor-mediated currents are evoked by paired-pulse electrical stimulation delivered from a stainless-steel electrode placed approximately 300 μm away from the transplant in the cortex (3 representative traces superimposed; * depicts stimulation artifact). Insets show respective traces on an expanded scale. Ctx = cortex.

139

lower (0.9±0.2%) as compared to 2 months, being similar to that of intrastriatal transplants. Many of the grafted cells displayed a neuronal morphology as shown by GFP (Figure 8D) and SC-121 (Figure 8E) immunostainings. Although the percentage of GFP+/NeuN+ remained high at 4 months after transplantation (77.2±3.2%), the GABA+ cells in the grafts (Figure 9, A-D) decreased to 8.8±0.8%. At this time point, we found populations of parvalbumin+ (11.9±1%), calretinin+ (2.0±0.5%), and calbindin+ cells (8.1±0.8%; Figure 9, P-S) in the intracortical grafts. Also when transplanted into cerebral cortex, the iPSC-derived lt-NES cells differentiated to cells expressing the DARPP-32 (Figure 9, T-W), the proportion of grafted HuNu+/DARPP-32+ cells (5.2±1.5%) resembling that in intrastriatal grafts.

Neurons generated from grafted human iPSC-derived lt-NES are functional and receive synaptic input from host neurons

We finally studied the electrophysiological properties of iPSC-derived lt-NES cell progeny at 4.5-5.5 months after transplantation into striatum or cerebral cortex of T- cell deficient rats by performing whole cell patch-clamp recordings in acute brain slice preparations (Figure 10, A-C; Figure 11, A and B). Grafted cells were classified as neuronal or glial based on resting membrane potential and input resistance (Table 1). A proportion of the cells were mature functional neurons with a resting membrane potential of about -50 mV and -58 mV in the striatum and cortex, respectively, the majority generating action potentials in response to depolarizing current injection (Figure 10D and Figure 11C). In voltage-clamp configuration, depolarizing voltage steps induced characteristic Na^+ and K^+ whole-cell currents, which were sensitive to the voltage-gated Na^+ channel blocker tetrodotoxin (TTX), and the voltage-gated K^+ channel blocker, tetraethylammonium (TEA), respectively (Figure 10E and Figure 11D).

Spontaneous postsynaptic currents were frequently observed in grafted cells in the striatum (Figure 10F). Spontaneous excitatory postsynaptic currents (sEPSCs) were recorded in the presence of the GABAA receptor antagonist, picrotoxin (PTX) (Figure 10G) and addition of glutamate receptor antagonists (2,3-dihydroxy-6-nitro-7-sulfamoyl-benzo[f]quinoxaline-2,3-dione (NBQX) and (2R)-amino-5-phosphonovaleric acid (D-AP5)) blocked all postsynaptic currents (Figure 10H), indicating that the cells had functional excitatory synapses. Spontaneous inhibitory postsynaptic currents (using high-chloride intracellular solution and blocking excitatory transmission with NBQX and D-AP5) were not observed (n = 5 cells).

We observed spontaneous postsynaptic currents also in iPSC-derived lt-NES neurons implanted in the cortex (Figure 11E). The sEPSCs in cortically grafted iPSCs were recorded in the presence of PTX (Figure 11G), and all events were blocked after application of NBQX (Figure 11H), indicating that the transplanted cells had developed excitatory synapses. In addition, we detected miniature postsynaptic currents which were action potential-independent and not blocked by TTX (Figure 11F). In 2 of 10 grafted cells, excitatory, 2-amino-3-(5-methyl-3-oxo-1,2- oxazol-4-yl) propanoic acid (AMPA) receptor-mediated currents could be evoked by stimulating a cortical region remote from the transplant (Figure 11I). This finding suggests that transplanted neurons generated from iPSC-derived lt-NES cells, similar to human ESC-derived neurons (26), receive synaptic input from host neurons and functionally integrate into host brain neural circuitries.

DISCUSSION

We show here that intrastriatal transplantation of lt-NES cells, derived from human iPSCs, gives rise to improved recovery of a clinically relevant motor deficit, i.e., impairment of fine forelimb movements in the staircase test, after stroke in mice. Although we found that at 10 weeks the majority of cells in the surviving grafts expressed neuronal markers, recov-

Table 1. Electrophysiological characteristics of human iPSC-derived lt-NES progeny at 4.5-5 months after transplantation into intact rat striatum and cerebral cortex

	Striatum (n = 2 rats, 13 cells)		Cortex (n = 2 rats, 12 cells)
	Neuronal (n = 6 cells)	Glial (n = 7 cells)	
Resting membrane potential (mV)	-51.4 ± 4.2	-81.6 ± 2.1	-57.8 ± 5.3
Input resistance (MΩ)	1478 ± 253	172 ± 40	656 ± 175
Membrane capacitance (pF)	8.7 ± 1.5	11.3 ± 2.5	11.8 ± 1.5
Cells exhibiting action potentials	5/6	0/7	7/12
Action potential threshold (mV)	-32.5 ± 1.3	-	-34.9 ± 1.3
Action potential amplitude (mV)	41.6 ± 5.0	-	47.0 ± 3.7
Action potential duration (ms)	1.4 ± 0.2	-	1.3 ± 0.1
Afterhyperpolarization amplitude (mV)	11.6 ± 2.7	-	7.1 ± 0.7
Afterhyperpolarization duration (ms)	58.4 ± 25.0	-	20.3 ± 7.2

ery was probably promoted earlier, before any functioning neurons could have been developed from the grafted human iPSC-derived lt-NES cells. Most likely, this early improvement is due to mechanisms other than neuronal replacement. In support of this interpretation, the enhancement of behavioral recovery in our experiment was observed irrespective of whether the grafts were surviving at 10 weeks or not. Similarly, human iPSCs improved performance in the cylinder test from 4 days after intrastriatal implantation into stroke-damaged rats (25).

The mode of action of human iPSC-derived lt-NES cells after transplantation in the stroke-damaged rodent brain resembles that of grafted human NSCs, which have been reported to induce recovery by a variety of mechanisms, e.g., modulation of inflammation, neuroprotection, and stimulation of angiogenesis (see, e.g., (1)), and to be independent from donor cell survival(4). In analogy to our findings, human fetal NSCs implanted into a cortical lesion 1 week after stroke in rats gave rise to improved fore-

limb placing already after 1 week (11). Secretion of vascular endothelial growth factor by the NSCs was important for the suppression of inflammation and neovascularization in the peri-infarct region probably underlying the improved recovery (11). It is conceivable that the grafted human iPSC-derived lt-NES cells promoted the early behavioral improvement found here by similar mechanisms. We obtained no evidence that the grafts acted by protecting the host neurons from dying following the insult. At the time of cell implantation 1 week following the insult, the stroke-induced striatal injury is already complete (29) and, consequently, we observed no difference in infarct volume between cell- and vehicle-implanted groups at 10 weeks after transsplantation.

The only study with human iPSCs in stroke published so far provided no evidence for the formation of neuroblasts or mature neurons (25). We found that at 10 weeks after transplantation into mouse striatum, almost 80% of grafted human iPSC-derived lt-NES cells expressed the

marker for young and mature neurons HuD and 13% the neuroblast marker DCX. Similarly, at 2 months after these cells had been implanted into the striatum or cerebral cortex of T-cell deficient rats in two different models of stroke, 66% and 72%, respectively, of grafted cells expressed the mature neuronal marker NeuN. Importantly, at 4 months after implantation, the proportion of cells in the grafts with mature neuronal phenotype (NeuN+) remained high in both striatum (73%) and cerebral cortex (77%). Our data indicate that grafted iPSC-derived lt-NES cells can efficiently differentiate to mature neurons in vivo and survive long-term in the stroke-damaged brain. In contrast, only a fraction of grafted cells expressed the glial marker GFAP.

The grafted cells exhibited characteristic neuronal morphologies and expressed markers providing evidence that they had differentiated to various subtypes of neurons. At 4 months, grafts placed in striatum and cerebral cortex contained human-derived cells expressing GABA (11 and 9%, respectively), parvalbumin (15% and 12%), or calretinin (4% and 2%). In addition, we found cells expressing calbindin (8%) in the intracortical grafts. At 4 months, the intrastriatal grafts also contained a population of cells (4%) expressing the specific striatal projection neuron marker DARPP-32. Surprisingly, a similar proportion of cells (5%) expressed comparable staining for this marker in transplants placed in cerebral cortex, where only weakly stained DARPP-32+ neurons are normally seen (30). Two important conclusions of relevance for cell replacement strategies can be drawn from this observation and from the finding of similar proportions of GABA+, parvalbumin+, and calretinin+ cells in the intrastriatal and intracortical grafts. First, that the spontaneous differentiation of the grafted human iPSC-derived lt-NES cells to specific subtypes of neurons in vivo is determined by intrinsic mechanisms and not significantly affected by external cues in the ischemically injured environment. Second, that effective neuronal replacement in different stroke-damaged brain regions will require

directed in vitro differentiation of the human iPSC-derived lt-NES cells to precursors, which give rise to the lost types of neurons after transplantation.

Our data show, for the first time, that transplanted NSCs generated from reprogrammed adult human fibroblast-derived iPSCs can differentiate into functional neurons in vivo. Similarly, grafted human ES cell–derived NSCs have previously been shown to differentiate to cells with electrophysiological properties of neurons and synaptic input from host neurons in a stroke-injured environment (6). We found here that at 4.5-5.5 months after transplantation into striatum or cortex, grafted cells exhibited the electrophysiological properties of mature neurons. The findings of sEPSCs, which were blocked by glutamate receptor antagonists, and of AMPA-receptor mediated currents evoked by stimulating a cortical region remote from the intracortical graft, provide evidence that the grafted neurons had developed excitatory synaptic input and were, at least partly, functionally integrated into host neural circuitries. The lack of sIPSCs in the grafted cells, seem to suggest that they were not fully differentiated at the time of recording.

Our findings using the retrograde tracer Fluoro-Gold indicated that a fraction of the grafted cells had established axonal projection to the globus pallidus. This brain region is the projection area of the majority of striatal neurons, the medium spiny neurons, and following a stroke, there is a major injury to the striato-pallidal system. Therefore, the ability of human-derived iPSCs to reestablish this system could potentially be important for restoration of function. Our data further illustrate the remarkable capacity of neurons derived from xenografted human iPSCs (19), ES cells (31), and fetal brain tissue (32) to extend specific, long axonal projections to their appropriate target areas in the rodent brain.

Tumor formation and graft overgrowth (33-35) from pluripotent stem cells and their derivatives are major hurdles for the application

of stem cell therapy in stroke and other brain diseases. Undifferentiated human iPSCs formed larger tumors at 14 and 28 days after transplantation in striatum and cortex of mice subjected to stroke as compared to sham-treated animals (23). In another study, human iPSCs showed high tumorigenicity at 4 weeks after intracerebral implantation in stroke-damaged rats (24). Here we used transplantation of iPSCs into immunocompromized, T-cell deficient rats subjected to stroke and a long-term observation period (up to 4 months) both to ensure lack of rejection of the xenotransplanted cells and to create optimum environment for assessing their tumorigenicity. No tumor formation or transplant overgrowth was detected in any animal grafted with iPSC-derived lt-NES cells. Moreover, the high proliferative activity of these cells in vitro and at 2 weeks after transplantation decreased at 2 and virtually disappeared at 4 months. Our data suggest that pre-differentiation of iPSCs and generation of long-term self-renewing neural cell lines is an effective strategy for minimizing the risk for tumor formation.

Our experimental study provides evidence that transplantation of human fibroblast-derived iPSCs is a new, promising approach for promoting functional recovery after ischemic stroke. Most importantly, our findings demonstrate for the first time the potential of iPSCs for neuronal replacement in the stroke-damaged brain. The iPS grafts survived long-term and contained a high proportion of cells with morphological and electrophysiological properties of neurons. These neurons received afferent inputs from the host brain and extended their axons to an appropriate target area. Before any clinical application can be considered, the mechanisms regulating the differentiation of the iPSC-derived lt-NES cells into specific neuron types in the stroke-damaged brain have to be much better understood and effectively controlled, and the behavioral recovery induced by neuronal replacement has to be optimized.

METHODS

Generation of human induced pluripotent stem cells. For production of retroviral particles, PhoenixGP cells (ATTC #3514) were transfected with plasmids encoding for the viral glycoprotein VSV-G (Addgene 12259) and the reprogramming factors (Oct4, Sox2, KLF4 and c-MYC (Addgene 17217-17220). Dermal fibroblasts were transduced twice with ultracentrifuge-concentrated virus in DMEM high glucose media containing 10% fetal calf serum (FCS), 1% sodium pyruvate (stock: 100 mM), 1% non-essential amino acids (stock: 10 mM) and 1% L-glutamine (stock: 200 mM) (all Invitrogen) in the presence of 10 ng/ml FGF2. Four days post transduction, cells were split into plates pre-seeded with mouse embryonic fibroblasts (MEFs). Medium was switched to human iPS cell culture medium containing DMEM/F12 supplemented with 20% KnockOut serum Replacement, 0.1 mM non-essential amino acids (all from Invitrogen), 1 mM L-glutamine, 0.1 mM ß-mercaptoethanol and 50 ng/ml zebrafish basic fibroblast growth factor (zbFGF) 6 days post-transduction and changed every other day. Four weeks after transduction, colonies with human ES cell morphology were manually picked, carefully triturated and expanded to establish human iPS cell lines.

Neural differentiation of human iPS cells. Human iPSCs were induced to differentiate as described (26). Briefly, iPS cell colonies were detached from the MEF layer using collagenase (Invitrogen), and embryonic body (EB) formation was induced by plating the colonies on non-adhesive plastic culture dishes in human iPSC media without zbFGF. Fifty percent of the media were changed every second day, and 5-day-old EBs were plated on tissue culture plates coated with 0.1 mg/ml poly-L-ornithine (Sigma). Neural rosette structures started to emerge about one week after plating. Rosettes were carefully picked with a needle, and isolated clusters were transferred to a non-adhesive culture plate in

143

DMEM/F12, 2mM L-glutamine, 1.6 g/l glucose, and N2 supplement (1:100) (all Invitrogen). To establish lt-NES cell lines, floating rosettes were dissociated 2 days later using trypsin (10 min) followed by inhibition of trypsin by trypsin inhibitor (both Invitrogen). Cells were centrifuged for 5 minutes at 300G and plated onto poly-L-ornithine and 10 µg/ml laminin (Sigma) coated plates into the same media supplemented with 10 ng/ml FGF2, 10 ng/ml EGF (both from R&D systems) and B27 (1 µl/ml, Invitrogen). These iPSC-derived lt-NES cells were passaged at a ratio of 1:2 to 1:3 every second to third day using trypsin. All transplantation studies were performed with lt-NES cells passages 20-30. To induce terminal differentiation, growth factors were omitted and cells were cultured in Neurobasal media supplemented with B27 (1:50, Invitrogen) and DMEM/F12 media supplemented with N2 (1:100) mixed in a 1:1 ratio. 300 ng/ml cAMP were added to the differentiation media.

Animals. All experimental procedures were approved by the Malmö-Lund Ethical Committee. We used male C57bl6 mice, weighing 25-28 g, or male Nude rats (Charles River) weighing 280-320 g at the beginning of experiments. Nude rats were housed in individually ventilated cages with free access to water but were fasted overnight before induction of stroke. Mice were housed in standard cages with free access to food and water. During the period of staircase and corridor tests, mice were food-restricted and maintained at 85% - 90% of free-feeding bodyweight.

Middle cerebral artery occlusion in mice and rats. Surgical procedures on rats and mice were performed under general 1.5–2.0% isofluorane anesthesia with a mixture of 30% O2 and 70% N2O. Constant body temperature, about +37 °C was maintained using a heating pad. Stroke was induced using the intraluminal filament model of middle cerebral artery occlusion (MCAO) with slight modifications in rats (36, 37) and in mice (38, 39). Thirty minutes of MCAO cause ischemic injury predominantly in the striatum.

Briefly, a midline sagittal skin incision was made on the ventral surface of the neck. The right common carotid artery (CCA) and its proximal branches were isolated. The CCA and external carotid artery (ECA) were ligated, and internal carotid artery (ICA) was temporarily clipped using a metal microvessel clip. Small (about 1 mm) incision was made on the anterior surface of the ECA, and a nylon monofilament (7-0 for mice and 0.25 mm for rats) coated with silicone or rounded, was advanced through the ICA until resistance was felt. The size of the tip of the filament was adjusted to the luminal diameter of distal part of ICA and, therefore, could not be advanced further. The silk suture, previously placed around the ECA, was used to secure the filament. Metal clips or silk sutures closed the skin incision temporarily, and the animal was then released from anesthesia.

Thirty minutes after the start of occlusion, the animal was reanesthetized, the nylon filament was carefully removed, and the incision on ECA was ligated permanently by silk suture. Intradermal self-absorbable Vikryl 5.0 sutures were used to close the skin and the animal was released from anesthesia. The cerebral blood flow (CBF) reperfusion after removal of the filament, as well as the blood flow stasis during the MCAO were monitored by the laser doppler flow meter probe (Mode l418-1; Perimed, Sweden) attached to skull surface, corresponding to the area of ipsilateral cortex supplied by MCA. Animals subjected to sham surgery were treated similarly, except that the filament was not advanced to ICA.

The CBF was continuously monitored in the area of cerebral cortex supplied by the occluded MCA using a laser doppler flowmeter probe during the whole MCAO procedure. Only animals with a sharp decrease in CBF (about 70% of basal value) after occlusion with subsequent reperfusion were included in further experiments. Sensorimotor and motor impairments were evaluated at 1h, 1 day, and 1 week after the stroke using the acute neurological assessment (27) for rats and Bederson's score (40) with minor modifications (23) for mice.

Distal middle cerebral artery occlusion in rats. Focal ischemic injury in cerebral cortex was induced by permanent occlusion of the distal cortical branch of MCA and transient (30 min) occlusion of both CCAs as described previously (41). Briefly, a 1.5-2 cm scalp incision was made at the midpoint between the eye and ear on the right side. The temporal muscle was separated bluntly along muscle fibers and then retracted to expose the zygomatic arch and squamosal part of temporal bone. A craniotomy of about 3-5 mm in diameter was made using the dental drill, 1 mm rostal to the junction of the zygoma and the squamosal bone. Surgical field was irrigated with saline to avoid thermal injury of cerebral cortex during the drilling procedure. The dura was carefully opened using the tip of a 27g needle, and the cortical branch of MCA was isolated and ligated by a 10.0 nylon suture. Through a ventral midline incision in the neck, both CCAs were isolated and temporarily ligated (for 30 minutes) using 5.0 silk sutures. Metal clips closed the wound temporarily. The integrity of the temporal muscle was restored to close the cranial window and the overlying skin was sutured using 5.0 Vikryl. At 30 minutes after the ligation, both CCAs were released and the surgical wounds were closed permanently.

Transplantation. Intracerebral transplantation of human iPSC-derived lt-NES cells was performed stereotaxically at 1 week and 48 h after MCAO in mice and rats, respectively. At the day of transplantation, iPSC-derived lt-NES cells transduced with lentivirus carrying enhanced GFP under the control of a phosphoglycerate kinase promoter and naïve cells for rats and mice, respectively, were centrifuged and resuspended in transplantation buffer (43.25g of Myo-inositol were dissolved in distilled water, 200 ml phosphate buffer saline (PBS) and 5g of polyvinylalchol were added and stirred, and the solution was filtered) to reach a final concentration of 100 000 cells/μl.

Mice received 1 μl of cell suspension as a single injection in the striatum ipsilateral to MCAO using a microcapillary connected to a Hamilton syringe. For vehicle injection, the same amount of transplantation buffer was used. Coordinates were: 0.5 mm anterior from bregma, 2.2 mm lateral from midline and 2.5 mm ventral from brain surface with tooth bar at -3.3 mm. Mice were given subcutaneous injections of 10 mg/kg Cyclosporine A every other day after transplantation.

Rats subjected to MCAO received 4 μl of cell suspension at two sites (2 μl/site) in ipsilateral striatum. Coordinates were: (1) 0.5 mm anterior from bregma, 3.0 mm lateral from midline, and 5.4 mm ventral from brain surface; (2) 0.5 mm posterior from bregma, 3.0 mm lateral from midline, and 5.4 mm ventral from brain surface with tooth bar at – 3.3 mm.

Rats with distal MCAO received 3 μl of cell suspension at two sites (1.5 μl/site) in the ipsilateral cortex. Coordinates were: (1) 1.5 mm anterior from bregma, 1.5 mm lateral from midline, and 2.5 mm ventral from brain surface; (2) 0.5 mm anterior from bregma, 1.5 mm lateral from midline, and 2.5 mm ventral from brain surface with tooth bar at – 3.3 mm.

Retrograde tracer injection. At 9 weeks after transplantation or vehicle injection, all mice with MCAO lesions were injected iontophoretically with 2% Fluoro-Gold (FG; Biotium), dissolved in distilled water, into globus pallidus ipsilateral to the transplant. Coordinates were: 0.4 mm posterior and 2.0 mm lateral from bregma and 3.7 mm ventral from brain surface with tooth bar at – 3.3 mm. Iontophoretic injections were made using microcapillaries with tip-diameters of 20-30 μm and 5 μA positive current pulsed for 7 out of every 14 seconds over 7 min using a constant current generator (Midgard; Stoelting)

Immunocytochemistry. Mice were sacrificed at 10 weeks and rats were sacrificed at 2 weeks, 2 or 4 months after transplantation, respectively. Animals were deeply anesthetized by sodium pentobarbital and perfused transcardially with saline followed by 4% paraformaldehyde

(PFA). After post-fixation overnight, brains were placed in 20% sucrose until they sunk. Coronal sections (30 μm) were cut on a freezing microtome (Leica, Germany) and kept at -20 °C in cryoprotective solution.

Incubation in primary antibodies was carried out overnight at 4°C. The following primary antibodies were used: mouse anti-human nucleus - HuNu; (1:400; Millipore), mouse anti-human cytoplasm - SC121; (1:3000; provided by Dr N. Uchida, StemCells, Inc., Palo Alto, CA), goat anti-doublecortin - DCX; (1: 400; Santa Cruz Biotechnologies, Santa Cruz, CA), rabbit anti Ki-67 (1:400; Novocastra), mouse anti-neuronal nuclei - NeuN (1:100 Millipore), human-specific mouse anti glial fibrillary acid protein (GFAP; 1:100; R&D Systems), rabbit anti-HuD (1:100; Millipore), rabbit anti-dopamine- and 3':5'-monophosphate-regulated phosphoprotein 32 (DARPP32) (1:400; Santa Cruz), rabbit anti-FG (1:3000; Millipore), rabbit anti-GABA (1:2000; Sigma), rabbit anti-calbindin (1:500; Sigma), rabbit anti-parvalbumin (1:1000; provided by Prof. P. Emson, Babraham Institute, Cambridge, UK), and goat anti-calretinin (1:1000; Millipore).

Primary antibodies were detected using appropriate fluorescent (Cy3, Cy5 and Dylight 488 conjugated; Jackson ImmunoResearch, West Grove, PA) or biotin-conjugated (Vector, Burlingame, CA) secondary antibodies (1:200). Biotin-conjugated antibodies were detected with Alexa 488-conjugated streptavidin (1:200; Molecular Probes, Eugene, OR) or Cy3 - conjugated streptavidin. For double-labeling, only one biotinylated secondary antibody was used at a time.

For staining of mouse tissue using mouse anti HuNu antibody, sections were pre-incubated with unconjugated monovalent fab fragments of anti-mouse antibody (1:15; Jackson) prior to primary antibodies to block the binding of anti-mouse secondary antibody to endogenous mouse tissue.

Tyramide Signal Amplification (TSA, Perkin-Elmer, Waltham, MA) combined with avidin-biotin complex method (Elite ABC kit, Vector) was used for HuD and GABA staining.

For chromogenic visualization, endogenous peroxidase activity was first blocked with potassium phosphate-buffered saline (KPBS) containing 3% H_2O_2 and 10% methanol. After consecutive rinses, sections were incubated with primary antibodies in KPBS containing 3% appropriate serum and 0.25% TritonX. The following day, sections were rinsed and incubated with biotinylated secondary antibodies. Sections were then rinsed, incubated with avidin–biotin complex (Elite ABC kit; Vector), and developed by intensified reaction with diaminobenzidine.

For performing immunocytochemical staining, the cultured iPSC-derived lt-NES cells were fixed with 4% PFA for 15 min and blocked in PBS containing 10% FCS. For GABA-staining, 0.02% glutaraldehyde was added to the PFA. Primary antibodies were: mouse anti-Tra1-60 and -Tra1-81 (1:500, respectively, Invitrogen), mouse anti-Sox2 (1:500, R&D Systems), mouse anti-nestin (1:600, R&D Systems), rabbit anti-Dach1 (1:100 Proteintech), mouse anti-PLZF (1:50, Calbiochem), mouse anti-beta III-tubulin (1:2500, Covance), mouse anti-MAP2ab (1:250, Chemicon), rabbit anti-GFAP (1:500, DAKO Cytomation), GABA (1:800, Sigma), and rabbit anti-ZO-1 (1:100, Zymed). Primary antibodies were detected using appropriate fluorescent (Alexa 488 and 555)-conjugated (1:200, Jackson Immuno Research, West Grove, PA) secondary antibodies.

Immediately after patch-clamp recording, brain slices were fixed for 12-24 h in 4% paraformaldehyde then rinsed in KPBS and stored in antifreeze medium at -20°C. For double staining of biocytin and GFP, free-floating sections were preincubated for 1 h in 5% serum in 0.25% Triton X-100 in KPBS, and then exposed to rabbit anti-GFP primary antibody (1:10000, Abcam) overnight at room temperature. Immunoreactivity was visualized using FITC-conjugated goat anti-rabbit secondary antibody and Cy3-streptavadin (both 1:200, Jackson ImmunoResearch). Sections were mounted on glass slides, cover-

slipped and analyzed using an Olympus BX61 epifluorescence microscope.

Staircase test. The staircase test was used to assess the "side-specific" skilled forelimb reaching and grasping abilities (42, 43). Animals were placed in the staircase apparatus (Campden Instruments, Loughborough, UK). Two sugar pellets (20mg, TestDiet, Richmond, VA, USA) were placed on each step of a double staircase divided by a wide central platform and 6 steps from the bottom were baited (12 on each side, total 24 pellets per test box). Mice were trained for 12 consecutive days before stroke surgery to retrieve and eat sugar pellets. The number of pellets retrieved (= pellets eaten + pellets taken but missed to eat) per side was used as a measure of forelimb reaching ability. In addition, the number of pellets eaten per side was used to assess the forelimb reaching and grasping abilities. The average from the last three days in this period was used as baseline performance. At 2, 5 and 9 weeks after MCAO, the mice were retested for 5 days using the same test paradigm and the average from the last three days in each week was used for analysis. Performance was calculated as the number of pellets on the impaired side divided by the total number of pellets on both sides, and expressed as the percent change compared to baseline. Animals which did not eat/retrieve any pellets at all on either side were excluded from analysis. Each test session lasted 15 minutes and the session in the last three days of each period lasted 30 minutes.

Corridor test. The corridor test, originally established for a rat model of Parkinson's disease(44) and later adapted to mice(45), was used to assess the sensorimotor impairment caused by the striatal damage. Briefly, animals were placed in a narrow plastic corridor (60 cm long, 4 cm wide and 15 cm high) with 10 pairs of adjacent pots containing 5 sugar pellets (20 mg; TestDiet) that were placed at 5-cm intervals along the length of the corridor. Animals were tested for 5 consecutive days 1week before and 2, 5, and 9 weeks after stroke surgery. On each testing day, the animals were first placed in an identical, but empty, corridor for habituation for 5 minutes. The animals were then transferred to one end of the testing corridor, and the number of retrievals ipsilateral and contralateral to the lesion was counted until the animal had made a total of 20 retrievals, or 5 minutes had passed. A new retrieval was defined as retrieval from a new pot. Performance was calculated by dividing the number of contralateral retrievals with the total number of retrievals from both sides. The average from the last three days in each week was used for analysis. During the staircase and corridor test periods, animals were food-restricted and maintained at 85% - 90% of free-feeding bodyweight.

Cell counting and volume measurement. For quantification of colocalization of HuNu+ cells with different markers, approximately 1000 HuNu+ cells in each animal were analyzed. Double-labeled cells identified in an Olympus BX61 epifluorescence/light microscope were validated with a confocal laser scanning microscope (Leica). For quantification of surviving grafted cells and FG+/HuNu+ cells in mice, all HuNu+ cells in all sections were counted. Sections close to the FG injection site were excluded from counting of FG+/HuNu+ cells. Total number of HuNu+ and GFP+ cells in rats were counted stereologically by using C.A.S.T – Grid software (Olimpus, Denmark) and cell numbers were calculated according to the optical fractionator formula (46).
The microscopic images of coronal sections though the striatum immunostained with NeuN were first digitized. Using NIH Image-J software, non-lesioned area of the striatum ipsilateral to MCAO was measured and subtracted from the area of the intact contralateral striatum. To calculate the lesion volume, the results were multiplied by section thickness and the distance between sections.

Electrophysiology. Rats were anesthetized with isofluorane and decapitated. Brains were rapidly removed and placed in ice-cold, gassed (95% O_2, 5% CO_2) cutting solution (pH 7.2-7.4, 295-300 mOsm), containing (in mM): 75 sucrose, 67 NaCl, 26 $NaHCO_3$, 1.25 NaH_2PO_4, 0.5 $CaCl_2$, 7 $MgCl_2$, and 25 glucose. Coronal slices (300 μm) were cut using a vibratome (Leica VT1200S) and were allowed to rest for at least 30 minutes in cutting solution before being transferred to the recording chamber, which was constantly perfused with heated (32-34°C), gassed (95% O_2, 5% CO_2) artificial cerebrospinal fluid (aCSF, pH 7.2-7.4, 295-300 mOsm) containing (in mM): 119 NaCl, 2.5 KCl, 1.3 $MgSO_4$, 2.5 $CaCl_2$, 26 $NaHCO_3$, 1.25 NaH_2PO_4, and 25 glucose. Cells for recording were visualized under infrared light with differential interference contrast using an Olympus upright microscope equipped with a digital camera and a 40x water-immersion lens. Recording pipettes were filled with solution (pH 7.2–7.4, 295–300 mOsm) containing (in mM): 122.5 potassium gluconate, 12.5 KCl, 10.0 KOH-Hepes, 0.2 KOH-EGTA, 2 MgATP, 0.3 Na3-GTP, and 8 NaCl, resulting in pipette resistances of 3–5 MΩ. For measurements of spontaneous inhibitory postsynaptic currents recording pipettes contained (in mM): 135.0 CsCl, 10.0 CsOH, 0.2 CsOH-EGTA, 2 Mg-ATP, 0.3 Na3-GTP, 8 NaCl and 5 lidocaine N-ethyl bromide (QX-314, Tocris), resulting in pipette resistances of 2.5-4 MΩ. Biocytin (0.5%; Sigma-Aldrich) was freshly dissolved in the pipette solution before recordings for post-hoc identification of recorded cells. Resting membrane potential was estimated in current–clamp mode immediately after breaking the membrane and establishing whole-cell configuration. For measurements of action potentials and voltage responses, cells were current–clamped at ~ -70 mV, and 500 ms hyperpolarizing and depolarizing current steps were delivered in 10 pA increments through the whole-cell pipette. For measurements of whole-cell currents, cells were voltage–clamped at −70mV, series resistance was compensated, and 200 ms voltage steps were delivered in 10 mV increments. Postsynaptic currents were measured in voltage-clamp at -70 mV. Evoked currents were measured after electrical stimulation (two 100 μs square-wave pulses of 150-300 μA timed 50 ms apart) delivered by a single stainless steel wire enclosed in a glass pipette filled with aCSF (~2 MΩ tip resistance) connected to a constant current isolated stimulator (Digitimer ltd., UK). Voltage-gated sodium and potassium channels were blocked with 1 μM tetrodotoxin (TTX, Tocris) and 2 mM tetraethylammonium (TEA, Sigma), respectively. N-Methyl-D-aspartate (NMDA) and 2-amino-3-(5-methyl-3-oxo-1,2- oxazol-4-yl)propanoic acid (AMPA) receptors were blocked using 50 μM (2R)-amino-5-phosphonovaleric acid (D-AP5, Tocris) and 5 μM 2,3-dihydroxy-6-nitro-7-sulfamoyl-benzo[f]quinoxaline-2,3-dione (NBQX, Tocris), respectively. $GABA_A$ receptors were blocked using 100 μM picrotoxin (PTX, Tocris). Data were filtered at 2.9 kHz and sampled at 10 kHz with an EPC9 patch-clamp amplifier (HEKA Elektronik). Capacitance was compensated. Tabulated values are means ± SEM. Input resistance was measured at a holding potential of –60 mV by delivering –10 mV test pulses. Action potential amplitude was measured from the threshold to the peak voltage deflection, whereas half-width was measured as the duration of the action potential at half maximum amplitude. After-hyperpolarization amplitude was measured as the difference between the resting membrane potential and the maximum hyperpolarization after the action potential, whereas duration was measured as the time between the start and end of the hyperpolarization.

Statistical analysis. Two-way repeated measures ANOVA followed by bonferroni post-hoc test were used to assess differences between groups in behavioral analysis. Data are expressed as means ± SEM and differences considered significant at $P < 0.05$.

REFERENCES

1. Lindvall, O., and Kokaia, Z. 2011. Stem Cell Research in Stroke: How Far From the Clinic? Stroke.
2. Daadi, M.M., Maag, A.L., and Steinberg, G.K. 2008. Adherent self-renewable human embryonic stem cell-derived neural stem cell line: functional engraftment in experimental stroke model. PLoS One 3:e1644.
3. Hicks, A.U., Lappalainen, R.S., Narkilahti, S., Suuronen, R., Corbett, D., Sivenius, J., Hovatta, O., and Jolkkonen, J. 2009. Transplantation of human embryonic stem cell-derived neural precursor cells and enriched environment after cortical stroke in rats: cell survival and functional recovery. Eur J Neurosci 29:562-574.
4. Ramos-Cabrer, P., Justicia, C., Wiedermann, D., and Hoehn, M. 2010. Stem cell mediation of functional recovery after stroke in the rat. PLoS One 5:e12779.
5. Buhnemann, C., Scholz, A., Bernreuther, C., Malik, C.Y., Braun, H., Schachner, M., Reymann, K.G., and Dihne, M. 2006. Neuronal differentiation of transplanted embryonic stem cell-derived precursors in stroke lesions of adult rats. Brain 129:3238-3248.
6. Daadi, M.M., Li, Z., Arac, A., Grueter, B.A., Sofilos, M., Malenka, R.C., Wu, J.C., and Steinberg, G.K. 2009. Molecular and Magnetic Resonance Imaging of Human Embryonic Stem Cell-Derived Neural Stem Cell Grafts in Ischemic Rat Brain. Mol Ther 17:1282-1291.
7. Darsalia, V., Kallur, T., and Kokaia, Z. 2007. Survival, migration and neuronal differentiation of human fetal striatal and cortical neural stem cells grafted in stroke-damaged rat striatum. Eur J Neurosci 26:605-614.
8. Darsalia, V., Allison, S.J., Cusulin, C., Monni, E., Kuzdas, D., Kallur, T., Lindvall, O., and Kokaia, Z. 2011. Cell number and timing of transplantation determine survival of human neural stem cell grafts in stroke-damaged rat brain. J Cereb Blood Flow Metab 31:235-242.
9. Kelly, S., Bliss, T.M., Shah, A.K., Sun, G.H., Ma, M., Foo, W.C., Masel, J., Yenari, M.A., Weissman, I.L., Uchida, N., et al. 2004. Transplanted human fetal neural stem cells survive, migrate, and differentiate in ischemic rat cerebral cortex. Proc Natl Acad Sci U S A 101:11839-11844.
10. Lee, S.T., Chu, K., Jung, K.H., Kim, S.J., Kim, D.H., Kang, K.M., Hong, N.H., Kim, J.H., Ban, J.J., Park, H.K., et al. 2008. Anti-inflammatory mechanism of intravascular neural stem cell transplantation in haemorrhagic stroke. Brain 131:616-629.
11. Horie, N., Pereira, M.P., Niizuma, K., Sun, G., Keren-Gill, H., Encarnacion, A., Shamloo, M., Hamilton, S.A., Jiang, K., Huhn, S., et al. 2011. Transplanted Stem Cell-Secreted Vascular Endothelial Growth Factor Effects Poststroke Recovery, Inflammation, and Vascular Repair. Stem Cells 29:274-285.
12. Bacigaluppi, M., Pluchino, S., Jametti, L.P., Kilic, E., Kilic, U., Salani, G., Brambilla, E., West, M.J., Comi, G., Martino, G., et al. 2009. Delayed post-ischaemic neuroprotection following systemic neural stem cell transplantation involves multiple mechanisms. Brain 132:2239-2251.

13. Lee, H.J., Kim, K.S., Park, I.H., and Kim, S.U. 2007. Human neural stem cells over-expressing VEGF provide neuroprotection, angiogenesis and functional recovery in mouse stroke model. PLoS One 2:e156.

14. Chen, J., Zhang, Z.G., Li, Y., Wang, L., Xu, Y.X., Gautam, S.C., Lu, M., Zhu, Z., and Chopp, M. 2003. Intravenous administration of human bone marrow stromal cells induces angiogenesis in the ischemic boundary zone after stroke in rats. Circ Res 92:692-699.

15. Andres, R.H., Horie, N., Slikker, W., Keren-Gill, H., Zhan, K., Sun, G., Manley, N.C., Pereira, M.P., Sheikh, L.A., McMillan, E.L., et al. 2011. Human neural stem cells enhance structural plasticity and axonal transport in the ischaemic brain. Brain 134:1777-1789.

16. Daadi, M.M., Davis, A.S., Arac, A., Li, Z., Maag, A.L., Bhatnagar, R., Jiang, K., Sun, G., Wu, J.C., and Steinberg, G.K. 2010. Human neural stem cell grafts modify microglial response and enhance axonal sprouting in neonatal hypoxic-ischemic brain injury. Stroke 41:516-523.

17. Liu, Z., Li, Y., Zhang, X., Savant-Bhonsale, S., and Chopp, M. 2008. Contralesional axonal remodeling of the corticospinal system in adult rats after stroke and bone marrow stromal cell treatment. Stroke 39:2571-2577.

18. Takahashi, K., and Yamanaka, S. 2006. Induction of pluripotent stem cells from mouse embryonic and adult fibroblast cultures by defined factors. Cell 126:663-676.

19. Hargus, G., Cooper, O., Deleidi, M., Levy, A., Lee, K., Marlow, E., Yow, A., Soldner, F., Hockemeyer, D., Hallett, P.J., et al. 2010. Differentiated Parkinson patient-derived induced pluripotent stem cells grow in the adult rodent brain and reduce motor asymmetry in Parkinsonian rats. Proc Natl Acad Sci U S A 107:15921-15926.

20. Wernig, M., Zhao, J.P., Pruszak, J., Hedlund, E., Fu, D., Soldner, F., Broccoli, V., Constantine-Paton, M., Isacson, O., and Jaenisch, R. 2008. Neurons derived from reprogrammed fibroblasts functionally integrate into the fetal brain and improve symptoms of rats with Parkinson's disease. Proc Natl Acad Sci U S A 105:5856-5861.

21. Ebert, A.D., Yu, J., Rose, F.F., Jr., Mattis, V.B., Lorson, C.L., Thomson, J.A., and Svendsen, C.N. 2009. Induced pluripotent stem cells from a spinal muscular atrophy patient. Nature 457:277-280.

22. Dimos, J.T., Rodolfa, K.T., Niakan, K.K., Weisenthal, L.M., Mitsumoto, H., Chung, W., Croft, G.F., Saphier, G., Leibel, R., Goland, R., et al. 2008. Induced pluripotent stem cells generated from patients with ALS can be differentiated into motor neurons. Science 321:1218-1221.

23. Kawai, H., Yamashita, T., Ohta, Y., Deguchi, K., Nagotani, S., Zhang, X., Ikeda, Y., Matsuura, T., and Abe, K. 2010. Tridermal tumorigenesis of induced pluripotent stem cells transplanted in ischemic brain. J Cereb Blood Flow Metab.

24. Chen, S.J., Chang, C.M., Tsai, S.K., Chang, Y.L., Chou, S.J., Huang, S.S., Tai, L.K., Chen, Y.C., Ku, H.H., Li, H.Y., et al. 2010. Functional improvement of focal cerebral ischemia injury by subdural transplantation of induced pluripotent stem cells with fibrin glue. Stem Cells Dev 19:1757-1767.

25. Jiang, M., Lv, L., Ji, H., Yang, X., Zhu, W., Cai, L., Gu, X., Chai, C., Huang, S., Sun, J., et al. 2011. Induction of pluripotent stem cells transplantation therapy for ischemic stroke. Mol Cell Biochem 354:67-75.

26. Koch, P., Opitz, T., Steinbeck, J.A., Ladewig, J., and Brustle, O. 2009. A rosette-type, self-renewing human ES cell-derived neural stem cell with potential for in vitro instruction and synaptic integration. Proc Natl Acad Sci U S A 106:3225-3230.

27. Andsberg, G., Kokaia, Z., Bjorklund, A., Lindvall, O., and Martinez-Serrano, A. 1998. Amelioration of ischaemia-induced neuronal death in the rat striatum by NGF-

secreting neural stem cells. Eur J Neurosci 10:2026-2036.

28. Schmued, L.C., and Fallon, J.H. 1986. Fluoro-Gold: a new fluorescent retrograde axonal tracer with numerous unique properties. Brain Res 377:147-154.

29. Kokaia, Z., Andsberg, G., Martinez-Serrano, A., and Lindvall, O. 1998. Focal cerebral ischemia in rats induces expression of P75 neurotrophin receptor in resistant striatal cholinergic neurons. Neuroscience 84:1113-1125.

30. Ouimet, C.C., Miller, P.E., Hemmings, H.C., Jr., Walaas, S.I., and Greengard, P. 1984. DARPP-32, a dopamine- and adenosine 3':5'-monophosphate-regulated phosphoprotein enriched in dopamine-innervated brain regions. III. Immunocytochemical localization. J Neurosci 4:111-124.

31. Steinbeck, J.A., Koch, P., Derouiche, A., and Brustle, O. 2011. Human embryonic stem cell-derived neurons establish region-specific, long-range projections in the adult brain. Cell Mol Life Sci.

32. Wictorin, K., Brundin, P., Gustavii, B., Lindvall, O., and Björklund, A. 1990. Reformation of long axon pathways in adult rat central nervous system by human forebrain neuroblasts. Nature 347:556-558.

33. Aubry, L., Bugi, A., Lefort, N., Rousseau, F., Peschanski, M., and Perrier, A.L. 2008. Striatal progenitors derived from human ES cells mature into DARPP32 neurons in vitro and in quinolinic acid-lesioned rats. Proc Natl Acad Sci U S A 105:16707-16712.

34. Brederlau, A., Correia, A.S., Anisimov, S.V., Elmi, M., Paul, G., Roybon, L., Morizane, A., Bergquist, F., Riebe, I., Nannmark, U., et al. 2006. Transplantation of human embryonic stem cell-derived cells to a rat model of Parkinson's disease: effect of in vitro differentiation on graft survival and teratoma formation. Stem Cells 24:1433-1440.

35. Tabar, V., Panagiotakos, G., Greenberg, E.D., Chan, B.K., Sadelain, M., Gutin, P.H., and Studer, L. 2005. Migration and differentiation of neural precursors derived from human embryonic stem cells in the rat brain. Nat Biotechnol 23:601-606.

36. Kokaia, Z., Zhao, Q., Kokaia, M., Elmér, E., Metsis, M., Smith, M.-L., Siesjö, B.K., and Lindvall, O. 1995. Regulation of brain-derived neurotrophic factor gene expression after transient middle cerebral artery occlusion with and without brain damage. Exp Neurol 136:73-88.

37. Zhao, Q., Smith, M.-L., and Siesjö, B.K. 1994. The w-conopeptide SNX-111, an N-type calcium channel blocker, dramatically ameliorates brain damage due to transient focal ischaemia. Acta Physiol Scand 150:459-461.

38. Andsberg, G., Kokaia, Z., and Lindvall, O. 2001. Upregulation of p75 neurotrophin receptor after stroke in mice does not contribute to differential vulnerability of striatal neurons. Exp Neurol 169:351-363.

39. Hara, H., Huang, P.L., Panahian, N., Fishman, M.C., and Moskowitz, M.A. 1996. Reduced brain edema and infarction volume in mice lacking the neuronal isoform of nitric oxide synthase after transient MCA occlusion. J Cereb Blood Flow Metab 16:605-611.

40. Bederson, J.B., Pitts, L.H., Tsuji, M., Nishimura, M.C., Davis, R.L., and Bartkowski, H. 1986. Rat middle cerebral artery occlusion: evaluation of the model and development of a neurologic examination. Stroke 17:472-476.

41. Chen, S.T., Hsu, C.Y., Hogan, E.L., Maricq, H., and Balentine, J.D. 1986. A model of focal ischemic stroke in the rat: reproducible extensive cortical infarction. Stroke 17:738-743.

42. Baird, A.L., Meldrum, A., and Dunnett, S.B. 2001. The staircase test of skilled reaching in mice. Brain Res Bull 54:243-250.

43. Montoya, C.P., Campbell-Hope, L.J., Pemberton, K.D., and Dunnett, S.B. 1991. The "staircase test": a measure of independent forelimb reaching and grasping abilities in rats. J Neurosci Methods 36:219-228.

44. Dowd, E., Monville, C., Torres, E.M., and Dunnett, S.B. 2005. The Corridor Task: a simple test of lateralised response selection sensitive to unilateral dopamine deafferentation and graft-derived dopamine replacement in the striatum. Brain Res Bull 68:24-30.

45. Grealish, S., Mattsson, B., Draxler, P., and Bjorklund, A. 2010. Characterisation of behavioural and neurodegenerative changes induced by intranigral 6-hydroxydopamine lesions in a mouse model of Parkinson's disease. Eur J Neurosci 31:2266-2278.

46. West, M.J. 1999. Stereological methods for estimating the total number of neurons and synapses: issues of precision and bias. Trends Neurosci 22:51-61.